Assessment of the Resilience of Indian River Basins to Droughts under Climate Change Scenarios

Thesis submitted in partial fulfilment of the requirements

for the award of the degree of

Doctor of Philosophy

in

Civil Engineering

by

Ashutosh Sharma

Under the supervision of

Dr. Manish Kumar Goyal

Prof. Arup Kumar Sarma

Department of Civil Engineering

Indian Institute of Technology Guwahati

Guwahati - 781039, India

October, 2019

Dedicated to my life-coach, my late grandfather:

Shri Kishan Chand Sharma

I owe it all to you.

Many thanks!

Declaration

I certify that

- The work contained in this thesis is original and has been done by myself and under the general supervision of my supervisor(s).
- The work reported herein has not been submitted to any other Institute for any degree or diploma.
- Whenever I have used materials (concepts, ideas, text, expressions, data, graphs, diagrams, theoretical analysis, results, etc.) from other sources, I have given due credit by citing them in the text of the thesis and giving their details in the references. Elaborate sentences used verbatim from published work have been clearly identified and quoted.
- I also affirm that no part of this thesis can be considered plagiarism to the best of my knowledge and understanding and take complete responsibility if any complaint arises.
- I am fully aware that my thesis supervisors are not in a position to check for any possible instance of plagiarism within this submitted work.

Ashutosh Sharma

Department of Civil Engineering
Indian Institute of Technology Guwahati
Guwahati - 781039, India

Certificate

This is to certify that this thesis entitled "**Assessment of the Resilience of Indian River Basins to Droughts under Climate Change Scenarios**" submitted by **Ashutosh Sharma (Roll No. 166104015)**, in partial fulfilment of the requirements for the award of the degree of Doctor of Philosophy, to the Indian Institute of Technology Guwahati, Assam, India, is a record of the bonafide research work carried out by him under our guidance and supervision at the Department of Civil Engineering, Indian Institute of Technology Guwahati, Assam, India. To the best of our knowledge, no part of the work reported in this thesis has been presented for the award of any degree at any other institution.

Dr. Manish Kumar Goyal
Associate Professor,
Discipline of Civil Engineering,
IIT Indore,
Indore - 453552, India.
Email : mkgoyal@iiti.ac.in
Phone : +91-7324-306697

Prof. Arup Kumar Sarma
Professor,
Department of Civil Engineering,
IIT Guwahati,
Guwahati - 781039, India.
Email : aks@iitg.ac.in
Phone : +91-361-258-2420

Acknowledgements

The PhD Journey is not only about engaging in the research. In fact, it is a life itself that we live it and learn a lot by several challenges, ups, and downs in this entire period. This work would not have been possible without the help and support I received from many people during this wonderful journey of PhD.

It goes without saying that this journey would not have been possible without the constant support, the unconditional love and profound encouragement of my mother and my father. They never questioned my intentions and whole-heartedly supported me in all my endeavours. There are no words to express my gratitude to them. I express my deepest sense of gratitude and veneration to my supervisors Prof. Arup Kumar Sarma, Department of Civil Engineering, Indian Institute of Technology Guwahati (IITG) and Dr. Manish Kumar Goyal, Associate Professor, Discpline of Civil Engineering, Indian Institute of Technology Indore (IITI), for their meticulous guidance, constructive suggestions, and sustained interest and patience throughout the present investigation. It is my sublime duty to express my deepest sense of reverence and indebtedness to the Chairman of my Doctoral Committee Dr. Bimlesh Kumar, Associate Professor, Department of Civil Engineering, IITG, for his constant encouragement and indelible inspiration provided during the study. I express my sincere thanks to the members of my Doctoral Committee Dr. Rishikesh Bharti, Assisstant Professor, Department of Civil Engineering and Dr. Subhash Thota, Associate Professor, Department of Physics, IITG for their valuable suggestions, eternal encouragement, and timely help provided at various stages of the investigation and compilation of thesis.

I am thankful to Shastri Indo Canadian Institute for providing me the Shastri Student Research Fellowship to carry out research work at McGill University. My sincere thanks goes to Dr. Jan Franklin Adamowski, Associate Professor, Department of Bioresource Engineering, Faculty of Agricultural and Environmental Sciences, McGill University, for providing me the opportunity to join his team as a visiting researcher. I am also thankful to Indo-U.S. Science and Technology Forum (IUSSTF) for providing me the internship opportunity under the Water Advanced and Ressearch Innovation (WARI) Program. I express my deepest graditude to Dr. Francisco Muñoz-Arriola, Associate Professor of Hydroinformatics and Integrated Hydrology, Biological Systems Engineering Department, University of Nebraska-Lincoln for providing me the opportunity to

join his research group as a an intern.

I thank my fellow labmates and friends at IITG for the stimulating discussions, for the sleepless nights we were working together before deadlines, and for all the fun we had during this journey. In particular, I am grateful to Dr. Vishal Singh, Scientist, National Institute of Hydrology, Roorkee, Dr. Shivam, Assisstant Professor, Central Agricultural University, Gangtok, and Dr. Uttam Puri Goswami, for enlightening me the first glance of research. It is often said good friends are rare to get. In this context I find myself very lucky to have so many good friends like Sameer, Chandan, Manas, Aparimita, Amrutha, Gilbert, Juna, Suman, Srinidhi, Vinay and Anjeneylu. Their friendly affection, timely help, and encouragements never let me feel away from home during my stay at the institute. Also, I thank my good friends, Vishnu, Rachit, Karan and Sobhan at McGill University and Manas, Alessandro, Lucia, Arun, Ved, Ravi and Meetpal at University of Nebraska-Lincoln, for supporting me during my stay. And finally, last but by no means least, I thank my dear friend, Aditi, who has provided me through moral and emotional support in my life. This list is obviously incomplete, but let me submit that the omissions are inadvertent and I once again record my deep felt gratitude to all those who have cooperated with me either directly or indirectly in this endeavor.

Ashutosh Sharma

Abstract

In the last few decades, climate change has emerged as a major threat to natural systems. Climate change has affected the climatic patterns around the globe and is affecting the hydrology and ecohydrology in different river basins. These changes are anticipated to aggravate in future. Therefore, it is essential to assess the capacity of our natural systems to withstand these hydroclimatic changes. The concept of resilience, defined as the ability of the ecosystem to absorb the disturbances and sustain the same functioning under disturbed conditions, has emerged as a tool to understand the response of system to disturbances. In this study, a framework is developed for the resilience analysis of the terrestrial ecosystems in India to droughts. The framework uses ecosystem water use efficiency (WUE_e) as an indicator for the ecosystem functioning. The framework is applied at multiple scales (river basin, district, land cover and climate type) for the resilience analysis of the terrestrial ecosystems. The ecosystem resilience analysis revealed that six out 22 basins and 241 out of 634 districts were resilient to droughts. Forests were found resilient to droughts, which contributed to the higher resilience of forest dominated regions. Out of 30 states and UTs, only 10 had more than 50% resilient area, which were mainly located in the lower Himalayan region. Further, WUE_e and its controlling factors are studied in detail. Large variation in WUE_e is found for different parts of the country. WUE_e was higher in the lower Himalayan regions and northeast India. In contrast to the decreasing trend in global WUE_e, an increasing trend was found for the country-average WUE_e. Precipitation was the main climatic factor affecting WUE_e in the western, central and eastern India; Temperature in the mountainous Himalayan regions; and Solar radiation in some parts of northeast and northwest. The negative impact of development activities on primary production was found for four forest-dominated states (3 in northeast and 1 in north).

In addition to ecosystem resilience analysis, a hydrological resilience analysis was performed in the Teesta river basin in Indian Himalayan regions. Two resilience measures (deviation and recovery time) were used for the resilience analysis. Analysis of changes and trend in precipitation, temperature and climate extremes (23 indices) was

performed in the basin for past and future climates. Four general circulation models (GCMs) were used to obtain the projected scenarios of precipitation and temperature under two representative concentration pathways (RCPs) in eight sub-basins of the Teesta river. Increase in precipitation and temperature was found in the basin for all the projected scenarios. Hydrological modelling (Soil and Water Assessment Tool) was used to simulate the hydrological processes in the basin for both past (1951-2010) and projected (2011-2100) climates. The simulated streamflow had an increasing trend in the basin for different projected scenarios. Drought analysis using standardized precipitation index (SPI) indicated a decrease in drought events in future. The resilience analysis revealed an increase in the basin's resilience to maintain streamflow under less precipitation conditions.

Climate change is affecting the pattern of precipitation and temperature around the world. Analysis of changes in precipitation, temperature and climate extremes is also performed for India at 0.5-degree grids. The outputs from 20 GCMs were corrected for bias using the observed data for four climate change scenarios (i.e. RCPs). Precipitation and temperature were found to increase under projected climate in India; however, there was large spatial heterogeneity in the changes in both precipitation and temperature. Higher increase in precipitation was found in Western parts of the country whereas a higher increase in temperature was found in Himalayan regions. Study of the climate extremes revealed an increase in extreme warm events such as warm nights, warm days, tropical nights and summer days, and decrease in extreme cool events such as cool nights, cool days, ice day and frost days. Substantial increase in precipitation extremes was also found for different parts of the country.

This study provides a framework for resilience analysis, which can be applied in different parts of the country. This study facilitates the identification of the most sensitive regions in the country for ecosystem management and climate policymaking, and highlight the need for taking sufficient adaptation measures to ensure the sustainability of ecosystems.

Keywords: Climate change; Droughts; India; Resilience.

Contents

List of Figures

List of Tables

List of Symbols

Symbols	Description
CO_2	Carbon dioxide
E_a	Evapotranspiration
gC	grams of carbon
km	kilometer
m	meters
mm	millimetre
Q	Discharge
Q_{surf}	Surface runoff
R^2	Coefficient of determination
R10	Number of heavy precipitation days
R20	Number of very heavy precipitation days
R95p	Very wet days
R_d	Resilience index
Rday	Daily rainfall
RX1day	Max 1-day precipitation amount
RX5day	Max 5-day precipitation amount
SW	Soil water content
TN10p	Cool nights
TN90p	Warm nights
TNn	Min Tmin
TNx	Max Tmin

TX10p	Cool days
TX90p	Warm days
TXn	Min Tmax
TXx	Max Tmax
W	watt
W_{seep}	water seepage
WUE	Water Use Efficiency
WUE_e	Ecosystem WUE
WUE_m	Mean WUE_e
WUE_d	WUE_e during the dry period

List of Abbreviations

Terms	Abbreviations
ANN	Artificial Neural Network
ANOVA	Analysis of Variance
AOGCM	Atmosphere-Ocean General Circulation Model
APAR	Absorbed Photosynthetically Active Radiation
AR3	Third Assessment Report of IPCC
AR5	Fifth Assessment Report of IPCC
ARS	Agricultural Research Service
AWiFS	Advanced Wide Field Sensor
CASA	Carnegie–Ames–Stanford Approach
CCI	Commission of Climatology
CDD	Consecutive Dry Days
CFSR	Climate Forecast System Reanalysis
CLIVAR	Climate Variability and Predictability
CMIP	Coupled Model Intercomparison Project
CMIP3	Third phase of CMIP
CMIP5	Fifth phase of CMIP
CN	Curve Number
CNRM-CM5	Centre National de Recherches Météorologiques - Climate Model, version 5
CNV	Cropland/Natural Vegetation Mosaic
CR	Croplands
CRU	Climatic Research Unit

CS	Closed Shrublands
CV	Coefficient of Variation
CWD	Consecutive Wet Days
DBF	Deciduous Broadleaf Forest
DEM	Digital Elevation Model
DGVM	Dynamic Global Vegetation Model
DNF	Deciduous Needleleaf Forest
DTR	Diurnal Temperature Range
EBF	Evergreen Broadleaf Forest
ENF	Evergreen Needleleaf Forest
EOS	Earth Observation System
ESM	Earth System Model
ET	Evapotranspiration
ETCCDI	Expert Team on Climate Change Detection and Indices
FAO	Food and Agriculture Organization
FD	Frost Days
FORM	First-Order Reliability Method
FSI	Forest Survey of India
GCM	General Circulation Model
GDP	Gross Domestic Product
GEP	Gross Ecosystem Productivity
GFDL-CM3	Geophysical Fluid Dynamics Laboratory - Coupled Physical Model, version 3
GFDL-ESM2G	Geophysical Fluid Dynamics Laboratory - Earth System Model 2G
GFDL-ESM2M	Geophysical Fluid Dynamics Laboratory - Earth System Model 2M
GLUE	Generalized Likelihood Uncertainty Estimation
GPP	Gross Primary Production
GR	Grasslands
GSDP	Gross State Domestic Product

GSL	Growing Season length
GWUE	GPP based WUE_e
HEC-HMS	Hydrologic Engineering Centre -Hydrological Modelling System
HRU	Hydrological Response Unit
ID	Ice Days
IDW	Inverse Distance Weightage Interpolation
IMD	Indian Meteorological Department
India-WRIS	India - Water Resources Information System
IPCC	Intergovernmental Panel on Climate Change
LAI	Leaf Area Index
LCI	Land Cover Institute
LULC	Land Use and Land Cover
MAP	Mean Annual Precipitation
MCMC	Markov Chain Monte Carlo
MF	Mixed Forests
MK	Mann-Kendall trend test
MMA	Multi Model Average
MODIS	Moderate Resolution Imaging Spectroradiometer
MUSLE	Modified Universal Soil Loss Equation
NCAR	National Center for Atmospheric Research
NCEP	National Center of Environmental Prediction
NPP	Net Primary Production
NPS	Non-Point Source
NRSC	National Remote Sensing Centre
NSE	Nash-Sutcliffe Efficiency
NTSG	Numerical Terradynamic Simulation Group
NWUE	NPP based WUE_e
OGD	Open Government Data

CWC	Central Water Commission
OS	Open Shrublands
PDF	Probability Distribution Function
PDSI	Palmer Drought Severity Index
PRCPTOT	Annual total wet-day precipitation
PRECIS	Providing Regional Climates for Impact Studies
PSO	Particle Swarm Optimization
RCM	Regional Climate Model
RCP	Representative Concentration Pathway
SCA	Snow Covered Area
SCS	Soil Conservation Service
SDII	Simple Daily Intensity Index
SPI	Standardized Precipitation Index
SPEI	Standardized Precipitation Evapotranspiration Index
SRES	Special Report on Emissions Scenarios
STD	Standard Deviation
SUFI2	Sequential Uncertainty Fitting
SU	Summer Days
SWAT	Soil and Water Assessment Tool
SWAT-CUP	SWAT – Calibration and Uncertainty Programs
Tmax or TX	Daily maximum temperature
Tmin or TN	Daily maximum temperature
TR	Tropical nights
UMT	University of Montana
UNFCCC	United Nations Framework Convention on Climate Change
USDA	United States Department of Agriculture
UT	Union Territories
VIC	Variable Infiltration Capacity

WMO	World Meteorological Organization
WS	Woody Savannas
WTR	Water
WUE	Water Use Efficiency
WUE_e	Ecosystem Water Use Efficiency
WUE_m	Mean WUE_e

1

Introduction

1.1 Background

Climate change has emerged as a major challenge for the 21st century. Currently, climate change is looked upon as one of the greatest environmental and socio-economic threat to the world. With improvements in both quality and quantity of hydro-climatological observations, climate change is now widely recognised by the scientific community (IPCC, 2014; Oreskes, 2004). In the Fifth Assessment Report (AR5), Intergovernmental Panel on Climate Change (IPCC) reported "*Human influence on the climate system is clear, and recent anthropogenic emissions of greenhouse gases are the highest in history. Recent climate changes have had widespread impacts on human and natural systems*" (IPCC, 2014). The Third Assessment Report (AR3) of IPCC in 2001 reported that the global average surface temperature (including both land and oceans) increased by about 0.6°C over the 20th century (IPCC, 2001). The AR5 of IPCC in 2014 reported that the global average surface temperature has increased by 0.85°C over the period between 1880 and 2012 (IPCC, 2014). The warming of Earth's surface is anticipated to intensify the water cycle (Huntington, 2006; Oki and Kanae, 2006). The impact of climate change on natural systems has been seen in all the continents around the world; however, there is large spatial heterogeneity in climate change impacts. The direct impacts of climate change can be seen on the physical systems in the form of an increase in temperature, changing rainfall and snowfall patterns, melting of glaciers and permanent ice, changing patterns of extreme hydro-climatological events like floods and droughts (IPCC, 2014). These changes in the Earth's climate have hydrological, ecological and biological implications (Peñuelas and Filella, 2001; Walther et al., 2002; Parmesan and Yohe, 2003; Cowie, 2012; IPCC, 2014). IPCC has reported

that changes in extreme weather and climate events have been observed since the mid-20th century (IPCC, 2014). Globally, the number of cold days and nights has reduced, whereas the number of warm days and nights has increased (Easterling, 2000; Reichstein et al., 2013; Trenberth et al., 2014). The alterations in spatiotemporal patterns of precipitation are affecting the hydrological systems leading to disturbance in quality and quantity of available water resources. In terms of the impacts of climate change on agriculture, IPCC reported that the negative impacts are more common than the positive impacts (Howden et al., 2007; IPCC, 2014). Also, the rise in temperature is leading to precipitation in the form of rainfall than snowfall, which may lead to a decrease in streamflow during the dry period in many river basins having significant snowmelt contributions (Berghuijs et al., 2014). Climate change is also contributing to the losses due to extreme events such as floods (Hallegatte et al., 2013). The variation in frequency or intensity of climate extremes is affecting both natural ecosystems as well as humans (Easterling, 2000).

The impacts of climate change are not limited to the atmosphere or hydrosphere, but it also has a profound influence on terrestrial ecosystem's functioning (Dale et al., 2000; Karl and Trenberth, 2003; Meehl and Tebaldi, 2004; Wheeler and Von Braun, 2013). The terrestrial ecosystems play an important role in the global carbon cycle as a major sink for atmospheric CO_2 (Cao and Woodward, 1998; Ciais et al., 1995; Yu et al., 2014). Terrestrial plants take out CO_2 from the atmosphere through photosynthesis along with the loss of water, which regulates the mass-energy exchange between the vegetation and the atmosphere (Keenan et al., 2013). Global food production and security are jeopardised by the changes in climate (Wheeler and Von Braun, 2013). The productivity of terrestrial ecosystems is adversely affected by the hydroclimatic disturbances such as droughts, which also has implications in food security (Breshears et al., 2005; Dale et al., 2000; Thomey et al., 2011; Xu et al., 2017; Zhao and Running, 2010).

1.2 Resilience Concept

The concept of resilience was introduced by Holling (1973) in the field of ecology to help understand the capacity of ecosystems to absorb change. This concept has emerged immensely over the last few decades in different fields (Folke, 2016). Resilience is defined as the ability of a system to maintain its structure and patterns

of behaviour in the face of disturbance (Holling, 1986). The term “disturbance” in ecology refers to a temporary change in environmental conditions that causes a noticeable change in an ecosystem. Resilience is having the capacity to persist in the face of change, to continue to develop with ever-changing environments (Folke, 2016). In simple terms, it relates to the ability of a system to recover after being hit by some disturbance (Walker and Salt, 2013). It quantifies the capacity of a system to adapt or even transform into new development pathways under the dynamic change. The resilience approach is perceived as a subset of sustainability science by many (Anderies et al., 2013; Walker and Salt, 2006). Resilience cannot be defined in terms of a single measurement or number; instead, it is determined based on a set of attributes (Walker and Salt, 2013). To assess the resilience of a system, the identity (a measure of the system’s response/functioning) of the system needs to be identified first. The resilience analysis focuses on how that identity might be changing over time, and what threatens that identity (Walker and Salt, 2013).

The resilience can be defined in two ways (Holling, 1996):

1. Engineering Resilience

This is a traditional approach that concentrates on the stability of the system with respect to a single equilibrium state. The focus is on the resistance of the system to disturbance and its ability to recover/return to the same equilibrium state.

2. Ecological Resilience

This approach emphasises the ability to the system to reorganise itself to a new equilibrium state. In this case, the resilience is measured in terms of the magnitude of disturbance that the system can absorb before undergoing the structure change or reorganisation.

Although, in theory, it may seem straightforward, measuring engineering resilience poses several challenges, which include deciding what measure or metric to use, using an accurate baseline, and accounting for disturbances of different types. Also, various components of a system may recover at different rates. Therefore, the selection of what is to be measured can significantly influence the quantification of resilience.

1.3 Problem Statement

As climate change has affected natural systems around the globe, developing countries are believed to be the most affected. India is one of these countries and has the

second largest population in the world. The agricultural sector in India, which accounts for around 18 percent of country's Gross Domestic Product (GDP) and offers employment to half of the country's workforce (Madhusudhan, 2015), is mainly dependent on climate, especially the Monsoon rainfalls. Therefore, it is essential to understand the impact of climatic changes on India's natural systems. One way to reduce the impacts of extreme rainfall events and droughts on the ecosystems is to invest in enhancing resilience (NRC, 2012). The concept of resilience provides an opportunity to understand the current state of natural systems to withstand the climatic disturbances anticipated under climate change. In this study, a framework is developed utilising the concept of resilience to understand the impact of changing climatic conditions on India's natural systems. The ecosystem resilience analysis is performed at multiple scales (river basin, district, land cover, and climate type) to understand the response of terrestrial ecosystems to droughts.

In addition, the prediction of future climatic changes plays an important role in policy making and adaptation strategies. Therefore, future climatic changes in the country are studied using the outputs from multiple climate models. The study is carried out considering precipitation, daily maximum temperature, daily minimum temperature, and 25 different extreme indices of precipitation and temperature. Further, a hydrological resilience framework was used in the Teesta river basin to understand the climate-induced changes in the basin's hydrology. The basin was chosen as the anthropogenic impact is low in the basin with low urbanization. Though many studies have been carried out in different parts of the country to examine the impact of anticipated climatic changes, these studies generally considered the impact of gradual climatic changes on the hydrological systems while looking into the trend and changes compared to past climates. However, the hydrological resilience framework analyses the changes in the response of basin to meteorological droughts conditions over time.

1.4 Research Objectives

The primary goal of this study is to evaluate the resilience of different Indian River basins to droughts. The objectives are defined as:

1. Development of a framework for resilience analysis of terrestrial ecosystems to droughts and its application at river basin scale in India.
2. Analysis of ecosystem water use efficiency and its controlling factors in India.

3. Assessment of ecosystem resilience to droughts at district scale in India.
4. Analysis of hydrological resilience to droughts in Teesta river basin.
5. Assessment of changes in precipitation, temperature and climate extremes in India.

1.5 Organization of the Thesis

This thesis contains seven chapters. Chapter 1 contains a brief overview of climate change impacts and resilience concept. Chapter 2 focuses on understanding the relevant literature on the climate change impact assessment, resilience analysis and hydrological modelling. Chapter 3 describes the proposed ecosystem resilience analysis framework and its application at different scales. Chapter 4 discusses the ecosystem water use efficiency, which is used as an indicator in resilience analysis, along with the controlling factors. Chapter 5 focuses on the hydrological resilience analysis of the Teesta river basin and the assessment of climate change impacts. Chapter 6 describes the analysis of precipitation, temperature and climate extremes in India under the observed and projected climates. Chapter 7 summarises the major findings from the present investigation and highlights recommendations for future studies in this field.

Chapter 1: It provides an overview of climate change and its impact, and the concept of resilience. The objectives of the study are described in this chapter.

Chapter 2: This chapter contains the review of literature on climate change impact assessment around the world and in India, and on the resilience analysis.

Chapter 3: This chapter describes the framework developed for the ecosystem resilience analysis and its application at different scales in India.

Chapter 4: This chapter presents an analysis of ecosystem water use efficiency and its controlling factor in India.

Chapter 5: In this chapter, the analysis of hydrological resilience of Teesta river basin is discussed. The impact of climate change on precipitation, temperature and streamflow in the basin is also discussed.

Chapter 6: This chapter describes the assessment of changes in precipitation, temperature and climate change in India using multiple climate model outputs.

Chapter 7: The final chapter summarises the major findings from the present investigation and highlights some of the recommendations for future studies in this field.

2

Review of the Literature

2.1 Climate Change

The energy balance of the Earth's climate is affected by the changes in atmospheric abundance of greenhouse gasses and aerosols, in solar radiation and land surface properties. The IPCC defines climate change as (IPCC, 2007):

"Climate change refers to a change in the state of the climate that can be identified (e.g., by using statistical tests) by changes in the mean and/or the variability of its properties and that persists for an extended period, typically decades or longer. Climate change may be due to natural internal processes or external forcings such as modulations of the solar cycles, volcanic eruptions and persistent anthropogenic changes in the composition of the atmosphere or land use."

The United Nations Framework Convention on Climate Change (UNFCCC), in its Article 1, defines climate change as (UNFCCC, 1992):

"A change of climate which is attributed directly or indirectly to human activity that alters the composition of the global atmosphere and which is in addition to natural climate variability observed over comparable time periods."

Based on a review of 928 scientific peer-reviewed articles published between 1993 and 2003, Oreskes (2004) concluded that there was a strong scientific consensus on climate change. There was not a single paper that disagreed with the consensus position. Thousands of studies carried out around the world have reported the adverse impacts of climate change on natural and human systems, although the severity of impact varies from region to region (IPCC, 2014). The impact of climate change on water supply has been a fundamental concern (Vorosmarty et al., 2014). Based on the linear trend, the

global average land and ocean surface temperature showed an increase of 0.85°C over the period from 1880 to 2012. Also, the difference between the average temperature of the period 1850-1900 and the period 2003-2012 was found about 0.78°C (IPCC, 2013). The AR5 of IPCC (IPCC, 2014) explores the literature on the scientific, and technological, economic and social aspects of mitigation of climate change. The report highlighted that the freshwater-related risks are anticipated to increase significantly with increasing greenhouse gas concentration in the atmosphere (IPCC, 2014). It adopted greenhouse gas concentration (not emissions) trajectories called Representative Concentration Pathways (RCPs), which succeeded Special Report on Emissions Scenarios (SRES) (Taylor et al., 2012; van Vuuren et al., 2011).

Climate change studies rely on global climate models for the projection of future climate scenarios. Climate models are based on well-established physical principles and simulate different processes of climate and its interactions in atmosphere, oceans, land surface and ice. These models have been widely used to understand the past climate and to predict the future climate based on different scenarios (Taylor et al., 2012). The General Circulation Models (GCMs) are a class of climate models, which mathematically models the general circulation of a planetary atmosphere or ocean. GCMs are widely used to study the impact of anthropogenic activities on climate, to climate predictions and to understand the climate. The Atmosphere-Ocean General Circulation Models (AOGCMs), which incorporate atmosphere, ocean, land and sea ice components of climate systems, were widely used in the Fourth Assessment Report (AR4) of IPCC. The Earth System Models (ESMs) is an advancement over the AOGCMs, which include the representations of different biochemical cycles on Earth (Flato et al., 2013). These models include atmosphere, ocean, sea, ice, land surface and vegetation on land and the biogeochemistry of the ocean.

To study the global climatic changes and to understand the past and future climate, Coupled Model Intercomparison Project (CMIP) framework was designed to improve the modeling capability of global coupled ocean-atmosphere GCMs. CMIP has gone through different phases of improvements. The most recent completed phase of the project is the fifth phase of CMIP (CMIP5). The experiments under this project were conducted during the period 2010-2014. The main objective of CMIP5 was to address the scientific question from the AR4 of IPCC. More than 50 models of more than 20 groups used the CMIP5 framework and provided the outputs of the models (Taylor

et al., 2012). Unlike the SRES scenarios used in CMIP3, CMIP5 used RCP based scenarios, which incorporated the adaptation policies in the GCM runs. Four RCPs were defined for CMIP5, which were based on the projections of future growth in population, development in technology and response of the society (Taylor et al., 2012). RCPs were specified based on the rough estimate of the radiative forcing by the end of the twenty-first century relative to the pre-industrial period (Taylor et al., 2012; van Vuuren et al., 2011). RCP2.6 is a low emission scenario or mitigation scenario, which is also called 'peak-and-decay' scenarios. Under this scenario, the radiative forcing peaks at about 3 Wm^{-2} near the middle of the twenty-first century and starts to decline. The value of radiative forcing in 2100 is assumed to be 2.6 Wm^{-2}. RCP4.5 and RCP6.0 are two intermediate pathways (stabilization scenarios) in which the radiative forcing are stabilized at the values of 4.5 Wm^{-2} and 6.0 Wm^{-2}, respectively, after 2100. RCP8.5 is the high emissions scenario in which the radiative forcing goes above 8.5 Wm^{-2} by 2100. Table 2.1 describes the different RCPs. The results of experiments carried out under CMIP5 were utilized for the preparation of AR5 of IPCC.

The coarser scale outputs of climate models are generally downscaled to a finer scale for better representation of the local atmospheric processes (Chen et al., 2012; Wilby et al., 1998). GCMs simulate several climate variables; however, it is worth mentioning the confidence in future projections or estimation is higher for some climate variables (e.g., temperature) than for others (e.g., precipitation) due to inherent complexities associated with the processes (Randall and Wood, 2007).

Table 2.1: Description of RCPs (IPCC, 2014; Taylor et al., 2012).

RCP	Radiative Forcing in 2100 compared to 1750 (Wm^{-2})	Climate policy associated with the scenario	CO_2 Equivalent by 2100 (ppm)	Projected global temperature increase from 1986-2005 (°C)
RCP2.6	2.6	Mitigation	475	1.0
RCP4.5	4.5	Stabilization	630	1.8
RCP6.0	6.0	Stabilization	800	2.2
RCP8.5	8.5	None	1313	3.7

2.2 Impact of climate change on water resources and hydrology

The impact of climate change on hydrology has been widely reported. Many parts of the world are facing moderate to severe water stress. An approximation by Arnell (1999) suggested that around one-third of the population across the globe was facing mild to high water stress. Using climate models and macro-scale hydrological model, the study further indicated that the scenario of water stress would aggravate by 2025 with a large section of the global population facing severe water scarcity. Approximately two-thirds of the people in 2025 could be under water stress arising due to the increase in population and water demands (Arnell, 1999). IPPC has also reported that the rise in CO_2 and other greenhouse gasses concentration will significantly affect the hydrological cycle (IPCC, 2013). More and more evidence is now available to support the idea that anthropogenic activities, mainly the release of greenhouse gasses, have caused the change in global climate (McMichael et al., 2004). It is widely reported that the patterns of precipitation have changed, resulting in arid or semiarid regions turning drier and other areas turning wetter (Arnell, 1999; Chou et al., 2013; McMichael et al., 2004; Trenberth, 2011). However, the increase in precipitation is also disproportionate. There is a change in the frequency of heavy precipitation events (Sillmann and Roeckner, 2008). With the warming of the Earth's climate, the intensification of the hydrological cycle has been reported (Déry et al., 2009; Huntington, 2006). With the intensification of the hydrological cycle, more evaporation and precipitation will happen, but it is believed that the extra precipitation will not be evenly distributed resulting in changes in the frequency and intensity of extreme events such as storms, flood, and droughts (Huntington, 2006). For example, Déry et al. (2009) used the observed streamflow data of 45 rivers in northern Canada over the period 1964-2007 to provide the observational evidence of an intensifying hydrological cycle in the region. Held and Soden (2006) examined the changes in different aspects of the hydrological cycle based on multiple experiments. The study found different robust responses such as the increase in horizontal moisture transport, reduction in convective mass fluxes, enhancement of the pattern of evaporation minus precipitation and its temporal variance, and the decrease in the horizontal sensible heat transport in the extratropics. The study further reported that these responses were due to the increase in the lower-tropospheric water vapor. Chou et al. (2013) showed that the annual range of precipitation had increased globally, which was attributed to an uneven increase in precipitation. Some parts of

the world may see significant reductions in precipitation or significant alterations in the timing of wet and dry seasons. Based on a statistical analysis of precipitation observations from 1951 to 2011, Singh et al. (2014) found statistically significant decreases in peak-season precipitation and statistically significant increases in the frequency of dry spells and intensity of wet spells during the South Asian monsoon season. The response of snow cover and glaciers to rising temperature is also a significant concern. With the rise in temperature, there is a reduction in the portion of precipitation falling as snow (Arnell, 1999). The northern hemisphere snow cover extent is anticipated to decrease (Mudryk et al., 2017). Marty (2008) found a drastic decrease in the winter snow in Switzerland, which was related to the increase in the mean winter temperature. Using remote sensing based snow products, Huang et al. (2017b) found an increase in snow-covered area (SCA) at elevations below 2000 m a.s.l. and decrease in SCA at altitudes above 2000 m a.s.l in Tibetan Plateau over the period 2001–2014. This has implications for the timing of streamflow in such regions, with a shift from spring snowmelt to winter runoff. In the following section, a review of the literature on impacts of climate change, particularly on water resources and hydrology is presented.

2.2.1 Impact of climate change around the world

Several studies around the world have reported the impact of climate change-induced variability on the hydrologic cycle and water resources. This section reviews some of the global studies.

Arnell (1999) carried out a GCM based analysis of the impact of climate change scenarios on the global water resources using GCMs from the Hadley Centre (HadCM2 and HadCM3) and a macro-scale hydrological model. The study found an increase in the annual runoff in high latitudes and decrease in the same for mid-latitudes. Also, in general, there was a reduction in the share of snowfall in precipitation. The study also highlighted that there were differences in the projections obtained from different models. Milly et al. (2002) studied the risk of great floods under climate change using the streamflow observations and simulations of anthropogenic climate change. The great floods were defined as the floods of flow exceeding the 100-year levels in large scale river basins (i.e., basins having an area greater than 200,000 km^2). The study found a substantial increase in the frequency of great floods over the twentieth century, which were anticipated to further increase in future. Based on the review of literature

on climate change impact on crop productivity, Kang et al. (2009) suggested that water availability might increase in many parts of the world, further affecting the water use efficiency. Based on modelling based studies, it was found that the crop yield was more sensitive to precipitation than temperature. Changes in precipitation patterns and an increase in temperature may significantly affect crop production. Besides, food and environment may also degrade under the changing climate. Abbaspour et al. (2009) developed a hydrological model for Iran using Soil and Water Assessment Tool (SWAT) to assess the impact of climate change on the water resources of the country. Various future scenarios were generated by downscaling a climate model (CGCM 3.1). The model was used to examine the climate change impact on precipitation, blue water, green water, and yield of wheat across the country. The results of the study suggested the wet regions would become more humid, and the dry areas would become drier. On the continent scale, Faramarzi et al. (2013) used SWAT hydrological model along with five GCMs under four emission scenarios to analyze the climate change impact on freshwater availability in Africa. The water availability over Africa was found to increase; however, there was considerable uncertainty associated with the results. On the other hand, the analysis of extremes suggested an increase in droughts and their durations. Based on numerous numerical experiments incorporating the outputs of climate models, water budget and socioeconomic information, Vorosmarty et al. (2014) demonstrated that a large section of the global population was facing water stress. Further, the study found that rising water demands play a more prominent role compared to greenhouse warming in the state of water availability to 2025. The study strongly emphasized that demographic and economic changes over the next 25 years would have a more significant impact on water availability than the mean climate.

The projections of climate change or hydrology are subjected to a lot of uncertainty arising from different sources. To understand the uncertainty associated with multi-model projections of climate change, Dams et al. (2015) used four different hydrological models in a catchment in Belgium. The hydrological models were forced with three separate climate change scenarios. The study found that the structure of the hydrological model induces a considerable uncertainty in the streamflow projections; however, the uncertainty caused by the climate change scenarios was more significant than the hydrological model induced uncertainty. Leng et al. (2015) investigated the climate change impact on different types of droughts in China using bias-corrected out-

puts of GCMs for RCP8.5. The projected scenarios indicated more severe and prolonged droughts in the future. Arnell and Gosling (2016) studied the impact of climate change on global river flood risk using a global hydrological model and 21 climate models. The study also incorporated the population growth in the analysis. The study found a drastic increase in flood risk of different parts of the world, putting millions of people at risk. For example, in one of the scenarios, it was found that the global flood risk would increase by 187% in 2050 relative to the threat without climate change. Kundzewicz et al. (2018) argued that uncertainty plays a vital role in global environmental change research. The study proposed a framework for the assessment of uncertainty, which included the use of ensembles and multi-model probabilistic approaches rather than relying on a single model.

2.2.2 Impact of climate change in the Indian subcontinent

This section presents the review of the literature for the study area of this thesis, i.e., India. Based on the instrumental observations, Thapliyal and Kulshrestha (1991) studied the long term changes in climatic parameters such as rainfall, surface temperature, atmospheric pressure, and total ozone. The study concluded that there was no systematic trend of climate change or ozone depletion in India. Kumar et al. (2006) used a regional climate modelling system (PRECIS – Providing Regional Climates for Impact Studies) for high-resolution climate change projections in India. The model projections indicated an increase in both precipitation and temperature over the 21st century. The west-central regions of the country had the highest growth in precipitation. The study further found that the minimum daily temperature was expected to increase faster than daily maximum temperature. Gosain et al. (2006) used the HadRM2 climate data and the SWAT model to quantify the climate change impact on Indian water resources. The study was carried out for 12 river basins in India, which concluded that the drought might become more severe and floods might become more intense in different parts of the country. Based on the observed data and reanalyzed models, Dash et al. (2007) found that the atmospheric surface temperature in the country increased by about 1°C and 1.1°C during winter and post-monsoon months, respectively. Dash and Hunt (2007) analyzed the meteorological measurements in India and found a trend of increase in temperature. Ghosh et al. (2009) examined the impact of change in the spatial scale of the data on the trends in the Indian summer monsoon. The study pointed out that results found in a coarse resolution previous study (Goswami et al., 2006)

contradicted with the new findings. Utilizing the extreme value theory, Ghosh et al. (2012) examined the trends in observed Indian rainfall extremes. The study found no statistically significant spatially uniform trends for annual maximum rainfall, whereas an increase in the spatial variability of rainfall extremes was found. A basin-scale study (Narsimlu et al., 2013) in Upper Sind River basin, conducted using SWAT hydrological model and PRECIS climate model, found an increase in the annual streamflow for the 21st century. However, the seasonal analysis revealed that though the monsoon season streamflow was found increasing, the non-monsoon season streamflow was found decreasing. Mallya et al. (2015) used multiple drought indices and different datasets to study the drought characteristics of Indian monsoon region over the period 1901-2004. An increasing trend in the drought severity and frequency was found for the period 1972–2004. Based on an integrated approach using hydrological modelling and glacier retreat modeling, Li et al. (2016) investigated the climate change impact on two Himalayan river basins, namely Chamkhar Chhu basin in Bhutan and Beas basin in India. The study utilized two Regional Climate Models (RCMs) along with three different RCPs. The study found a significant warming trend and inconsistent trends for precipitation. The size of glaciers and the availability of water resources was found to decrease in projected climate. Mishra et al. (2016) examined the drought of 2015 in the Indo-Gangetic Plains. The extreme drought event was linked to rainfall deficit in the previous year and reduction in the terrestrial water storage. Mishra and Lilhare (2016) used the downscaled and bias-corrected climate model projections along with SWAT hydrological model to examine the hydrologic changes in 18 major river basins in India. The study found that most of the river basins were shifting towards a warmer and wetter climate in the future. Roxy et al. (2017) presented an analysis of widespread extreme precipitation events in central India along with the driving factors. The study found that despite a decline in other factors, there was a threefold increase in widespread extreme rain events over central India during 1950–2015.

2.3 Resilience analysis

Holling (1973) gave the concept of resilience in the field of ecology. Holling highlighted the difference between resilience and stability in the view of ecosystem behaviour. The stability approach focussed on the equilibrium of the system and maintaining a particular behaviour under different conditions with least alteration in the system's functioning. On the other hand, the resilience approach focuses on domains

of attraction and the need for persistence (Holling, 1973; Peterson et al., 1997). The concept of resilience has been used in different disciplines, including economics, natural resource management, engineering, psychology, sociology, etc. (Folke, 2006; NRC, 2012). Holling (1996) defined two different types of resilience, engineering resilience and ecological resilience. The engineering resilience focuses on the recovery speed of the system, and the ecological resilience focusses on the magnitude of disturbance that can be absorbed by the system before shifting to a new state. Figure 2.1 illustrates engineering and ecological resilience. Engineering resilience is defined based on the system's response to disturbance and its recovery to the same state. It has one equilibrium state. The ability of the system to resist the change under disturbance and to recover quickly defines the resilience of the system. Ecological resilience measures the value of disturbances that the system can withstand without moving into the new state.

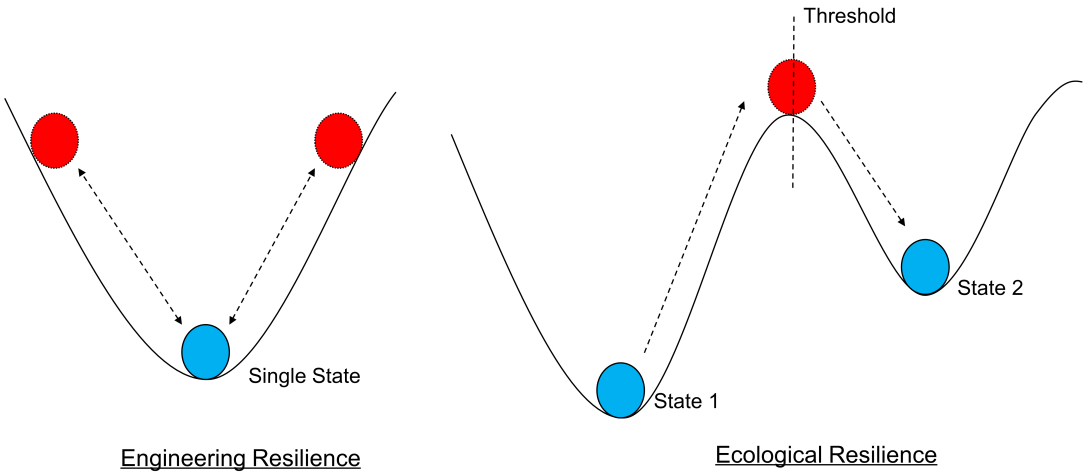

Figure 2.1: Schematic of (a) engineering and (b) ecological resilience. This is a cup and ball representation, in which ball represents the system and the cup/basin represents the state of the system. The blue ball shows the system in its equilibrium state, whereas red ball shows system in disturbed state.

A review of the literature on resilience is presented in the following section:

Hashimoto et al. (1982) discussed three criteria for evaluating the performance of the water resources systems, which included reliability, resiliency, and vulnerability. The study suggested that these three criteria were useful for the choice of water resources projects. Fiering (1982a) emphasized on the concept of resilient water resources system, which was termed as a system that does not respond precipitously to a major surprise during its economic life. The study suggested that stability is not necessarily a desirable characteristic of system performance. Stability does not imply resilience,

which is the ability of a system to accommodate surprise and to survive or even to recover and thrive under unanticipated perturbation. Fiering (1982b) proposed some new indices of resilience, which were based on the time required to pass from one state to another and involve the passage to or from a state defined as failure. Fiering (1982d) used canonical correlation analysis to quantify the linear estimates of the information on the performance of water resource systems. Fiering (1982c) calculated various resilience indices proposed in Fiering (1982b) for several reservoir configurations which constitute a set of sample plans for a river basin. The study found that the indices were useful to assess system performance. Moy et al. (1986) proposed two indices for system performance, namely, system vulnerability and system resilience, for reservoir operations. The system vulnerability was defined as the maximum shortfall from the target, whereas the system resilience was defined as the number of consecutive periods of the deficit during a record. The study found that as the resilience increased with the increase in the reliability, the system's vulnerability to larger deficit also increased.

Bergkamp (1998) studied the resilience of oak-dominated communities in Spain. The hydrological conditions of the system were linked to its resilience through a conceptual model. As an alternative to the computationally intense simulation-based methodology of measuring resilience, Maier et al. (2001) proposed a First-Order Reliability Method (FORM) based method for the computation of different measures such as reliability, vulnerability, and resilience. The proposed method was used in a river basin in the U.S. and was found efficient in computing these measures. Adger et al. (2005) discussed the socio-ecological resilience aspect of coastal disasters. The study suggested that a resilient system should have a different mechanism for withstanding and recovering from any unanticipated disturbances. Gerten et al. (2005) used the resilience concept to examine the capacity of terrestrial ecosystems to water-limited conditions. The analysis utilized a Dynamic Global Vegetation Model (DGVM) and multiple GCMs for projections of Net Primary Production (NPP). The study found heterogeneity in the response of NPP to water-limited conditions.

Li and Lence (2007) stated that in water resources systems, the resilience was defined as a probabilistic measure for examining the risk-cost trade-offs. The study proposed two methods for resilience analysis in the discrete time domain. These methods were based on the bivariate normal distribution and stochastic linear prediction. These methods were robust under different types of problems and were applicable to

both stationary and non-stationary input conditions. Botter et al. (2013) proposed an index for determining the resilience of the flow regime of rivers, which was based on climate and landscape attributes. The index-based assessment found that erratic flow regimes having less discharge were more resilient due to the lesser sensitivity to climate fluctuations. Harder et al. (2015) carried out an analysis of different climatic and hydrological parameters in Marmot Creek Research Basin in Canada to understand the resilient nature of the basin's streamflow despite drastic changes in meteorological conditions and land cover. Ganin et al. (2016) developed quantitative measures to effectively use the engineering resilience concept in different domains such as social, information and physical. The proposed methods include interdependent coupled networks and multi-level directed acyclic graphs.

Based on the annual discharge value of the river, Qi et al. (2016) introduced an index based on a convex model and principle of critical slowing down to examine the change in the resilience of the river. The proposed index was based on the autocorrelation of streamflow at a time. The application of this method in Yellow and Yangtze Rivers revealed that the downstream regions of the river were less resilient compared to the upstream areas. Amarasinghe et al. (2016) proposed three resilience indicators for the assessment of the resilience of water supply system with a case study of the same on the Water Grid system of Queensland State, Australia. The indicators were useful in finding critical conditions for the operation of the system. Similarly, the concept of resilience was used in many other studies to examine the system's response to disturbances (Francis and Bekera, 2014; Peterson et al., 2012; Ponce Campos et al., 2013; Walker and Salt, 2006; Walker et al., 2004).

2.4 Hydrological modelling

A model is a simplified representation of a real-world system (Sharma et al., 2008). The best model is the one which gives results close to reality with the use of least parameters and model complexity (Devi et al., 2015). Models are generally used to predict the behaviour of complex systems such as hydrological systems (Mondal et al., 2016). Models contain typically a set of equations and parameters which represent a different physical process that is modelled. For example, a simple runoff model will have some equations relating the runoff to watershed characteristics and meteorological forcing through a set of parameters (Chow et al., 1988; Devi et al., 2015). The two primary

inputs needed for the hydrological model are precipitation and catchment area (Devi et al., 2015). In addition to these two basic inputs, many other inputs are required to improve the model simulation to achieve better agreement between the model outputs and actual measurements. These inputs include watershed characteristics like soil properties, vegetation cover, watershed topography, soil moisture content, characteristics of the groundwater aquifer. Hydrological models are now considered as an important and necessary tool for water and environment resource management.

Nowadays, many hydrological models are available. There are many different ways these models can be classified. For example, a model can be lumped or distributed based on the spatial distribution of parameters; deterministic or stochastic based on randomness; empirical, conceptual or physically-based based on the structure of the model. Table 2.2 summarized the differences between empirical, conceptual, and physically based models.

Table 2.2: Differences between empirical, conceptual, and physically based models. (Adapted from Devi et al. (2015))

Empirical model	**Conceptual model**	**Physically based model**
Data based or black box model	Parametric or gray box model	Mechanistic or white box model
Less consideration of the processes of the system	Field data and calibration based parameterization	Initial state of model and catchment characteristics are needed
High predictive power, low explanatory depth	Simple and can be easily implemented in computer code	Complex model. Require human expertise and computation capability
Cannot be generated to other catchments	Require large hydrological and meteorological data	Suffer from scale related problem
e.g. ANN, unit hydrograph	e.g. HBV model, TOPMODEL	e.g. SHE or MIKE SHE model, SWAT
Valid within the boundary of a given domain	Calibration involves curve fitting, make difficult physical interpretation	Valid for a wide range of situations

Some of most widely used hydrological models include: Catchment Model (CM), U.S. Department of Agriculture Hydrograph Laboratory Model (USDAHL), HBV model (Hydrologiska Byrans Vattenavdelning model), Physically Based Runoff Production Model (TOPMODEL), Hydrologic Engineering Centre -Hydrological Modelling System (HEC-

HMS), MIKE SHE model (Systeme Hydrologique European), Variable Infiltration Capacity (VIC) Macroscale Model, and Soil Water Assessment Tool (SWAT). SWAT model development team maintains a large database on the SWAT model related peer-reviewed journal articles. The database can be accessed through: https://www.card.iastate.edu/swat_articles/.

2.5 Conclusions from the literature review

There is significant scientific evidence to support the role of anthropogenic activities in climate change. As per IPCC, every place around the globe is facing the impacts of climate change in different ways. The intensification of the hydrological cycle due to the warming of Earth's atmosphere is leading to spatial heterogeneity in the distribution of precipitation. The intensity and frequency of climate extremes, such as droughts and floods, are changing and are getting worse in different parts. India has also faced many hydroclimatic changes in last few decades and is expected to face many such changes in the future.

Literature review revealed that many studies had been carried out in different parts of the country, highlighting the adverse impact of climate change on hydrology or water resources. However, most of the studies focused on the assessment of gradual changes/trends in hydroclimatic variables such as precipitation, streamflow, temperature, etc. or climate extremes. It has been found that the gradual changes in climatic variables do not pose much threat to humans and natural systems as compared to extreme events. Therefore, it becomes imperative to understand the response of natural systems to climate change-induced extreme events. Considering this research gap, this study focuses on the analysis of the response of natural systems (terrestrial ecosystems and hydrological systems) to extremely dry conditions in India.

The concept of resilience, which has found its application in different fields, can be a useful tool to understand the behaviours of natural systems under disturbances. But, so far, the concept has not been used much in the field of hydrology. This study utilizes the resilience concept to examine the behaviour of natural systems.

3

Ecosystem Resilience Analysis at Different Scales

3.1 Introduction

As per IPCC, the global surface temperature will rise and the precipitation regimes around the globe will change substantially under climate change in the 21st century (IPCC, 2014). However, the impacts of climate change are not limited to the atmosphere or hydrosphere, but it also has a profound influence on terrestrial ecosystem's functioning (Dale et al., 2000; Karl and Trenberth, 2003; Meehl and Tebaldi, 2004; Wheeler and Von Braun, 2013). The productivity of terrestrial ecosystems is adversely affected by the hydroclimatic disturbances such as droughts (Breshears et al., 2005; Dale et al., 2000; Thomey et al., 2011; Xu et al., 2017; Zhao and Running, 2010). Terrestrial ecosystems also play an essential role in the global carbon cycle as a major sink for atmospheric CO_2 (Cao and Woodward, 1998; Ciais et al., 1995; Yu et al., 2014). Terrestrial plants take out CO_2 from the atmosphere through photosynthesis along with the loss of water, which regulates the mass-energy exchange between the vegetation and the atmosphere (Keenan et al., 2013). The terrestrial Net Primary Production (NPP) is defined as the difference between the plant photosynthesis and the autotrophic respiration (Roxburgh et al., 2005). NPP is an effective indicator for ecosystem functioning and carbon fluxes from ecological and physiological processes (Cao and Woodward, 1998).

The primary productivity is linked to climatic conditions such as precipitation, temperature, and solar radiation (Running et al., 2004). For example, the increase in NPP during 1982-1999 was attributed to the eased critical climatic constraints on plant

growth (Nemani et al., 2003). Water stress is one of the most important controlling factors, which directly or indirectly constrains vegetation productivity (Mu et al., 2011a). The water loss from the ecosystem can be divided into two parts: 1) 'physiologically productive water' which represents the transpiration during the growing season, and 2) 'non-productive' water loss which includes the water loss from canopy interception and evaporation from bare soil (Sun et al., 2016). These two parts of ecosystem water loss are controlled differently by the climatic factors. The reduction in NPP during 2000-2009 was attributed to the large-scale droughts, which indicated the importance of water as a limiting factor for vegetation productivity (Zhao and Running, 2010). In Europe, the reduction in gross primary productivity was also attributed to the rainfall deficit and extreme summer heat in 2003 (Ciais et al., 2005). Therefore, water stress or drought is seen as one of the significant constraints on the productivity of terrestrial ecosystems or vegetation growth. Ecosystem water use efficiency (WUE_e), defined as the ratio of the rate of carbon uptake and the water loss, indicates the interaction of carbon and water fluxes between the terrestrial ecosystem and atmosphere (Equation 3.1) (Jones, 2004; Niu et al., 2011; Song et al., 2017; Tang et al., 2014).

$$WUE_e = \frac{CarbonUptake}{WaterUsed} \tag{3.1}$$

WUE_e is one of the most critical factors controlling plant productivity in dry environments (Mu et al., 2011a). The hydroclimatic conditions play a crucial role in the spatiotemporal variation of WUE_e by affecting the ecosystem evaporation, transpiration and carbon uptake (Niu et al., 2011; Yang et al., 2016). The spatiotemporal pattern of WUE_e and its environmental controls play an important role in understanding the responses of terrestrial ecosystems to climate change. Several global and regional studies have been carried out around the globe, but there are very few studies in India (Huang et al., 2015, 2016; Song et al., 2017; Tang et al., 2014). The quantification of the patterns of WUE_e is needed to assess the natural and human impacts on terrestrial ecosystems in the country. A better understanding of how WUE_e responds to hydroclimatic changes will provide insight into how carbon and water cycles will change under hydroclimatic alterations caused due to global climate change (Huang et al., 2015).

During the early twenty-first-century drought, the ecosystems in North America

and Australia showed remarkable cross-biome resilience, which was assessed using WUE_e by Ponce Campos et al. (2013). A resilient ecosystem absorbs the disturbances and sustains its productivity by increasing or maintaining WUE_e under water-limited conditions induced by lesser annual precipitation, whereas a non-resilient ecosystem is not able to sustain productivity under such conditions.

In this study, the assessment of ecosystem resilience was carried out on multiple scales (river basin, district, land cover and climate type) in India. Due to the lack of ground measurements, satellite datasets such as terrestrial NPP product (MOD17A3) and Evapotranspiration product (MOD16A3) from the Moderate Resolution Imaging Spectroradiometer (MODIS) were used for spatiotemporal assessment of WUE_e for the period 2000 to 2014. The satellite datasets were utilized due to the unavailability of eddy covariance sites in India. These satellite products have been used in many regional and global studies (Anav et al., 2015; Turner et al., 2006; Xue et al., 2015; Zhao and Running, 2010). The comparative assessment of different river basins is essential for helping to understand how future climate change will affect the carbon and energy budgets in different regions. However, the diversity of responses to disturbances among various ecosystem components play an important role in defining the overall ecosystem resilience (Elmqvist et al., 2003) and hence, the assessment of the contribution of different factors is necessary.

This chapter discusses the methodology developed for the resilience analysis. The developed method is applied at different spatial scales. The results for different scales are presented under different sections, along with the description of the data used and study area.

3.2 Methodology for resilience analysis

Figure 3.1 gives an overview of the methodology developed for the ecosystem resilience analysis.

3.2.1 Computation of WUE_e

The annual WUE_e was computed at pixel level using raster of annual MODIS NPP and ET. First, the pixels corresponding to the valid and non-fill values of NPP and ET were identified and then, WUE_e was computed for every valid pixel to represent its spatial variations within a basin. The average WUE_e was computed as the average for

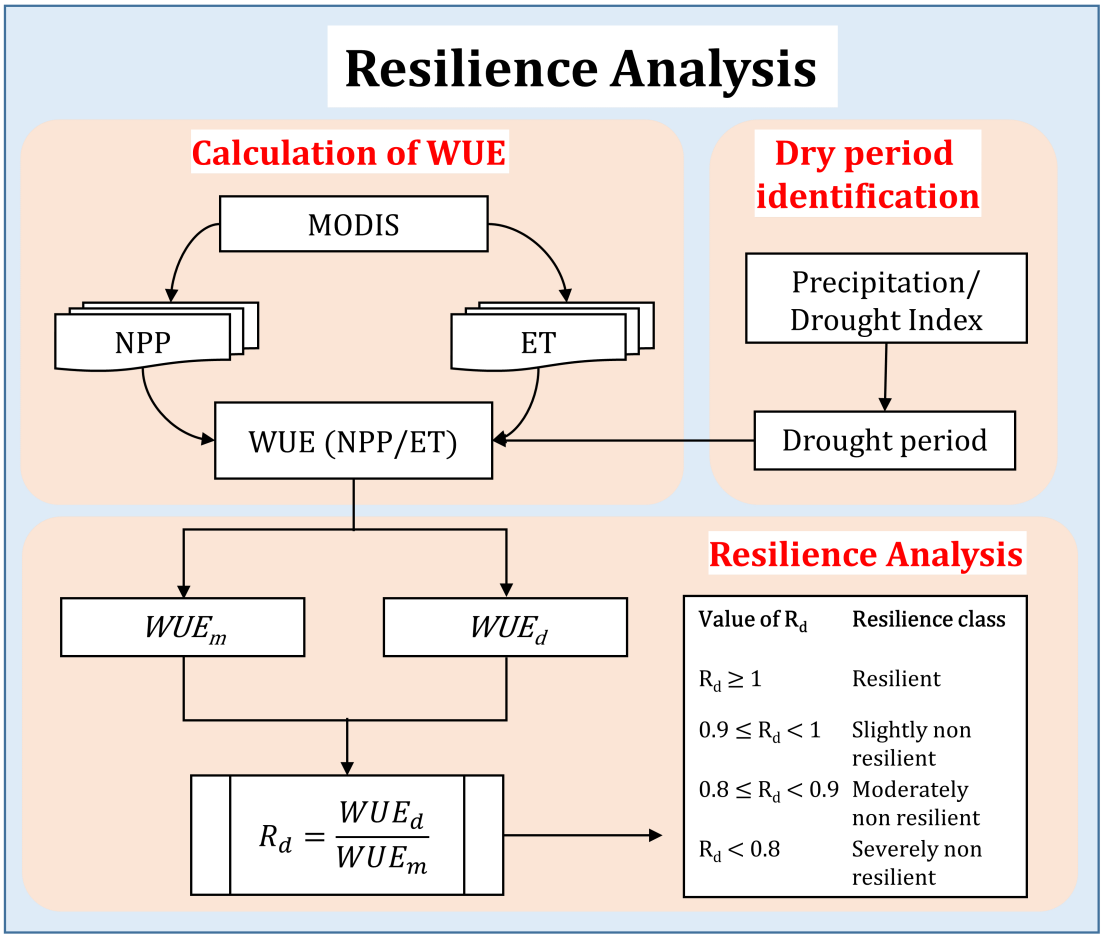

Figure 3.1: Methodology flowchart for ecosystem resilience analysis.

all pixels falling within the basin boundaries. The mean annual WUE_e (denoted as WUE_m) over 15 years (2000-2014) was computed by averaging all rasters of annual WUE_e.

3.2.2 Ecosystem resilience analysis

The ecosystem resilience analysis was carried out using WUE_e as an indicator. WUE_e during the driest year, denoted as WUE_d, in the study duration was compared with the WUE_m for each basin to examine the ecosystem resilience. The driest year was chosen based on the annual precipitation, the Standardized Precipitation Index (SPI) and the Standardized Precipitation Evapotranspiration Index (SPEI) (Mckee et al., 1993; Vicente-Serrano et al., 2010). SPI for the period 2000-2014 was computed based on long-term precipitation series (1901-2015), whereas the SPEI was calculated based on long-term precipitation and temperature series (1951-2014). The negative values of SPI represent dry conditions. As the productivity of resilient ecosystems should not

be affected by the disturbance (i.e., water-limited conditions), the ecosystem that sustains its productivity by increasing or maintaining its WUE_m during the driest year was considered as resilient. The resilience index (R_d) (Equation 3.2) was defined that represents the ratio of WUE_d and WUE_m.

$$R_d = \frac{WUE_d}{WUE_m} \tag{3.2}$$

The dimensionless R_d can be used for comparative assessment of ecosystem resilience of different basins. Different classes were formed based on the value of R_d (Table 3.1). If R_d is greater than or equal to 1, the ecosystem is resilient to disturbances as it sustained its productivity despite the disturbed conditions by increasing the WUE_e. If R_d lies between 0.9 and 1, the basin is termed as slightly non-resilient, as the productivity of the basin is not much affected by the disturbances. If R_d is between 0.8 and 0.9, the basin is termed as moderately non-resilient, and if R_d is less than 0.8, the basin is termed as severely non-resilient.

Table 3.1: Resilience classes based on resilience index (R_d)

Value of R_d	**Resilience class**
$R_d \geq 1$	Resilient
$0.9 \leq R_d < 1$	Slightly non resilient
$0.8 \leq R_d < 0.9$	Moderately non resilient
$R_d < 0.8$	Severely non-resilient

3.2.3 Standardized Precipitation Index

SPI was developed by Mckee et al. (1993), which can be defined on different time scales. The time required for lack of precipitation to generate different type of droughts varies from a week to years. For example, soil moisture conditions (i.e., agricultural drought) respond to precipitation on a short scale, whereas groundwater and reservoir storage deficit respond on a longer scale. SPI is calculated for different time scales like 1, 3, 6, 12, 24 or 48 months. Classification of weather based on SPI values is given in Table 3.2. A drought occurs when the value of SPI is continuously below zero and reaches an intensity of -1.0 or less. The drought ends when SPI value goes above zero. The duration of drought is defined by its beginning and end, and intensity as the value

of SPI. The magnitude of the drought is defined as the positive sum of the SPI values of all the months within the drought duration.

Table 3.2: Weather classification based on SPI

SPI Values	**Weather Class**
>2	Extremely wet
1.5 to 1.99	Very wet
1.0 to 1.49	Moderately wet
-0.99 to 0.99	Near normal
-1.0 to -1.49	Moderately dry
-1.5 to -1.99	Severely dry
<-2	Extremely dry

3.2.3.1 Computation of SPI

SPI is computed by fitting a probability density function to the frequency distribution of the precipitation summed over any time scale of interest. This is performed separately for all the months and all the stations. Each probability distribution is then transformed into a standardized normal distribution.

The probability density function for gamma distribution is defined as (for $x > 0$):

$$g(x) = \frac{1}{\beta^{\alpha}\Gamma(\alpha)} x^{\alpha-1} e^{-x/\beta} \tag{3.3}$$

where $\alpha(0)$ is a shape factor, $\beta(0)$ is a scale factor, and $x > 0$ is precipitation value. $\Gamma(\alpha)$ is the gamma function which is defined as

$$\Gamma(\alpha) = \int_0^{\infty} y^{\alpha-1} e^{-y} dy \tag{3.4}$$

Shape factor and scale factor required for fitting the distribution to the data are obtained using the following equations.

$$\widehat{\alpha} = \frac{1}{4A}\left(1 + \sqrt{1 + \frac{4A}{3}}\right) \tag{3.5}$$

$$\widehat{\beta} = \frac{\bar{x}}{\widehat{\alpha}} \tag{3.6}$$

where $A = \ln(\bar{x}) - \frac{\sum \ln(x)}{n}$ for n observations.

Then, the cumulative probability distribution of precipitation for any time scale is calculated using the following equation

$$G(x) = \int_0^\infty g(x)dx = \frac{1}{\widehat{\beta}^{\widehat{\alpha}}\Gamma\left(\widehat{\alpha}\right)} \int_0^x x^{\widehat{\alpha}-1} e^{-x/\widehat{\beta}} dx \tag{3.7}$$

Substitution t for $x/\widehat{\beta}$ in the above equation, reduces the equation to incomplete gamma function:

$$G(x) = \frac{1}{\Gamma\left(\widehat{\alpha}\right)} \int_0^x t^{\widehat{\alpha}-1} e^{-1} dt \tag{3.8}$$

Gamma function is defined for $x > 0$ but the precipitation records may contain zero values, so the cumulative precipitation function becomes:

$$H(x) = u + (1-u)G(x) \tag{3.9}$$

where u is the probability of the zero value of precipitation.

The cumulative probability function, $H(x)$ is then transformed to the standard normal random variable Z with mean as zero and variance as one using Normal inverse cumulative distribution function. The normal inverse function is defined in terms of the normal cumulative distribution function as:

$$x = F^{-1}\left(\rho|\mu,\sigma\right) = \{x : F(x|\mu,\sigma) = \rho\} \tag{3.10}$$

where,

$$\rho = F\left(x|\mu,\sigma\right) = \frac{1}{\sigma\sqrt{2\pi}} \int_{-\infty}^{x} e^{\frac{-(-t-\mu)^2}{2\sigma^2}} dt \tag{3.11}$$

x is the solution of the equation above for a desired value of probability p. x is SPI Values (Z) and probability p is $H(x)$ obtained from above equation.

Advantages of SPI are (Hayes et al., 1999; Mishra and Desai, 2005):

- It requires only rainfall as input. So, it can be easily used for catchments where other hydro-meteorological parameters are not known.
- It can be computed for different time scales. This property can be used to study a different kind of droughts like meteorological, hydrological and agricultural.
- SPI is not adversely affected by topography.
- As SPI is based on normal distribution, it ensures that the frequencies of extremes at any location and on any time scale are consistent.

3.2.4 Trend analysis

The non-parametric Mann-Kendall (MK) trend test (Mann, 1945; Kendall, 1975) was used for the trend analysis. The MK test has been widely used for the detection of the trend in various hydroclimatic variables (Anghileri et al., 2014; Jain and Kumar, 2012). MK test evaluates the magnitude of change in the time series. The statistical significance of the trend was assessed at a significance level of 0.05. The null hypothesis (H_0) for the test is the absence of any trend in the time series and the alternate hypothesis is that there is the presence of trend (increasing or decreasing) in the time series. Under the null hypothesis, the data are independent and identically distributed.

The test first computes the S statistics as:

$$S = \sum_{k=1}^{n-1} \sum_{j=k+1}^{n} sgn\,(x_j - x_k) \tag{3.12}$$

where n represents the number of observation, x_j is the j^{th} observation, and $sgn(*)$ is the sign function, which is calculated as:

$$sgn\,(x_j - x_k) = \begin{cases} +1 & \text{if } (x_j - x_k) > 0 \\ 0 & \text{if } (x_j - x_k) = 0 \\ -1 & \text{if } (x_j - x_k) < 0 \end{cases} \tag{3.13}$$

The mean and variance of S statistic are given as:

$$E(S) = 0 \tag{3.14}$$

$$var(S) = \frac{n(n-1)(2n+5) - \sum_{p=1}^{m} t_p\,(t_p-1)\,(2t_p+5)}{18} \tag{3.15}$$

where m is the number of tied ranks, each with t_p tied pairs. The Mann Kendall (MK) Z statistic is given by:

$$Z = \begin{cases} \frac{S-1}{\sqrt{var(S)}} & \text{if } S > 0 \\ 0 & \text{if } S = 0 \\ \frac{S+1}{\sqrt{var(S)}} & \text{if } S < 0 \end{cases} \tag{3.16}$$

The positive values of the Z statistic indicate the upwards (increasing) trend in the time series, whereas the negative values indicate the downward (decreasing) trend. When $|Z| > Z_{1-\alpha/2}$, the null hypothesis (H_0) is rejected and a significant trend exists in the time series. The critical value of $Z_{1-\alpha/2}$ for a p-value of 0.05 from the standard normal table is 1.96. Therefore, the value of Z greater than +1.96 indicates a significant increasing trend; on the other hand, the value of Z less than -1.96 indicates the significant decreasing trend. The problem with MK test is that the time series should be serially independent and if there is the presence of autocorrelation in the series, MK test may lead to erroneous rejection of null hypothesis (i.e., Type I error) (Hamed and Rao, 1998). The most common methods applied to deal with auto-correlated time series is to remove the serial correlation by prewhitening. Therefore, in this study, the modified MK test proposed by Hamed and Rao (1998) was used, which accounts for the autocorrelation in the time series. The presence of autocorrelation in the data affects the variance of S statistics of the MK test. The modified method incorporated a revised value of variance based on a theoretical relationship, which was found suitable for the autocorrelated data also. The modified variance calculation is as follows (Hamed and Rao, 1998):

$$var^*(S) = var(S).\left(\frac{n}{n_e^*}\right) = \left(\frac{n(n-1)(2n+5)}{18}\right)\left(\frac{n}{n_e^*}\right) \tag{3.17}$$

where n/n_e^* represents the correlation due to correlation in timeseries and is calculated

as:

$$\frac{n}{n_e^*} = 1 + \left(\frac{2}{n(n-1)(n-2)}\right) \sum_{i=1}^{n-1} (n-f)(n-i-1)(n-i-2)\ \rho_e(i) \tag{3.18}$$

where n is the actual sample size and n^* is the effective sample size required to account for the autocorrelation factor in the data. $\rho(i)$ is the autocorrelation function of the ranks of the observations and can be calculated by the inverse of the following equation (Hamed and Rao, 1998).

$$\rho(i) = 2\ sin\left(\frac{\pi}{6}\ \rho_e(i)\right) \tag{3.19}$$

3.3 River basin scale

3.3.1 Study Area

For this study, river basins in India were defined as per the India-WRIS (Water Resources Information System) report "Watershed Atlas of India" (India-WRIS, 2014). The study was carried out at 22 river basins (Figure 3.2). Table 3.3 shows the watershed details and mean annual precipitation (MAP, mm/year) for different basins. Figure 3.2 shows the location of basins and the spatial distribution of precipitation in India. Ganga Basin (Basin Id. 2a) is the largest basin in terms of the geographical area (8,61,452 km^2) whereas East flowing rivers between the Godavari and Krishna Basin (Basin Id. 16) is the smallest basin (12,289 km^2). West flowing rivers South of Tapi Basin (Basin Id. 14) receives the highest amount of annual rainfall amount of 2755 mm/year due to the presence of Western Ghats. West flowing rivers of Kutch and Saurashtra including Luni Basin (Basin Id. 20), which covers the arid and semi-arid regions of Rajasthan and Gujarat, receives the least mean annual rainfall amount of 560 mm/year.

3.3.2 Data used

3.3.2.1 MODIS NPP

The global annual MOD17A3 products (Version: 055) from the NASA Earth Observation System (EOS) program was used in this study. The global dataset was developed by Numerical Terradynamic Simulation Group (NTSG) at the University of Montana (UMT). MOD17A3 product was generated using the MOD17 algorithm (Running et al.,

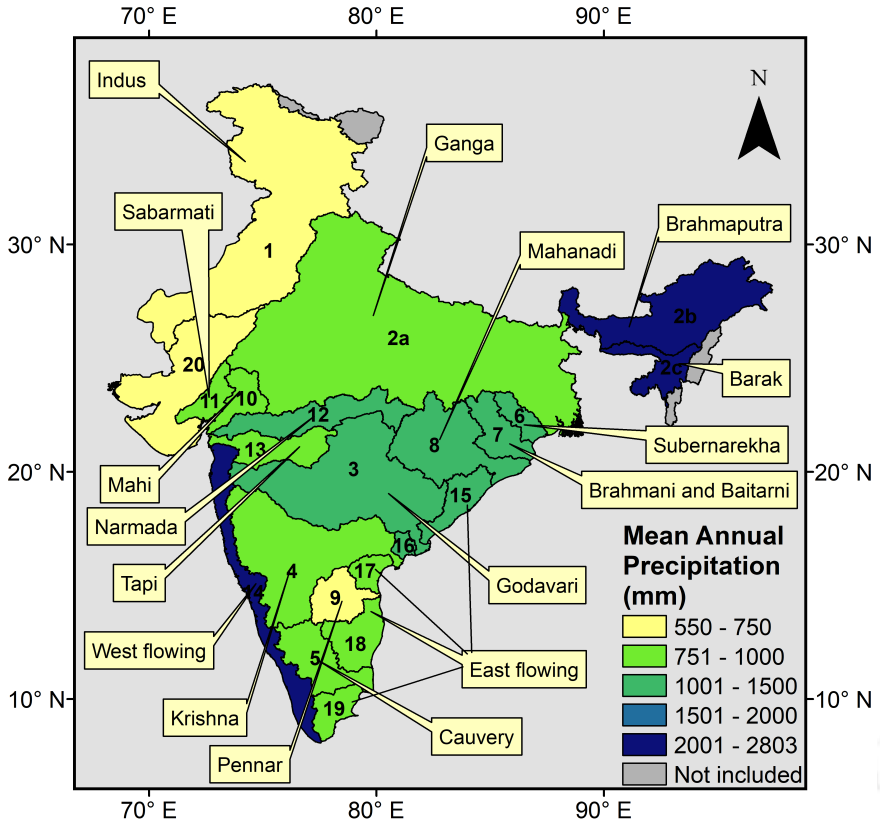

Figure 3.2: The spatial variation in mean annual precipitation (MAP) across different river basins in India.

2004; Zhao et al., 2005). The MOD17 algorithm is based on the radiation use efficiency procedure of Monteith (1972). The algorithm considers that the productivity of vegetation under well-watered and fertilized conditions is linearly related to the amount of Absorbed Photosynthetically Active Radiation (APAR). A conversion efficiency parameter (ϵ) is used to convert APAR to actual productivity estimates. The parameter (ϵ) varies for vegetation types and climate conditions. To calculate NPP, MOD17 also estimates daily leaf and fine root maintenance respiration, annual growth respiration, and annual maintenance respiration of live cells in woody tissue. The MODIS NPP dataset has been validated and used in many studies (Turner et al., 2006; Zhao et al., 2005, 2006). The global MODIS NPP and Gross Primary Productivity (GPP) products showed no overall bias across multiple biomes (Turner et al., 2006). NPP dataset is used in this study for the period 2000-2014 at a spatial resolution of 1 km. There was a significant spatial variation of mean annual MODIS NPP across India (Figure 3.3). Northeastern and Western Ghats regions have higher mean annual NPP (>1500 gC m^{-2}), whereas

Table 3.3: Watershed details and mean annual precipitation (MAP) for different river basins. The river basin definition is as per the India-WRIS report "Watershed Atlas of India" (India-WRIS, 2014).

India-WRIS Basin Id	Basin Name	Watershed area (km^2)	MAP (mm/year)
1	Indus (Up to border) Basin	453929	643
2a	Ganga Basin	861452	990
2b	Brahmaputra Basin	194413	2291
2c	Barak and others Basin	41723	2658
3	Godavari Basin	312812	1109
4	Krishna Basin	258948	832
5	Cauvery Basin	81155	989
6	Subernarekha Basin	29196	1426
7	Brahmani and Baitarni Basin	51822	1480
8	Mahanadi Basin	141589	1342
9	Pennar Basin	55213	741
10	Mahi Basin	34842	868
11	Sabarmati Basin	21674	802
12	Narmada Basin	98796	1032
13	Tapi Basin	65145	829
14	West flowing rivers South of Tapi Basin	112117	2756
15	East flowing rivers between Mahanadi and Godavari Basin	49685	1242
16	East flowing rivers between Godavari and Krishna Basin	12289	1101
17	East flowing rivers between Krishna and Pennar Basin	24669	926
18	East flowing rivers between Pennar and Cauvery Basin	65049	984
19	East flowing rivers South of Cauvery Basin	35090	942
20	West flowing rivers of Kutch and Saurashtra including Luni Basin	321851	561

the arid areas of western India have the least NPP.

3.3.2.2 MODIS ET

The evapotranspiration data from the global annual MOD16A3 product from the NASA EOS program was used in this study. The dataset is available at same resolution from as MODIS NPP for the period from 2000 to 2014 (available from http://ntsg.

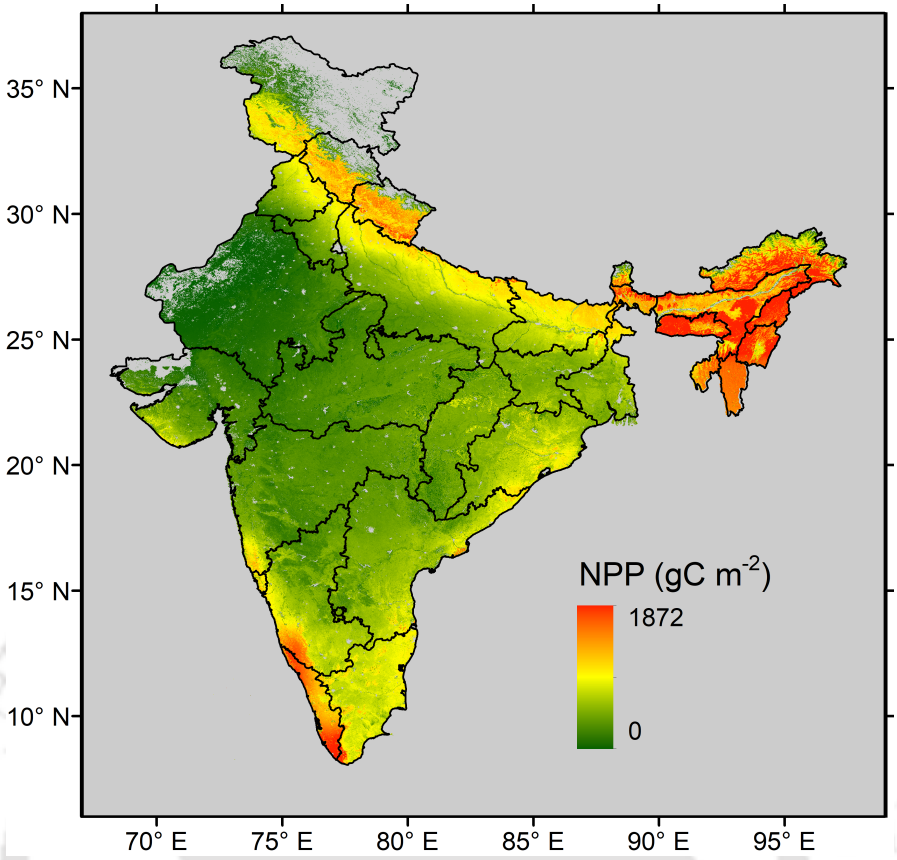

Figure 3.3: Spatial distribution of mean annual MODIS NPP in India over 2000-2014. The background is the administrative map of India.

umt.edu/project/mod16). MOD16 algorithm is based on the improved ET algorithm of Mu et al. (2011b), which uses the Penman-Monteith equation (Mu et al., 2007, 2011a, 2013). ET includes evaporation from wet and moist soil, from rainwater intercepted by the canopy before it reaches the ground, and the transpiration through stomata on plant leaves and stems. The remote sensing data from MODIS provides input for surface biophysical variables affecting ET, including albedo, biome type, and Leaf Area Index (LAI). The detailed algorithm of MOD16 is available at http://www.ntsg.umt.edu/project/modis/mod16.php. This global ET product was validated by Mu et al. (2011b) using 46 eddy flux towers dataset and it was found that the dataset can be used to estimate actual ET with satisfactory accuracy in Asia. Previous studies in India used MOD16 ET as an estimate of actual ET (e.g. Shah and Mishra (2016)). Like MODIS NPP, there was substantial variation in mean annual ET across India (Figure 3.4).

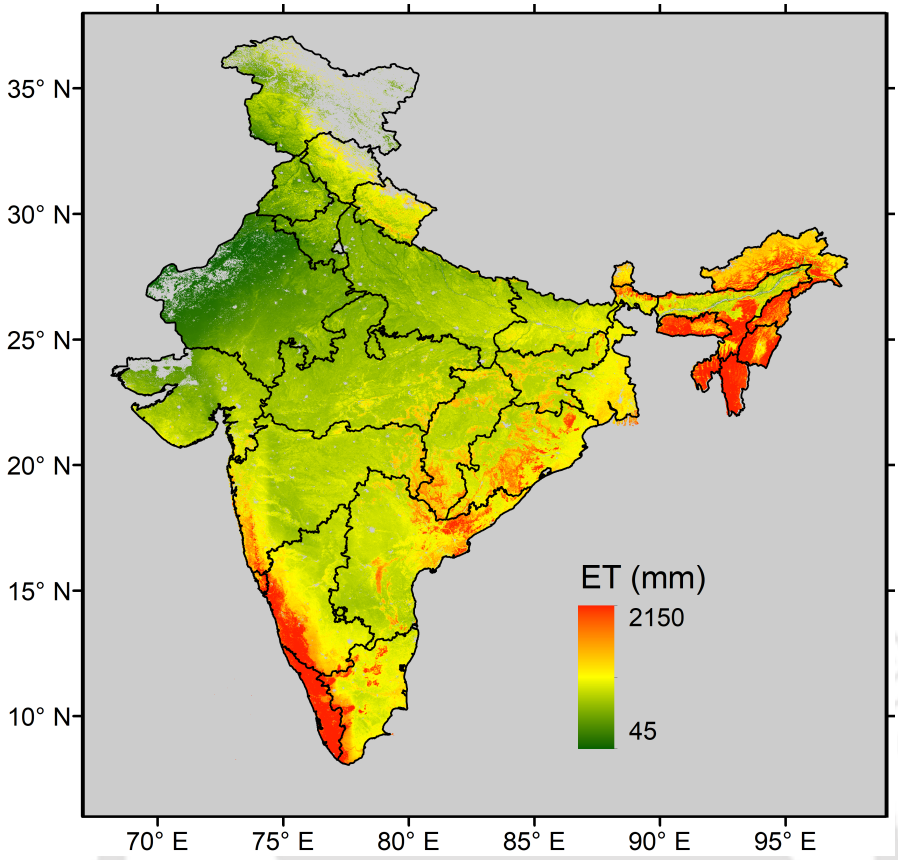

Figure 3.4: Spatial distribution of mean annual MODIS ET in India over 2000-2014. The background is the administrative map of India.

3.3.2.3 Koppen-Geiger climate classification

The Koppen-Geiger climate classification maps were prepared based on recent data sets from the Climatic Research Unit (CRU) of the University of East Anglia and the Global Precipitation Climatology Centre (GPCC) at the German Weather Service (Kottek et al., 2006; Rubel and Kottek, 2010) (available from http://koeppen-geiger.vu-wien.ac.at/present.htm). India has a diverse spatial distribution of different climate types (Peel et al., 2007). Figure 3.5 shows the spatial distribution of Koppen-Geiger climate classes in India, which was derived from Kottek et al. (2006). Southern parts of the country have tropical (A) climate, north-western parts have dry (B) climate, northern and north-eastern parts have temperate climate (C) and Himalayan regions have polar climate (E). Out of thirty-one different climate types identified in India by Kottek et al. (2006), only climate types having spatial coverage over more than 2.5% of the total geographical area of the country were considered in this study.

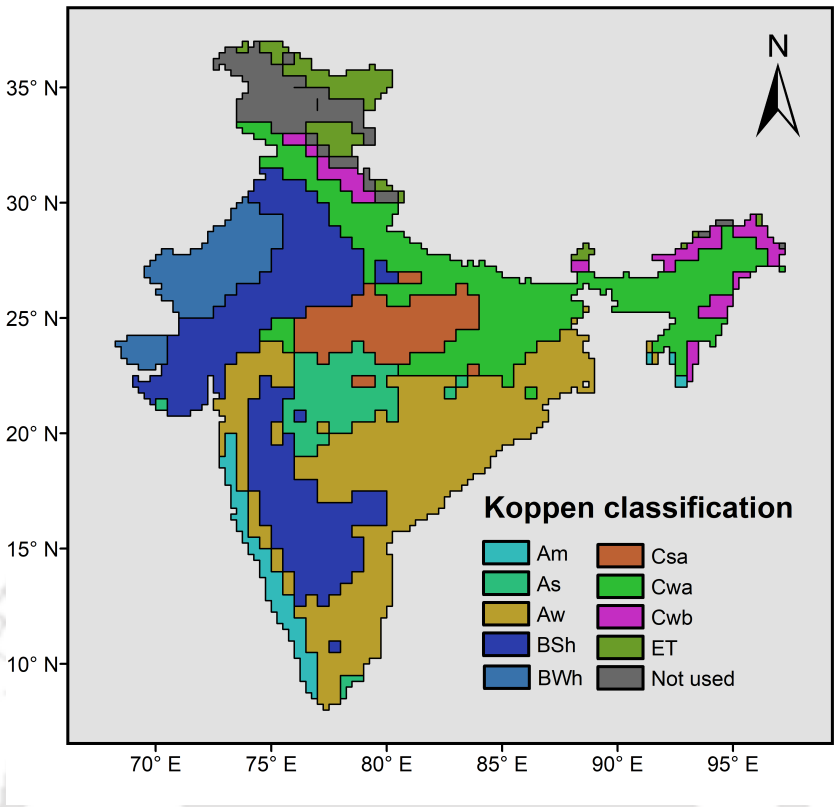

Figure 3.5: Koppen-Geiger climate classification for India.

3.3.2.4 Land cover classification

Different vegetation types differ in carbon uptake and water consumption, leading to the differences in WUE_e. The land cover classification used in this study is based on 10 years (2001-2010) of Collection 5.1 MCD12Q1 land cover type data and was obtained from the USGS Land Cover Institute (Broxton et al., 2014). Figure 3.6 shows the spatial distribution of different land cover types in India. Croplands (CR) is the most dominant land cover type in India, covering about 50% of the total geographical area. This dataset has 17 different classes of land cover types.

3.3.2.5 Meteorological data

Daily gridded rainfall dataset (IMD4) from the Indian Meteorological Department (IMD) at a high spatial resolution (0.25° × 0.25°) was used in this study (Pai et al., 2014). The dataset is prepared from daily rainfall records from 6955 rain gauge stations in India and is available from 1901 to 2015. The total annual precipitation (sum of daily precipitation, mm/year) and MAP (mean of annual precipitation, mm/year) at same resolution were computed from daily values.

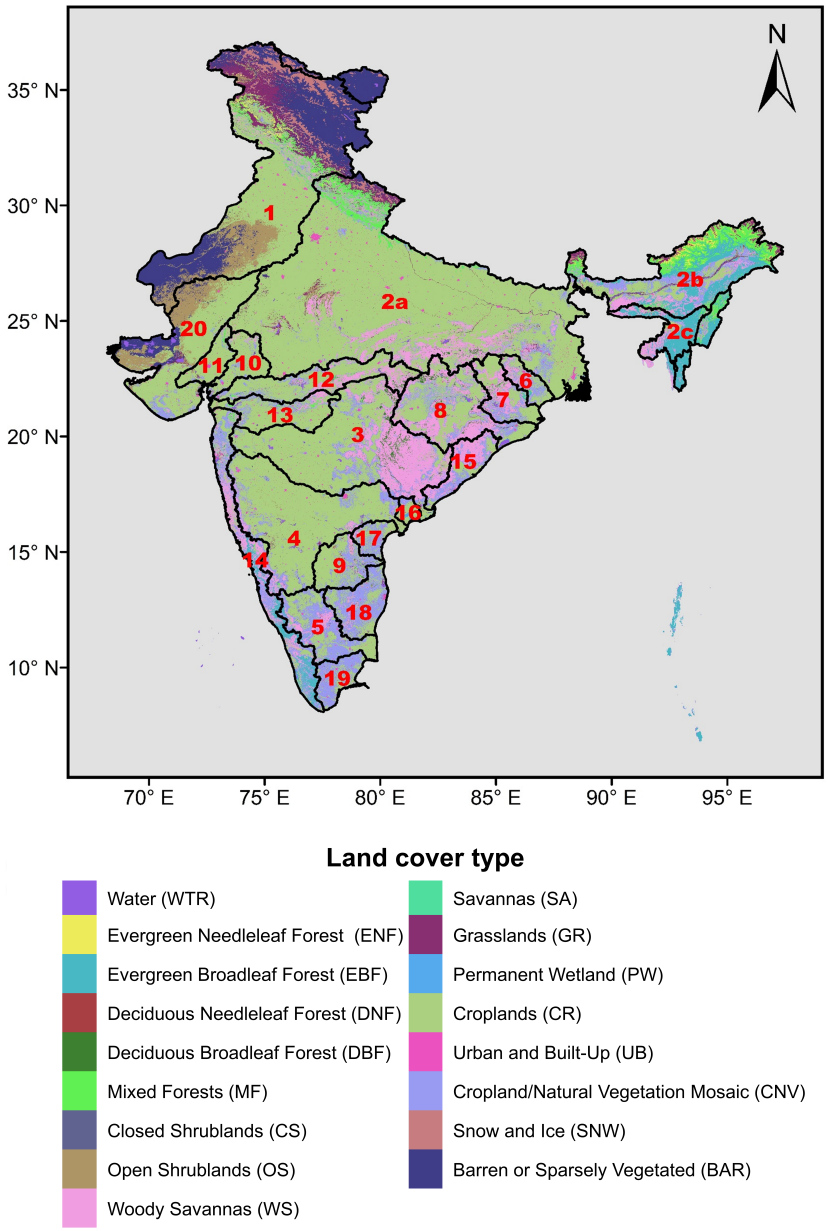

Figure 3.6: Land cover types in India.

3.3.3 Results and discussion

3.3.3.1 Basin scale WUE_e

The mean annual WUE_e (denoted as WUE_m) showed considerable spatial variations over India due to different climate, soils and vegetation types. Figure 3.7 show the WUE_m and standard deviation (STD) for different river basins in India. There was a significant difference, $F(21,308) = 127.35$, p-value < 0.01 (ANOVA), in WUE_m across basins. The basins in the northeastern parts of the country had higher WUE_m followed

by northern, eastern, southern, and western regions, respectively (Figure 3.7a). The spatial variation in WUE_m is closely related to the variations in the mean annual precipitation (see Figure 3.2) and NPP (see Figure 3.3). WUE_m for Brahmaputra basin (Basin Id. 2b, WUE_m = 1.111 gC m^{-2} mm^{-1}) in the northeastern regions was significantly higher (p-value < 0.01) than for other basins, whereas Mahi basin (Basin Id. 10) in the western region had the least WUE_m (= 0.249 gC m^{-2} mm^{-1}). The standard deviation (STD, Figure 3.7b) of the pixel values of WUE_m was highest for the Indus basin (Basin Id. 1), followed by Ganga (Basin Id. 2a) and Brahmaputra basins (Basin Id. 2b), respectively, due to larger geographical areas and presence of different climate and vegetation types in the basins. STD was less than 0.2 gC m^{-2} mm^{-1} for all other basins, indicating lesser spatial variations within the basins.

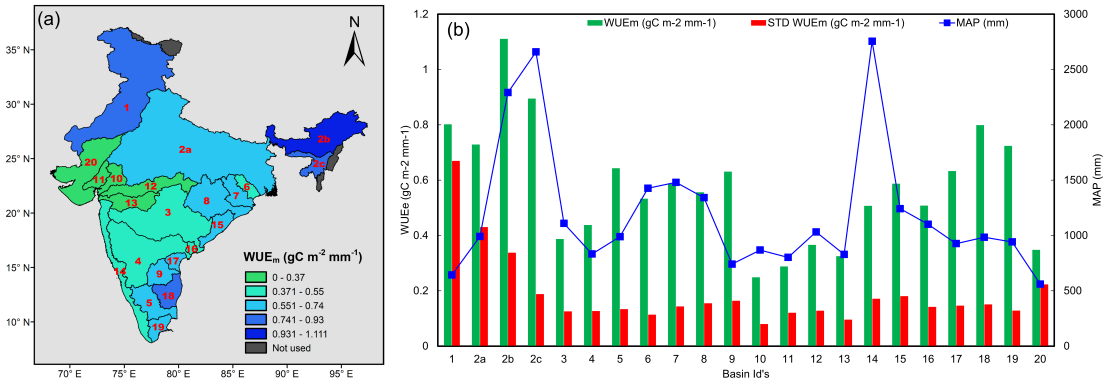

Figure 3.7: Mean annual ecosystem water use efficiency (WUE_e = NPP/ET) across different basins in India over 2000–2014. Spatial distribution of WUE_m across basins (a) and variation in mean and standard deviation (STD) of WUE_m (b). MAP is the mean annual precipitation (mm/year) of the basin.

3.3.3.2 Land cover scale WUE_m

Different vegetation types differ in carbon uptake and water consumption, leading to the differences in WUE_m. Figure 3.8 shows the WUE_m for major land cover types. Forest classes had higher WUE_m compared to other vegetation types, which was consistent with the global studies (Tang et al., 2014). The highest WUE_m(= 1.087 gC m^{-2} mm^{-1}) was found for Mixed Forests (MF), followed by Deciduous Needleleaf Forest (DNF, WUE_m = 1.001 gC m^{-2} mm^{-1}), Evergreen Needleleaf Forest (ENF, WUE_m = 0.959 gC m^{-2} mm^{-1}) and Evergreen Broadleaf Forest (EBF, WUE_m = 0.948 gC m^{-2} mm^{-1}). In contrast to other forest types, Deciduous Broadleaf Forest (DBF) had much smaller WUE_m (= 0.416 gC m^{-2} mm^{-1}); however, DBF accounts for only 0.56% area in the country. All non-forest land covers had WUE_m less than 0.7 gC m^{-2} mm^{-1}.

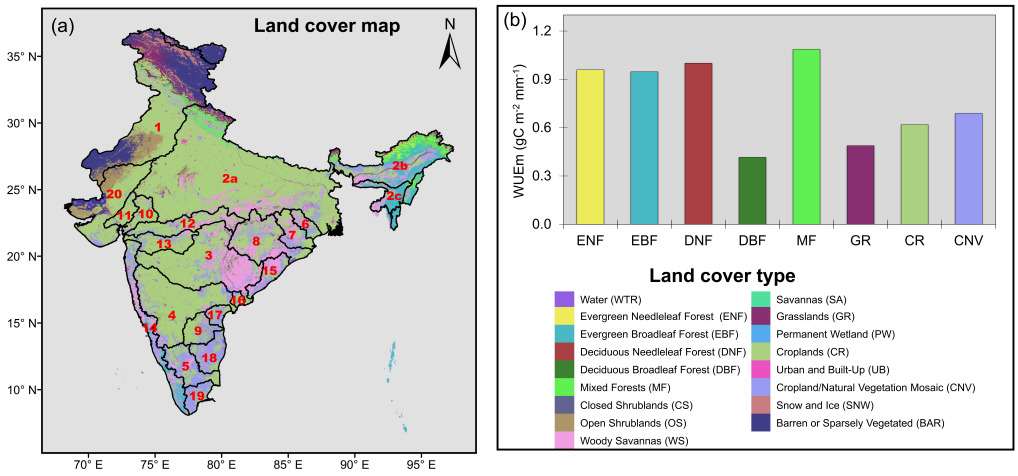

Figure 3.8: Mean annual ecosystem water use efficiency (WUE_m) of different land cover types in India. Annual ecosystem water use efficiency (WUE_e = NPP/ET) was computed using MODIS NPP and ET products over 2000–2014.

3.3.3.3 Climate type scale WUE_m

India has a diverse spatial distribution of different climate types (Peel et al., 2007). Temperate climate types, Cwa and Cwb, had highest WUE_m of 1.055 gC m^{-2} mm^{-1} and 1.009 gC m^{-2} mm^{-1}, respectively, followed by equatorial and arid climates (Figure 3.9), which was consistent with global studies (Xia et al., 2015). Arid climates, BWh and BSh, had least WUE_m of 0.175 gC m^{-2} mm^{-1} and 0.475 gC m^{-2} mm^{-1}, respectively.

3.3.3.4 Ecosystem resilience analysis at the river basin scale

Table 3.4 shows the results of the ecosystem resilience analysis of different river basins. The table shows the computation of R_d, which indicates the degree to which an ecosystem is resilient to the droughts. Higher the value of R_d, higher the resilience of the ecosystem. The results of this study found that only six basins (Basin Ids. 1, 2b, 9, 17, 18, and 20) out of 22 river basins were resilient to droughts in the study duration (Figure 3.10). Indus basin (Basin Id. 1) had the highest R_d, which indicated that the ecosystems in this basin sustained their productivity by increasing the WUE_e under water-limited conditions. The value of R_d for Brahmaputra basin (Basin Id. 2b) was slightly above 1, indicating the resilient characteristics of ecosystems in the basin. Basin Id. 20, which had low WUE_m (= 0.348 gC m^{-2} mm^{-1}) and located in arid and semi-arid regions of Rajasthan and Gujarat, was also found resilient (R_d = 1.189). The ecosystems in arid regions are habituated to the water-limited conditions due to frequent droughts and hence, have an inherent resilience to such conditions. Also, three

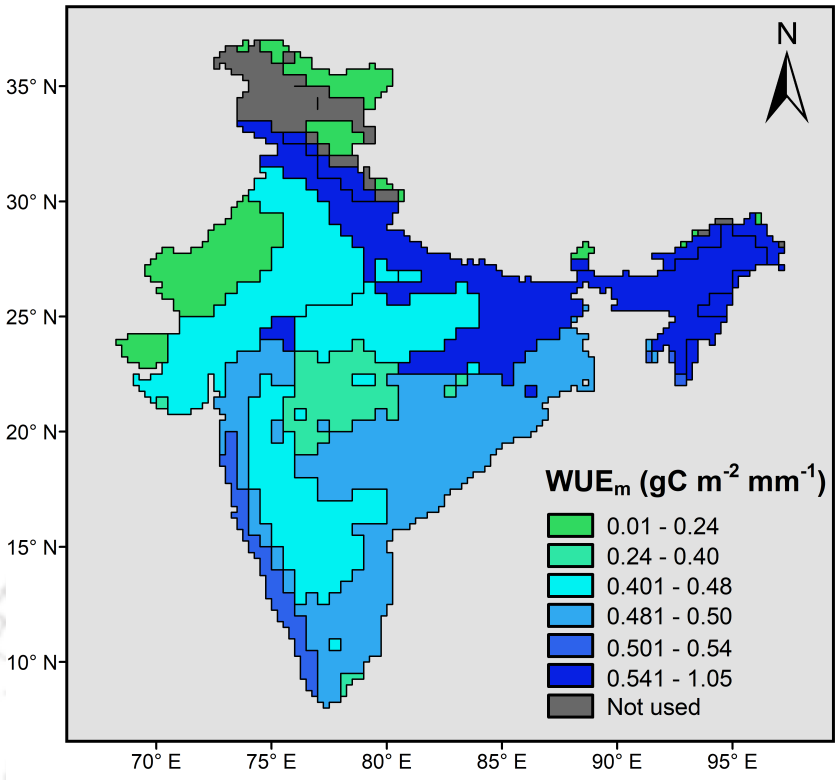

Figure 3.9: Mean annual ecosystem water use efficiency (WUE$_m$) for different climate types in India. Climate classes with an area less than 2.5% of the total area were not used in this study.

basins along coastal south India (Basins Ids. 9, 17 and 18) were also found resilient. Seven basins, including the Ganga basin (Basin Id. 2a), the largest and most populous basin, were found slightly non-resilient ($0.9 \leq R_d < 1$). The basins along the Western Ghats (Basin Id. 14), which are generally water surplus because of high annual rainfall, failed to maintain their WUE$_e$ during the driest year. Three basins (Basin Ids. 4, 8 and 16) were found moderately non-resilient ($0.8 \leq R_d < 0.9$). Ecosystems in the central and eastern regions of the country were least resilient to dry conditions as R_d was less than 0.8 for all the basins in the region. Among all basins, the Mahi basin (Basin Id. 10) had the highest degree of non-resilience ($R_d = 0.592$).

3.3.3.5 Ecosystem resilience analysis at land cover scale

The ecosystem resilience analysis for the dominant land cover types was carried out to understand the factors controlling the ecosystem resilience at the basin scale. Table 3.5 shows the ecosystem resilience analysis at land cover scale. Only evergreen forests (ENF and EBF) were found resilient (i.e., $R_d \geq 1$), which partially explains the

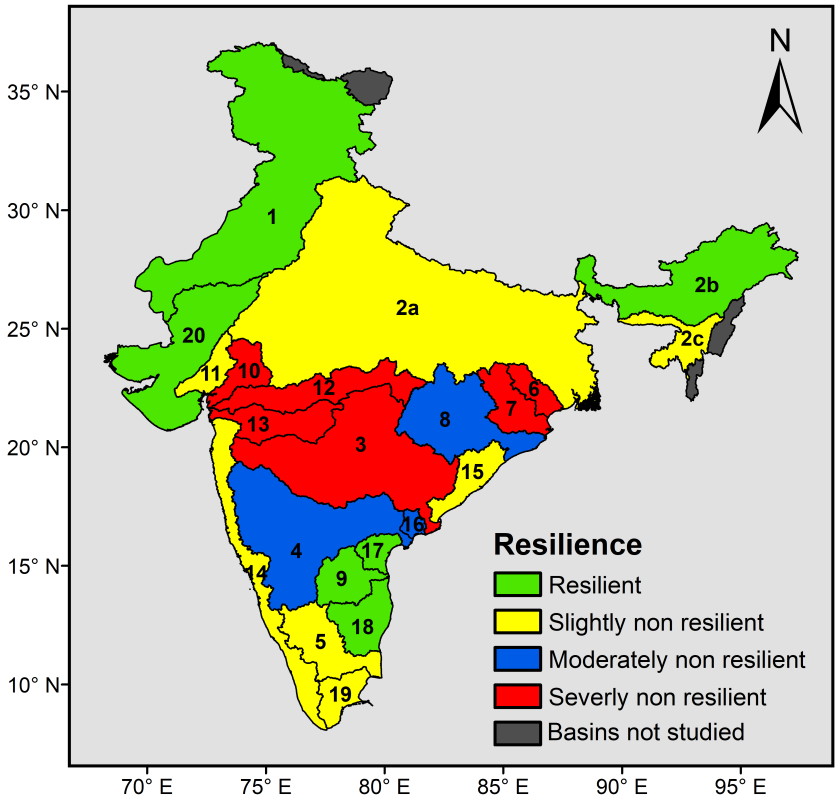

Figure 3.10: Ecosystem resilience of different river basins in India.

resilience of forest dominated Brahmaputra basins (Basin Id. 2b). Deciduous Broadleaf Forest (DBF), which had least WUE_m among forest covers, was the least resilient (R_d = 0.70). WUE_e for Grasslands (GR), the most sensitive biome to water availability, decreased slightly for the driest year (R_d = 0.98). Croplands (CR and CNV), the most significant land cover in India, had similar behaviour as GR under dry conditions. The ecosystem resilience of Ganga basin (Basin Id. 2a) is consistent with the presence of vast croplands.

3.3.3.6 Ecosystem resilience analysis at climate type scale

Ecosystem resilience analysis of different climate types indicated that only three climate types, namely Csa, Cwb and ET, were resilient to hydroclimatic disturbances during the study duration (Table 3.6). Csa was found the most resilient (R_d = 1.060). The ecosystem productivity of BWh climate type was most affected by the dry conditions (R_d = 0.627).

Table 3.4: Ecosystem resilience analysis at the basin scale. SPI6 and SPEI6 represent the six-month standardized precipitation index and standardized precipitation evapotranspiration index.

Basin Id.	**WUE$_m$**	**Driest year**	**Mean SPI6 for the driest year**	**Mean SPEI6 for the driest year**	**Precipitation in the driest year (mm)**	**WUE$_d$**	**R_d**	**Resilient (R_d >1)**
1*	0.802	2002	− 0.89	− 1.2	466	1.055	1.315	TRUE
2a	0.729	2009	− 2.09	− 1.02	812	0.67	0.92	FALSE
2b*	1.111	2001	− 1.32	− 0.71	1982	1.115	1.004	TRUE
2c	0.895	2006	− 1.25	− 0.73	1741	0.845	0.944	FALSE
3	0.387	2009	− 1.39	− 1.37	861	0.277	0.716	FALSE
4	0.438	2003	− 1.37	− 1.09	554	0.373	0.851	FALSE
5	0.643	2002	− 2.79	− 1.69	488	0.635	0.988	FALSE
6	0.533	2010	− 1.73	− 0.9	891	0.37	0.695	FALSE
7	0.586	2010	− 1.51	− 1.5	1081	0.449	0.766	FALSE
8	0.556	2000	− 1.3	− 0.59	888	0.493	0.887	FALSE
9*	0.631	2014	− 0.87	− 0.75	490	0.715	1.134	TRUE
10	0.249	2000	− 0.88	− 0.92	454	0.147	0.592	FALSE
11	0.288	2002	− 1.15	− 1.18	382	0.283	0.982	FALSE
12	0.366	2000	− 0.99	− 0.47	681	0.236	0.643	FALSE
13	0.325	2000	− 0.55	− 0.32	563	0.203	0.624	FALSE
14	0.507	2002	− 1.2	− 0.59	2220	0.487	0.961	FALSE
15	0.587	2002	− 0.47	− 0.98	911	0.533	0.909	FALSE
16	0.508	2002	− 0.96	− 0.59	697	0.438	0.862	FALSE
17*	0.633	2014	− 0.7	− 0.98	582	0.792	1.25	TRUE
18*	0.799	2002	− 2.2	− 1.52	464	0.844	1.056	TRUE
19	0.724	2003	− 2.4	− 1.94	312	0.7	0.968	FALSE
20*	0.348	2002	− 0.92	− 1.08	232	0.414	1.189	TRUE

* represents the resilient (WUE$_d \geq$ WUE$_m$) basins.

3.3.3.7 Relation between WUE$_e$ at different scales

Water is the most critical limiting factor for primary productivity in India (Running et al., 2004). Addition of water due to high precipitation will simulate the primary productivity more than the ET, leading to an increase in WUE$_e$. Figure 3.7 shows that Brahmaputra basin (Basin Id. 2b) had the highest WUE$_m$ (= 1.111 gC m^{-2} mm^{-1}), which can mainly be attributed to the present of forests in the basin (Figure 3.6), as forest classes had higher WUE$_m$ compared to other land cover types (Figure 3.8). Among all river basins, the Brahmaputra basin has a large forest cover. EBF and MF, respectively, covers about 24.45% and 21.82% of the area in the Brahmaputra basin, with total forest cover approximately 50% of the basin area. Similar to Brahmaputra basin,

Table 3.5: Ecosystem resilience analysis at land cover scale.

Land cover type	**WUE$_m$**	**Driest year**	**Precipitation in the driest year (mm)**	**WUE$_d$**	**R_d**	**Resilient**
Evergreen Needleleaf Forest (ENF)*	0.959	2001	1612	0.99	1.03	TRUE
Evergreen Broadleaf Forest (EBF)*	0.948	2012	1934	0.951	1	TRUE
Deciduous Broadleaf Forest (DBF)	0.416	2002	983	0.29	0.7	FALSE
Mixed Forests (MF)	1.087	2012	1440	1.034	0.95	FALSE
Grasslands (GR)	0.488	2009	1030	0.478	0.98	FALSE
Croplands (CR)	0.619	2002	743	0.609	0.98	FALSE
Cropland/Natural Vegetation Mosaic (CNV)	0.689	2002	1008	0.671	0.97	FALSE

* represents the resilient (WUE$_d \geq$ WUE$_m$) land covers.

Table 3.6: Ecosystem resilience analysis at Koppen-Geiger climate type scale.

Climate Type	**Percent Area (%)**	**WUE$_m$**	**Driest year**	**Precipitation in the driest year (mm)**	**WUE$_d$**	**R_d**	**Resilient**
Am	2.99	0.535	2002	1930.38	0.513	0.958	FALSE
As	5.51	0.4	2000	787.19	0.261	0.653	FALSE
Aw	25.88	0.504	2002	892.21	0.425	0.844	FALSE
BWh	6.48	0.175	2002	95.21	0.11	0.627	FALSE
BSh	21.45	0.475	2002	440.07	0.429	0.903	FALSE
Csa*	6.63	0.476	2007	692.14	0.505	1.06	TRUE
Cwa	19.32	1.055	2009	1257.54	1.041	0.987	FALSE
Cwb*	3.16	1.009	2001	1515.1	1.027	1.018	TRUE
ET*	3.29	0.242	2014	545.71	0.257	1.06	TRUE

* represents the resilient (WUE$_d \geq$ WUE$_m$) climate types.

neighboring Barak and other basins (Basin Id. 2c) also have large forest cover about 60.81% of the basin area and therefore, have higher WUE$_m$. On the other hand, Mahi basin (Basin Id. 10) has the least WUE$_m$ (= 0.249 gC m^{-2} mm^{-1}) due to the absence of forest area (<1%), where cropland covers about 83% of basin area (Figure 3.6). The basin had least WUE$_m$ due to the low productivity and high ratio of evaporation to ET associated with sparse vegetation. It should be noted that Brahmaputra basin has one of the highest mean annual precipitation (MAP), whereas the Mahi basin has much

smaller MAP (Figure 3.8), which shows the dependence of WUE_m on precipitation. In contrast to the good correlation between WUE_m and MAP for different basins, the west flowing rivers South of Tapi Basin (Basin Id. 14) had the highest MAP but lesser WUE_m (= 0.507 gC m^{-2} mm^{-1}). Basin Id. 18 had relatively higher WUE_m (= 0.799 gC m^{-2} mm^{-1}) compared to other basins in southern regions due to the significant presence of CNV. The moderate WUE_m (= 0.802 gC m^{-2} mm^{-1}) of Indus basin (Basin Id. 1) was due to the presence of forests in lower Himalayan regions.

Due to different patterns of eco-hydrological process among different vegetation types, the land cover type was one of the major factor controlling the WUE_m at the basin scale. In addition to vegetation types, the hydroclimatic conditions also control the ecological and hydrological process such as evapotranspiration, plant respiration etc. For the Indian region, Cwa and Cwb climate types had the highest WUE_m. These climate types are mainly present in the Brahmaputra basin (Basin Id. 2b), which had the highest WUE_m. On the other hand, the arid climate types (i.e., BWh and BSh) had least WUE_m, which was consistent with the lesser WUE_m of basins (Basin Ids. 10, 11, 12, 13 and 20) in the western regions.

3.3.3.8 Relation between ecosystem resilience at different scales

The primary productivity of the ecosystems is affected differently by the hydroclimatic conditions at different scales because the response of the ecosystems at different scales is controlled by different ecohydrological processes. For example, in arid regions, the productivity is controlled by the water availability, whereas in mountain regions solar radiation is the controlling factor. The resilience of an ecosystem to the disturbance represents the cross-biome capability to tolerate the disturbed conditions (Ponce Campos et al., 2013). For Indian conditions, the primary climatic control on the vegetation productivity is the water availability or precipitation (Running et al., 2004) A decrease (increase) in water availability to the vegetation will result in lower (higher) primary productivity. This study evaluated the ecosystem resilience in terms of the capability of an ecosystem to maintain its productivity during the drought period (i.e., water-limited conditions). The results show that only 6 (out of 22) river basins were able to sustain their primary productivity by increasing the WUE_e under driest year. As the ecosystem response to the hydroclimatic changes is driven by the dominant species, the ecosystem resilience of a basin was related to the land cover types and climate types present in the

basin. The land cover scale ecosystem resilience analysis indicated that only two forest classes (ENF and EBF) were resilient during the study duration. The presence of these biomes in the Brahmaputra basin could be the reason for the resilient characteristics of the basin. Also, Brahmaputra basin has Cwa and Cwb climate types, which were found resilient. A dynamic vegetation modelling based study on Indian forests also found that the northeastern forests were resilient to climatic changes (Chaturvedi et al., 2011).

The least resilient basins include Basin Ids. 3, 6, 7, 10, 12 and 13, which are mainly located in central India. CR and Woody Savannas (WS) are the dominant land cover types in these regions; whereas Aw, As and BSh are the dominant climate types. These land cover or climate types were not-resilient, which had resulted in non-resilient characteristics of central India. Forests in some parts of the Western Ghats and central India were found more vulnerable (least resilient) to climate change (Chaturvedi et al., 2011), which was consistent with results of the present study. Ganga basin, the most populous and agriculturally important basin, (Basin Id. 2a) was also found slightly non-resilient (R_d = 0.920). CR is the most dominant land cover type in the basin, and Csa, Aw and Cwa are the major climate types. Though Csa was found resilient, the contribution from other climate types has resulted in overall non-resilient characteristics of the basin. The anthropogenic factors such as population growth, deforestation, agricultural activities, urbanization and construction activities have deteriorated the ecology in the basin (Sarkar et al., 2003), which could be the possible reason behind the non-resilient characteristics of the basin. Aw climate type, the most dominant climate in the eastern and southern regions, was found moderately non-resilient (R_d = 0.844), which was also consistent with basins falling in these regions except for Basin Ids. 9, 17, and 18. Climate type 'As', mainly limited to the central parts, was found severely non-resilient (R_d = 0.653) and was consistent with basins in central parts (Basin Ids. 3, 12 and 13). The non-resilient characteristics of the ecosystem in these basins were consistent with the higher vulnerability of forests in the region to climate change (Chaturvedi et al., 2011). Ecosystems in arid climate were found non-resilient, which was consistent with the Krishna basin (Basin Id. 4). On the other hand, Basin Id. 20 was found resilient, which was inconsistent with the presence of arid climates. Though land cover and climate type were related to the ecosystem resilience of some basins, the ecosystem response in other basins cannot be entirely related to these two factors due to substantial ecohydrological variations within the basins.

3.4 District scale

3.4.1 Study area

The study area for this analysis was districts and states in India (Figure 3.11). Districts represent the administrative divisions within the states in the country. There are a total of 29 states and 7 union territories (UTs) in India. Out of these, a total of 30 states and UTs were considered for this study, which includes all states and one UT, namely Delhi. As per 2011 Census of India, there are a total of 640 districts. 634 districts were considered leaving those having no valid pixels of MODIS NPP and ET raster and those on islands. There is a considerable variation in the area of districts ranging from 9 km^2 (Mahe in the state of Puducherry) and 45,652 km^2 (Kachchh in the state of Gujarat). Mahe was not included in this study.

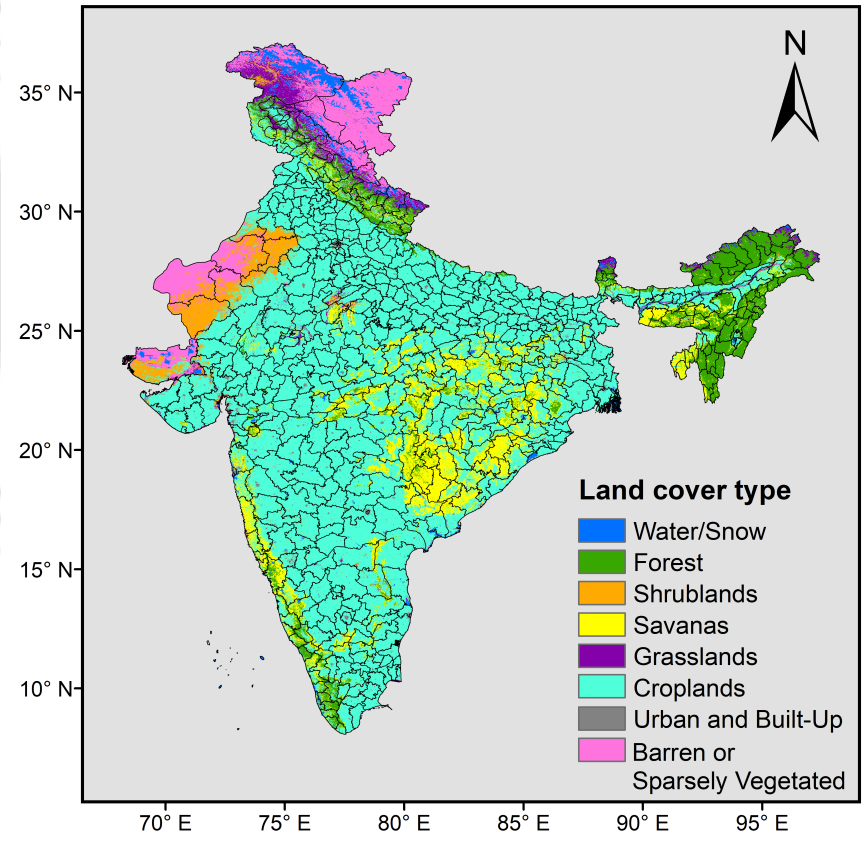

Figure 3.11: Spatial variation of reclassified land cover types in India.

3.4.2 Data used

3.4.2.1 MODIS NPP and ET

For the computation of district-scale NPP, ET and WUE_e, the NPP and ET dataset from MODIS based product as discussed in the Sections 3.3.2.1 and 3.3.2.2 were used.

3.4.2.2 Land cover data

Land cover data used for this analysis was the same as described in Section 3.3.2.4. In Section 3.3.3.2, it was found that different forest classes or cropland classes had nearly the same values of WUE_e. WUE_e value for all forest classes was nearly same ($\approx$0.95 gC m^{-2} mm^{-1}). Among five forest classes, only Deciduous Broadleaf Forest (DBF) had lesser value of WUE_e, but it covers only 0.56% of the area in India. Similarly, the value of resilience index (R_d) was also nearly the same for different forest types except for DBF (Section 3.3.3.4). Likewise, crop classes also had similar behaviour. Therefore, the land cover map was reclassified to reduce the number of classes by merging similar classes. For example, Evergreen Needleleaf Forest, Evergreen Broadleaf Forest, Deciduous Needle leaf Forest, Deciduous Broadleaf Forest and Mixed Forests were considered as a single forest class. Croplands and Cropland/Natural Vegetation Mosaic were merged into a single cropland class. Closed Shrublands and Open Shrublands were merged to form Shrublands class. Similarly, Savannas and Water/Snow classes were formed by merging similar classes of MCD12Q1 land cover type. Figure 3.11 shows the distribution of different land cover types (i.e., the classes used in this study) in India. To estimate the potential role of vegetation type on WUE_e, average WUE_e was calculated for districts dominated by different land covers. A threshold of 40% was taken to determine the dominance of a land cover in a district.

3.4.2.3 Precipitation and drought index

Daily gridded rainfall dataset (IMD4) from the IMD at a high spatial resolution (0.25° × 0.25°) was used in this study. The district level MAP for the duration 2000 to 2014 is shown in Figure 3.12. To identify the drought condition, the Palmer Drought Severity Index (PDSI) was used. The monthly PDSI dataset was obtained from Dai and NCAR (2017) at monthly timescale. PDSI is a measure of dryness, which is computed based on precipitation and temperature. It is a standardized index and its value ranges from -10 to +10. The negative values of PDSI indicate the dry conditions, whereas the

positive values indicate the wet conditions. Further details of PDSI and drought classifications based on PDSI can be found at http://droughtmonitor.unl.edu/AboutUSDM/DroughtClassification.aspx.

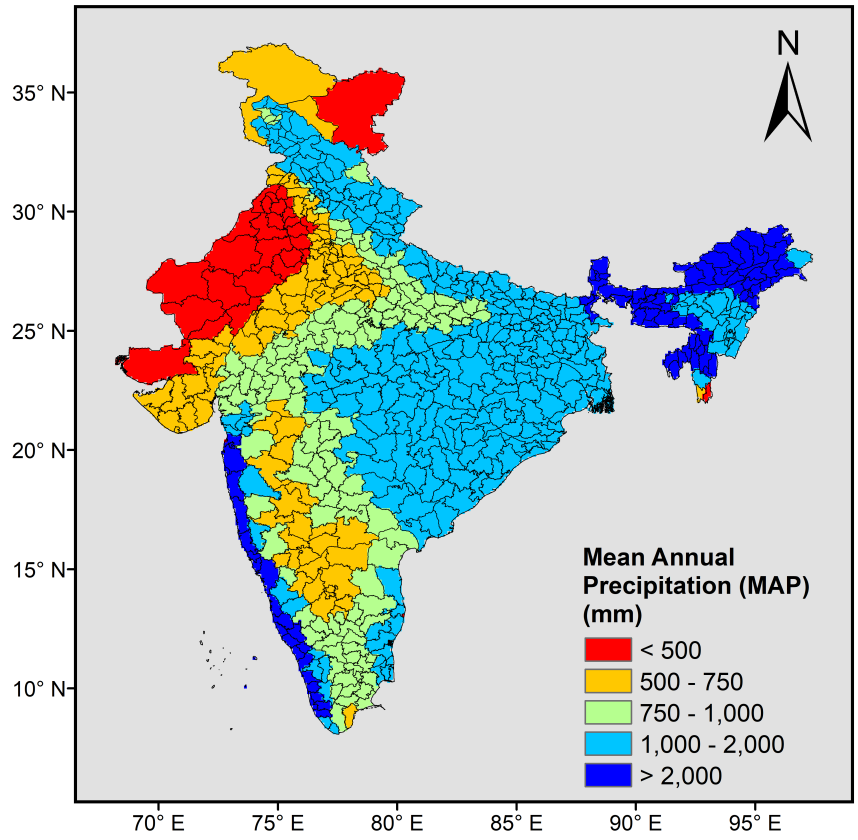

Figure 3.12: Spatial variation of district level mean annual precipitation (MAP) in India over the period 2000-2014.

3.4.3 Results and discussion

3.4.3.1 Spatial variation in NPP and ET

The spatial variations of district-level MODIS NPP and ET are shown in Figure 3.13, which are the average values over the period 2000-2014. Both NPP and ET had large spatial variation in the country. Northeast and Western Ghats had higher NPP and ET compared to the remaining parts of the country, which can mainly be attributed to the higher precipitation and the presence of forests in these regions (see Figures 3.11 and 3.12). The agricultural lands of Indo-Gangetic plains (i.e., the northern parts of the country) had moderate NPP ranging between 500-1000 gC m^{-2}. The lower Himalayan regions in the north had moderate NPP (ranging between 400 and 900 gC m^{-2}), whereas the region had lesser ET (ranging between 300 and 600 mm). The

arid and semi-arid regions in the west had the least NPP. These regions receive very less annual precipitation and have very sparse vegetation. Some regions in the north (e.g. upper parts of Jammu and Kashmir) also had very less NPP. The spatial pattern of MODIS NPP was partly consistent with the Carnegie–Ames–Stanford Approach (CASA) model simulated NPP over the period 1981 to 2005 (Nayak et al., 2013).

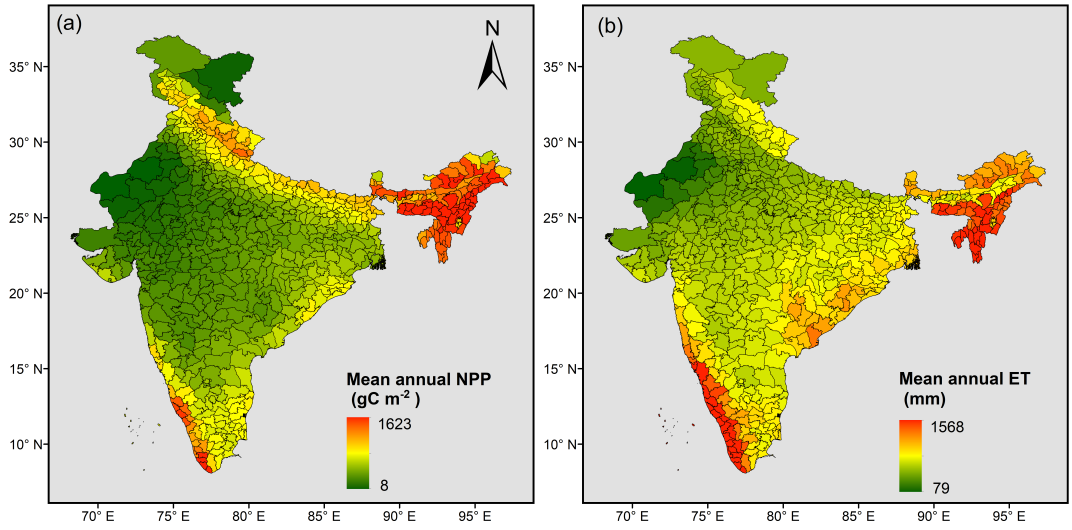

Figure 3.13: District-level mean annual MODIS (a) NPP and (b) ET in India for the duration 2000-2014. Northeast and the Western Ghats had higher NPP and ET due to higher precipitation and presence of forests.

3.4.3.2 Spatial variation and trend in WUE_e

Figure 3.14 shows the spatial pattern of mean annual WUE_e (WUE_m) at district scale in India for the period 2000-2014. Due to the large variation in the controlling factors such as precipitation, temperature, and solar radiation, WUE_e showed a large spatial variation across the country. The district level WUE_m ranged between 0 and 2.19 gC m^{-2} mm^{-1}. Higher WUE_m was found in the northeast and lower Himalayan regions. In northeast India, the higher WUE_m can mainly be attributed to the higher NPP due to the presence of the forest. Western Ghats had higher NPP but showed lesser WUE_m, which is due to the high rate of ET (Figure 3.13). Figure 3.15 shows the distribution of the linear trend for districts across the country. A decreasing trend was found for districts along the lower Himalayan regions in the north and northeast India. These regions had higher WUE_e. Significant increasing trend (as per MK test) of magnitude > 0.01 gCm^{-2} mm^{-1} yr^{-1} was observed for central India. This region had moderate WUE_e. In general, regions with higher WUE_e showed a decreasing trend,

whereas the regions with lesser WUE_e showed an increasing trend. However, there were very few districts with a significant decreasing trend (only 10 districts). About 68% of the districts had an increasing trend (only 22% were significant), whereas the remaining districts had a decreasing trend (only 1.6% were significant).

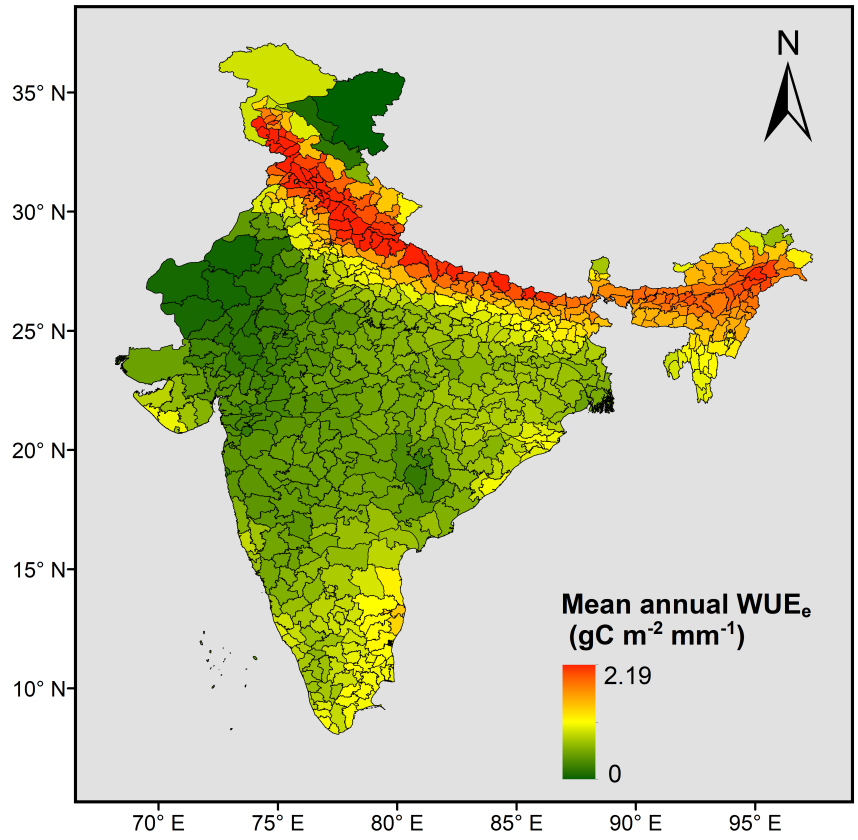

Figure 3.14: Mean annual ecosystem water use efficiency (WUE_e) at district scale in India. Annual WUE_e was computed as the ratio of annual NPP and ET. The districts in the lower Himalayan region had higher WUE_e compared to rest of the country, whereas the arid regions in the west had least WUE_e.

3.4.3.3 Relation with land cover and climate types

NPP and WUE_e are dependent on the vegetation types as different vegetation types have variations in carbon uptake and water consumption. Figure 3.16 shows the average WUE_m for districts dominated by different land covers (i.e., vegetation types). Forest dominated districts had the highest WUE_e, which is consistent with other studies (Tang et al., 2014). This explains the higher WUE_e in northeast India. It should be noted that the average WUE_e is the average of annual WUE_e of the districts dominated by a particular land cover, not the average for that land cover as the district dominated by one land cover also has other land covers. The average WUE_e for Ever-

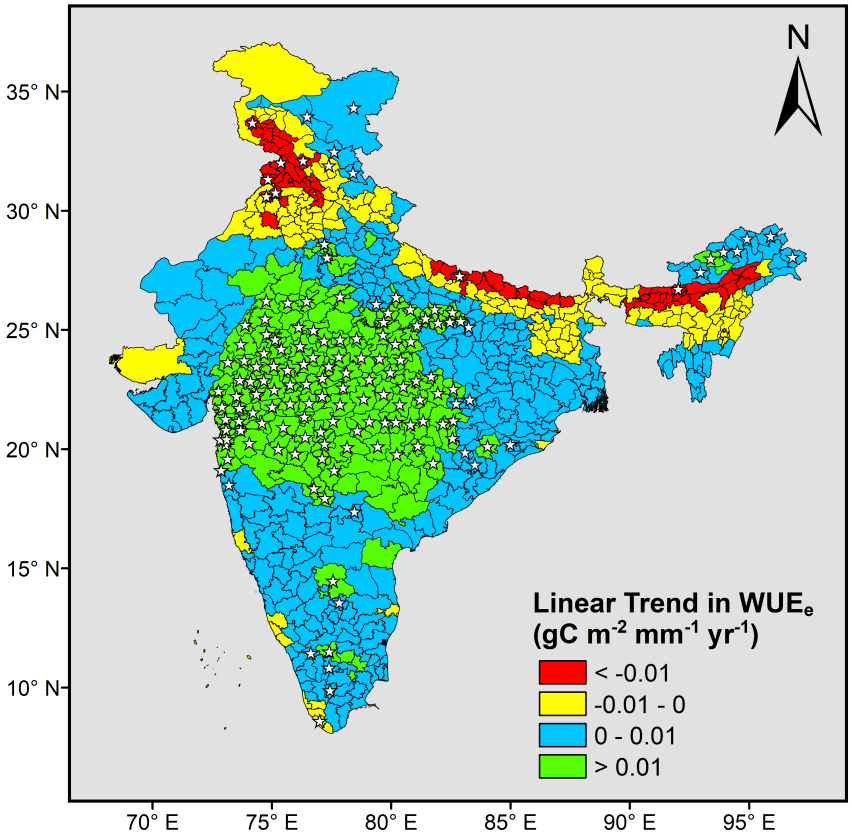

Figure 3.15: The linear trend analysis of district-level WUE_e. Star symbol (white) represents the district with the statistically significant trend at 5% significance level. Out of 634 districts, only 22% had significant increasing trend (mostly in central regions) and only 1.6% had significant decreasing trend. The regions with high WUE_e (i.e., the lower Himalayan regions) had decreasing trend.

green Needleleaf Forest (ENF), Evergreen Broadleaf Forest (EBF), Deciduous Broadleaf Forest (DBF), and Mixed Forests (MF) in India were 0.959, 0.948, 0.416, and 1.087 gCm^{-2} mm^{-1}, respectively. The average WUE_e for forest dominated districts was found as 1.00 gCm^{-2} mm^{-1}, which is close to the values for individual forest classes. The average WUE_e for Grasslands (GR) was 0.488 gCm^{-2} mm^{-1}, whereas the average WUE_e for the GR dominated districts found was 0.77 gC m^{-2} mm^{-1}. The average WUE_e for Cropland (CR) and Cropland/Natural Vegetation Mosaic (CNV) were 0.619 and 0.689 gCm^{-2} mm^{-1}, whereas the average WUE_e for the cropland dominated districts was 0.72 gCm^{-2} mm^{-1}. Similarly, average WUE_e for the Shrubland, Savanas and Barren land dominated districts were 0.17, 0.54 and 0.19 gCm^{-2} mm^{-1}. This indicates that the WUE_e of districts dominated by a particular vegetation type was related to WUE_e of the corresponding vegetation types. Though, there were differences in the values of WUE_e, which was due to the presence of different vegetation types within the district.

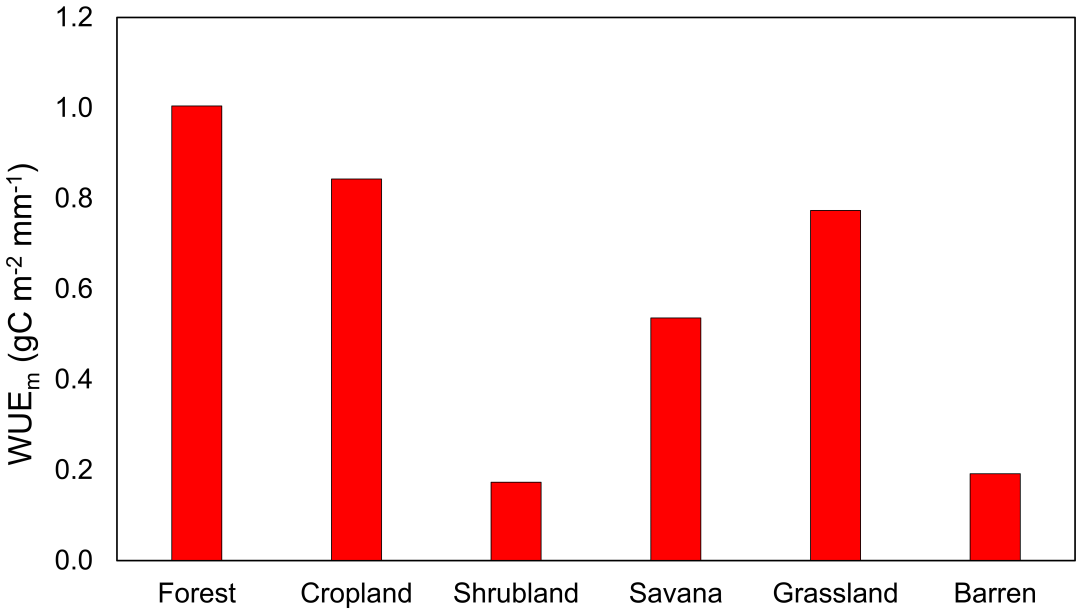

Figure 3.16: Average WUE$_m$ for districts dominated by different land covers. A district with more than 40% of a particular land cover was considered dominated by that land cover.

3.4.3.4 Dry period identification

Annual PDSI was computed for every district in India for the study duration. Figure 3.17 shows the values of PDSI for every district in their respective driest years. It is clear from the Figure 3.17 that most parts (600/634 districts) of the country experienced drought conditions (PDSI < -1) during their respective driest year, which accounts for about 94.64% of the districts. Only 34 districts had the value of PDSI greater than -1 but less than 0, which also represent below average precipitation conditions. Out of 634 districts, 501 districts had moderate to exceptional drought conditions (i.e., PDSI < -2).

3.4.3.5 Resilience Analysis

Figure 3.18 shows the results of the district level resilience analysis. R_d was calculated based on the mean and driest year values of WUE$_e$ as discussed in the methodology. Out of 634 districts considered for this study, 241 ($\approx$ 38%) districts were resilient. Remaining 62% districts were found non-resilient under different classes of non-resilience. The number of districts with slightly, moderately and severely non-resilient classes was 180 ($\approx$28.4%), 80 ($\approx$12.6%) and 133 ($\approx$21%), respectively. In terms of area under different classes, the resilient, slightly, moderately and severely non-resilient classes covered 31.65%, 27.51%, 11.52%, and 29.32%, respectively, of

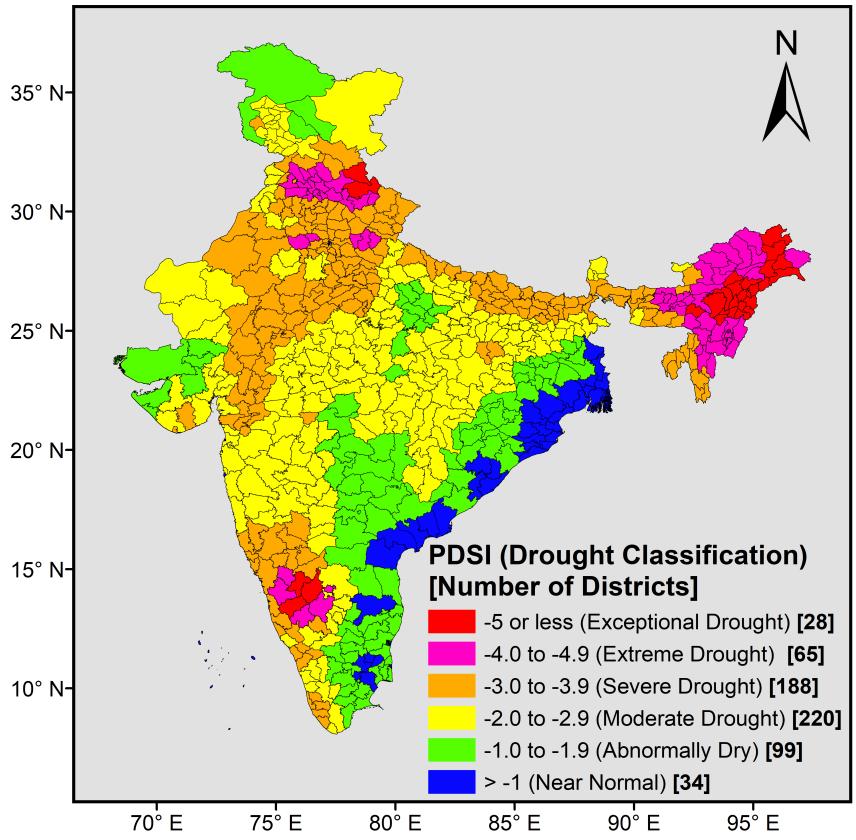

Figure 3.17: Map showing the Palmer Drought Severity Index (PDSI) values and drought classification for every district during the respective driest years in the study duration. Numbers in the square brackets ([ ]) represent the number of districts having respective drought class.

the area of the country. This indicates the around 68% of the area was not resilient. Most of the districts in the northeast and north India were either resilient or slightly non-resilient. The arid or semi-arid regions in the west were non-resilient. Some parts of eastern states were also found non-resilient. Figure 3.19(a) shows the distribution of number of districts for ranges of R_d. Most of the districts are falling either in resilient or slightly non-resilient classes. The range 0.9 – 1.0 holds the most number of districts (=180). Also, around 63% of the districts fall in the range of 0.8 to 1.1; this shows that only 37% of the stations had shown clear characteristics of either resilient or non-resilient. Recent studies have shown that different biomes tended to increase its WUE_e under water stress conditions (Huang et al., 2017a; Liu et al., 2015), therefore, a correlation analysis was performed between the ratio of driest year precipitation to mean precipitation and the R_d (Figure 3.19b). Pearson's correlation was found 0.125, indicating no dependencies between these two variables. This shows that the behaviour

of WUE_e was not controlled only by the precipitation, but it also represents other eco-hydrological processes.

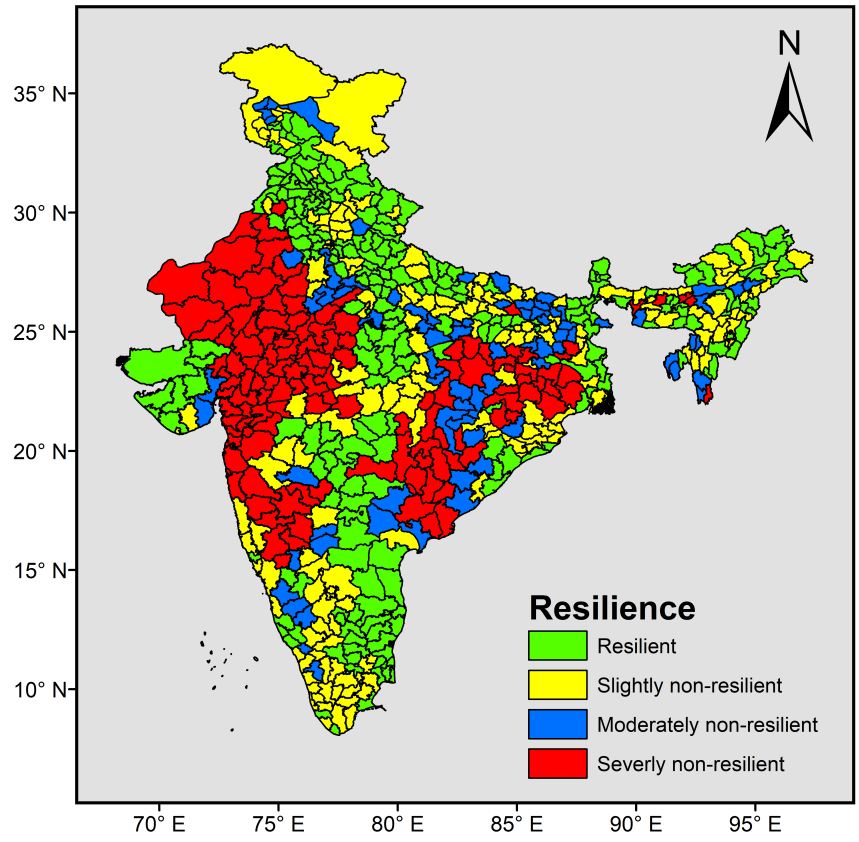

Figure 3.18: Map showing the resilience of different districts in India.

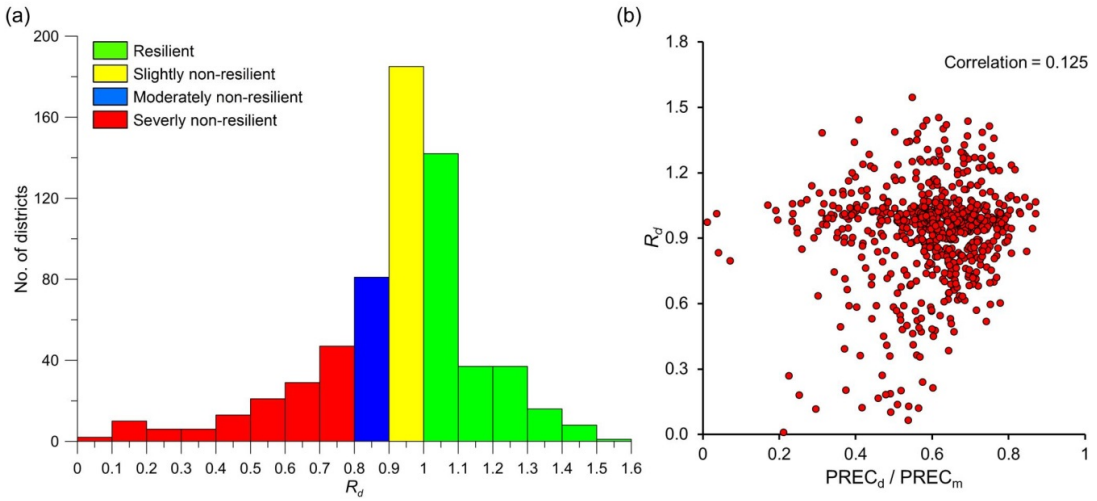

Figure 3.19: Number of districts for different ranges of R_d (a) and scatter plot between R_d and PREC$_d$/PREC$_m$. PREC$_d$ is the precipitation for the driest year and PREC$_m$ is the mean precipitation.

3.4.3.6 Relation of resilience with controlling factors

Different factors affect the ecosystem functioning, including climatic factors such as precipitation, temperature and solar radiation, and biome types. To find out the factor controlling the ecohydrological resilience, the contribution of different biome types and climate types was analyzed. There was a significant difference (p-value $<$ 0.05) in the average R_d value for different biomes and climate types. The average R_d for forest, shrubland, savannas, grassland, cropland and barren land dominated districts were 0.99, 0.28, 0.83, 0.98, 0.92 and 0.77, respectively, which shows that biome type doesn't completely relate to resilience. However, the forest class showed higher resilience compared to other biomes. 75 districts had forest cover greater than 40% of district area. Out of these districts, more than 50% were resilient. Whereas, about 65% of the districts with less than 20% forest cover were not resilient. This also indicates the higher resilience of forest dominated districts. It can also be seen that the forest dominated area in the northeast and north India are mostly resilient. On the other hand, only 35% of cropland dominated districts were found resilient. The R_d values for Cropland (CR) and Cropland/Natural Vegetation Mosaic (CNV) were 0.98 and 0.97, whereas the cropland dominated districts had slightly lesser R_d value (=0.92). It should be noted that croplands cover more than 50% area in India. The R_d value for Grasslands (GR) was 0.98, which was equal to the average R_d value for the grassland dominated districts.

Koppen-Geiger climate classes A (Tropical), B (Dry) and C (Temperate) cover about 30%, 20% and 48% of the country's districts respectively. The average R_d for district dominated by these classes was 0.89, 0.89, and 0.9, respectively. The percent of districts under these climates that were found resilient were 32%, 38% and 42%, respectively. This shows that districts in the temperate climate had a higher tendency to be resilient. The average R_d values for A, B and C climate types were 0.818, 0.787, and 1.02, respectively, which also indicated that climate type C was more resilient. However, similar to the biome types, the resilience at the district level did not wholly relate to climate type. There were resilient districts with land cover and climates that were found less resilient. Some global studies showed that different biomes had contrasting responses to droughts (Huang et al., 2017a; Yang et al., 2016). The results of the present study are not consistent with these studies for the reason that there are multiple vegetation types within the geographical area of a district. For example, within

a district, there can be a forest as well as croplands. The district level response of WUE_e is the combined response of multiple biomes/climates rather than that of a single biome/climate. Some relation between these controlling factors and the resilience were identified, but there is still a need for more observation and research to determine the other eco-hydrological factors controlling the resilience.

3.4.3.7 State scale analysis

In addition to the district-level resilience assessment, the resilience at the state scale was also examined. Figure 3.20 shows the percentage of resilient area in every state. The percentage of the resilient area was computed using the sum of areas of resilient districts and total area of the state. Sikkim (SK) was the only state with 100% resilient area. All four districts in the state were found resilient. Two states, namely Rajasthan (RJ) and Chhattisgarh (CH), had 0% resilient area. RJ is located in the western arid regions and has very less vegetation. It should be noted that all three classes of non-resilience were considered non-resilient. These states had districts with different classes of non-resilience but did not have a single resilient district. Out of 30 states and UTs considered, only 10 had more than 50% resilient area. In general, it was found that the states in the lower Himalayan regions had higher resilient areas (in terms of percent of total state area), for example, Sikkim (SK, 100%), Punjab (PB, 88.11%), Haryana (HR, 76.02%), Uttarakhand (UK, 75.26%), Himachal Pradesh (HP, 73.19%), and Arunachal Pradesh (AR, 64.04%). In the south, Tamil Nadu (TN, 56.74%) was the most resilient, followed by Andhra Pradesh (AP, 53.43%) and Telangana (TL, 48.61%). Whereas, Karnataka (KR, 17.38%) and Kerala (KL, 19.13%) had the minimum percentage of resilient area in the south. Among northeastern states, Assam (AS, 20.72%) had the minimum percentage of resilient area.

This study highlights the resilience of the terrestrial ecosystems in different parts of India at state and district scale. India is a developing nation, which has been expanding its infrastructure exponentially. Economic growth in India requires rapid industrialization and infrastructure development. The infrastructural and economic developments come at the cost of damage to natural ecosystems. Anthropogenic activities such as Land Use and Land Cover (LULC) alterations, deforestation, and urbanization affect the ecological process and primary production. Every state in India has shown a consistent increase in Gross State Domestic Product (GSDP), which indicates that continuous de-

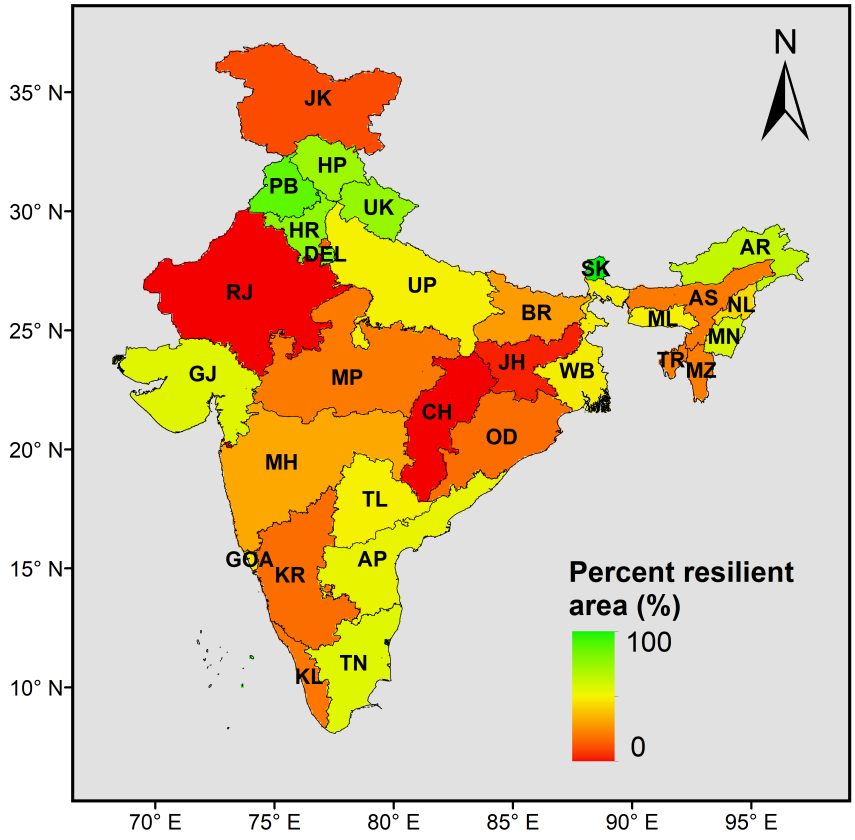

Figure 3.20: Map showing the percentage of resilient area in each state. The resilient area is the total area of all resilient districts within the state. All the 29 states and one UT, Delhi, were considered in this study.

velopment occurring in different sectors. On the other hand, an increase in the extreme hydroclimatic events in India has increasingly been reported (Mallya et al., 2015; Roxy et al., 2017; Sharma and Mujumdar, 2017). The ongoing climatic changes may lead to more extreme hydroclimatic events, which will put tremendous pressure on terrestrial ecosystems to maintain its functioning and productivity. The reduction in primary productivity under dry condition, as found in this study, may also lead to a risk of food shortage, as both population and demand for food have been increasing.

3.5 Resilience analysis using GPP

Gross Primary Production (GPP) is the amount of chemical energy as biomass that primary producers create in a given length of time. The previous analysis was carried out based on WUE_e computed using NPP as the estimate of carbon uptake. However, GPP has also been widely used for the calculation of WUE_e. Therefore, a comparison of NPP and GPP based resilience analysis was carried out to understand the difference

between these two measures.

3.5.1 Study area

This comparison was carried out at the basin scale same as described in Section 3.3.1.

3.5.2 Data used

All the dataset used for this analysis were the same as described in Section 3.3.2 except for MODIS GPP.

3.5.2.1 MODIS GPP

The global annual MOD17A3 products, which was used for NPP, also provides GPP data for the whole globe at the same spatial and temporal resolution. Therefore, the GPP data from the same source was used for this analysis. Details about this datasets are discussed in Section 3.3.2.1.

3.5.3 Methodology

The methodology adopted for this analysis was the same as described in Section 3.2 For GPP based analysis, the NPP was replaced with GPP. Figure 3.21 shows the difference between GPP and NPP based analyses.

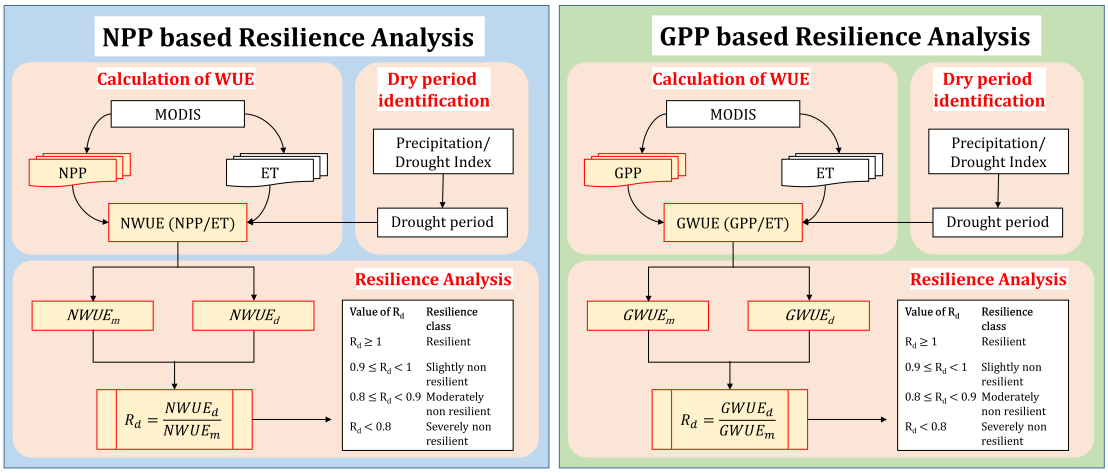

Figure 3.21: Difference between NPP and GPP based resilience analyses.

3.5.4 Results and Discussion

3.5.4.1 Spatial variation of GPP and GWUE

Like NPP, GPP also had large variation for river basins in India (Figure 3.22). The Barak Basin (Basin Id. 2c) in northeast India had the highest GPP of 2,304 gCm^{-2}. The neighbouring Brahmaputra basin also had high GPP of 1,590 gCm^{-2}. The Basin Id. 14, which is the group of basins along the Western Ghats, also had higher GPP of 1,644 gCm^{-2}. West flowing rivers of Kutch and Saurashtra including Luni Basin (Basin Id. 20) had the least GPP of 412 gCm^{-2}. Figure 3.23 compares the GPP based WUE (GWUE) and NPP based WUE (NWUE) for different basins. Both NWUE and GWUE had similar variations for different river basins. GWUE was higher than NWUE due to higher values of GPP as compared to NPP. GWUE was highest for Indus basin (Basin Id. 1) and Barak basin (Basin Id. 2c) of 1.92 gC m^{-2} mm^{-1}, whereas the NWUE was highest for Brahmaputra basin. The GWUE for Brahmaputra basin (= 1.80 gC m^{-2} mm^{-1}) was slightly less than that of Indus basin. The Mahi basin (Basin Id. 10) had the least GWUE of 1.06 gC m^{-2} mm^{-1}. The Indus basin (Basin Id. 1) had the largest spatial variability of GWUE within the basin. The standard deviation (SD) of pixel values within the basin for Indus basin was 0.46 gC m^{-2} mm^{-1}. The Basin Id. 20 had the second highest SD of 0.24 gC m^{-2} mm^{-1}.

3.5.4.2 Resilience Analysis

Out of 22 basins, 7 basins were found resilient (Figure 3.24), which shows that the GWUE of the terrestrial ecosystems in these basins either increased or remained the same under dry conditions compared to the mean values. These basins include Basin Ids. 1, 2b, 9, 11, 17, 18 and 20. Basins with lesser GWUE were found non-resilient, whereas the basins with higher GWUE were found resilient. Indus basin was found the most resilient with R_d = 1.35. Basins in the central parts of the country (Basin Ids. 10, 12 and 13) were found severely non-resilient, which shows that GWUE under dry conditions was less than 80% of the mean values.

3.5.4.3 Comparison of NPP and GPP based resilience analysis

Figure 3.25 compares the resilience analysis based on GWUE and NWUE. Seven basins were found resilient based on GWUE-based resilience analysis, whereas six basins were found based on NWUE-based resilience analysis. The resilient basins were the

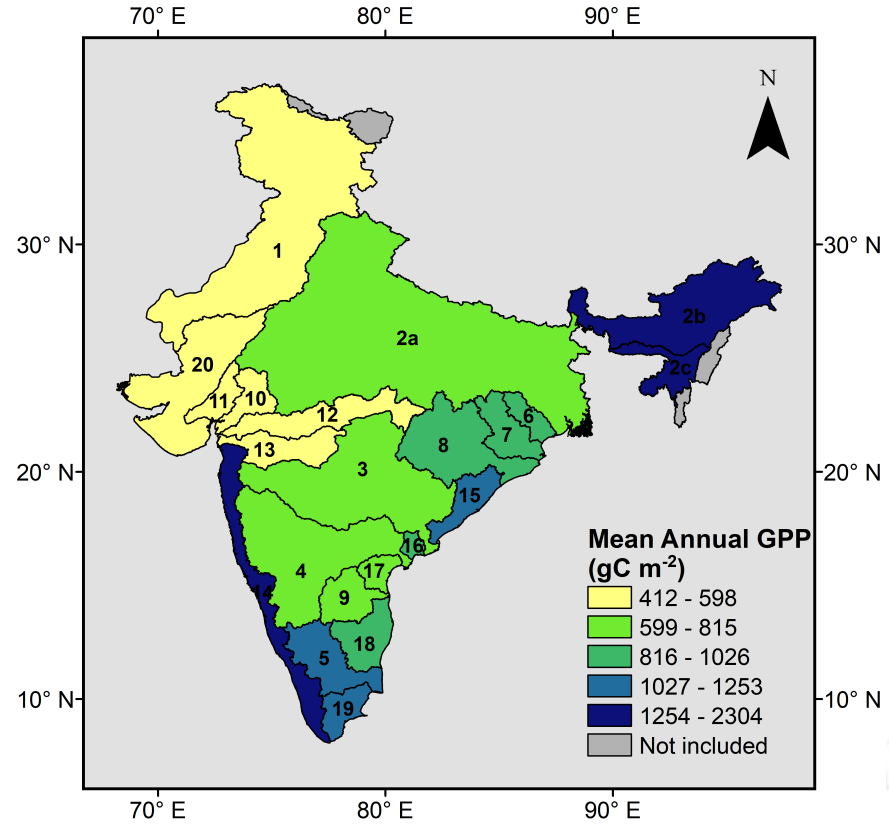

Figure 3.22: The mean annual GPP for different river basins in India.

same except for the Sabarmati Basin, which was not resilient for NWUE-based analysis. The number of basins with 'severely non-resilient' class were 6 and 3 for NWUE and GWUE-based analyses, respectively. Godavari Basin, which is one of the largest basins in the country, was found moderately non-resilient for GWUE based analysis, whereas it was found severely non-resilient for NWUE based analysis. In general, the GPP (or GWUE) based analysis indicated higher resilience for river basins compared to NPP (or NWUE) based analysis.

3.6 Use of high resolution land cover map

The land cover wise analysis of WUE_e plays a vital role in understanding the spatial variation in WUE_e. The MODIS based land cover maps were compared with high-resolution land cover maps obtained from National Remote Sensing Centre (NRSC) to examine the impact of land cover maps resolution on average WUE_e computation. The NRSC land cover map was available only for Northeast (NE) India; therefore, this analysis was carried out for only the NE part of the country. Table 3.7 compares MODIS and

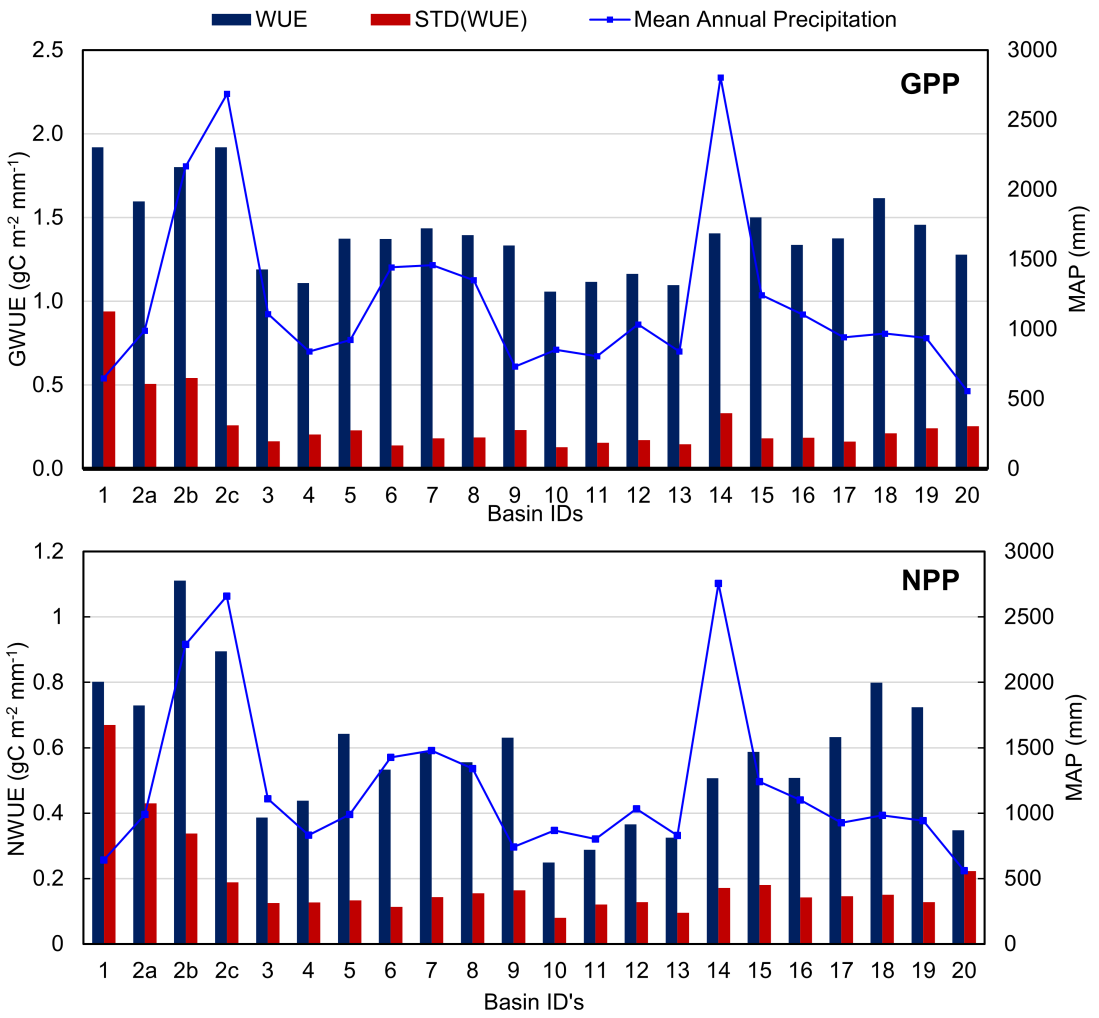

Figure 3.23: Comparison of GPP based WUE (GWUE) and NPP based WUE (NWUE).

NRSC LULC maps. To analyze the maps, NRSC LULC was resampled to the resolution of MODIS using MAJORITY algorithm of ArcGIS 10.4 to use with NPP and ET products. Majority algorithm determines the new value of the cell based on the most popular values within the filter window.

3.6.1 Comparison of LULCs

As both the products come with a different set of classes, the maps were reclassified to standard 6 classes. Tables 3.8 and 3.9 show the details of LULC classes of MODIS and NRSC LULCs, respectively, along with the new assigned classes. Figure 3.26 shows the reclassified land cover maps of MODIS LULC, NRSC LULC and resampled NRSC LULC. The overall pattern of reclassified classes was similar for MODIS and NRSC LULCs. Table 3.10 compares the percent area under reclassified map classes for different LULC maps. MODIS LULC had higher area as forests and croplands compared to NRSC LULC. On the

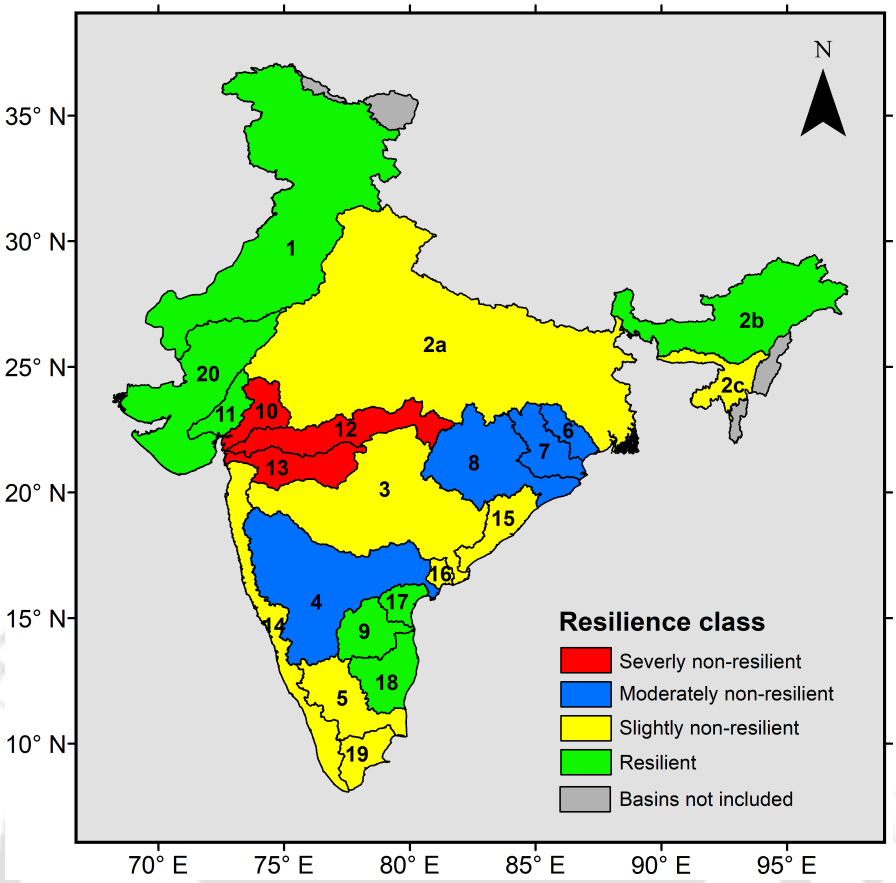

Figure 3.24: GWUE based resilience analysis.

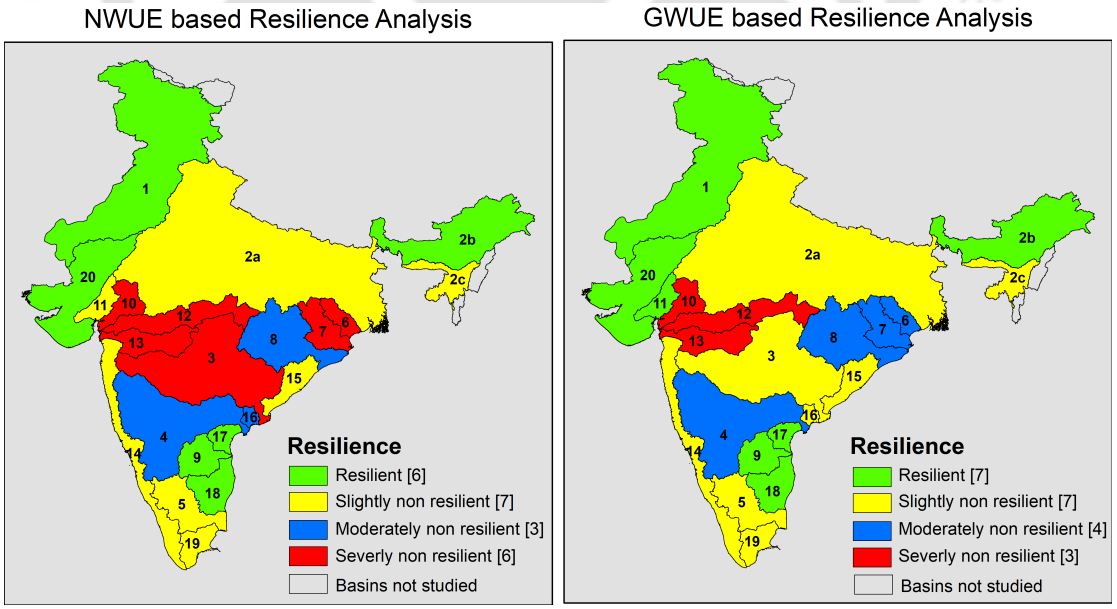

Figure 3.25: Comparison of resilience analysis using GWUE and NWUE.

other hand, the NRSC LULC showed about 4% more area in the form of water/snow. NRSC LULC also had 2% larger area as Barren compared to MODIS LULC.

Table 3.7: Comparison of MODIS and NRSC land cover maps products.

Product Name	MODIS LULC	NRSC LULC
Product Id	MOD12Q2	NRSA/LULC/1 : 250K
Developed by	USGS Land Cover Institute (LCI)	National Remote Sensing Centre (NRSC)
Satellite & Sensor	IRS-P6 Advanced Wide Field Sensor (AWiFS)	NASA MODIS
Spatial Resolution	(0.00417 × 0.00417) ∼1000m	(0.000509 × 0.000509) ∼125m
Number of classes	17	18

Table 3.8: Class details of MODIS LULC and the new assigned classes.

CODE	**Class**	**New class**
0	Water	Water/Snow/Ice
1	Evergreen Needle leaf Forest	Forest
2	Evergreen Broadleaf Forest	Forest
3	Deciduous Needle leaf Forest	Forest
4	Deciduous Broadleaf Forest	Forest
5	Mixed Forests	Forest
6	Closed Shrublands	Shurbland/Grassland
7	Open Shrublands	Shurbland/Grassland
8	Woody Savannas	Forest
9	Savannas	Forest
10	Grasslands	Shurbland/Grassland
11	Permanent Wetland	Water
12	Croplands	Cropland
13	Urban and Built-Up	Urban
14	Cropland/Natural Vegetation Mosaic	Cropland
15	Snow and Ice	Water/Snow/Ice
16	Barren or Sparsely Vegetated	Barren

3.6.2 Comparison of average NPP, ET and WUE$_e$

Figure 3.27 and Table 3.11 show a comparison of land cover wise average NPP, ET and WUE$_e$ computed using MODIS and NRSC LULCs. The values of NPP, ET and WUE$_e$ were nearly the same for forest and croplands. These two classes cover about 85% of the area in NE India. There were differences in the values for Barren and Shrub/Grasslands.

Table 3.9: Class details of NRSC LULC and the new assigned classes.

Value	Description	New class
1	Built-up	Urban
2	Kharif Crop	Cropland
3	Rabi Crop	Cropland
4	Zaid Crop	Cropland
5	Double/Triple Crop	Cropland
6	Current Fallow	Barren
7	Plantation	Cropland
8	Evergreen Forest	Forest
9	Deciduous Forest	Forest
10	Degraded/Scrub Forest	Shurbland/Grassland
11	Littoral Swamp	Water
12	Grassland	Shurbland/Grassland
13	Shifting Cultivation	Barren
14	Wasteland	Barren
15	Rann	N/A
16	Waterbodies max	Water/Snow/Ice
17	Waterbodies min	Water/Snow/Ice
18	Snow Cover	Water/Snow/Ice

Table 3.10: Percent area under different LULC classes for different sources.

Class	MODIS	NRSC	NRSC - Resampled
Water/Snow	2.03	6.24	6.23
Forest	70.31	67.1	68.34
Shrub/Grassland	4.53	4.66	3.8
Barren	0.41	2.5	1.75
Cropland	22.52	18.72	19.31
Urban	0.2	0.78	0.56

3.7 Conclusions

A framework was developed for the ecosystem resilience analysis at different scales in India. The resilience framework was based on the ecosystem water use efficiency (WUE_e), which was defined as the ratio of Net Primary Production and Evapotranspiration. A considerable variation in WUE_e was found at the river basin scale in India. The

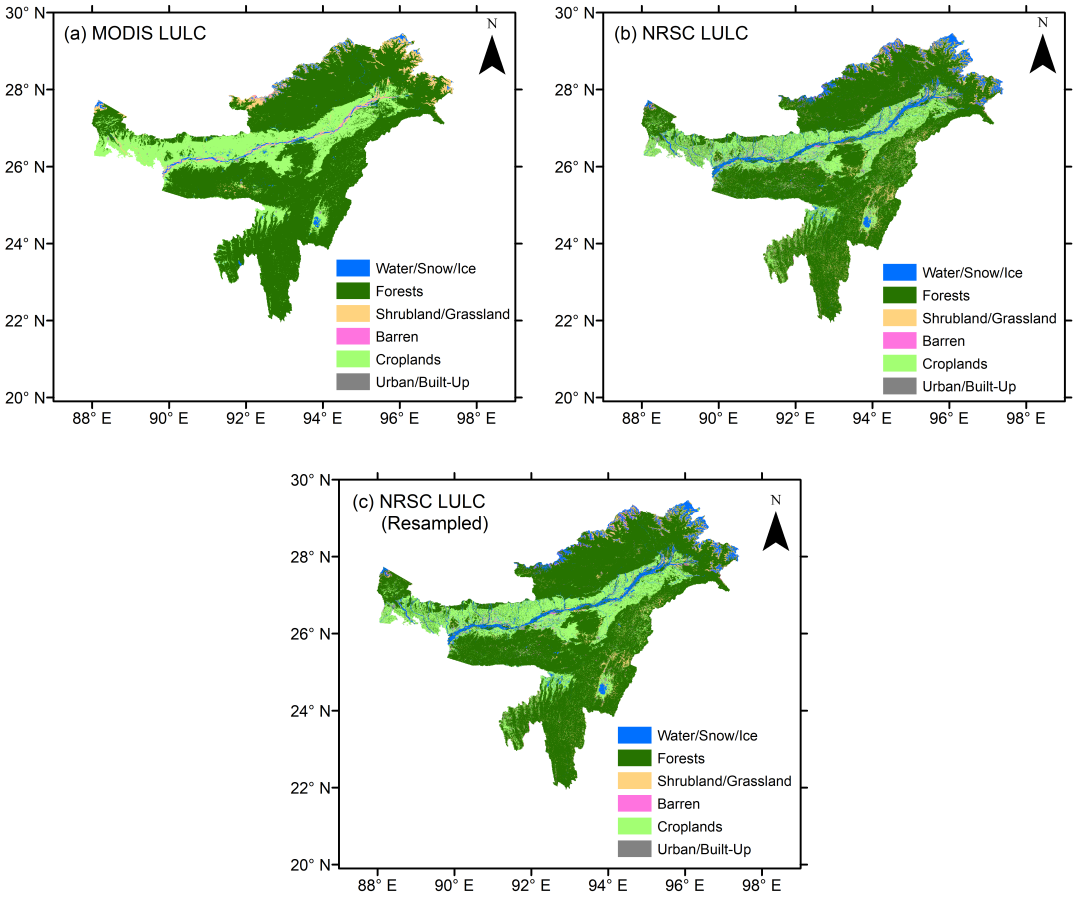

Figure 3.26: The land cover maps obtained after the reclassification of (a) MODIS LULC, (b) NRSC LULC and (c) resampled NRSC LULC.

Table 3.11: Average WUE_e for different land cover types computed using MODIS and NRSC LULCs.

Class	**Average WUE_e ($gCm^{-2}mm^{-1}$)**	
	MODIS	NRSC
Forest	1.03	1.03
Shrub/Grass	0.43	0.86
Barren	0.56	0.9
Cropland	1.26	1.26

Brahmaputra basin in northeastern India had the highest WUE_e, which was attributed to the presence of the vast forest cover. Mahi basin in western India had the least WUE_e. The land cover scale analysis revealed that the forests had higher WUE_e compared to other land cover types; however, there was heterogeneity in WUE_e for different forest types. Among different climate types, the temperate climate was found to have higher WUE_e. The ecosystem resilience analysis revealed that only 6 out of 22 river basins

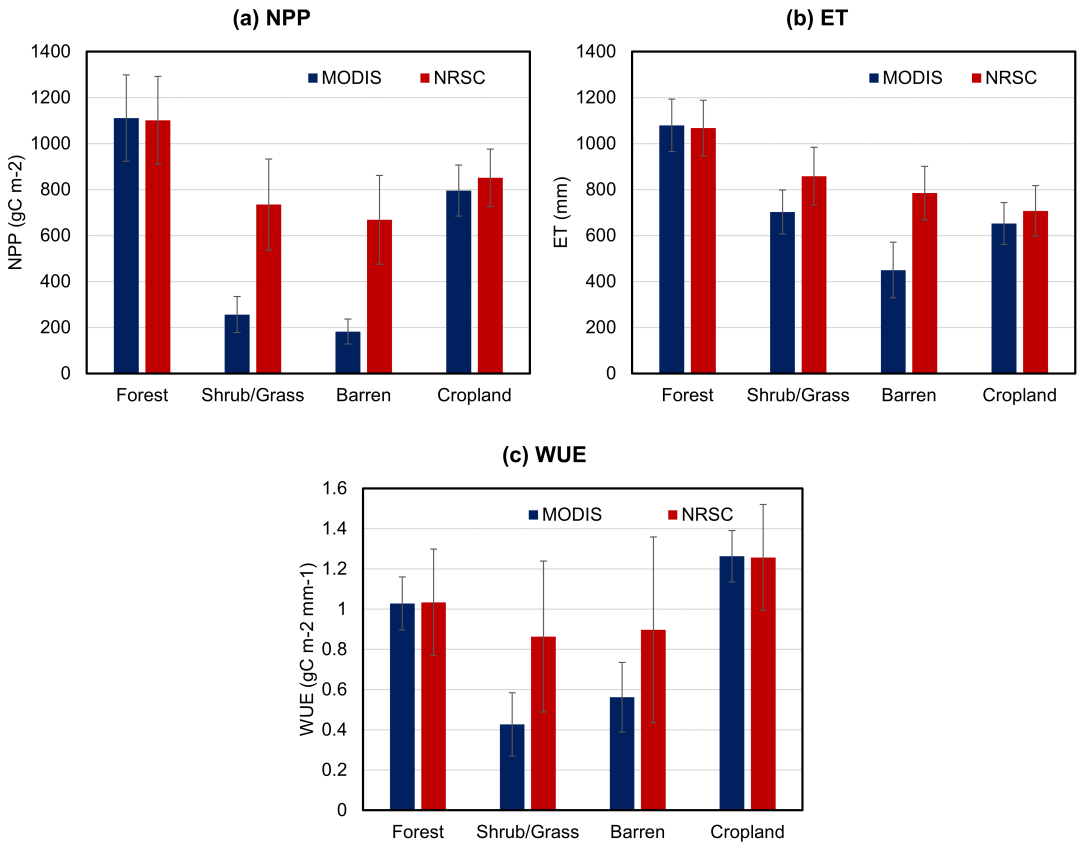

Figure 3.27: Comparison of land cover wise average NPP, ET and WUE_e computed using MODIS and NRSC LULCs. The bars shows the average values and the error bars show the standard deviation in the pixel values.

were resilient to dry conditions. Seven basins were found slightly non-resilient, three were found moderately non-resilient and remaining six basins were found severely non-resilient. Among different land cover types, only evergreen forests were found resilient. Among climate types, temperate climate-type was found most resilient.

The district scale analysis found that the lower Himalayan region had higher WUE_e compared to other parts of the country. The trend analysis of the WUE_e revealed that the central parts of the country had an increasing trend, whereas the lower Himalayan region had a decreasing trend. Out of 634 districts, only 22% had a significant increasing trend (mostly in central regions) and only 1.6% had a significant decreasing trend. Out of 634 districts, only 241 (≈38%) districts were found resilient. On the other hand, number of districts with slightly, moderately and severely non-resilient was 180 (≈28.4%), 80 (≈12.6%) and 133 (≈21%), respectively. In general, the forest dominated district had higher resilience. Out of 30 states and UTs, only 10 had more than 50% resilient area. The states in the lower Himalayan region had higher resilience.

The basin-scale resilience analysis was carried out using Gross Primary Production (GPP) based WUE_e. Out of 22 basins, 7 basins were found resilient in this analysis, whereas the number of severely non-resilient basins reduced to 3. Therefore, it was concluded that GPP based analysis indicated higher resilience. A high-resolution land cover dataset was compared with the MODIS dataset used in this work for the northeast part of the country. The analysis revealed that MODIS land cover had an equal area for the two largest classes (forest and cropland) compared to high-resolution land cover. WUE_e computed using both land cover maps was nearly the same for both major classes.

4

Spatiotemporal Analysis of Ecosystem Water Use Efficiency

4.1 Introduction

The ecosystem water use efficiency (WUE_e) is defined as the carbon uptake per unit the water consumption by the vegetation (Xue et al., 2015). It highlights the link between the physical process (i.e., evaporation) and the biological processes (i.e., photosynthesis and transpiration), which governs the water and carbon budget on Earth (Huang et al., 2017a; Ponce Campos et al., 2013). It is an important indicator to understand the response of ecosystem productivity to climate change due to the strong coupling of the carbon and water cycles (Yang et al., 2016).

In general, water use efficiency (WUE) is defined in different ways, such as at leaf, canopy, and ecosystem levels (Niu et al., 2011). Leaf or plant WUE is defined as the ratio of plant photosynthesis to transpiration; Canopy WUE is defined as the ratio of Gross Ecosystem Productivity (GEP) to canopy transpiration (Loomis and Connor, 1992); and WUE_e is defined as the ratio of NPP, net ecosystem production or GPP to water use or evapotranspiration (ET) (Ponce Campos et al., 2013; Song et al., 2017; Tang et al., 2014; Yang et al., 2016). The carbon and water fluxes are regulated by the leaf stomatal conductance and the other controlling factors that affect leaf functioning (Sun et al., 2016); however, the WUE_e is affected by other processes such as water loss from the soil surface (i.e., evaporation) and vegetation morphology (Tang et al., 2014). WUE_e is also controlled by the climate regimes (Still et al., 2003), local resource limitations (Huxman et al., 2004), and species composition (Niu et al., 2011). The assessment of controlling factors is crucial in ecosystem modeling. Global warming or

climate change is affecting the terrestrial ecosystems, which act as a major carbon sink (Dale et al., 2000; White et al., 1999). Different biomes have different responses to the warm conditions (Ellison et al., 2017). A better understanding of how the ongoing climatic changes affect the WUE_e will improve our ability to predict the carbon and water fluxes for better water management and designing the regional climate change mitigation policies. For this analysis, the WUE_e is defined as the ratio of NPP to ET.

Global and regional studies have investigated the spatial variations in WUE_e and its climatic factors (Huang et al., 2017a; Liu et al., 2015; Sun et al., 2016; Tang et al., 2014, 2017). For example, Tong et al. (2009) found both diurnal and seasonal variations in WUE_e, estimated using eddy covariance technique and the cuvette method on irrigated winter wheat and summer maize crops in the North China Plain. Similarly, based on the measurement of 47 different study sites across different forest biome types, Peñuelas et al. (2011) reported that the increase in the atmospheric CO_2 concentration and the intrinsic WUE_e did not result into a significant increase in tree growth (as measured by tree ring growth), which suggested that the potential growth benefits were controlled by other factors. Tang et al. (2014) used flux tower observations of evaporation and productivity to examine the spatial distribution and latitudinal trend in WUE_e. The study found that the trend peaks at approximately 51°N, and then decreases afterward. Huang et al. (2015) used data-driven models derived from satellite observations and process-oriented carbon cycle models to investigate the ecosystem WUE_e (defined as GPP/ET) trends from 1982 to 2008. The study found positive trends under different scenarios of rising CO_2, climate change, and nitrogen deposition. Utilizing a process-based ecosystem model, Liu et al. (2015) assessed the magnitude, spatial patterns, and trends of WUE_e (defined as NPP/ET) of China's terrestrial ecosystems. The study found that the national average annual WUE_e of China was 0.79 $gC\ kg^{-1}\ H_2O$ and the WUE_e in different regions had different responses to droughts. Sun et al. (2016) showed that the precipitation was strongly correlated with the spatial gradients of WUE_e for temperate and tropical regions, whereas temperature dominated in the regions north of 50° N. In the high latitudes, WUE_e increased with increasing solar radiation. Using continuous Eddy Covariance (EC) measurements and satellite data, Tang et al. (2017) found distinct seasonal cycles in GPP, ET and WUE_e for grassland and cropland ecosystems in the arid and semi-arid areas of Northwest China. The Pearson correlation analysis showed that local precipitation and temperature were the two most important climatic

factors. Likewise, there is a wide range of literature available on the WUE_e across the globe. However, the literature on the spatiotemporal patterns of WUE_e and its climatic factors in India is scarce. Though a few studies have assessed the spatial and temporal patterns of ecosystem productivity and its controlling factors in India (Banger et al., 2015; Goroshi et al., 2014; Nayak et al., 2013, 2011, 2010; Singh et al., 2011; Tripathi et al., 2017), there is no detailed study on WUE_e in India.

India's terrestrial ecosystems are diverse due to the presence of different climates, land covers and the seasonality of vegetation phenology (Nayak et al., 2015). The major controlling factors for vegetation productivity are water and temperature (Nayak et al., 2010). The climatic patterns over India are changing due to global warming and climate change, which is further affecting the vegetation patterns (Nayak et al., 2013, 2015).

This study presents a high-resolution spatiotemporal assessment of WUE_e in India. This chapter describes:

- Spatial pattern and trend in WUE_e in India.
- Role of different climatic parameters controlling the WUE_e.
- Assessment of the impact of development activities on ecosystem productivity.

4.2 Study area

The study area for this study is India, excluding the islands. The study was carried out at the pixel level. The resolution of the analysis was that of MODIS products (i.e., 1 km).

4.3 Data used and methods

4.3.1 Climate data

The precipitation data used in this study was obtained from IMD, as discussed in Section 3.3.2.5. The average annual precipitation of India is about 119 cm, but there is great spatial variation in the distribution of rainfall in India (Figure 4.1a). The amount of rainfall varies from heavy in the northeast and the Western Ghats to scanty in western India. Over 80% of the annual rainfall is received in the four rainy months (June to September) during the summer monsoon. IMD provides temperature data at coarser resolution ($1° \times 1°$); therefore, temperature data set from Sheffield et al. (2006) was

used. The dataset was developed using global observations and National Center of Environmental Prediction (NCEP) and the National Center for Atmospheric Research (NCAR) reanalysis (Kalnay et al., 1996). This temperature dataset was found comparable to IMD data (Mishra et al., 2014) and has been used for studies in India (Mishra and Lilhare, 2016). Data for solar radiation was obtained from the NCEP Climate Forecast System Reanalysis (CFSR) (Fuka et al., 2014). The temperature and solar radiation data sets were re-gridded to IMD data grid points using inverse distance weighting (IDW) interpolation. The land cover classification used for this study was as described in Section 3.3.2.4. There is a diverse pattern of land cover types in India (Figure 4.1b). High rainfall regions of the northeast and the Western Ghats have dense forests (FSI, 2015). A significant decrease in forests (from 89 million ha to 63 million ha) occurred during 1880-2010; however, the rate of decline has reduced after the 1980s due to government policies to protect the forests (Tian et al., 2014). Cropland is the prevailing land cover type, which spreads over about 50% of the total geographical area of the country. Cropland area increased from 92 million ha to 140.1 million ha during 1880–2010 (Tian et al., 2014). India has a diverse spatial distribution of different climate types (Peel et al., 2007). The country is home to six major climatic subtypes. It has arid deserts in the west, humid tropical regions supporting rain forests in the southwest and the island territories, and alpine tundra and glaciers in the north (Figure 4.1c).

4.3.2 NPP and ET data

The MODIS based NPP and ET products were used for this study. These datasets are discussed in Section 3.3.2.

4.3.3 Trend analysis

The non-parametric Mann-Kendall (MK) trend test was used to determine the trend in WUE_e and climatic variables (i.e., precipitation, temperature and solar radiation) for 2000–2014. The trend was assessed at a significance level of 0.05. The method is described in Section 3.2.4. Also, Sen's slope estimator was used to quantifying the magnitude of the trend (Sen, 1968). The MK test was performed at the pixel level to assess the spatial patterns of the trend in WUE_e. The Sen's slope was estimated

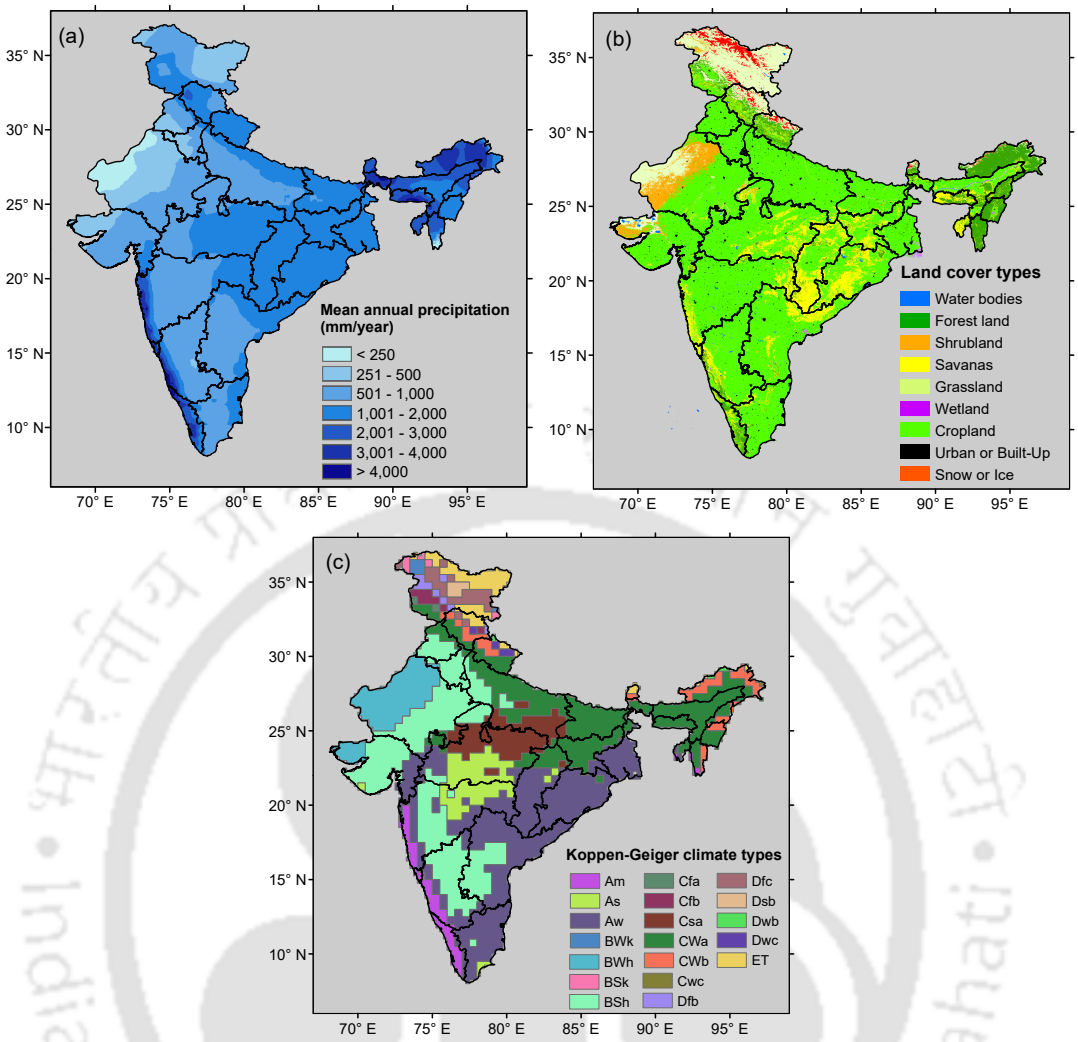

Figure 4.1: Spatial distribution of (a) mean annual precipitation, (b) land cover types, and (c) Koppen-Geiger climate types in India.

using the following equation:

$$S_i = \frac{x_j - x_k}{j - k}, \quad i = 1, ..., N \tag{4.1}$$

where x_j and x_k are the values of timeseries at timestep j and k $(j > k)$ respectively. The median value of N values of S_i gives the Sen's estimator of the slope. A positive value of Sen's estimator of the slope indicates an upward trend and a negative value indicates a downward trend in the timeseries.

4.3.4 Pearson correlation coefficient

To analyze the relationship between the WUE_e and climatic variables, the Pearson correlation coefficient was used. It is a measure of the linear correlation between two variables, X and Y.

$$\rho = \frac{cov(X,Y)}{\sqrt{var(X) \times var(Y)}} \tag{4.2}$$

where $cov(X,Y)$ is the covariance between two variables (i.e., X and Y), and $var(X)$ and $var(Y)$ represent the variance of variables X and Y, respectively.

4.4 Results and discussion

4.4.1 Spatial pattern of MODIS NPP and ET

NPP showed a large spatial variation over the country (Figure 4.2). Higher NPP (>1500 gC m^{-2}) was found for the forest dominated northeastern and Western Ghats regions, whereas the arid northwestern areas had the least NPP. Indo-Gangetic plains had moderate NPP ranging between 500 and 1500 gC m^{-2}. The interannual variations (presented in the form of the coefficient of variation, CV) in NPP was very high for the northwestern arid regions compared to the rest of India. The vegetation productivity in these regions is controlled by water availability or precipitation, which has very erratic behaviour. In this region, the standard deviation in annual NPP is much higher compared to lower values of mean annual NPP, resulting in a higher CV. However, CV was less for regions with higher NPP (i.e., for the Western Ghats and northeast India). The spatial variation in NPP over India was consistent with the distribution of different land covers (Figure 4.1b). ET followed the same spatial pattern as NPP (Figure 4.2 c and d). Forest dominated the northeastern region and the Western Ghats in the south had higher ET (>1000 mm/year) with lesser inter-annual variations (CV <30%). Indo-Gangetic plains and the eastern regions had moderate ET (500-1200 mm/year). The interannual variation in ET was high (CV > 50%) for the arid northwestern regions due to erratic precipitation behavior.

4.4.2 Spatial pattern of WUE_e

Figures 4.3(a) and 4.3(b) show the spatial pattern of mean and CV, respectively, of annual WUE_e in India over the period 2000-2014. Due to the large variation in

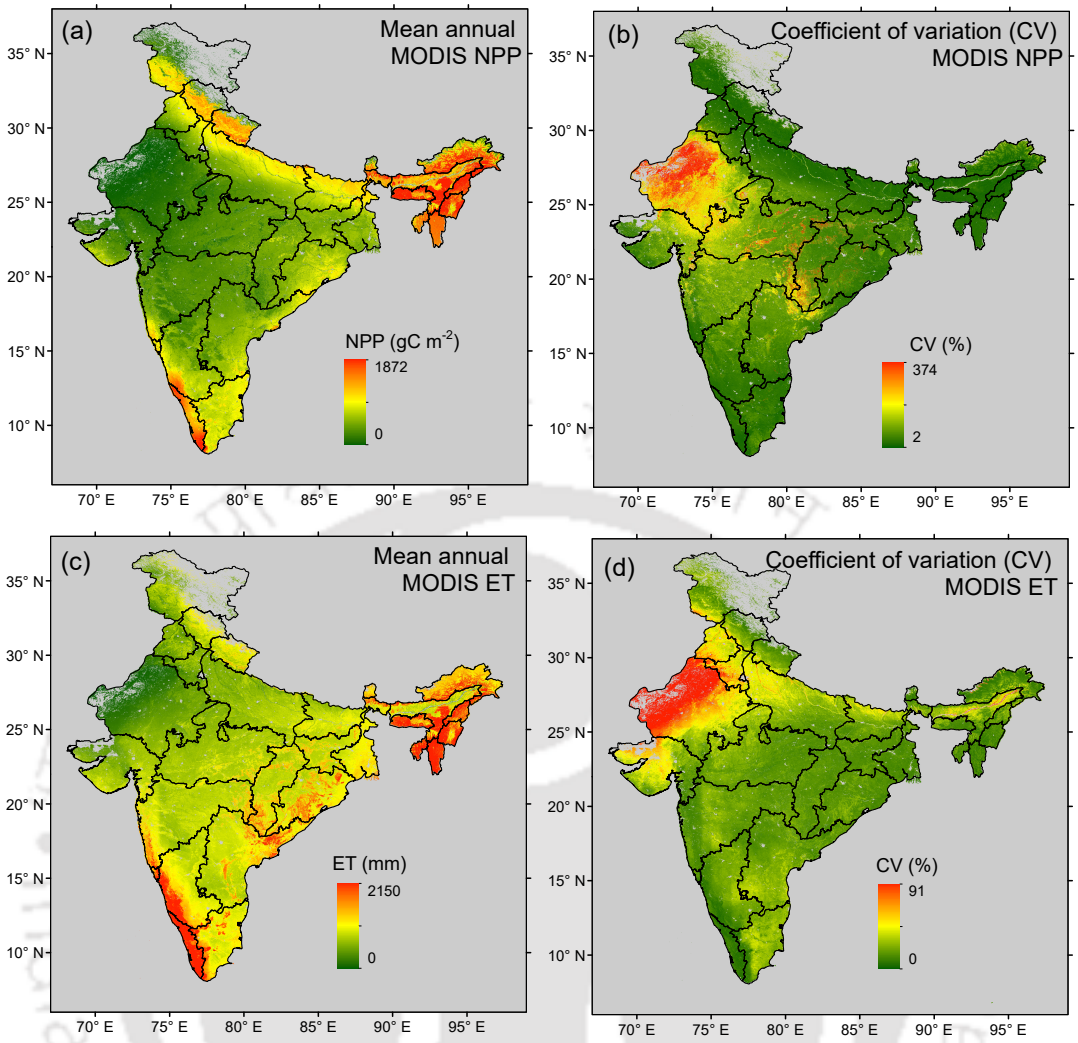

Figure 4.2: Variation in MODIS Net Primary Production (NPP) and Evapotranspiration (ET). Spatial distribution of mean (a) and coefficient of variation (CV, b) of annual MODIS NPP, and mean (c) and CV (d) of annual MODIS ET over India during 2000-2014.

the controlling factors such as precipitation, temperature and solar radiation, WUE_e showed a large spatial variation across the country. The pixel-level mean WUE_e ranged between 0 and 5.9 gC m^{-2} mm^{-1}. The spatial pattern of WUE_e was consistent with NPP, i.e., the regions with high WUE_e had higher NPP. Higher WUE_e was found along the Indo-Gangetic plains and in some parts of northeast India. Western Ghats had high NPP but showed relatively lesser WUE_e due to the high rate of ET. Some parts of north India (lower Himalayan regions) had higher WUE_e due to moderate NPP and less ET. The interannual variability (in terms of CV) in WUE_e followed the same pattern as that of NPP (Figure 4.3b), which show that WUE_e in India is controlled by NPP to a greater extent compared to ET. The CV in WUE_e was higher for the arid regions (western India)

and some parts of central India. The biome-level differences in the WUE_e are shown in Figure 4.3(c). Forests and Closed Shrublands (CS) had higher WUE_e. CS has the highest WUE_e (= 1.24 gC m^{-2} mm^{-1}) as well the highest inter-annual variability. Among different forest classes, Deciduous Broadleaf Forest (DBF) had lower WUE_e (= 0.42 gC m^{-2} mm^{-1}). Non-forest land cover classes showed relatively lesser WUE_e (< 0.6 gC m^{-2} mm^{-1}). The presence of these land covers in different regions of the country explains the WUE_e of the regions.

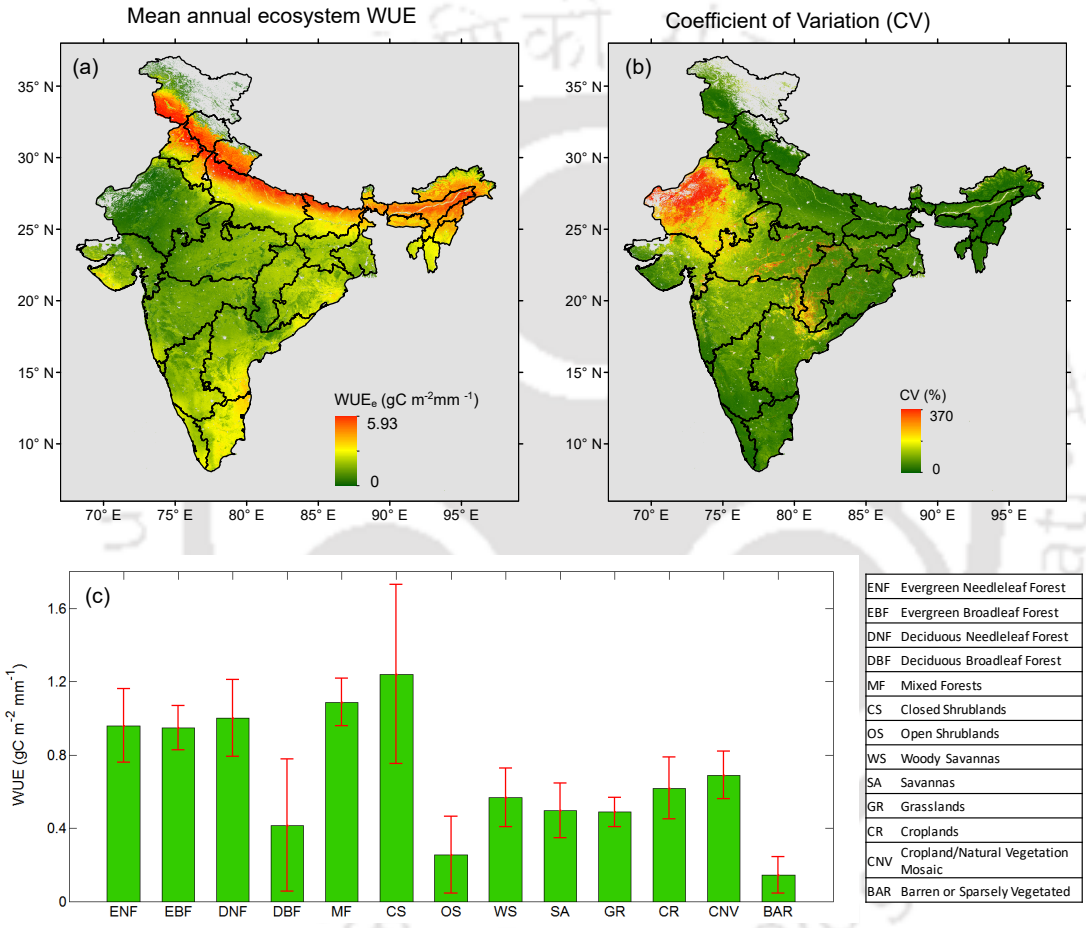

Figure 4.3: Distribution and variability of ecosystem water use efficiency (WUE_e) in India over 2000-2014. Spatial distribution of (a) mean and (b) coefficient of variation of annual WUE_e , and (c) differences in the WUE_e among different biome types. The interannual variation of biome type WUE_e in (c) is shown by the standard error bar. Lower Himalayan regions in the north and northeast India has higher WUE_e , whereas the western regions with lesser WUE_e has higher inter-annual variability. Forest and CS has higher WUE_e compared to other land covers.

4.4.3 Trend analysis of WUE_e

The trend analysis of annual WUE_e at the country level and the pixel level was carried out over the period 2000-2014. The country level average annual WUE_e showed a significant increasing trend (p-value < 0.05) with the magnitude of 0.0058 gC m^{-2} mm^{-1} yr^{-1} (Figure 4.4). Out of total vegetated area, around 21% area showed a significant increasing trend (p-value < 0.05) in WUE_e, whereas about 55% of the area had a non-significant increasing trend in the WUE_e (Figure 4.5a and 4.5b). The significant increasing trend was found for central India and some parts of western, eastern and northeastern India. Around 21% of the vegetated area had non-significant decreasing trend, and only 2% area had a significant decreasing trend. The decreasing trend was mainly found in the Indus and Brahmaputra basins, which had higher WUE_e. The magnitude of the decreasing trend in these regions was greater than 1.5 gC m^{-2} mm^{-1} yr^{-1} (Figure 4.5b). The magnitude of the increasing trend was limited to 0.07 gC m^{-2} mm^{-1} yr^{-1} in central India. The biome level trend analysis of WUE_e showed that Deciduous Broadleaf Forest (DBF) and Woody Savannas (WS) had a significant increasing trend (p-value < 0.05, Figure 4.5c). DBF had the highest increasing trend of 0.014 gC m^{-2} mm^{-1} yr^{-1}, whereas CS had the highest decreasing trend of -0.016 gC m^{-2} mm^{-1} yr^{-1}, which was statistically non-significant (p-value > 0.05). It should be noted that CS had the highest mean WUE_e (=1.24 gC m^{-2} mm^{-1}).

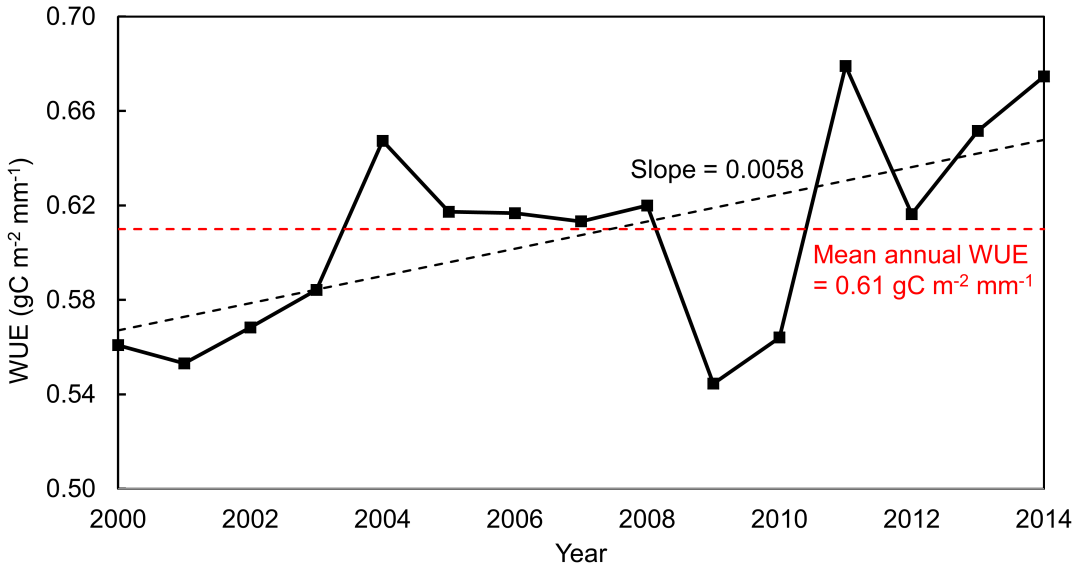

Figure 4.4: Trend analysis of annual WUE_e in India over the period 2000-2014. The dashed horizontal (red) line shows the mean annual value of WUE_e during this period.

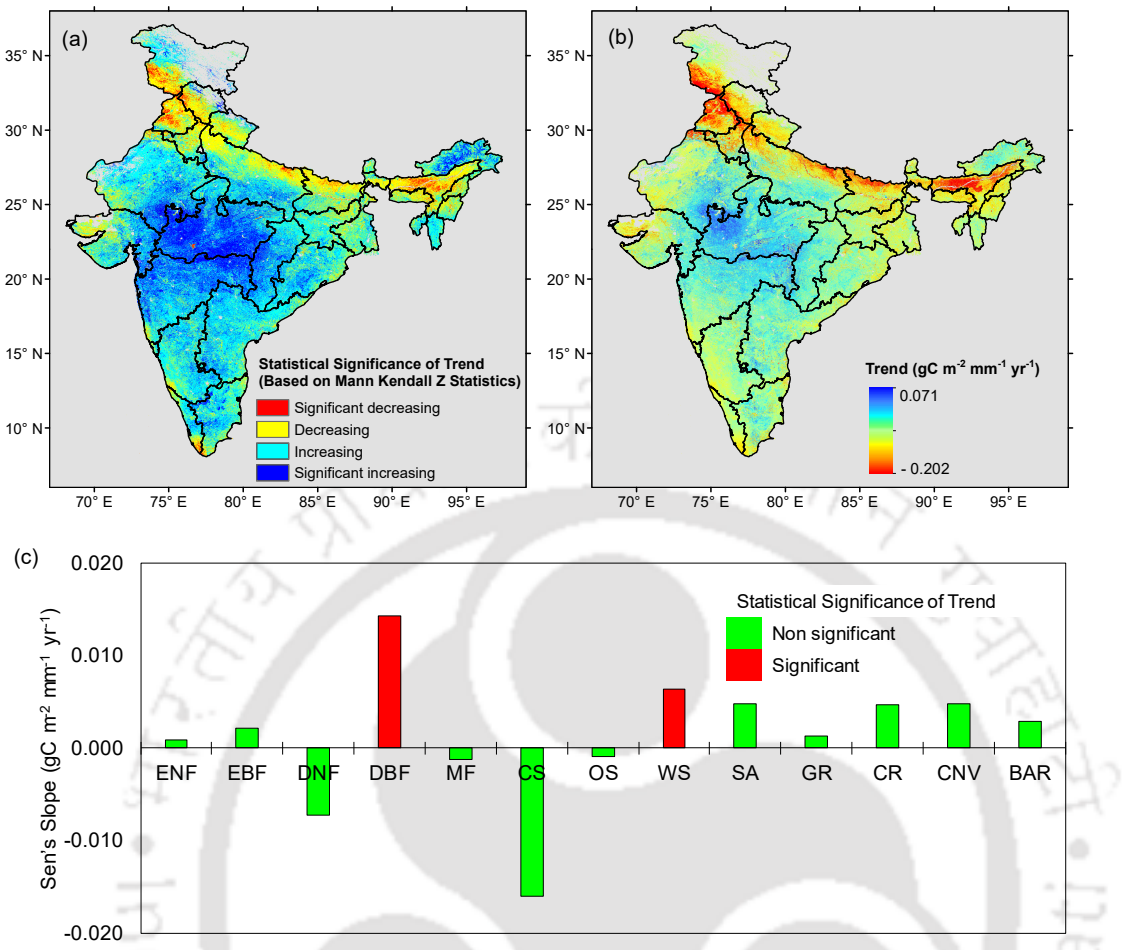

Figure 4.5: Trend analysis of annual ecosystem water use efficiency (WUE_e). (a) Mann Kendall test based statistical significance, (b) Sen's slope based magnitude of the trend and (c) Trend analysis for different biome types. The significance level was assessed at p-value < 0.05.

4.4.4 Controlling factors of WUE_e

A map of the relative contribution of different climatic constraints on vegetation growth (as per Nemani et al. (2003)) was prepared (Figure 4.6). Precipitation is the major climatic constraint on vegetation growth in most parts of the central, western, eastern and southern India, whereas both precipitation and temperature together were the climatic constraints in Western Himalayan region of north India. The vegetation growth in the forest dominated northeastern and Western Ghats regions was controlled by solar radiation. To determine the climatic factors controlling the WUE_e in different parts of the country, a correlation analysis was performed. The annual WUE_e raster was resampled to the resolution of the climatic data to carry out the pixel-level correlation analysis. Figure 4.7 shows the positive and negative correlation between the WUE_e and

climatic factors. Each pixel shows the influence of three climatic factors through the additive colour synthesis of the three prime colour (red, green and blue). Red represents the correlation between annual WUE_e and annual precipitation; green represents the correlation between annual WUE_e and annual temperature, and blue represents the correlation between the annual WUE_e and annual solar radiation. Figure 4.7 shows that WUE_e in the central parts of India had a positive correlation with precipitation and negative correlation with the temperature, which is consistent with Figure 4.6. Solar radiation was positively correlated with the WUE_e in forest dominated northeastern regions and coastal regions of south India. Both precipitation and solar radiation were positively correlated with WUE_e in the Western Ghats, whereas temperature was negatively correlated in the region. Temperature was positively correlated with WUE_e in mountainous Himalayan regions of Jammu and Kashmir, Himachal Pradesh, Uttarakhand, Sikkim and Arunachal Pradesh, which generally have low temperature due to higher elevations. Arid and semi-arid areas of western India showed a high positive correlation with precipitation.

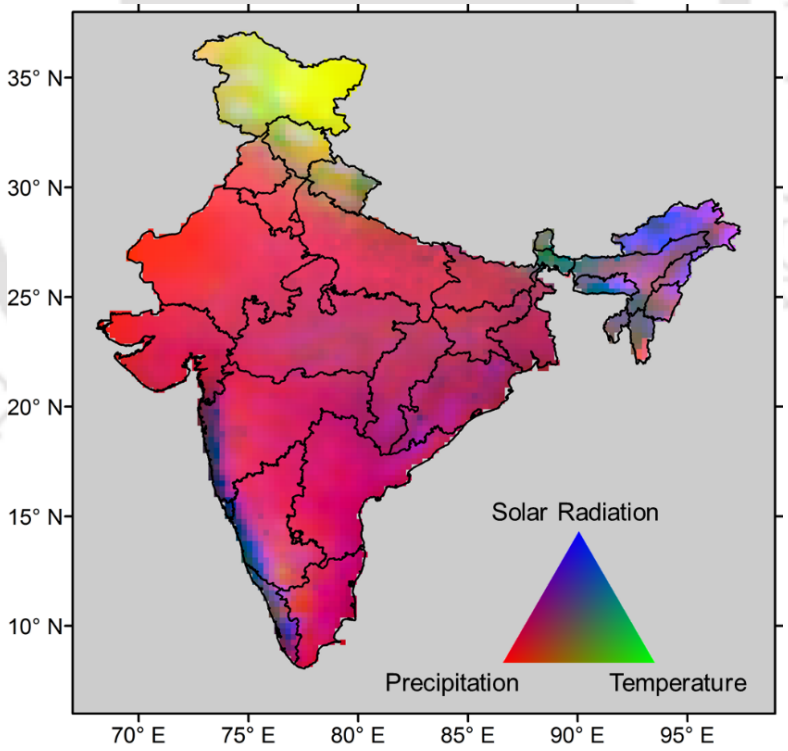

Figure 4.6: Climatic constraints on plant growth in India. Composite of red, green and blue colors is used to represent the relative contribution of water, temperature and solar radiation, respectively. Plant growth in the central and west parts of the country is constrained by precipitation. In some parts of northeast and the Western Ghats, the solar radiation controls the plant growth. Temperature is the climatic constraint in the Himalayan region of north India.

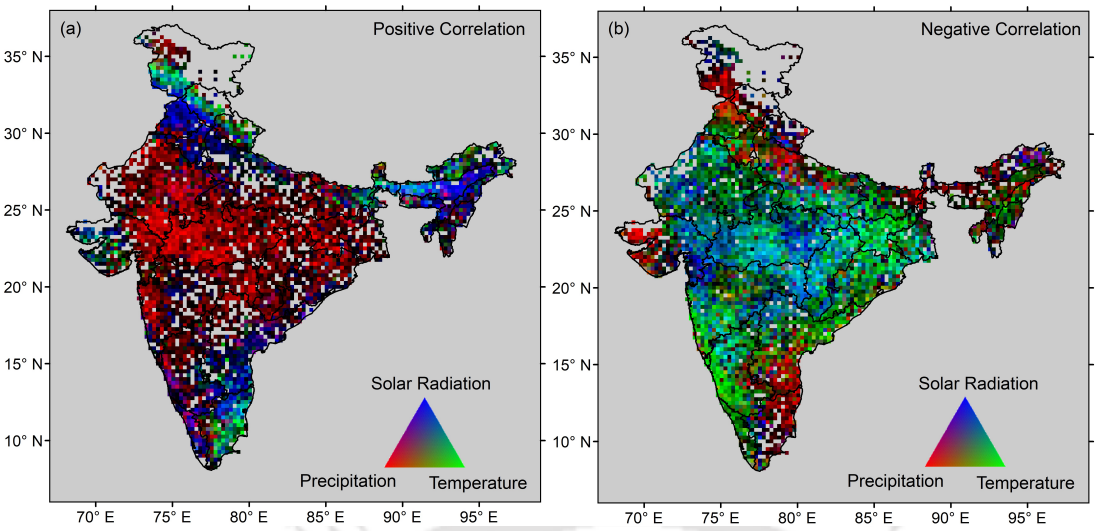

Figure 4.7: Correlation between WUE_e and climatic factors over 15 years in India. Composite of red, green and blue colors is used to represent the relative contribution of water, temperature and solar radiation, respectively.

4.4.5 State level NPP and GSDP growth

In addition to climatic factors, human activities, such as LULC alterations, deforestation, and urbanization, also affect the ecological process, which influences the vegetation productivity (i.e., NPP). To assess the impact of different development activities on the NPP, state-level comparison of Gross State Domestic Product (GSDP) and the annual NPP was carried out. The data for GSDP was obtained from Open Government Data (OGD) Platform India portal (http://data.gov.in). Every state in India has shown consistent growth in GSDP between 2000 and 2014 and hence has a monotonic increasing trend. Figure 4.8(a) shows the average NPP across different states in India. Northeastern states, such as Assam, Arunachal Pradesh, Manipur, Meghalaya, Mizoram and Nagaland had higher NPP due to the presence of vast forest cover. Kerala also had higher NPP due to the presence of Western Ghats. Rajasthan had the least NPP due to the presence of the Thar Desert and arid climate. Figure 4.8(b) shows Pearson's correlation coefficient between the annual NPP and GSDP for different states. GSDP was adopted as an indicator of industrial and infrastructural development in the states. Most of the states showed a positive correlation between NPP and GSDP, which indicated that NPP was not adversely affected by the development activities in the states. However, there was a significant negative correlation for one state, namely Meghalaya in the northeast, and non-significant negative correlation for three northeastern states, namely Assam and Nagaland in northeast and Uttarakhand in the north. Forest Survey

of India (FSI) had reported a decrease in the forest cover in these four states (FSI, 2009, 2011, 2015). Encroachment in forest land, biotic pressure, and shifting cultivation are the main reason behind the decrease in forest cover in the northeastern state, whereas diversion of forest land for development activities was the main factor in Uttarakhand (FSI, 2015).

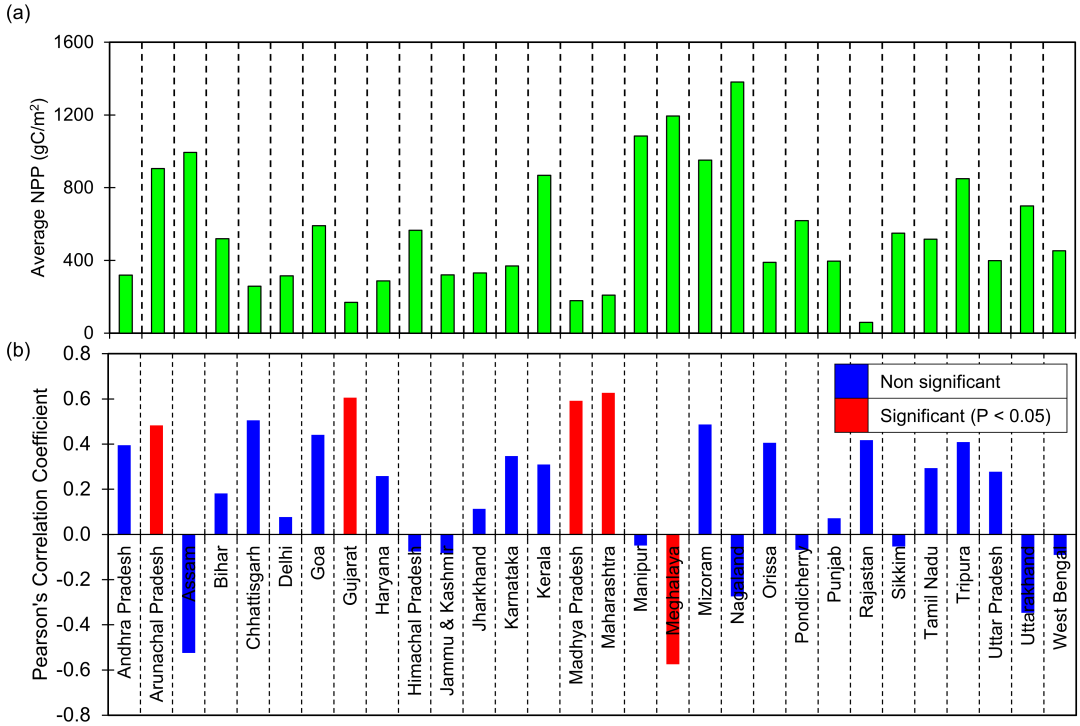

Figure 4.8: The impact of economic growth on NPP. (a) State-wise average NPP and (b) the correlation coefficient between the NPP and GSDP. Northeastern states have higher average NPP due to presence of forest. Only states with higher forest cover had negative correlation between GSDP and NPP. A decrease in forest in these states has been reported in these states.

4.4.6 Discussion on results

The spatial pattern of MODIS NPP was consistent with the previous studies (Nayak et al., 2013, 2010). Carnegie–Ames–Stanford Approach (CASA) model simulated NPP over the period 1981 to 2005 had a similar spatial variation (Nayak et al., 2013). Previous studies using MODIS data also showed a same behavior of WUE_e for different biomes (Huang et al., 2017a; Tang et al., 2017).

MODIS NPP showed a large variation between regions and biomes. In general, the northeast and the Western Ghats regions of India had higher NPP compared to rest of the country, which was consistent with the presence of forests. On the other hand, the

arid and semi-arid regions in the west had the least NPP. The inter-annual variability was higher for arid regions (i.e., western parts). The spatial pattern of NPP over India was closely related to the patterns of precipitation and land cover types.

The spatial variation in WUE_e was consistent with the previous global studies (Huang et al., 2017a). WUE_e, which relates the water and carbon cycles, showed substantial spatial variation across India. The lower Himalayan regions in Indus, Ganga and Brahmaputra river basins had higher WUE_e compared to other parts of the country, which can be attributed to the presence of the forest. These regions had higher NPP but lower ET, resulting in higher WUE_e. The differences in WUE_e of different biomes in India was similar to global studies (Huang et al., 2017a; Tang et al., 2017). In general, forest and closed shrublands had higher WUE_e. The variability in WUE_e was closely related to the variability in NPP, which indicated that the WUE_e is controlled by NPP rather than ET.

Tang et al. (2014) showed that the global annual WUE_e (calculated as the ratio of GPP and ET) had decreasing trend from 2000 to 2013. Contrastingly, a significant increasing trend (p-value < 0.05) in country-average annual WUE_e was found. This indicates that ecosystems in India responded differently to the global climate change compared to other parts of the world. The sharp decrease in WUE_e in the year 2009 can be attributed to the reduction in country average NPP ($= 318$ gC m^{-2}) in 2009 compared to mean NPP ($= 365$ gC m^{-2}) over 2000-2014. It should be noted that 2009 was a drought year and had annual precipitation of 987 mm compared to MAP of 1106 mm/year over 2000-2014. Huang et al. (2017a) showed that most parts of India had a negative correlation between drought index and WUE_e, which indicated that WUE_e in India decreases with a reduction in precipitation.

To understand the spatial variation in the trend in WUE_e, the trend analysis of three main climatic factors (precipitation, temperature and solar radiation) affecting the WUE_e was performed (Figure 4.9). The correlation analysis (Figure 4.7) suggested that WUE_e in central India was positively correlated with precipitation, and negatively correlated with temperature and solar radiation. Increasing and decreasing trends (p-value > 0.05) in precipitation and temperature, respectively, in the region, whereas the solar radiation had a decreasing trend were found. The combined effect of these factors resulted in the increasing trend in WUE_e in central India. Similarly, in the Himalayan region, the WUE_e was positively correlated with the temperature and solar

radiation. There was no significant trend found for temperature in the region, but there was a significant decreasing trend in solar radiation. Solar radiation had a significant decreasing trend in the lower Himalayan areas including the states of Punjab in the north and Assam in the northeast, which resulted in the decreasing trend of WUE_e in Himalayan regions. The highly elevated Himalayan areas (parts of the state of Sikkim and Arunachal Pradesh in the northeast) showed a significant increasing trend in WUE_e. WUE_e in these regions had a strong positive correlation with temperature as it is the main climatic constraint on vegetation growth. A non-significant increasing trend in temperature for these regions was found, which partially explains the rising trend in WUE_e.

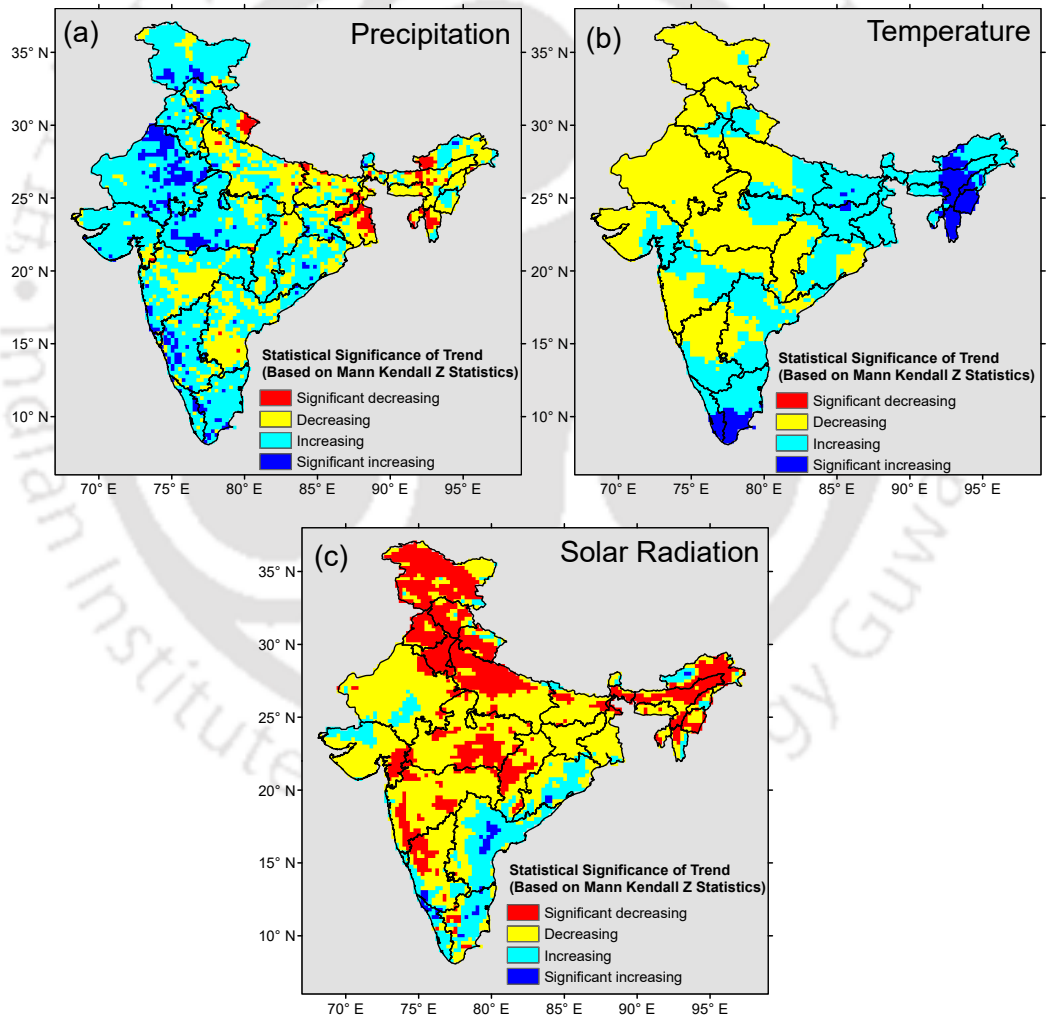

Figure 4.9: Trend analysis of main climatic variables (precipitation, temperature and solar radiation) affecting the ecosystem water use efficiency (WUE_e).

Among different biomes, most of the biomes had non-significant trends in WUE_e (p-value $>$ 0.05) except for Deciduous Broadleaf Forest and Woody Savannas. These

two biomes had significant increasing trends. Among different forest types, DBF had the least the WUE_e, but it showed the highest increasing trend. Similarly, CS had the highest WUE_e, but it showed the highest decreasing trend. This indicates that the biomes with lower WUE_e showed an increasing trend and vice versa. This is consistent with the fact that the lower Himalayan region (this region had the highest WUE_e) showed a significant decreasing trend in WUE_e.

The anthropogenic activities have affected terrestrial ecosystem productivity over the globe. India is a developing nation, which has transformed substantially in the recent past. Economic growth in India requires rapid industrialization and infrastructure development. Every state in India has shown a consistent increase in GSDP, which indicates that continuous development occurring in different sectors. GSDP in 17 states has increased more than six times between 2000 and 2014. Four states, namely Andhra Pradesh, Maharashtra, Tamil Nadu and Uttar Pradesh, had a rate of increase in GSDP greater than INR 60000 crores/years. NPP in these states was highly unstable, which shows the relationship between growth rate and fluctuation in NPP. The NPP in one state (namely Meghalaya) showed significant (p-value < 0.05) negative correlation with GSDP (Figure 4.8). The state is situated in forest dominated northeast India, and FSI had reported a decrease in the forest cover in the state, which was attributed to different anthropogenic factors such as encroachment in forest land, biotic pressure and shifting cultivation (FSI, 2015). In addition, other northeastern states such as Assam, Nagaland and Sikkim also had a negative correlation between NPP and GSDP. Uttrakhand in north India has significant forest presence (Figure 4.1b). The GSDP in Uttrakhand has increased more than 10 times between 2000 and 2014 and was negatively correlated ($= -0.3335$) with NPP. As per FSI, forest cover in Uttrakhand has reduced due to the diversion of forest land for development activities. Moreover, it can be concluded that NPP in the states having significant forest cover has been affected by economic development, whereas other states were not much affected. The conversion of one non-forest land cover to another non-forest land cover may not affect the NPP as the major non-forest land covers have similar NPP, which could be the reason that NPP didn't reflect any change for states with lesser forest cover. The terrestrial primary production is the largest global CO_2 flux, driving several ecosystem functions, and the forest is a major contributor to primary production (Beer et al., 2010). This study shows that as the development activities are happening in the forest dominated

states, the NPP is decreasing, which is mainly due to the conversion of forest to other land covers. Forests play an important role in fixing the anthropogenic carbon dioxide. Keeping in mind the increasing CO_2 concertation in the atmosphere, a decrease in the forest could worsen the conditions. This study will help understand the impact of development activities on forest and primary production.

4.5 Conclusions

The spatiotemporal variation in ecosystem water use efficiency (WUE_e = NPP/ET) and its climatic controls in India were analyzed using MODIS datasets. Higher WUE_e for northeastern regions and the lower Himalayan belt was found, whereas the arid areas of western India had the least WUE_e. The inter-annual variability in WUE_e was higher for the arid western region due to highly fluctuating rainfall patterns. Among different biome types, closed shrublands had the highest WUE_e, followed by the forests, which was consistent with previous global and regional studies. Trend analysis of national average WUE_e indicated an increasing trend with a magnitude of 0.0058 gC m^{-2} mm^{-1} yr^{-1}, which did not follow the decreasing trend of global average WUE_e as reported by past studies. The spatial assessment of the trend in WUE_e revealed a significant increasing trend in central India and a significant decreasing trend along the lower Himalayan belt. Analysis of climatic factors affecting WUE_e showed that precipitation was positively correlated with WUE_e in central and western India, whereas temperature was negatively correlated in these regions. Solar radiation was positively correlated along the lower Himalayan belt, whereas precipitation was negatively correlated in this region. Temperature was positively correlated with WUE_e in mountainous Himalayan regions. India is one of the fastest growing economies. To assess the impact of development activities on NPP, Pearson's correlation coefficient-based analysis between NPP and gross state domestic product (GSDP) was carried out. Most of the states had a positive correlation between NPP and GSDP, which indicated that development activities were not adversely affecting the NPP. However, four states (3 from northeast India and 1 from north India) showed a negative correlation, which indicated that NPP is reducing in these states as GSDP is growing. Forest Survey of India (FSI) had also reported a reduction in forests in these states in recent decades, which was attributed to different human activities.

5

Hydrological Resilience in Teesta River Basin

5.1 Introduction

The assessment of the impacts of climate change on regional hydrology plays a vital role in the management of water resources. The scientific community has utilized different tools such as climate, hydrological, ecological or biological models to predict the potential impacts of climate change on different natural systems (Fowler et al., 2007; Pearson and Dawson, 2003; Xu et al., 2005). In the field of hydroclimatology, the standard approach for impact assessment consists of the use of GCMs and hydrological modelling. The GCMs provide future climate projections based on different greenhouse gasses emission scenarios (Taylor et al., 2009). These climate projections are then forced into hydrological models to simulate future hydrology for a region/basin. This standard practice has been used at multiple scales across the globe (Xu et al., 2005).

This study presents a resilience-based climate change impact assessment for a river basin in India. Several studies have been carried out in different parts of the country, highlighting the adverse impact of climate change on hydrology or water resources (Gosain et al., 2011, 2006; Mishra and Lilhare, 2016; Shah and Mishra, 2016). These studies focused on the assessment of gradual changes in hydroclimatic variables such as precipitation, streamflow, temperature etc. or climate extremes. However, extreme events are a bigger threat than gradual changes (Sillmann and Roeckner, 2008). Therefore, it is crucial to understand the response of natural systems to extreme events. This study focuses on the analysis of the response of a river basin to extremely dry conditions under the projected climate. The water availability during the dry period (i.e., mete-

orological drought) is dependent on streamflow generated from the water storage in subsurface or melting of snow/ice (Andermann et al., 2012). These transient reservoirs of water are strongly dependent on the wet period precipitation characteristics such as timing, amount and form (i.e., snow or rain) (Andermann et al., 2012). Snowmelt forms a substantial contribution to the annual discharge in the Himalayan catchments (Bookhagen and Burbank, 2010).

The mountainous regions of India (in Western and Eastern Himalayas) are immensely affected by the climate change (Bhutiyani et al., 2010; Shekhar et al., 2010; Singh and Goyal, 2016, 2017b). A consistent increase in temperature is leading to precipitation in the form of rainfall than snowfall. Accumulated snow/ice acts as a reservoir of water, which maintains the river flow during the melt season. Lesser snowfall and accelerated melting are affecting the streamflow patterns.

5.2 Study Area

The Teesta River basin in the eastern Himalayan region of India was chosen as the study area of this work. The basin is located between the latitudes 27 °N and 28 °N and longitudes 88 °E and 90 °E (Figure 5.1). The total area of the basin is 7,733 km^2 and covers the state of Sikkim. The elevation in the basin varies from 200 m to 8376 m, with an average value of 3292 m and a standard deviation of 1625 m. The climate in the basin ranges from sub-tropical in the south to tundra in the north. The mean annual precipitation in the basin was 2779 mm during the period from 1951 to 2010. The mean daily maximum and minimum temperatures for the same period were 13.7 °C and 1.87 °C, respectively. Forest and Grassland are the most dominant land cover types in the basin covering 46% and 30% area, respectively, in the basin followed by Snow/Ice (12.2%). Cropland covers only 5% of the basin area. The basin has an urban area on only 0.02% of the basin area, which is very less maintained. Sikkim is very less populated and accounts for only 0.05% of the total population of India. The basin was divided into eight subbasins (SBs) based on the elevation variation and the tributaries (as shown in Figure 5.1).

Limited amount of observed streamflow data was available due to the presence of basin in high mountainous terrain. Therefore, hydrological modelling was carried out for simulation of hydrological components in basins. The resilience analysis was carried out on simulated streamflow.

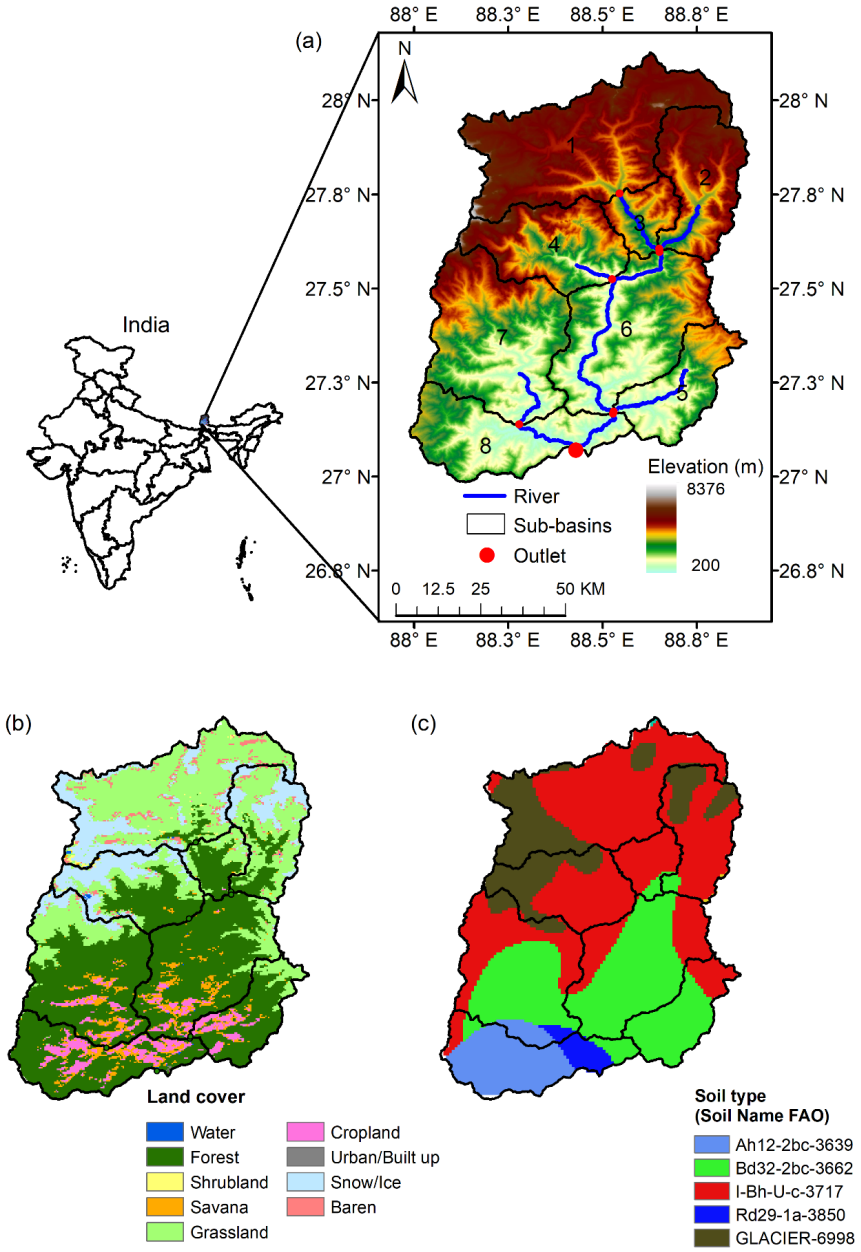

Figure 5.1: Geographic, topographic, land use/land cover type and soil type description of the basin. (a) Location of basin in India and the elevation variation in the basin. (b) Variation in different land covers in the basin. (c) Variation in the soil type in the basin.

5.3 Input data

5.3.1 Meteorological data

High resolution (0.25° × 0.25°) gridded precipitation dataset was obtained from IMD (Pai et al., 2014). The data is available from 1901 to 2015. IMD provides temperature data at coarse resolution (1° × 1°), which was not suitable for this study. Therefore,

temperature data (i.e., maximum and minimum daily temperature) from Sheffield et al. (2006) was used. The dataset was developed by Terrestrial Hydrology Research Group, Princeton University and is available at 0.25° × 0.25° resolution. Mishra et al. (2014) used this temperature dataset and compared with the IMD temperature records for the overlapping period (1969-2005) in India. The comparison suggested that temperature data from Sheffield et al. (2006) follows the seasonal cycle and temporal and spatial variability in India.

5.3.2 Observed streamflow data

The basin is located on the hilly Himalayan range, and data scarcity is a major issue. Daily streamflow data at Teesta Bazar gauging station was obtained from Central Water Commission (CWC). The data was available from January 2001 to December 2010. First six years data was used for calibration of the hydrological model, whereas the remaining four years data was used for validation purpose.

5.3.3 GCM data

Daily outputs of precipitation and air temperature were obtained from the CMIP5 based GCMs. These GCMs provide outputs for four RCPs. Two RCPs, RCP4.5 (medium mitigation scenario) and RCP8.5 (high emissions scenario), were used, which assumes that radioactive forcing will increase to 4.5 Wm^{-2} and 8.5 Wm^{-2}, respectively, by the end of the twenty-first century (Taylor et al., 2009). To take into account uncertainty in the climate model projections, four different GCMs, namely Centre National de Recherches Météorologiques Coupled Global Climate Model, version 5 (CNRM-CM5), Geophysical Fluid Dynamics Laboratory Coupled Physical Model version 3 (GFDL-CM3), Geophysical Fluid Dynamics Laboratory Earth System Model 2M with the Modular Ocean Model version 4.1 (GFDL-ESM2M), and Geophysical Fluid Dynamics Laboratory Earth System Model 2G with Generalized Ocean Layer Dynamics (GOLD) (GFDL-2G) were used. The outputs for precipitation and temperature for these GCMs were obtained for two RCPs (i.e., RCP4.5 and RCP8.5) and the historical run. Nine GCM grids covering the study area were selected, and their outputs were adjusted to sub-basin centroids using Inverse distance weighted (IDW) interpolation technique.

5.3.4 Inputs for hydrological modelling

For hydrological modelling of the basin, Soil and Water Assessment Tool (SWAT) was used. SWAT is discussed in Section 5.4.2. SWAT requires different spatial and temporal input data. One of the most important spatial inputs required for hydrological modelling is the Digital Elevation Model (DEM), which is used for generating the topographic characteristics of the basins. The choice of DEM affects many processes in hydrological modelling such as runoff generation, flow routing, sediment export, and transport etc. The effect of DEM on SWAT model has been widely studied. For example, Goyal et al. (2018) studied the effect of different DEM scenarios of varying resolution, sources and resampling methods on two catchments in India. One of the catchments is a part of the river basin in the present study. The study highlighted that the choice of DEM affected topographic characteristics in the Himalayan basin (Upper Teesta basin). In this study, ASTER GDEM v2 (≈30 m) was used, which is the second version of ASTER DEM released in October 2011. It was produced using elevations recorded by ASTER instrument aboard Terra satellite of NASA. This version has better horizontal and vertical accuracy, good quality water body coverage and detection with 260,000 additional stereo-pairs, enhancing coverage and decreasing data artefacts (http://asterweb.jpl.nasa.gov/GDEM.ASP). The other important spatial input for SWAT is LULC map due to its significant impacts on water quality and quantity processes such as surface runoff, groundwater, and non-point source (NPS) pollutions (Babar and Ramesh, 2015). LULC classification used in the present study is Moderate-resolution Imaging Spectroradiometer (MODIS) based Collection 5.1 MCD12Q1 land cover type data and was obtained from the USGS Land Cover Institute (LCI, https://landcover.usgs.gov/global_climatology.php). A soil map is used for the soil characterization in the model. Soil map was obtained from the Food and Agriculture Organization (FAO) (http://www.fao.org/soils-portal/soil-survey/soil-maps-and-databases/harmonized-world-soil-database-v12/en/).

SWAT requires five meteorological parameters: precipitation, temperature (daily maximum and minimum), net solar radiation, relative humidity, and wind speed. These variables are needed at daily temporal resolution. Precipitation was obtained from IMD, whereas the Temperature data was obtained from Terrestrial Hydrology Research Group, Princeton University (Sheffield et al., 2006). Data for remaining variables (net solar radiation, relative humidity, and wind speed) was obtained from the SWAT model's

'Global Weather Data for SWAT' portal (available at https://globalweather.tamu.edu/). These datasets were developed based on the National Centers for Environmental Prediction (NCEP) Climate Forecast System Reanalysis (CFSR) (Dile and Srinivasan, 2014; Fuka et al., 2014).

5.4 Methodology

The study was conducted in three steps: 1) Analysis of precipitation, temperature and climate extremes for past/observed climate and projected climate; 2) Set up of a SWAT model for Teesta River basin and its calibration using SWAT-CUP; and 3) Resilience analysis of the basin using SWAT-simulated streamflow. Following methods were used in this study:

5.4.1 Bias correction of GCM outputs

The outputs from the GCMs are generally biased and are rarely used directly. The bias arises due to the systematic errors in the climate model simulations, which occur because of the limited spatial resolution and simplified physics and thermodynamics. Our lack of understanding of different atmospheric processes also leads to deviation of model outputs from the actual scenarios. Therefore, it becomes essential to bias-correct the GCM outputs so that it adequately represents the actual climatic patterns of the regions. Many techniques have been used by researchers for the bias correction of climatic variables. For this work, methods suggested by Mahmood and Babel (2013) was used. The bias in precipitation was estimated as the ratio of long-term observed monthly mean precipitation data (IMD data in this study) to the same values obtained from the GCMs simulated data (historical run). The bias correction in the future/projected daily time series was carried out by multiplying this ratio with the daily time series of their respective months. The bias in temperature was estimated as the difference between the mean monthly temperature values from GCM's historical run and the long-term monthly mean value of observed temperature data over the same duration. The bias-corrected temperature for the projected period was obtained by subtracting this calculated bias from projected temperature time series. Observed precipitation and temperature datasets were used for the bias correction of model outputs. The bias-corrected data for the observed period was compared with observed data in terms of magnitude and frequencies.

Following equations were used for bias-correction of daily precipitation and tem-

perature data (Mahmood and Babel, 2013):

$$P_{deb} = P_{rcp} \times \left(\frac{\overline{P_{obs}}}{\overline{P_{gcm}}} \right) \tag{5.1}$$

where P_{deb} represents the de-biased daily precipitation timeseries for future/projected period. P_{rcp} represents the RCP's data from GCMs. $\overline{P_{obs}}$ and$\overline{P_{gcm}}$ are the mean monthly values of observed precipitation and historical simulation precipitation, respectively.

$$T_{deb} = T_{rcp} - \left(\overline{T_{gcm}} - \overline{T_{obs}} \right) \tag{5.2}$$

where T_{deb} represents the de-biased daily temperature timeseries for future/projected period. T_{rcp} represents the RCP's temperature data from GCMs. $\overline{T_{obs}}$ and $\overline{T_{gcm}}$ are the mean monthly values of observed temperature and historical simulation temperature, respectively.

5.4.2 Hydrological modelling using SWAT

SWAT, developed by United States Department of Agriculture (USDA) Agricultural Research Service (ARS), is a semi-distributed, continuous time step, physically based, computationally efficient model (Arnold et al., 1998, 1993). The model was developed to quantify the influence of different agricultural and management practices on water discharge, sediment and non-point source (NPS) chemical yields (Arnold et al., 1998; Neitsch et al., 2011; Srinivasan et al., 1998). It is one of the most widely used hydrological models for simulation of water flows, sediment exports, and nutrient cycling. It is capable of working for watershed ranging in area from a few hundred to several thousand km^2. The model is physically based and requires a large set of spatial and temporal data (Arnold et al., 2012). SWAT has different components which include weather, hydrology, soil temperature and properties, plant growth, nutrients, pesticides, bacteria and pathogens, and land management (Arnold et al., 2012). In SWAT, the basin is divided into several sub-basins based on the topographical characteristics. The sub-basins are further divided into hydrological response units (HRUs), which are the smallest spatial units of the model. An HRU consists of unique homogeneous combinations of the slope, soil and land use properties in a sub-basin (Neitsch et al., 2011). The basic water balance equation used by SWAT to simulate the hydrologic cycle is (Neitsch et al.,

2011):

$$SW_t = SW_0 + \sum_{i=1}^{t} (R_{day} - Q_{surf} - E_a - w_{seep} - Q_{gw}) \tag{5.3}$$

where $SW_t$and SW_0 represents the final and initial soil water content (mm/d), respectively; t represents the time step (in days); R_{day} represents the precipitation amount on i^{th} day (mm); Q_{surf} represents the amount of surface runoff on i^{th} days (mm); E_a is the amount of evapotranspiration on i^{th} day (mm); w_{seep} represents the amount of water percolating for the vadose zone on i^{th} day (mm); and Q_{gw} represents the return flow on i^{th} day (mm).

SWAT has two alternative methods to simulate the surface runoff: 1) Soil Conservation Service (SCS) Curve Number (CN) method (USDA, 1972), and 2) the Green & Ampt infiltration method (Green and Ampt, 1911). SCS-CN method was used in this study.

5.4.3 Calibration and uncertainty analysis using SWAT-CUP

Hydrological modelling is subjected to large uncertainty, which can mainly be divided into three types: conceptual model uncertainty, input uncertainty, and model parameter uncertainty. SWAT – Calibration and Uncertainty Programs (SWAT-CUP) is a public domain program that integrates different calibration/uncertainty analysis procedures for SWAT model (Abbaspour, 2007). These procedures include Sequential Uncertainty Fitting (SUFI2), Particle Swarm Optimization (PSO), Generalized Likelihood Uncertainty Estimation (GLUE), solution parameters (ParaSol), and Mark chain Monte Carlo (MCMC) (Abbaspour et al., 2004; Abbaspour, 2007). In this work, SUFI2 procedure was used for the calibration and uncertainty analysis of the SWAT model. SUFI2 procedure incorporates the uncertainty from different sources in the form of ranges of parameters (uniform distribution). The uncertainty in the model output due to parameter uncertainty is propagated using Latin hypercube sampling. The uncertainty is expressed as 95% probability distributions (95PPU), which are calculated at 2.5% and 97.5% levels of the cumulative distribution of output variable. The SUFI2 algorithm aims at enveloping most of the observation in 95PPU band of model output, which is assessed based on two statistics: P-factor and R-factor. P-factor represents the percentage of the observed data enveloped by 95PPU band, whereas R-factor represents the

thickness of 95PPU band (Abbaspour, 2007).

The performance of the SWAT model was assessed based on the following statistics:

1. Coefficient of Determination (R^2)

R^2 indicates the proportion of variance in the dependent variable that is predictable from the independent variable. The higher value of R^2 (close to 1) indicates that the model accurately replicates the observed values. It is calculated using equation below.

$$R^2 = \frac{\left[\sum_i \left(Q_{m,i} - \overline{Q_m}\right)\left(Q_{s,i} - \overline{Q_s}\right)\right]^2}{\sum_i \left(Q_{m,i} - \overline{Q_m}\right)^2 \sum_i \left(Q_{s,i} - \overline{Q_s}\right)^2} \tag{5.4}$$

where Q is a variable (e.g., discharge), and m and s stand for measured and simulated, respectively. i is the i^{th} measured or simulated data. The bar stands for average.

2. Nash-Sutcliffe Efficiency (NSE)

NSE is widely used in hydrological studies to assess the predictive performance of models (Nash & Sutcliffe, 1970). It ranges from - ∞ to 1. The value of NSE = 1 indicates a perfect match, whereas NSE = 0 suggests that the model predictions are as accurate as the mean of observed data. It is mathematically calculated using the equation below.

$$NSE = 1 - \frac{\sum_i \left(Q_{s,i} - Q_{m,i}\right)^2}{\sum_i \left(Q_{m,i} - \overline{Q_m}\right)^2} \tag{5.5}$$

where Q is a variable (e.g., discharge), and m and s stand for measured and simulated, respectively, and the bar stands for average. i is the i^{th} measured or simulated data.

5.4.4 Resilience analysis

The resilience analysis was performed on the SWAT-simulated streamflow for past as well as projected climates. The resilience was assessed based on two measures (Figure 5.2):

1. Deviation from normal:

It represents the deviation in the value of system function from the baseline sce-

nario. The baseline scenario was computed based on the long-term monthly average of the system function. The deviation is expressed in terms of percent change in system function.

2. Time to recover:

It is the number of months the system function takes to return to the normal state. The number of months is counted from the month for which the deviation goes below -10% up to the month for which the deviation goes above -10%.

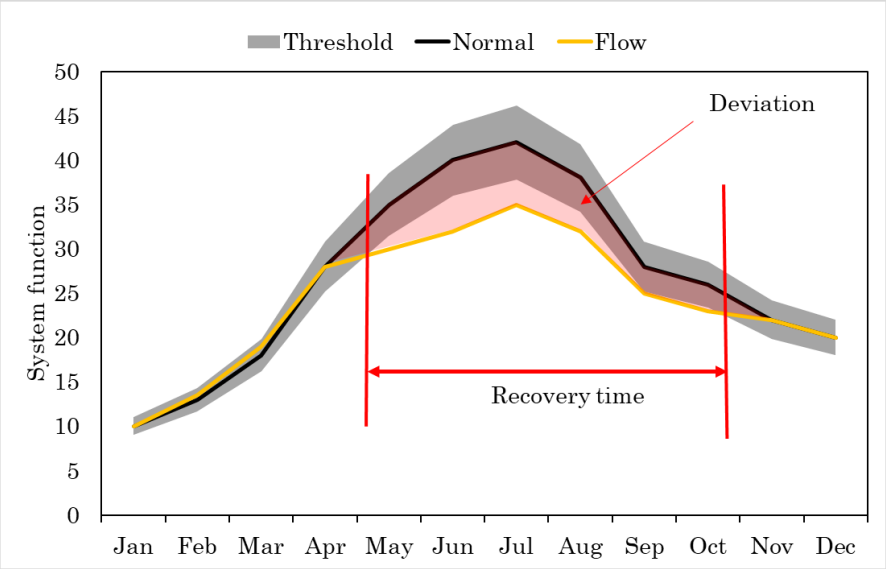

Figure 5.2: Computation of "Recover time" and "Deviation".

The disturbance in this study is the dry period, which was identified based on a drought index. The Standardized Precipitation Index (SPI) was used (Mckee et al., 1993). SPI is one of the most widely used drought indices (Dalezios, 2017). It was proposed by Mckee et al. (1993) and, after that, has been used in many drought studies (Kumar et al., 2009). It represents the actual precipitation in terms of the standardized departure from precipitation probability distribution function (PDF). It can effectively be used for comparisons of drought conditions across space and time. SPI is described in Section 3.2.3.

5.4.5 Trend analysis

The non-parametric Mann-Kendall (MK) trend test (Mann, 1945; Kendall, 1975) was used to determine the trends in precipitation, temperature and streamflow. The statistical significance of the trend was assessed at a significance level of 0.05. MK test is described in Section 3.2.4

5.4.6 Climate Extremes

The Expert Team (ET) on Climate Change Detection and Indices (ETCCDI) jointly sponsored by the World Meteorological Organization (WMO) Commission of Climatology (CCI) and the Climate Variability and Predictability (CLIVAR) project developed 27 indices for monitoring the changes in climate extremes (Peterson, 2005). The computation of these indices requires daily precipitation and temperature (minimum and maximum) dataset. In this study, 9 precipitation and 14 temperature indices were used (listed in Table 5.1). All indices used in this study were calculated on an annual basis from 1951-2100. The whole time period (1951-2100) was divided into five parts: observed period from 1951 to 1980 (P1), observed period from 1981 to 2010 (P2), bias-corrected data period from 2011 to 2040 (F1), bias-corrected data period from 2041 to 2070 (F2), and bias-corrected data period from 2071 to 2100 (F3).

Table 5.1: List of extreme indices of temperature and precipitation as recommended by the ETCCDI along with their definition.

S. N.	Index	Index name	Index definition	Units
1	TN10p	Cool nights	Let Tn_{ij} be the daily minimum temperature on day i in period j and let $Tn_{in}10$ be the calendar day 10th percentile centered on a 5-day window. The percentage of days in a year is determined where $Tn_{ij} < Tn_{in}10$	%
2	TX10p	Cool days	Let Tx_{ij} be the daily maximum temperature on day i in period j and let $Tx_{in}10$ be the calendar day 10th percentile centered on a 5-day window. The percentage of days is determined where $Tx_{ij} < Tx_{in}10$	%
3	TN90p	Warm nights	Let Tn_{ij} be the daily minimum temperature on day i in period j and let Tn_in 90 be the calendar day 90th percentile centered on a 5-day window. The percentage of days is determined where $Tn_{ij} > Tn_{in}90$	%
4	TX90p	Warm days	Let Tx_{ij} be the daily maximum temperature on day i in period j and let Tx_in 90 be the calendar day 90th percentile centered on a 5-day window. The percentage of days is determined where $Tx_{ij} > Tx_{in}90$	%
5	TXx	Max Tmax	Let Tx_{kj} be the daily maximum temperature in month k, period j. The maximum daily maximum temperature each month is then $TXx_{kj} = max(TX_{kj})$	°C
6	TXn	Min Tmax	Let Tx_{kj} be the daily maximum temperature in month k, period j. The minimum daily maximum temperature each month is then $TXx_{kj} = min(TX_{kj})$	°C
7	TNx	Max Tmin	Let Tn_{kj} be the daily minimum temperature in month k, period j. The maximum daily minimum temperature each month is then $TNx_{kj} = max(TN_{kj})$	°C
8	TNn	Min Tmin	Let Tn_{kj} be the daily minimum temperature in month k, period j. The minimum daily minimum temperature each month is then $TNn_{kj} = min(TN_{kj})$	°C
9	FD	Frost days	Let Tn_{ij} be the daily minimum temperature on day i in period j. Count the number of days where $Tn_{ij} < 0$ °C	days

10	ID	Ice days	Let Tx_{ij} be the daily maximum temperature on day i in period j. Count the number of days where $Tx_{ij} < 0$ ℃	days
11	SU	Summer days	Let Tx_{ij} be the daily maximum temperature on day i in period j. Count the number of days where $Tx_{ij} > 25$ ℃	days
12	TR	Tropical nights	Let Tn_{ij} be the daily minimum temperature on day i in period j. Count the number of days where $Tn_{ij} > 20$ ℃	days
13	GSL	Growing Season length	Let T_{ij} be the mean temperature on day i in period j. Count the number of days between the first occurrence of at least six consecutive days with $T_{ij} > 5$ ℃ and he first occurrence after 1st July (NH) or 1st January (SH) of at least six consecutive days with $T_{ij} < 5C$	days
14	DTR	Diurnal temperature range	Let Tn_{ij} and Tx_{ij} be the daily minimum and maximum temperature respectively on day i in period j.If I represents the number of days in j, then $DTR_j = \sum \frac{(Tx_{ij} - Tn_{ij})}{I}$?	
15	RX1day	Max 1-day precipitation amount	Let RR_{kj} be the precipitation amount for the 1-day interval ending k, period j. Then maximum 1-day values for period j are $Rx1day_j = max(RR_{kj})$	mm
16	RX5day	Max 5-day precipitation amount	Let RR_{kj} be the precipitation amount for the 5-day interval ending k, period j. Then maximum 5-day values for period j are $Rx5day_j = max(RR_{kj})$	mm
17	SDII	Simple daily intensity index	Let RR_{wj} be the daily precipitation amount on wet days, $RR \geq 1mm$ in period j.If W represents number of wet days in j, then $SDII_j = \frac{\sum_{w=1}^{W} RR_{wj}}{W}$	mm/d
18	R10	Number of heavy precipitation days	Let RR_{ij} be the daily precipitation amount on day i in period j. Count the number of days where $RR_{ij} \geq 10mm$	days
19	R20	Number of very heavy precipitation days	Let RR_{ij} be the daily precipitation amount on day i in period j. Count the number of days where $RR_{ij} \geq 20mm$	days
20	CDD	Consecutive dry days	Let RR_{ij} be the precipitation amount on day i in period j. Count the largest number of consecutive days where $RR_{ij} < 1mm$	days
21	CWD	Consecutive wet days	Let RR_{ij} be the daily precipitation amount on day i in period j. Count the largest number of consecutive days where $RR_{ij} > 1mm$	days

22	R95p	Very wet days	Let RR_{wj} be the daily precipitation amount on a wet day w ($RR_{ij} \geq 1.0mm$) in period j and let $RR_{wn}95$ be the 95th percentile of precipitation on wet days in the 1961-1990 period. If W represents the number of wet days in the period, then $R95p_j = \sum_{w=1}^{W} RR_{wj}$ where $RR_{wj} > RR_{wn}95$	mm
23	PRCP TOT	Annual total wet-day precipitation	Let RR_{ij} be the daily precipitation amount on day i in period j.If I represents the number of days in j, then $PRCPTOT_j = \sum(RR_{ij})$	mm

5.5 Results and discussion

5.5.1 Bias correction of precipitation and temperature

The precipitation and temperature outputs of GCMs were bias-corrected separately for every SB. The outputs from the historical run of the GCMs and observed data were used for bias correction. The bias-corrected precipitation and temperature for the historical period (i.e., 1975 to 2005) were compared with the observed data for the same period. R^2 between the observed and bias-corrected precipitation and temperature for 1975-2005 on a daily basis was checked. Also, the differences in mean daily values of observed and bias-corrected precipitation and temperature were also evaluated. A criterion of R^2 greater than 0.75 and difference less than 0.05 was set for selecting the GCMs. Figure 5.3 shows the R^2 value for bias-corrected daily precipitation and temperature, which was found reasonably good for all four models.

5.5.2 Basin average analysis of precipitation and temperature

Figure 5.4 shows the annual precipitation, daily maximum (Tmax) and daily minimum temperature (Tmin) for the basin over the period from 1951 to 2100. For the period from 1951 to 2010, the observed data is shown, whereas, for the period from 2011 to 2100, the bias-corrected data from GCMs is shown. Precipitation had a decreasing trend during the period from 1951 to 2010, which was not statistically significant (p-value $>$ 0.05). For the projected climate, an increasing trend was found for both RCP4.5 and RCP8.5 (p $<$ 0.05). Both RCP4.5 and RCP8.5 showed equivalent precipitation amounts before 2070, whereas the RCP8.5 scenario showed considerably higher precipitation after 2070. The basin is expected to receive higher precipitation under the climate change scenarios. Tmax showed an increasing trend (p-value $<$ 0.05) during

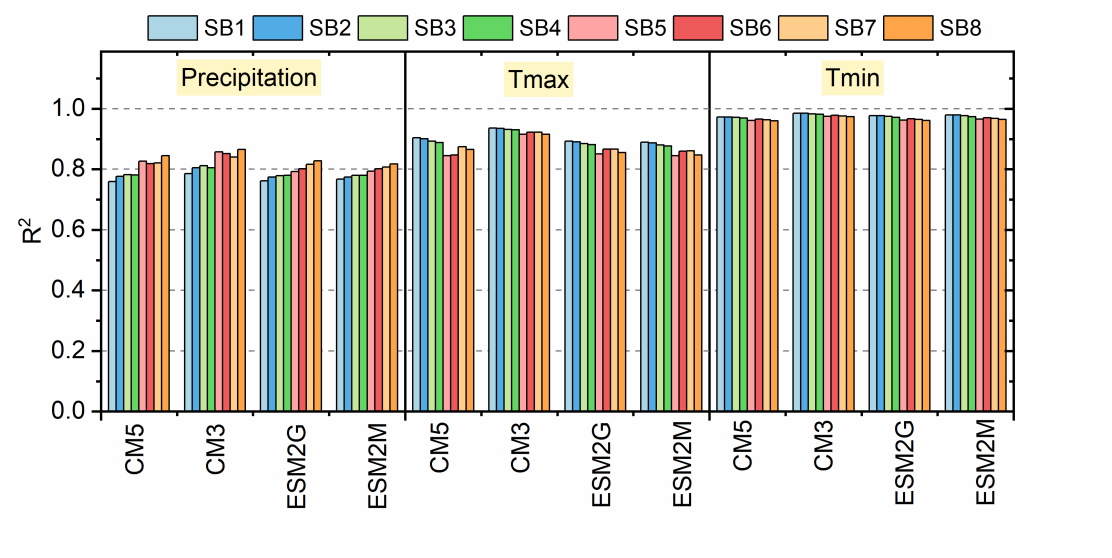

Figure 5.3: Coefficient of determination (R^2) between the observed and bias-corrected precipitation, daily maximum temperature (Tmax) and daily minimum temperature (Tmin) for the period from 1975 to 2005.

the period from 1951 to 2010. The increasing trend escalated under GCM based projections for the period from 2011 to 2100. Both RCPs had consistency in terms of the rising trend in Tmax, but the RCP8.5 projected about 2 °C higher temperature at the end of the 21st century compared to RCP4.5. Tmin followed the same trend as Tmax. Tmin showed an increasing trend during both the observed period and projected period. The difference between RCP8.5 and RCP4.5 projections, in this case, was more than 2°C by the end of the 21st century. The findings of this analysis are consistent with the previous studies within the basin (Goswami et al., 2018; Singh et al., 2017). As the basin is located in the Himalayan region and receives snowfall, the increasing trend in temperature is expected to disrupt the snow patterns over the area. Previous studies over the eastern Himalayas have reported the decrease in snow cover and glacial extent (Krishna, 2005; Racoviteanu et al., 2015).

Figure 5.5 shows the boxplots for precipitation, Tmax and Tmin over three 40-year periods: 1) P1: Observed climate (1971 to 2010), 2) P2: Projected climate (2021 to 2060), and 3) P3: Projected climate (2061 to 2100). Precipitation increased for P2 and P3 compared to P1 for both RCPs, which was consistent with the increasing trend in annual precipitation (as shown in Figure 5.4). One-way ANOVA test indicated that mean of precipitation for P1, P2 and P3 were significantly different ($p < 0.05$). The mean precipitation values for Observed (P1), RCP4.5 (P2), RCP4.5 (P3), RCP8.5 (P2) and RCP8.5 (P3) were 2826 mm, 2966 mm, 3093 mm, 2981 mm and 3414 mm, re-

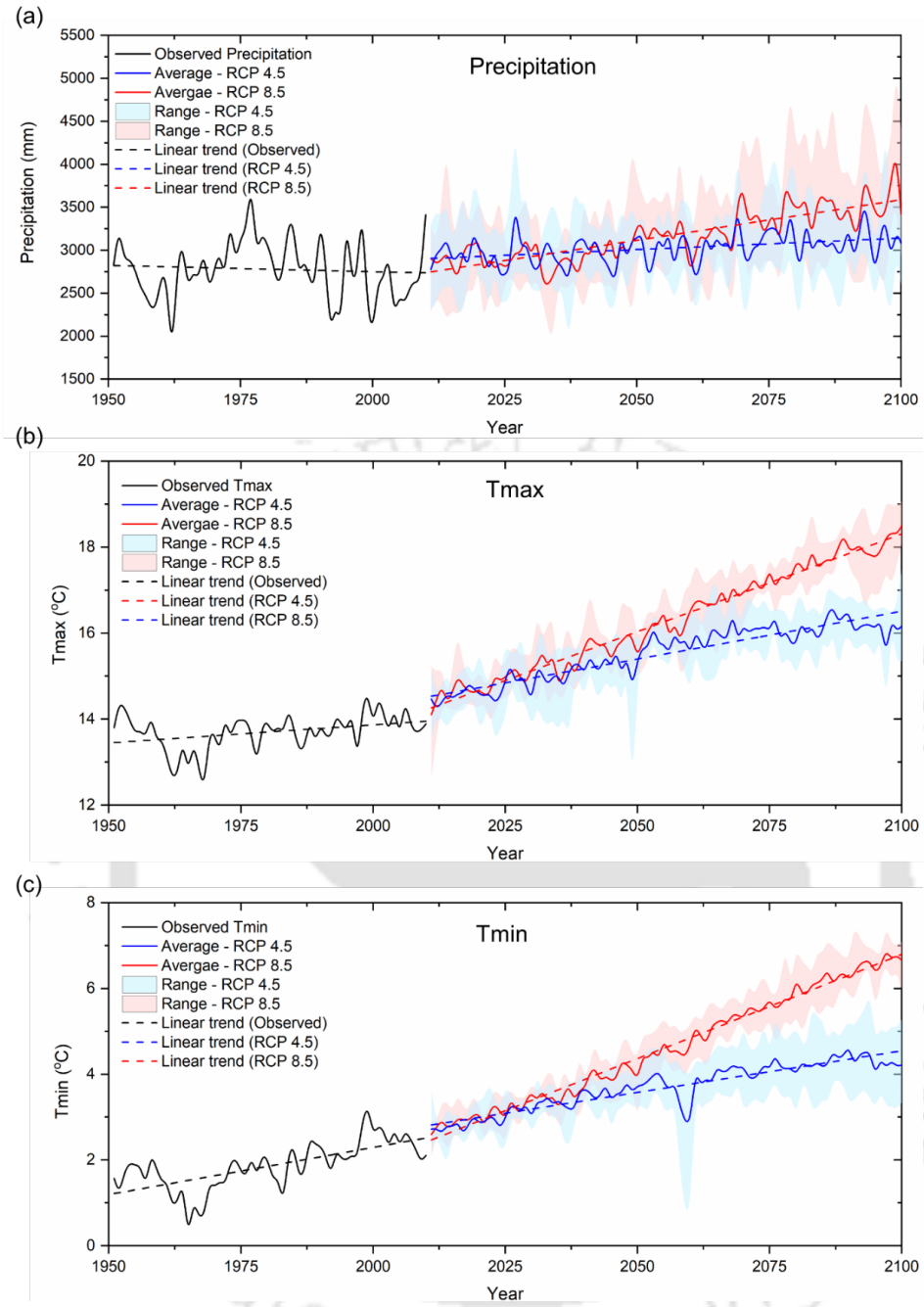

Figure 5.4: Temporal variation in annual precipitation, daily maximum temperature (Tmax) and daily minimum temperature (Tmin) for the past and projected climate. The solid blue and red curves show the average of multi-model projections for RCP4.5 and RCP8.5, respectively. The shaded blue and red area show the range of multi-model projection for RCP4.5 and RCP8.5, respectively. Dotted lines show the linear trend.

spectively. The range of precipitation for projected climate (P2 and P3) was found lesser compared to the observed period (P1). The P3 (2061 to 2100) for RCP8.5 showed about 20% higher mean precipitation compared to the observed period (P1), which indicates that basin is anticipated to have higher precipitation under extreme scenarios. The findings are consistent with the previous studies on precipitation in a smaller portion of the

basin (Singh and Goyal, 2017a). Both Tmax and Tmin showed a significant increase during P2 and P3 compared to P1 (Figure 5.5). The mean values of Tmax for Observed (P1), RCP4.5 (P2), RCP4.5 (P3), RCP8.5 (P2) and RCP8.5 (P3) were 13.82 °C, 15.2 °C, 16.09 °C, 15.52 °C, and 17.47 °C, respectively. One-way ANOVA test confirmed the statistical difference between these scenarios. Unlike precipitation, the interannual variability increased for Tmax under climate change scenarios. The mean values of Tmin for Observed (P1), RCP4.5 (P2), RCP4.5 (P3), RCP8.5 (P2) and RCP8.5 (P3) were 2.11 °C, 3.4 °C, 4.19 °C, 3.81 °C, and 5.9 °C, respectively. One-way ANOVA test confirmed the statistical difference between these scenarios. The interannual variability increased for all scenarios except for RCP4.5 (P3).

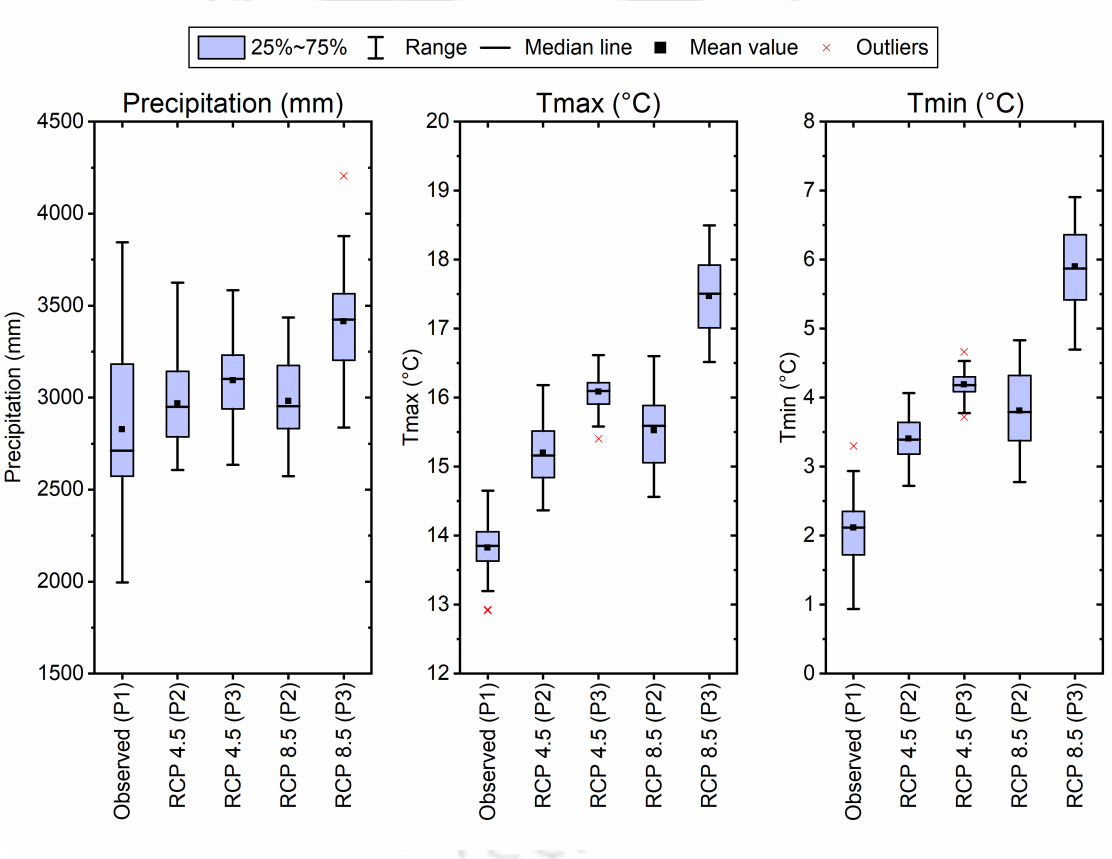

Figure 5.5: Boxplot of annual precipitation, daily maximum temperature (Tmax) and daily minimum temperature (Tmin) for P1 (1971 to 2010), P2 (2021 to 2060) and P3 (2061 to 2100). The RCP scenarios shown in the figure are the average of four GCMs used in this study.

5.5.3 Sub-basin scale analysis of precipitation and temperature

5.5.3.1 Observed period

Figure 5.6 shows the mean annual precipitation and temperatures for the basin for period P1 and P2, and the differences between the mean values for these two periods (i.e., P2-P1). Table 5.2 shows the results of the trend analysis of temperature and precipitation for both observed and projected climates. Figure 5.6(a) shows the spatial variation of mean annual precipitation (MAP) for the period from 1951 to 1980. All SBs had nearly the same precipitation (≈2700-2800mm) except for SB5 which had a slightly higher MAP (≈3100mm). SB7 had the least precipitation (≈2743mm). The spatial pattern of the MAP remained same for P2 (1981-2010); however, there were some changes in the magnitude of the MAP (Figure 5.6b). During P2, SB4 received the least MAP of 2495mm whereas SB5 received the highest MAP of 3375mm. There was a decrease MAP between P1 and P2 for six out of eight SBs (Figure 5.6c). Only SB5 and SB6 had an increase in MAP of magnitude 249mm and 17mm, respectively. The basin average MAP for P1 and P2 were 2833mm and 2726mm, which shows there was a decrease in the basin average precipitation. Among all SBs, SB4 and SB7 had significant decreasing trend for the observed period, whereas only SB5 had a significant increasing trend (Table 5.2). The increasing trend in SB6 was found non-significant (i.e., p-value > 0.05).

The SB-wise mean annual daily maximum temperature (TX) varied between 7.20°C (SB1) and 19.47°C (SB8) for P1 and between 7.74°C (SB1) and 19.89°C (SB8) for P2 (Figure 5.6d and 5.6e). The high elevation areas in SB1 and SB2 had lower temperature compared to other SBs. The basin average TX was 13.40°C and 13.86°C for P1 and P2, respectively, which shows an increase of 0.46°C in TX between P1 and P2. There was an increase in TX in all SBs with the magnitude of increase greater than 0.52°C in SB1 to SB4 (Figure 5.6f). SB5 reported the least increase in TX of 0.38°C. Trend analysis of the TX revealed that all basins except SB5 and SB8 had significant increasing trend for the observed period (Table 5.2). SB5 and SB8 had an increasing trend in TX, but the trend was not significant.

The SB-wise mean annual daily minimum temperature (TN) varied between− 6.45°C (SB1) and 9.03°C (SB8) for P1 and between− 5.77°C (SB1) and 9.77°C (SB8) for P2 (Figure 5.6g and 5.6h). Similar to TX, high elevation SBs has lower temperatures.

The basin average values of TN for P1 and P2 were 1.52 °C and 2.21 °C respectively, which clearly shows an increase of 0.7°C in TN between P1 and P2. There was an increase in TN of magnitude greater than 0.6°C in all SBs between P1 and P2. SB7 had the highest increase in TN (0.74°C) whereas SB2 had the least magnitude of increase (0.65°C) (Figure 5.6i). Trend analysis of TN also revealed a significant increasing trend for all SBs (Table 5.2).

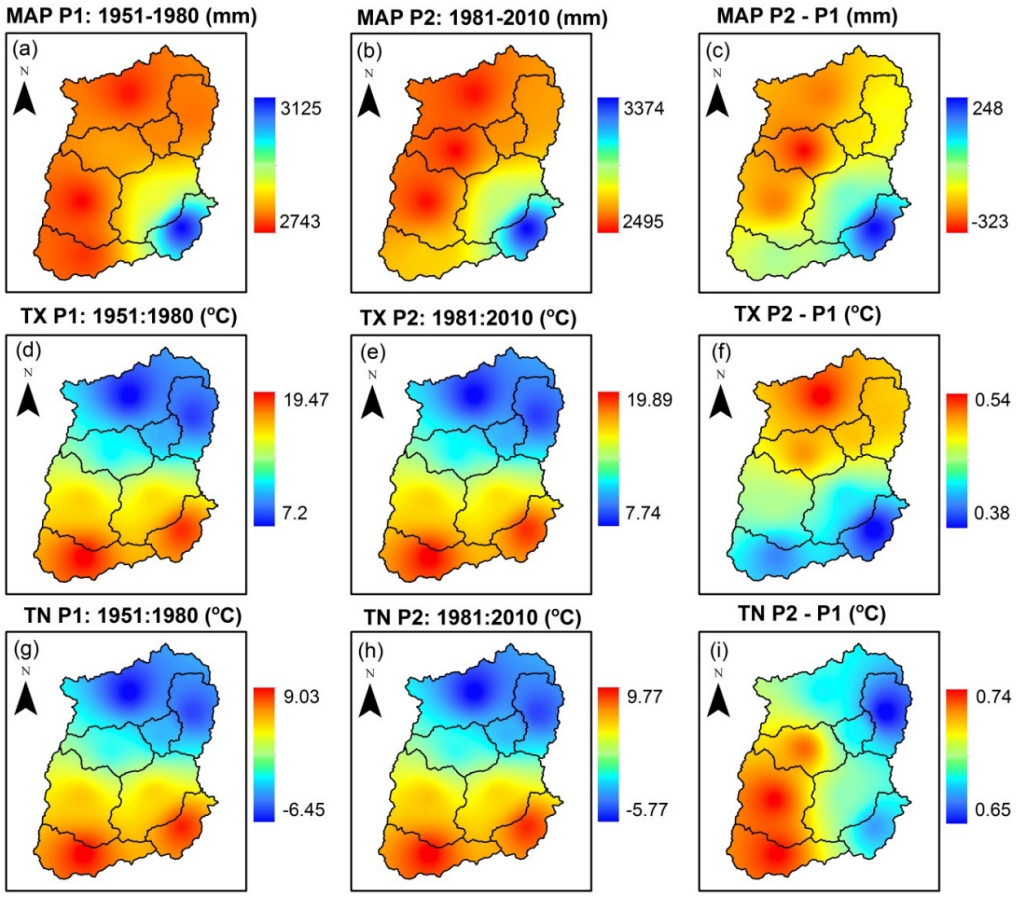

Figure 5.6: Mean annual precipitation (MAP), maximum daily temperature (TX), and minimum daily temperature (TX) for observed periods of 1951-1980 (P1) and 1981-2010 (P2), and the differences between P2 and P1.

5.5.3.2 Projected climate

Figure 5.7 shows the changes in precipitation and temperature for projected climate compared to observed climate. Here, the average of different GCMs is shown for both RCPs. Figure 5.7(a and b) show the changes in MAP for F1, F2 and F3 compared to the observed period (1951-2010) for every SB under RCP4.5 and 8.5 respectively. Increase in precipitation was found for all SBs for the 21st century. A consistent increase

Table 5.2: Sub-basin wise trend analysis of annual average precipitation and temperature (maximum and minimum) for past (1951-2010) and projected (2011-2100) climates using Mann-Kendall trend test.

Variable	Period	Scenario	Sub-basins							
			SB1	SB2	SB3	SB4	SB5	SB6	SB7	SB8
Precipitation	Past	Observed	-	-	-	↓	↑	+	↓	+
	Projected	RCP4.5	+	+	+	+	+	+	+	+
		RCP8.5	↑	↑	↑	↑	↑	↑	↑	↑
TX (Tmax)	Past	Observed	↑	↑	↑	↑	+	↑	↑	+
	Projected	RCP4.5	↑	↑	↑	↑	↑	↑	↑	↑
		RCP8.5	↑	↑	↑	↑	↑	↑	↑	↑
TN (Tmin)	Past	Observed	↑	↑	↑	↑	↑	↑	↑	↑
	Projected	RCP4.5	↑	↑	↑	↑	↑	↑	↑	↑
		RCP8.5	↑	↑	↑	↑	↑	↑	↑	↑

↑ represents the significant increasing trend at significance level of 0.05 (i.e., MK Z value > 1.96).
↓ represents the significant decreasing trend (i.e., MK Z value < -1.96).
+ represents the non-significant increasing trend (p-value > 0.05).
- represents the non-significant decreasing trend (p-value > 0.05)

in precipitation from F1 to F2 and then, F2 to F3 was found for all SBs. Under RCP4.5, the basin-average MAP increased by 225mm, 283mm and 385mm for F1, F2 and F3, respectively, compared to the observed period. On the other hand, under RCP8.5, basin-average MAP increased by 160mm, 418mm and 751mm for F1, F2 and F3, respectively. This indicates the higher precipitation under the high emissions scenario. The high elevated SBs had a higher increase in precipitation compared to low elevation SBs. The MK test based trend analysis of the precipitation revealed that all SBs had non-significant increasing trend under RCP4.5, whereas all SBs had significant increasing trend under RCP8.5 (Table 5.2).

Figure 5.7(c and d) show the changes in mean daily maximum temperature (TX) for F1, F2 and F3 compared to the observed period (1951-2010) for every SBs under RCP4.5 and RCP8.5 respectively. There was a consistent increase in TX under both RCPs for all SBs; however, the magnitude of increase was higher for high emission scenario (i.e., RCP8.5). Under RCP4.5, the basin average TX increased by 0.46°C, 0.90°C and 1.13°C for F1, F2 and F3, respectively. Under RCP8.5, the basin average TX increased by 0.54°C, 1.18°C and 1.92°C for F1, F2 and F3, respectively. In general, the high

elevated SBs showed a higher increase in TX compared to low-elevated SBs. SB1 had an increase of 2.01°C in F3 compared to observed period. MK trend test showed a significant increasing trend in TX for all SBs for the projected climate (Table 5.2).

Figure 5.7(e and f) shows the changes in mean daily minimum temperature (TN) for F1, F2 and F3 compared to the observed period (1951-2010) for every SBs under RCP4.5 and RCP8.5 respectively. A consistently increase in the TN was found for all SBs. There was an increase of about 0.4°C, 0.75°C, and 1°C for F1, F2 and F3, respectively, under RCP4.5. On the other hand, there was an increase of about 0.5°C, 1.2°C and 2°C for F1, F2 and F3 respectively under RCP8.5. Like TX, the high elevated SBs showed a higher increase in TN. The basin-average TN increased by 0.43°C, 0.76°C and 1.01°C for F1, F2 and F3, respectively under RCP4.5, whereas the basin average TN increased by 0.49°C, 1.18°C and 1.96°C for F1, F2 and F3 respectively under RCP8.5. Like TX, TN also had significant increasing trend for all SBs for the projected period (Table 5.2). The increase in temperature under projected climate is consistent with the increase in temperature under the observed climate. However, under projected climate, precipitation increased for SBs whereas there was a decrease in precipitation under observed climate.

5.5.4 Analysis of climate extremes

5.5.4.1 Changes in the Observed (1951–2010) Climate Extremes

Twenty-three climate indices were computed to assess the changes in the climate extremes (for details see Table 5.1). Figure 5.8 shows the spatial pattern of mean values of extreme indices of precipitation for the observed (1951-2010) period and Figure 5.9 shows the changes in the mean values of extreme indices of precipitation for the P2 (1981-2010) with respect to P1 (1951-1980). Precipitation indices followed the same spatial pattern as precipitation, i.e., higher in SB5 and lower values in other SBs.

The maximum 1-day precipitation amount (RX1day) varied between 95.94mm (SB4) and 135.9mm (SB5) (Figure 5.8a). There were significant differences in the RX1day for different SBs between the periods P1(1951-1980) and P2 (1981-2010). RX1day decreased in all SBs between P1 and P2 except for SB5, which showed a small increase (Figure 5.9a). The basin average value of RX1day decreased from 127.92mm for P1 to 86.85mm for P2.

The maximum 5-day precipitation amount (RX5day) ranged between 223.58mm

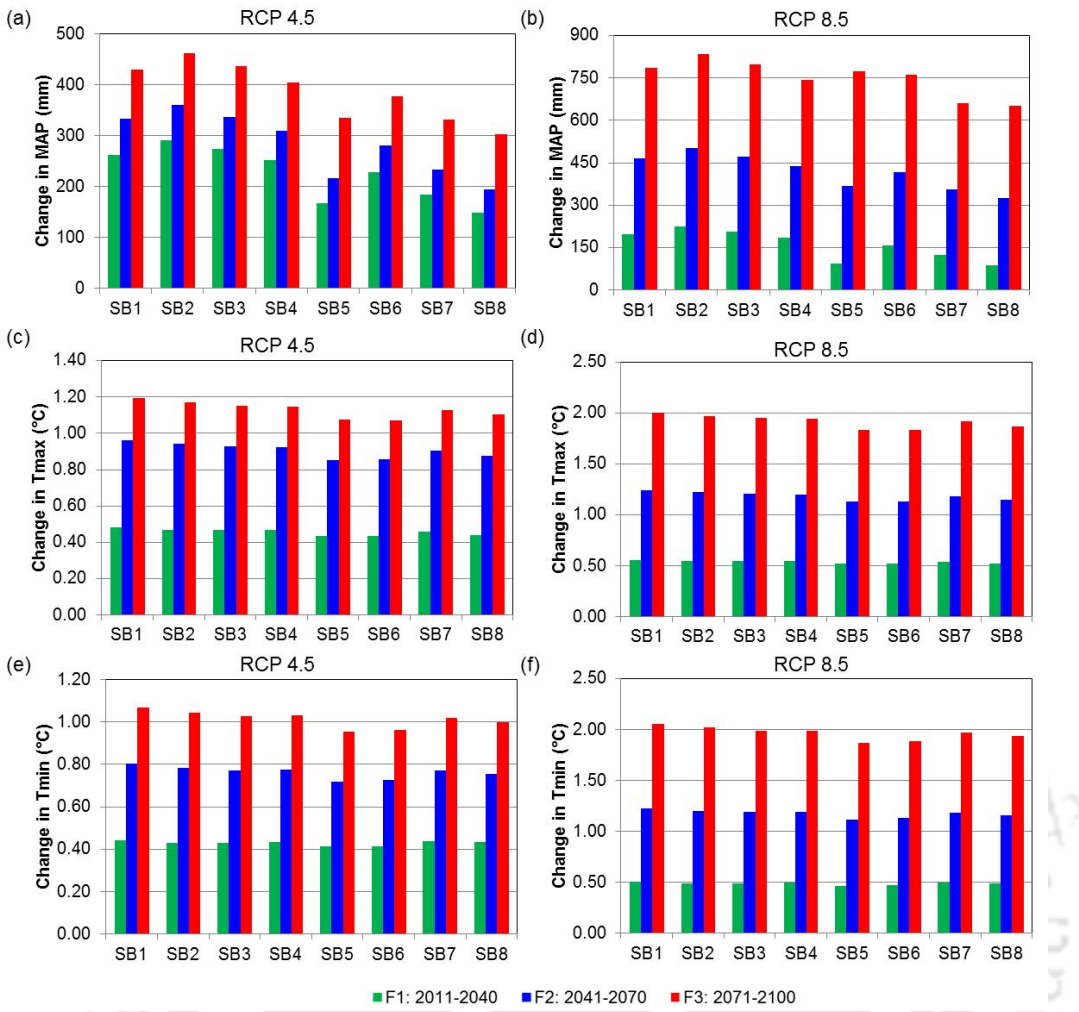

Figure 5.7: Changes in the precipitation and temperature under projected climate compared to observed climate.

(SB1) and 334.82mm (SB5) (Figure 5.8b). Like RX1day, the RX5day decreased for all SBs between P1 and P2 except for SB5 (Figure 5.9b). The basin average RX5day decreased from 286.65mm during P1 to 220.90mm during P1.

The simple daily intensity index (SDII) ranged between 17.33mm/day (SB5) and 13.61mm/day (SB7) (Figure 5.8c). There was a decrease in SDII for all SBs from P1 to P2 (Figure 5.9c). SB5 had the least decrease in SDII compared to other SBs. SB4 had the highest decrease in SDII of− 3.18 mm/day. Overall, the basin average SDII decreased from 15.85 mm/day during P1 to 13.39 mm/day during P2.

The number of heavy precipitation days (R10) ranged between 85.62 (SB7) and 94.59 (SB5) (Figure 5.8d). In contrast to other precipitation indices, an increase in R10 was found (Figure 5.9d). All SBs had an increase in R10 except SB4, which had a slight decrease in R10 of− 0.20 days. The basin average R10 increased from 85.01

days during P1 to 91.57 days during P2.

The number of very heavy precipitation days (R20) ranged between 39.7 (SB1) and 52.85 (SB5) (Figure 5.8e). The high elevation SBs had the least number of very heavy precipitation days. Unlike R10, most of the basins showed a decrease in R20 except for SB5 (Figure 5.9e). The high elevation SBs had a significant reduction in R20. Overall, the basin average R20 decreased from 45.65 days during P1 to 40.82 days during P2.

There was not much variation in the number of consecutive dry days (CDD) (Figure 5.8f). It ranged between 49.03 days for SB1 and 51.03 days for SB5. SB5 received the highest amount of precipitation and also had the highest number of CDD. It could be explained by the high values of SDII and R10. The basin average value of CDD was 49.81 days. There was a decrease in CDD for all SBs from P1 to P2 (Figure 5.9f). SB2 had the most substantial reduction in CDD from 60.23 days during P1 to 41.07 days during P2. On the other hand, consecutive wet days (CWD) showed considerable spatial variation over the basin (Figure 5.8g). The less rainfall receiving southwestern regions of the basin had highest CWD. CWD ranged between 55.65 days (SB2) and 70.82 days (SB8). The basin average CWD was 63.61 days. There was a decrease in CWD for the high elevation SBs (SB1-SB4), whereas the other SBs showed an increase in CWD (Figure 5.9g). Overall, the basin average CWD decreased from 64.43 days during P1 to 62.80 days during P2.

Precipitation during very wet days (days with precipitation greater than the 95th percentile, R95p) followed the same pattern as precipitation, i.e., higher for SB5 and lesser for other SBs (Figure 5.8h). The R95p for SB5 was 730.92 mm compared to the basin average 649.60 mm. There was a substantial decrease in R95p for all SBs except for SB5 (Figure 5.9h). Four SBs (SB2, SB3, SB4 and SB7) had a reduction of more than 500mm between P1 and P2. SB5 showed an increase in R95p from 661.95 mm during P1 to 799.89 mm during P2. A drastic change in the spatial pattern of R95p was observed between P1 and P2. During P1, SB5 had least R95p of 661.95 mm compared to basin average of 837.44 mm, whereas during P2, SB5 had the highest R95p of 799.89 mm compared to the basin average of 461.75 mm. There was a considerable decrease (44.8%) in basin average R95p from 837.44 mm during P1 to 461.75 mm during P2. This decrease is consistent with the decrease in other indices such as RX1day, RX5day, SDII and PRCPTOT.

The annual total wet-day precipitation (PRCPTOT) is similar to MAP and therefore had the same spatial pattern as well as the changes. The PRCPTOT ranged between 2606.28 mm for SB7 and 3233.75 mm for SB5 (Figure 5.8i). The basin average PRCPTOT was 2763.67 mm. All SBs showed a decrease in PRCPTOT from P1 to P2 except SB5 and SB6 (Figure 5.9i). SB4 had the most significant reduction in PRCPTOT of 323.94 mm between P1 and P2. The basin average PRCPTOT decreased from by 107.79 mm from 2817.57 mm during P1 to 2709.78 mm during P2. The PRCPTOT increased for SB5 by 242.77 mm between P1 and P2.

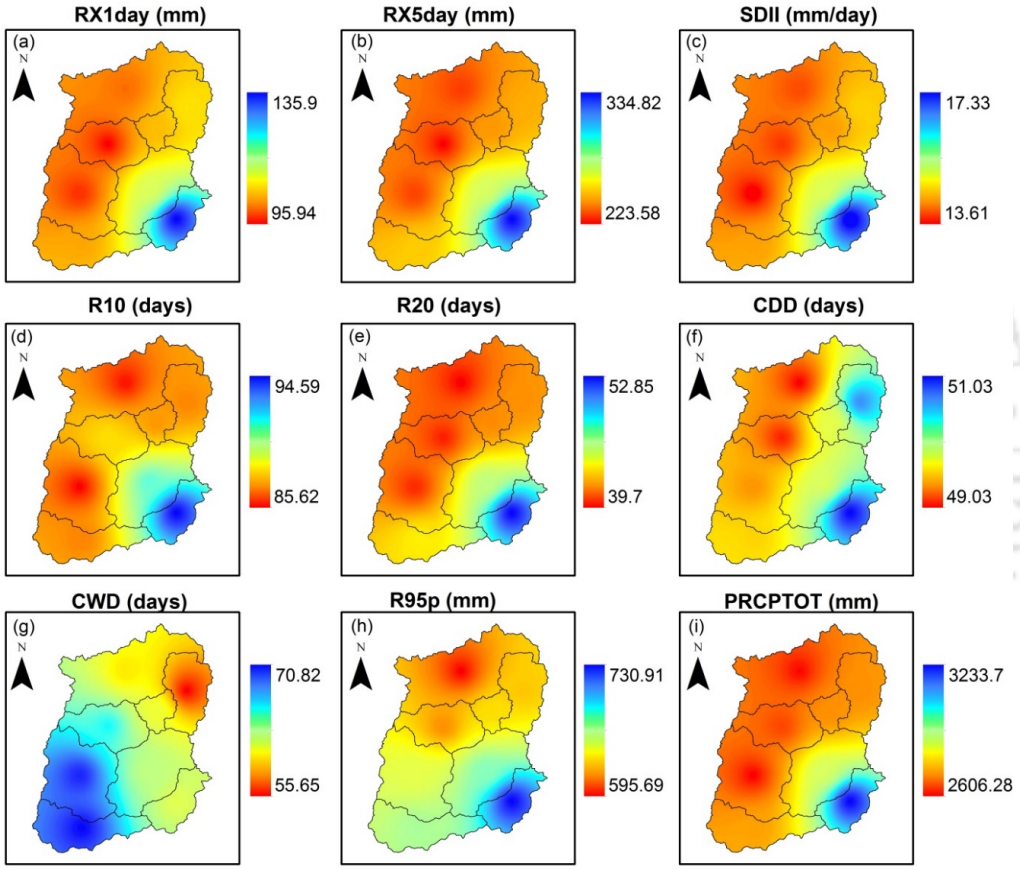

Figure 5.8: Mean values of extreme indices of precipitation for the observed (1951-2010) period.

Figure 5.10 shows the spatial pattern of mean values of extreme indices of temperature for the observed (1951-2010) period and Figure 5.11 shows the changes in the mean values of extreme indices of temperature for the P1 (1951-1980) and P2 (1981-2010) periods.

The cool nights (TN10p) ranged between 10.58% for SB2 and 11.54% for SB7 (Figure 5.10a) with basin average value of 11.03%. There was a decrease in TN10p for

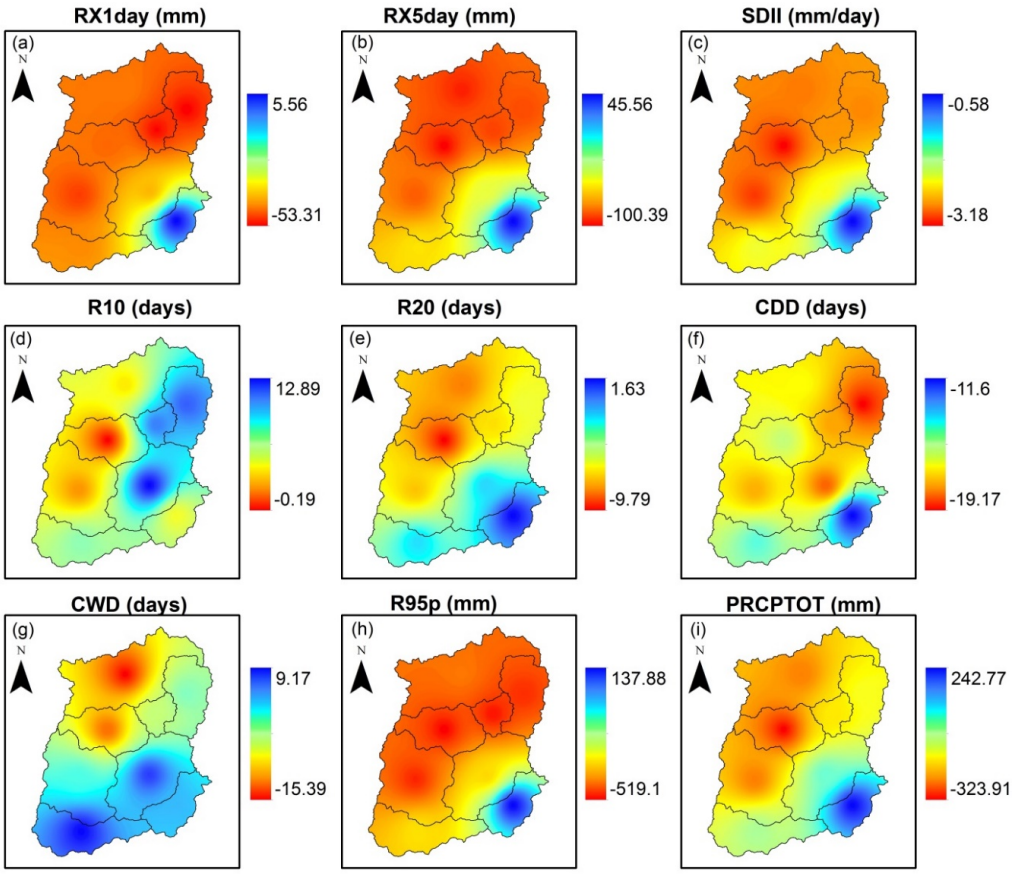

Figure 5.9: Changes in the mean values of extreme indices of precipitation from P1 (1951-1980) to P2 (1981-2010) periods (i.e., P2-P1).

all SBs from P1 to P2 (Figure 5.11a). The basin average TN10p decreased from 13.15% during P1 to 8.90% during P2. The decrease in cool nights was consistent with the increase in daily minimum temperature. The cool days (TX10p) ranged between 9.97% for SB8 and 10.63% for SB1 (Figure 5.10b) with basin average value of 10.38%. The high elevation SBs had more cool days. Similar to cool nights, there was a decrease in cool days for all SBs (Figure 5.11b). The basin average TX10p decreased from 11.32% during P1 to 9.44% during P2. The high elevation SB1 had the largest decrease in cool days of 2.53%.

The warm nights (TN90p) ranged between 8.8% for SB7 and 9.93% for SB2 (Figure 5.10c). There was an increase in warm nights over the basin (Figure 5.11c). The basin average TN90p increased drastically from 5.10% during P1 to 13.37% during P2, which indicates that there was increase of 8.27% in warm nights. Compared to warm nights, there was less spatial variation in warm days (TX90p), ranging between 9.33% for SB4 and SB, and 9.74% for SB8 (Figure 5.10d). The basin average TX90p was

9.51%. There was a consistent increase in TX90p for all SBs, ranging between 2.85% for SB8 and 3.72% for SB4 (Figure 5.11d). Overall, the basin average TX90p increased from 7.87% during P1 to 11.15% during P2. Maximum daily maximum temperature (TXx) had a large spatial variation in basin, which ranged between 15.99°C for SB1 and 26.94°C for SB8 (Figure 5.10e). There was consistent increase in TXx for all SBs (Figure 5.11e). The basin average TXx was 21.44°C, which increased from 21.34°C during P1 to 21.54°C during P2. SB5 has the largest increase in TXx of 0.42°C.

The minimum daily maximum temperature (TXn) ranged between− 3.71°C for SB1 and 9.13°C for SB8 (Figure 5.10f). The basin average value for TXn was 2.80°C, which increased from 2.61°C during P1 to 3°C during P2. There was increase in TXn for all SBs (Figure 5.11f). SB1 and SB2 experienced an increase of more than 0.6°C from P1 to P2. The maximum daily minimum temperature (TNx) also had large spatial variation over the basin ranging between 5.63°C for SB1 and 17.97°C for SB8 (Figure 5.10g). The basin average value of TNx was 11.94°C, which increased from 11.60°C during P1 to 12.27°C during P2. Every SB recorded an increase of greater than 0.45°C in TNx (Figure 5.11g). Like TNx, there was large spatial variation in minimum daily minimum temperature (TNn) ranging between− 24.06°C for SB1 and− 5.5°C for SB8 (Figure 5.10h). The basin average TNn was− 14.54°C, which decreased slightly from− 14.49°C during P1 to− 14.58°C during P2. In contrast to other temperature indices, TNn decreased in five out of eight SBs from P1 and P2 (Figure 5.11h).

There was a large variation in frost days (FD) in the basin (Figure 5.10i). The high elevated SBs (SBs1-4) had more than 200 FD, whereas low elevated SBs (SBs5-8) has less than 100 FD. FD ranged between 22.59 for SB8 to 252.7 for SB1. There was a consistent decrease in FD for every SB between P1 and P2 (Figure 5.11i). The basin average FD decreased from 143.36 days during P1 to 133.80 during P2. SB7 had large decrease in FD of magnitude 17.67 days. There were no ice days (ID) for half of the SBs (i.e., SBs 5-8) (Figure 5.10j). The ID for SB1, SB2, SB3 and SB4 were 26.02, 14.77, 3.03 and 1.03, respectively. The ID changed for SB1, SB2, SB3 and SB4 by− 5.30,− 2.67, 0.13, and 0.87, respectively, between P1 and P2, which shows that it decreased for two SBs and increase for other two SBs (Figure 5.11j). Summer days (SU) had opposite spatial variation compared to that of ID. There were no SU for first six SBs (i.e., SBs 1-4, 6 and 7) (Figure 5.10k). SB5 and SB8 had 9.02 and 14.08 SU, respectively. For SB5, SU increased from 6.27 for P1 to 11.77 for P2, whereas for SB8, it increased from

11.27 for P1 to 16.90 for P2 (Figure 5.11k). There were no tropical nights (TR) in the basin for P1 and P2 (Figure 5.10l). The growing season length (GSL) ranged between 123.8 days for SB1 and 360.7 days for SB8 (Figure 5.10m). The basin average GSL was 244.67 days. It increased from 241.52 days during P1 to 247.82 days during P2, which recorded an increase of 6.3 days (Figure 5.11m). There was increase in GSL for all SBs except for SB8, which had a slight decrease in GSL for 0.13 days. The diurnal temperature range (DTR) has small spatial variation within the basin (Figure 5.10n). It had higher value for higher elevated SBs compare to low elevated SBs. DTR ranged between 10.34°C for SB5 and 13.66°C for SB1. The basin average DTR was 11.83°C. Between P1 and P2, the basin average DTR decreased from 12.02°C to 11.64°C (Figure 5.11n). There was a decrease in DTR for all SBs, and the highest decrease was observed for SB8 of magnitude of 0.5°C.

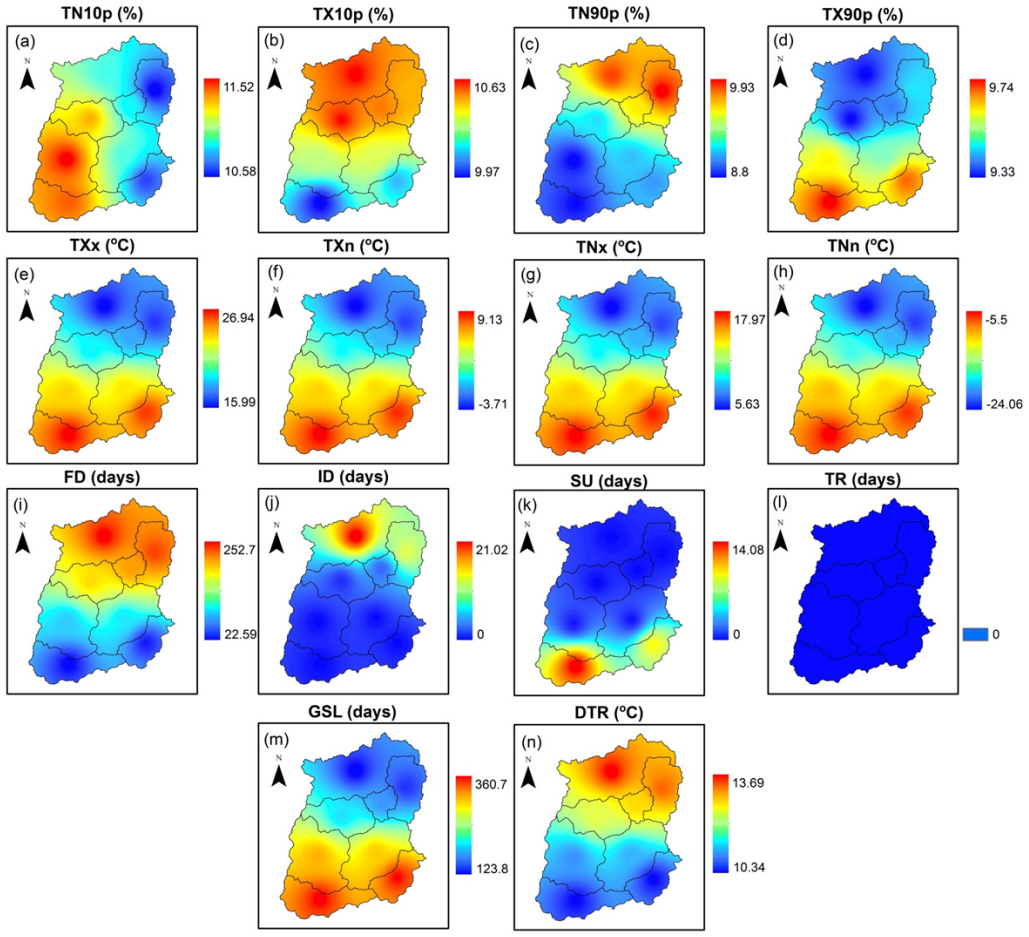

Figure 5.10: Mean values of extreme indices of temperature for the observed (1951-2010) period.

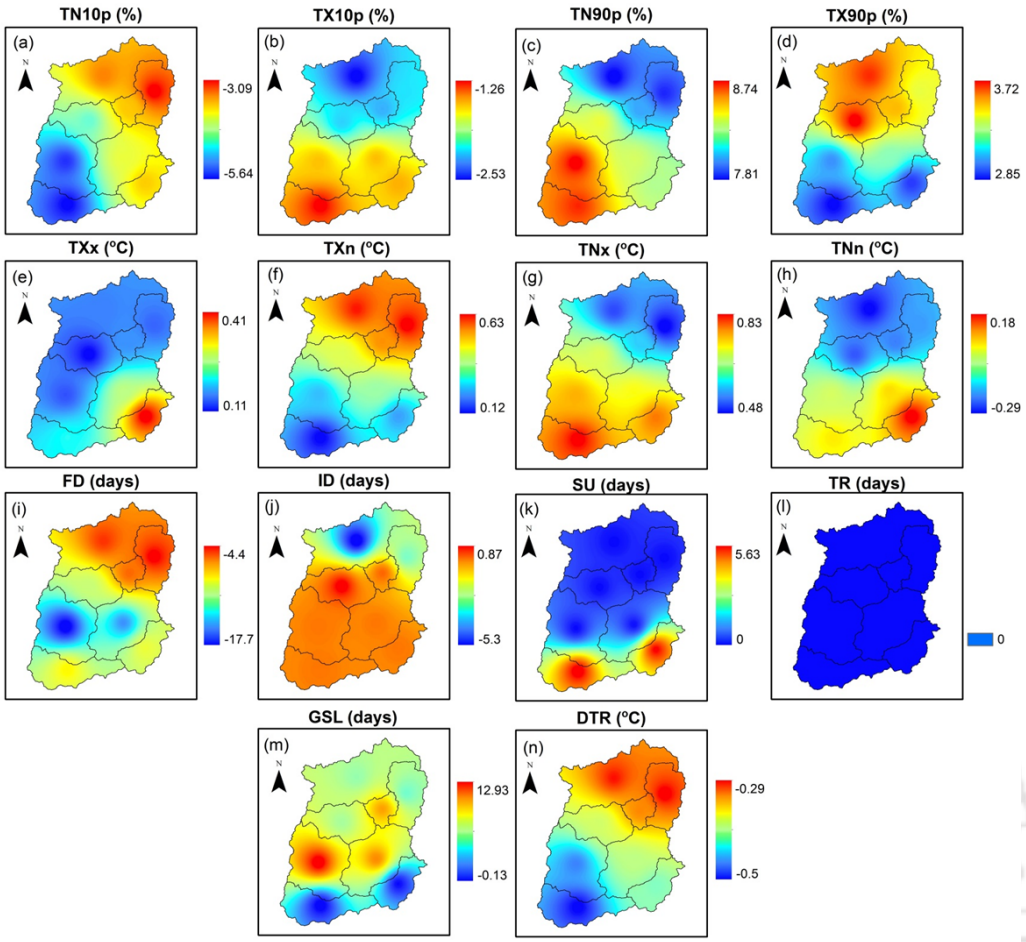

Figure 5.11: Changes in the mean values of extreme indices of temperature for the P1 (1951-1980) and P2 (1981-2010) periods (i.e., P2-P1).

5.5.4.2 Changes in Climate Extremes under Projected (2011-2100) Climate

Figure 5.12 shows the values of 30-year average precipitation indices for projected climate for all SBs. Consistent with the increase in precipitation for all SBs (Figure 5.7a, b), the precipitation indices were also expected to increase. In general, most of the indices showed an increase from F1 to F2 and from F2 to F3, and also from RCP4.5 to RCP8.5. Both RCPs showed an increase in RX1day (Figure 5.12a). Compared to observed climate (P2), RX1day increased by 1.11mm, 9.53mm and 17.37mm for F1, F2, and F3 under RCP4.5 and by 3.42mm, 15.11mm and 30.01mm under RCP8.5. It should be noted that P2 showed a decrease in precipitation (and in precipitation indices as well) compared to the period P1. Here, the projected climate was compared with the past 30 years (i.e., P2). RX5day also increase consistently for all SBs (Figure 5.12b). Comparing with observed climate (P2), an increase of 20.33mm, 26.61mm and 32.97mm was found for F1, F2 and F3 for RCP4.5 and increase of 19.40mm, 79.29mm

and 110.08mm for RCP8.5. There was a drastic increase in RX5day for F2 and F3 under high emission scenario (i.e., RCP8.5). Projected climate showed an increase in the intensity of precipitation (i.e., SDII) for F2 and F3 compared to F1 (Figure 5.12c) but compared to observed climate P2, the values are less. The changes in SDII for F1, F2 and F3 compared to P2 are− 3.16mm/day,− 2.10mm/day and 0.53 mm/day under RCP4.5 and− 3.51mm/day, 0.24mm/day and 1.60 mm/day for RCP8.5. The SDII exceeds the values in P2 during the projected climate F2 and F3. There was an increase in both heavy (R10) and very heavy precipitation (R20) days (Figure 5.12d, e). Compared to observed climate (P2), R10 increased by 13.07, 14.38 and 17.94 days for F1, F2 and F3, respectively, under RCP4.5 and by 11.42, 15.85 and 23.22 days, respectively, for RCP8.5. For R20, a decrease in projected climate F1 was found compared to observed climate P2. There was a decrease of 0.28 and 2.75 days under RCP4.5 and 8.5, respectively. For F2 and F3, there was an increase in R20. The CDD decreased under both RCPs. For RCP4.5, there was a decrease of 10.13, 8.32 and 12.64 days for F1, F2 and F3, respectively, compared to observer climate P2. There was a consistent increase in CWD for all SBs for both SBs (Figure 5.12g). R95p (i.e., very wet days) also increased for both RCPs (Figure 5.12h), but there was a drastic increase for RCP8.5. R95p increased by 383.81 mm and 634.58 mm for F2 and F3 respectively under RCP8.5. PRCPTOT also increase for both RCPs (Figure 5.12i).

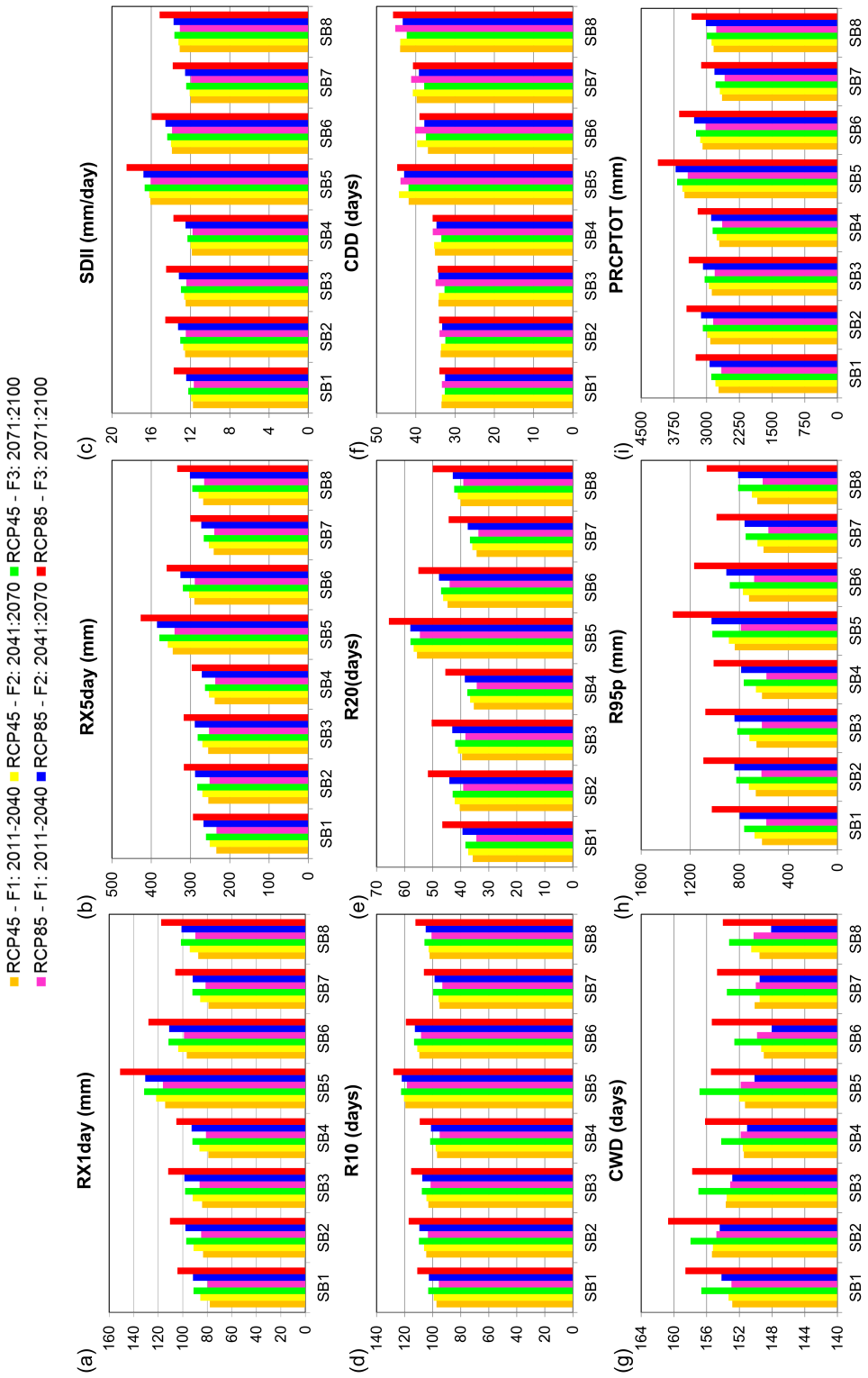

Figure 5.12: Mean values of extreme indices of precipitation for the projected (2011-2100) climate.

Figure 5.13 shows the changes in temperature indices for the projected climate. Cool nights (TN10p) decreased in the projected climate (Figure 5.13a). TN10p decreased by 0.816%, 4.663%, and 5.844% for F1, F2 and F3, respectively, under RCP4.5 and by 0.982%, 6.394% and 8.328%, respectively, under RCP8.5. Cool nights were less than 1% for F3 under RCP8.5. Like cool nights, cool days (TX10p) also decreased for projected climate (Figure 5.13b). TX10p decreased by 0.98%, 5.14% and 6.24% for F1, F2 and F3, respectively, under RCP4.5 and by 1.65%, 6.29% and 8.26%, respectively, under RCP8.5. Increase in both warm nights (TN90p) and warm days (TX90p) was found under both RCPs (Figure 5.12c and d). There was a drastic increase in TN90p and TX90p for F3 under RCP8.5. TXx, TXn, TNx and TNx increased consistently for the projected climate (Figure 5.13e-h). Among these indices, TNn had a drastic increase under all scenarios, which shows that daily minimum temperature increased more compared to daily maximum temperature. There was a large decrease in FD and ID (Figure 5.13i and 9j). The ID decreased to nearly zero by the end of for 21st century for low elevated SBs. FD decreased by 24.78 and 46.90 days for F3 under RCP4.5 and RCP8.5, respectively. There was a huge increase in summer days (SU) for SB5 and SB8 (Figure 5.13k). For these two SBs, SU crossed 100 days for F3 under RCP8.5, indicating a large number of summer days by the 21st century. There was no change in tropical nights (TR) for most of the SBs, expect for SB5 and SB8, which showed an increase in TR for F3 under RCP8.5 (Figure 5.13m). GSL increased significantly for SBs1-4 under all scenarios, whereas for SBs5-8, GSL was always greater than 300days (Figure 5.13n). The basin average GSL increased by 17.88, 27.33, and 33.24 days for F1, F2 and F3, respectively, under RCP4.5 and by 19.21, 36.79, and 51.61days, respectively, under RCP8.5. The projected climate showed a decrease in DTR (Figure 5.13o). In general, DTR was higher for SBs1-4 compared to low elevated SBs.

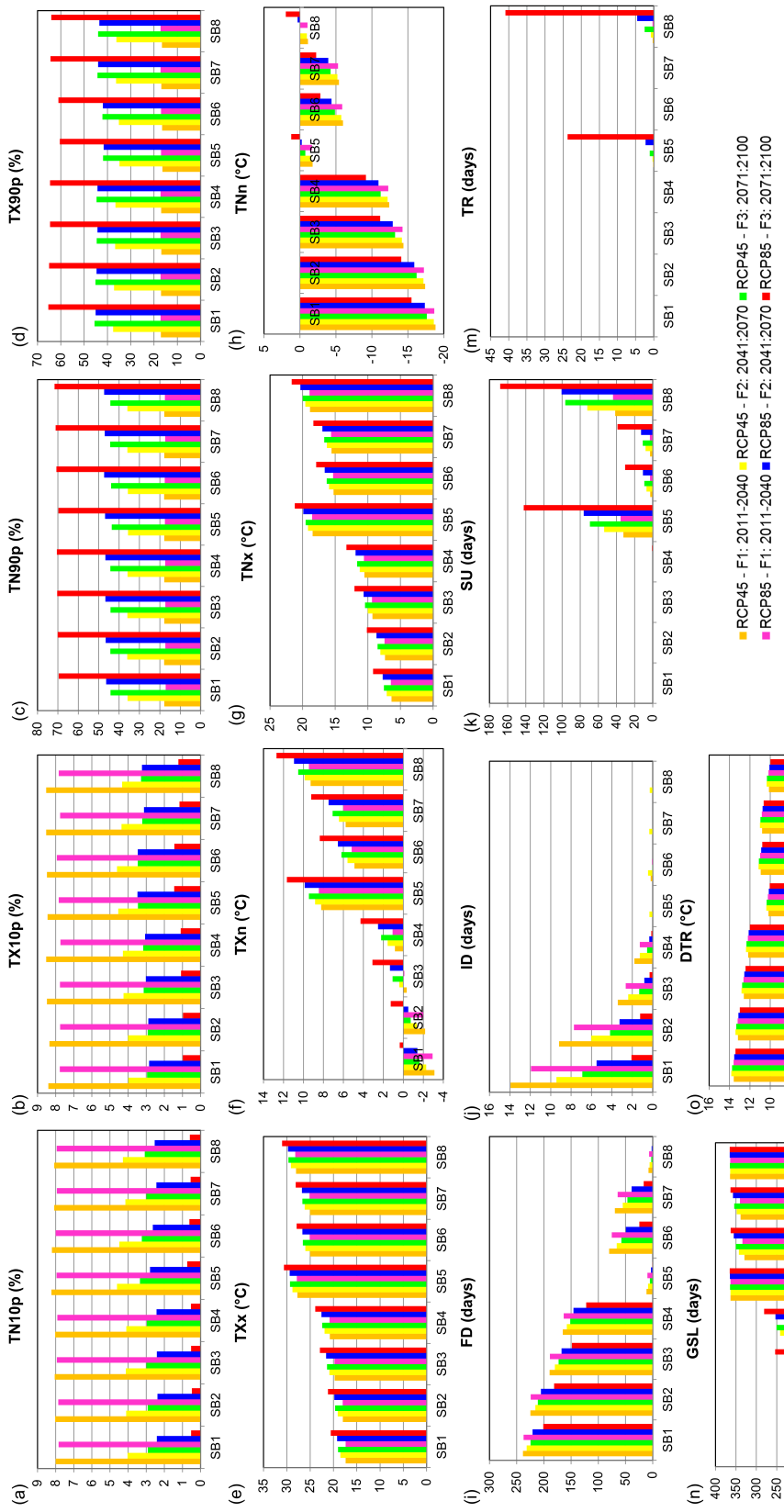

Figure 5.13: Mean values of extreme indices of temperature for the projected (2011-2100) climate.

5.5.5 Trend Analysis of Seasonal Precipitation

In addition to trend analysis of annual precipitation, trend analysis of seasonal precipitation was performed. The study area receives most of its precipitation during the southwest monsoon. Therefore, the trend analysis performed for two seasons, i.e., monsoon and non-monsoon season. Table 5.3 shows the results for the sub-basin wise trend analysis of seasonal precipitation using MK trend test. Most of the SBs (except SB5) had a decreasing trend in monsoon precipitation during the observed climate (1951-2010). Five SBs had significant decreasing trends, whereas two SBs had a non-significant decreasing trend. Only SB5 had an increasing trend in monsoon precipitation, but it was not significant (i.e., p-value $>$ 0.05). For projected climate (2011-2100), all SBs had significant increasing trend for monsoon precipitation. As monsoon precipitation forms the major component of annual precipitation, the trend in monsoon precipitation was somewhat like the trend in annual precipitation. Multi-model assessment of changes in Indian summer monsoon in India also suggested an increase in monsoon rainfalls under climate change (Sharmila et al., 2015). For the non-monsoon season, the precipitation had an increasing trend for both observed and projected (both RCPs) climates. Overall, the precipitation in the region is expected to increase under climate change. The results of this study are consistent with the findings of previous studies on a smaller part (covering 1 out of 4 districts in the state of Sikkim) of the basin (Goswami et al., 2018; Singh and Goyal, 2016, 2017a).

5.5.6 Streamflow simulation using SWAT

The SWAT model was set up for the basin. Based on the topography of the basin, the basin was divided into eight subbasins. 118 HRUs were created during the model set up. SWAT model has a large number of parameters to be calibrated; however, it is not advisable to incorporate all the parameters in calibration. Global Sensitivity tool in SWAT-CUP was used for selecting the most sensitive parameters. The monthly streamflow data from Jan 2001 to Dec 2006 was used for the calibration of the model and the remaining data from Jan 2007 to Dec 2010 was used for validation purpose. The selection of parameters for model calibration was made based on the basin's characteristics and similar studies carried out in the regions (Singh and Goyal, 2017a,b). The most sensitive parameters were (Table 5.4): Groundwater delay (GW_DELAY), Soil evaporation compensation factor (ESCO), Available water capacity of the soil layer (SOL_AWC),

Table 5.3: Sub-basin wise trend analysis of seasonal precipitation for past (1951-2010) and projected (2011-2100) climates using Mann-Kendall trend test.

Season	Period	Scenario	Sub-basins							
			SB1	SB2	SB3	SB4	SB5	SB6	SB7	SB8
Monsoon	Past	Observed	↓	↓	↓	↓	+	-	↓	-
	Projected	RCP4.5	↑	↑	↑	↑	↑	↑	↑	↑
		RCP8.5	↑	↑	↑	↑	↑	↑	↑	↑
Non-monsoon	Past	Observed	↑	↑	↑	↑	↑	↑	↑	↑
	Projected	RCP4.5	↑	↑	↑	↑	↑	↑	↑	↑
		RCP8.5	↑	↑	↑	↑	↑	↑	↑	↑

↑ represents the significant increasing trend at significance level of 0.05 (i.e., MK Z value > 1.96).
↓ represents the significant decreasing trend (i.e., MK Z value < -1.96).
+ represents the non-significant increasing trend (p-value > 0.05).
- represents the non-significant decreasing trend (p-value > 0.05)

Deep aquifer percolation fraction (RCHRG_DP) and Effective hydraulic conductivity in main channel alluvium (CH_K2).

Due to the presence of basin in the Himalayas and of larger snow cover, some parameters important to snow-water mass balance were also included. These parameters include Snowfall temperature (SFTMP), Snow pack temperature lag factor (TIMP), Snow water equivalent that corresponds to 50% snow cover (SNO50COV), Maximum melt rate for snow during year (SMFMX), Minimum melt rate for snow during the year (SMFMN) and Snowmelt base temperature (SMTMP). The model calibration was carried out in multiple iterations with updated parameters. Figure 5.14 shows the observed and simulated streamflow along with the scatter plots for calibration and validation periods. The agreement between observed and simulated streamflow was comparable for calibration and validation, hence eliminating the possibility of over-fitting. From scatter plots, it is clear that the model performance appears to be reasonably good. The performance of the model was also assessed based on statistical measures (p-factor, r-factor, NSE and R^2). The p-factor and r-factor were 0.81 and 0.69, respectively, for calibration and 0.64 and 0.33, respectively, for validation. The NSE and R^2 for calibration were 0.915 and 0.941, respectively, whereas, for the validation period, the NSE and R^2 were 0.898 and 0.888, respectively. Overall, the model's performance in simulating the observed flow was reasonably good.

Table 5.4: Description, sensitivity analysis and range of SWAT parameters used for calibration in SWAT-CUP.

Parameter	Description	Sensitivity analysis		Initial range		Final fitted value
		p-value	t-stat	Minimum	Maximum	
v__GW_DELAY.gw	Groundwater delay (days)	0	− 11.32	30	450	165.03
v__ESCO.hru	Soil evaporation compensation factor	0	6.52	0	1	0.36
r__SOL_AWC(..).sol	Available water capacity of the soil layer	0	− 5.56	− 0.2	0.4	0.17
v__RCHRG_DP.gw	Deep aquifer percolation fraction	0	− 5.03	0	1	0.87
v__CH_K2.rte	Effective hydraulic conductivity in main channel alluvium	0.01	2.51	5	130	69.44
r__OV_N.hru	Manning's "n" value for overland flow	0.03	2.22	− 0.2	0	− 0.14
v__ALPHA_BNK.rte	Baseflow alpha factor for bank storage	0.04	− 2.06	0	1	0.04
r__CN2.mgt	SCS runoff curve number	0.17	− 1.37	− 0.2	0.2	0.19

v__EPCO.bsn	Plant uptake compensation factor	0.29	1.07	0	1	0.77
v__SNO50COV.bsn	Snow water equivalent that corresponds to 50% snow cover	0.29	− 1.06	0.05	0.8	0.45
r__SNOCOVMX.bsn	Minimum snow water content that corresponds to 100% snow cover	0.34	− 0.95	0	0.1	0.09
v__GWQMN.gw	Threshold depth of water in the shallow aquifer required for return flow to occur (mm)	0.35	0.94	0	2	1.99
r__SMFMX.bsn	Maximum melt rate for snow during year (occurs on summer solstice)	0.38	− 0.88	− 0.2	0.2	− 0.03
r__HRU_SLP.hru	Average slope steepness	0.4	0.84	0	0.2	0.03
v__TIMP.bsn	Snow pack temperature lag factor	0.42	0.82	0	1	0.49
r__SLSUBBSN.hru	Average slope length	0.43	− 0.8	0	0.2	0.03

a__SMTMP.bsn	Snow melt base temperature	0.5	− 0.67	− 5	5	0.18
r__SMFMN.bsn	Minimum melt rate for snow during the year (occurs on winter solstice)	0.54	0.62	− 0.2	0.2	− 0.07
v__SFTMP.bsn	Snowfall temperature	0.57	− 0.56	− 1	1	− 0.82
v__CH_N2.rte	Manning's "n" value for the main channel	0.57	0.56	0	0.3	0.1
v__REVAPMN.gw	Threshold depth of water in the shallow aquifer for "revap" to occur (mm)	0.58	0.55	0	100	48.55
r__SOL_K(..).sol	Saturated hydraulic conductivity	0.83	0.22	− 0.2	0.2	0.16
v__GW_REVAP.gw	Groundwater "revap" coefficient	0.86	0.18	0	0.2	0.19
v__ALPHA_BF.gw	Baseflow alpha factor (days)	0.86	0.17	0	1	0.22
v__SURLAG.bsn	Surface runoff lag time	0.99	− 0.02	5	24	9.25

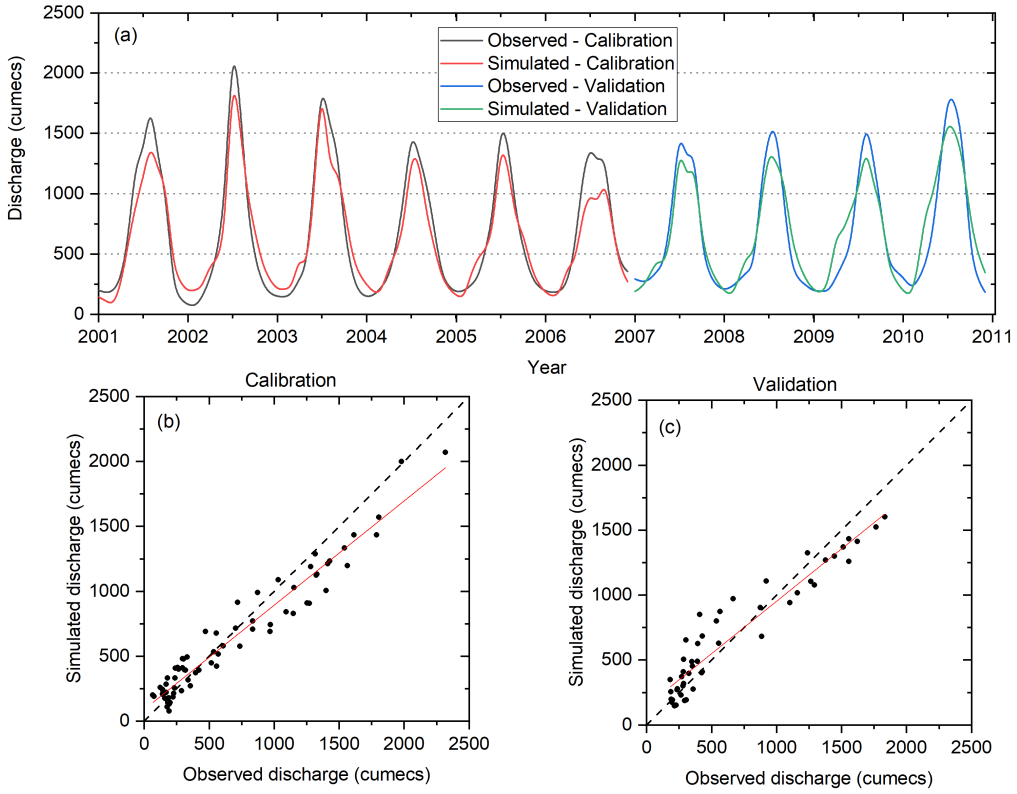

Figure 5.14: Comparison of observed discharge and SWAT simulated discharge. (a) Hydrographs of observed and simulated discharge for calibration and validation periods. (b) and (c) Scatter plots between observed and simulated discharge for calibration and validation periods respectively.

The calibrated SWAT model was used to simulate streamflow over the past and projected climate. The basin is located in mountainous regions of Eastern Himalayas. The area is scarcely populated and has very less anthropogenic impact. The state of Sikkim has least populated state in India and it accounts for only 0.05% of the total population of the country. Around 75% of the population live in rural areas. It is therefore assumed that there will not be significant changes in other conditions (e.g., LULC, soil etc.) apart from the climatic conditions. SWAT-simulated streamflow with different scenarios of GCM based climatic conditions were used for further analysis. Figure 5.15 shows the SWAT simulated streamflow for past and projected climate. The streamflow pattern was closely related to the precipitation. Like precipitation, streamflow during the past climate showed a decreasing trend, but it was not statistically significant ($p > 0.05$). The average annual flow for the observed period decreased from the value of 694.69 cumecs for the period from 1951 to 1980 to 647.52 cumecs for the period from 1981 to 2010. Under the projected climate, streamflow showed a significant increasing trend for both RCP4.5 and RCP8.5 ($p < 0.05$). The average annual flow under RCP4.5

was found to be 718.85 cumecs for the period from 2011 to 2040, 733.53 cumecs for the period from 2041 to 2070, and 739.96 cumec for the period from 2071 to 2100, which indicated the consistent increase in streamflow. Likewise, under RCP8.5, the average annual flow was found to be 699.63 cumecs for 2011-2040, 768.64 cumecs for 2041-2070 and 830.3 cumecs for 2071-2100. There was a substantial increase in streamflow under extreme scenario by in the last few decades; however, there was a large uncertainty associated with these predictions. The width of the range band increased towards the end of the 21st century. During the period 2071-2100, the average streamflow under RCP8.5 was 90 cumecs greater compared to RCP4.5. Figure 5.16 shows the cumulative density functions (CDF) of monthly flows for different GCMs and RCPs. The RCP based future streamflow showed a more frequent occurrence of higher flows compared to past climate.

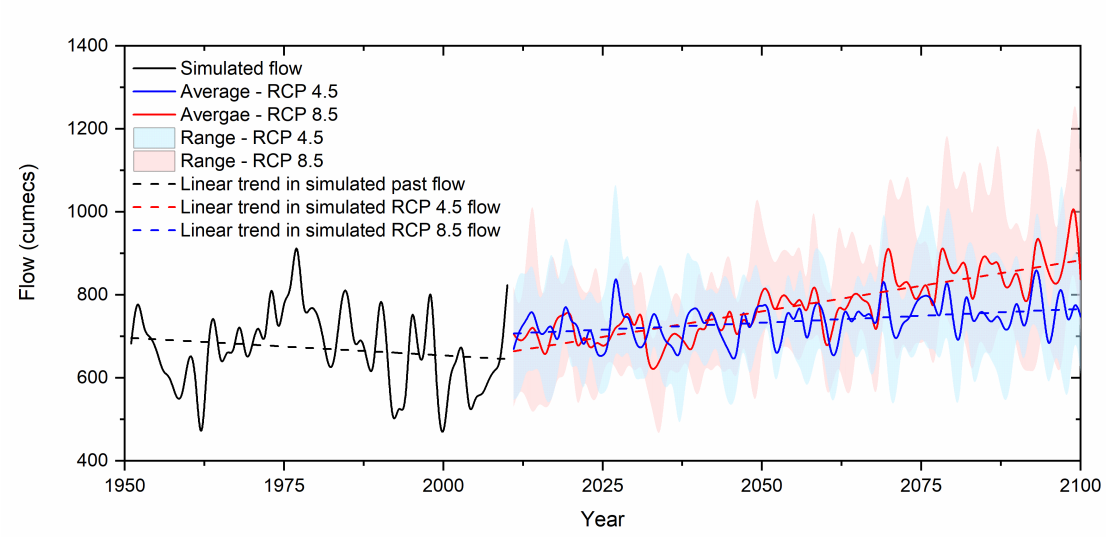

Figure 5.15: SWAT simulated streamflow for past and projected climates. The solid blue and red curves show the average of muti-model projections for RCP4.5 and RCP8.5 respectively. The shaded blue and red area shows the range of multi-model projection for RCP4.5 and RCP8.5 respectively. Dotted lines shows the linear trend.

Figure 5.17 shows the month-wise percent change in streamflow (Figure 5.17 a and b) and precipitation (Figure 5.17 c and d) during the period P2 (from 2021 to 2060) and P3 (from 2061 to 2100) compared to past climate P1 (from 1971 to 2010). Figure 5.18 shows the changes in monthly daily maximum temperature (Tmax), daily minimum temperature (Tmin), snowfall and snowmelt. It is evident from Figure 5.17 (a, b) that most of the months showed an increase in streamflow; however, there was a substantial increase in streamflow during the winter period (December to March).

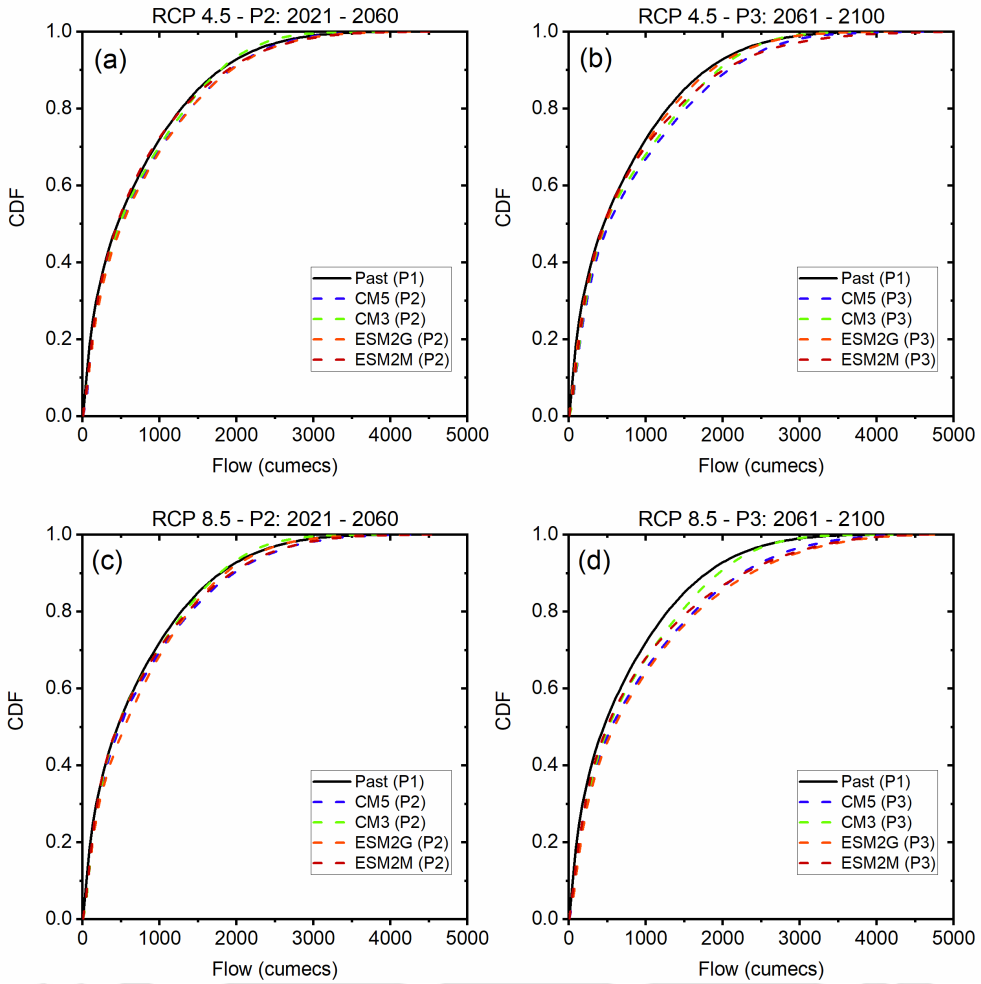

Figure 5.16: CDFs for monthly flow for past climate and for different models projections for RCP4.5 and RCP8.5 for different time periods.

Under RCP8.5, the winter streamflow was projected to increase by more than 50% during the period P3 compared to P1. The precipitation pattern in the basin is dominated by the southwest monsoon during the monsoon period from May to September, which occurs mainly in the form of rainfall. Precipitation in these months showed an increase for projected climate (Figure 5.17 c and d). During winter months, the precipitation showed both increase and decrease for P2 for different scenarios, whereas it had clear increase for P3. There was a consistent increase in both Tmax and Tmin for all month for RCP4.5 and RCP8.5 (Figure 5.18 a, b). Whereas, there was a decrease in snowfall for all months having snowfall, which was consistent with the increase in temperature. The projections of the increase in precipitation along with a decrease in snowfall indicate that more precipitation would occur in the form of rainfall than snow during winters. The snowmelt contribution to the water yield was higher during the spring period (March and April). However, the projected snowmelt obtained from SWAT in-

dicated a decrease in snowmelt during these periods, whereas snowmelt during winter months remained the same. This suggests that the snowfall happening during the winters would melt during winter period leaving lesser snow cover for spring months. The increased contribution of snowmelt during winter months explained the large increase in winter month streamflow (Figure 5.17 a, b).

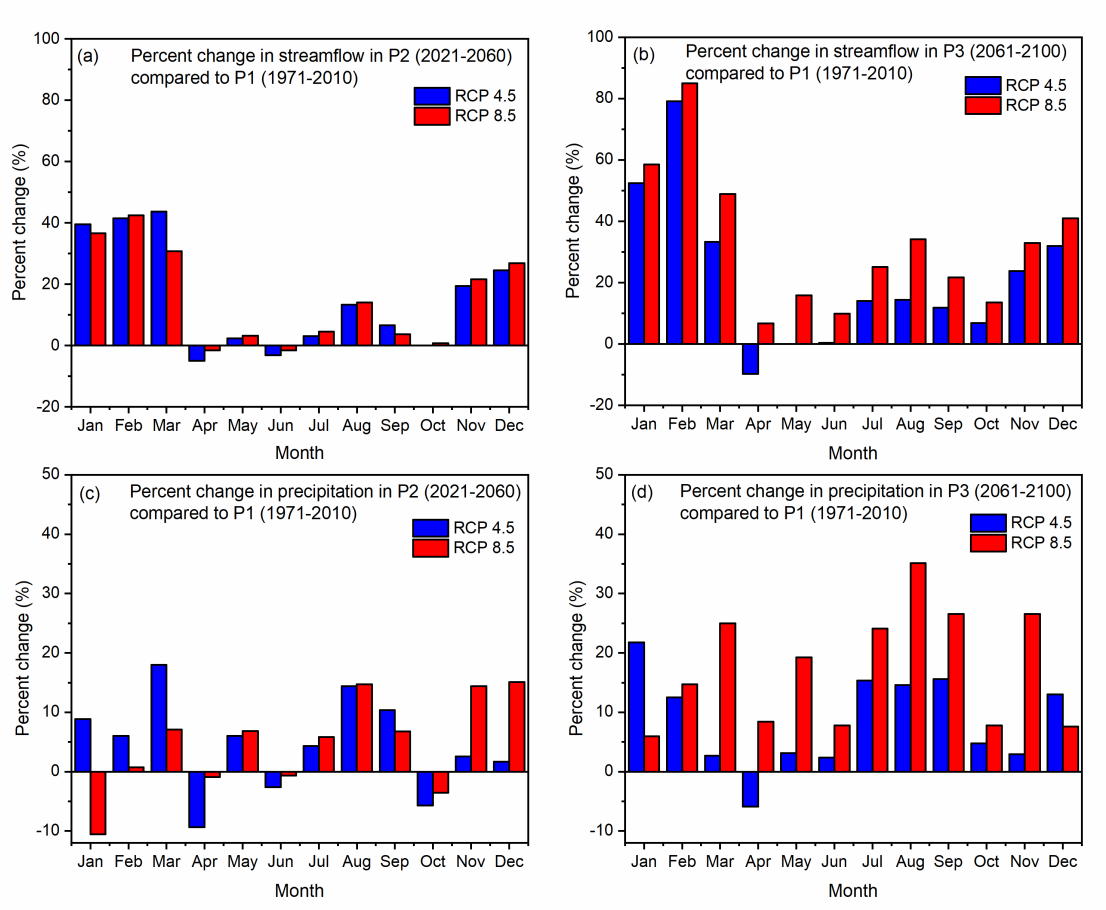

Figure 5.17: Month-wise percent change in streamflow and precipitation for the periods P2 (2021 to 2060) and P3 (2060 to 2100) compared to the period P1 (1971 to 2010) for RCP4.5 and RCP8.5. The streamflow is generated using SWAT model. The RCP scenarios represent the average of four GCMs used in the study.

5.5.7 Resilience analysis

Table 5.5 shows the statistics of the resilience analysis for past climate and projected climate under two RCPs. For this analysis, only the drought events of duration of more than three months were considered. The number of droughts for the past climate (1951-2010) was 9, whereas, for projected climate (2011-2100), the number of droughts was found to be 14.25 for RCP4.5 and 14 for RCP8.5. The average duration of drought events slightly increased from 6.08 months for the past climate to

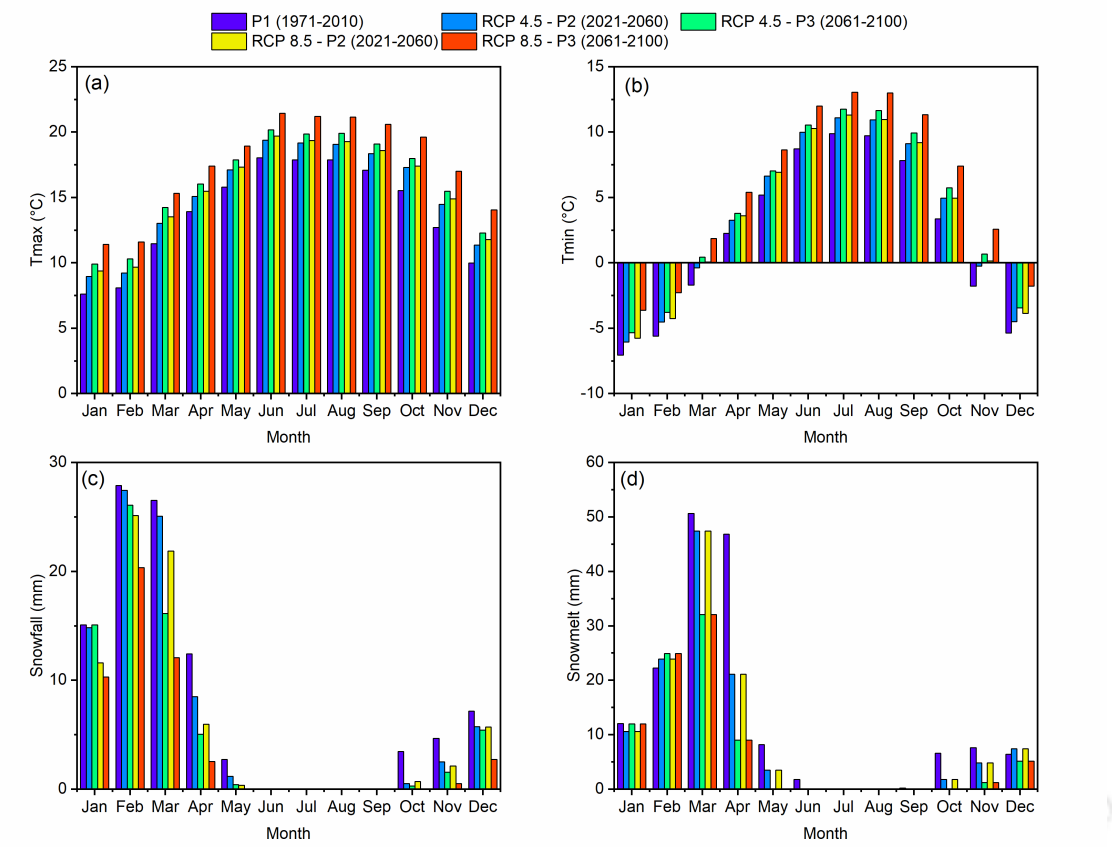

Figure 5.18: Month-wise mean value of annual daily maximum temperature (Tmax), daily minimum temperature (Tmin), snowfall and snowmelt for the periods: P1 (1971 to 2010), P2 (2021 to 2060) and P3 (2060 to 2100). The RCPs scenarios represents the average for four GCMs used in this study.

6.22 and 6.31 months for RCP4.5 and RCP8.5, respectively. However, the average SPI value for drought events increased for projected climate (-1.59 for RCP4.5 and− 1.52 for RCP8.5) compared to the value of− 1.62 for past climate. This suggests that the droughts in projected climate would be less intense. The resilience of the basin to dry period was assessed based on 'deviation' and 'recovery time' as discussed in methodology. The average deviation for the past climate was− 41.29%. The negative value of deviation indicates the reduction in system function (i.e., streamflow). The average deviation for RCP4.5 and RCP8.5 scenarios was found to be− 32.42% and− 29.55%, respectively. This shows that the deviation in streamflow was lesser under the projected climate. It should be noted that for resilience analysis, the changes in flow only during the dry period were analyzed. The lesser deviation under projected climate indicated the higher resilience of the basin to dry conditions. The average recovery time decreased from 5.42 months to 4.63 and 4.42 months during RCP4.5 and 8.5, respectively, which also indicates the higher resilience of the basin. Both statistics (deviation and recovery

time) clearly showed a sign of higher resilience of the basin in terms of maintaining the streamflow during meteorological drought conditions.

Table 5.5: Statistics of the resilience analysis for past and projected climate for different GCMs and two different RCPs. Only drought events of duration greater three months were considered.

Scenario	Model	Number of droughts	Average Duration (months)	Average SPI for drought events	Average Deviation (%)	Average Recovery Time (months)
Past climate (1951-2010)		9	6.08	− 1.62	− 41.29	5.42
RCP4.5 (2011-2100)	CM5	15	6.47	− 1.61	− 30.86	4.8
	CM3	13	6.46	− 1.58	− 23.88	4.38
	ESM2G	13	6.08	− 1.61	− 31.89	4.77
	ESM2M	16	5.88	− 1.58	− 43.04	4.56
	Average	14.25	6.22	− 1.59	− 32.42	4.63
RCP8.5 (2011-2100)	CM5	16	5.81	− 1.49	− 25.36	3
	CM3	13	6.31	− 1.55	− 32.77	4.15
	ESM2G	16	7.13	− 1.48	− 36.97	6.44
	ESM2M	11	6	− 1.55	− 23.1	4.09
	Average	14	6.31	− 1.52	− 29.55	4.42

Table 5.6 shows the statistics of resilience analysis over 30-year intervals from 1951 to 2100. During the past climate, the number of droughts increased from 3 during the period from 1951 to 1980 to 6 during the period from 1981 to 2010, whereas the average drought duration increased from 5.67 months to 6.5 months between these periods. The drought intensity decreased between these periods. The average deviation was - 56.49% for the period from 1951 to 1980 and - 26.1% for the period from 1981 to 2010, which indicated the higher resilience for the period from 1981 to 2010 period, whereas, on the other hand, the average recovery time increased from 4.67 months for the period from 1951 to 1980 to 6.17 months for the period from 1981 to 2010, which indicated the lower resilience for the period from 1981 to 2010. This implies that the streamflow was less affected by dry conditions during the period from 1981

to 2010, but the basin took a longer duration to recover to its normal state. Under the RCP4.5 scenario, the number of droughts significantly decreased towards the end of the 21st century, whereas there was no significant increase/decrease in average drought duration and average SPI. A substantial reduction in average recovery time was found, whereas the average deviation remained somewhat the same. Like RCP4.5, RCP8.5 also showed higher resilience for the 21st century. The number of droughts reduced to 2 during the period from 2071 to 2100 under RCP8.5. This analysis revealed a clear sign of increasing resilience of river basin to dry period, which could be attributed to the increase in the precipitation in the basin under climate change, which helped the basin in maintaining enough water storage in the form of groundwater that available during the dry period. The presence of glaciers and snow cover in the basin could also contribute to the flow. Increasing temperature, as clearly found in this study and previous studies, will result in the melting of glaciers, which could act as a source of water during the dry period; however, it is not a sustainable source of water.

Table 5.6: Statistics of the resilience analysis for past and projected climate for different time periods (30 year intervals). Only drought events of duration greater 3 months were considered.

Scenario	Time period	Number of droughts	Average Duration (months)	Average SPI for drought events	Average Deviation (%)	Average Recovery Time (months)
Past climate	1951-1980	3	5.67	− 1.77	− 56.49	4.67
	1981-2010	6	6.5	− 1.47	− 26.1	6.17
RCP4.5	2011-2040	7.3	5.9	− 1.59	− 31.9	4.8
	2041-2070	3.8	6.7	− 1.59	− 33	4.7
	2071-2100	3.3	6.1	− 1.56	− 31.9	4
RCP8.5	2011-2040	9	6.8	− 1.54	− 31.1	5.3
	2041-2070	5.4	6.3	− 1.57	− 32.1	4.5
	2071-2100	2	4.9	− 1.47	− 27.1	2.6

5.6 Conclusions

The hydrological resilience analysis of Teesta river basin in the Eastern Himalayan Region to dry periods was carried out. The hydrological resilience of the basin was defined as its ability to maintain the streamflow during the period of lesser precipitation (i.e., meteorological drought). The analysis of changes in precipitation, temperature, streamflow and snow was carried out over the period from 1951 to 2100. For projected climate (i.e., 2011 to 2100), four GCMs along with two RCPs were used. A decreasing trend for observed period precipitation and an increasing trend for precipitation in projected climate was found. For both observed and projected climates, a rising trend was found for both daily maximum and minimum temperature. SWAT-simulated streamflow showed a decreasing trend for observed climate and an increasing trend for the projected climate. RCP8.5 based projections showed a considerably higher increase in precipitation, temperature, and streamflow compared to RCP4.5 based projections. Monthly analysis of streamflow indicated a substantial increase in streamflow for the winter months under the projected climate. The snowfall decreased for all the months under both RCPs; however, the snowmelt did not show any significant change for winter months. Snowmelt during the winter period was linked to an increase in discharge during the same period. The standardized precipitation index (SPI) based drought analysis indicated a reduction in drought events under the projected climate. The intensity and duration of drought events were also found to decrease towards the end of the 21st century. 'Deviation from normal' and 'Time to recover' were used to assess the resilience of the basin. These measures suggested an increase in the basin's resilience to dry period under projected climate. Both average deviation and recovery time decreased for projected climate for both RCPs, which clearly shows the higher resilience of the basin to dry conditions. This could be due to the increasing trend of precipitation and streamflow.

6

Changes in Precipitation, Temperature and Climate Extremes

6.1 Introduction

As per IPCC, the anthropogenic greenhouse gas emissions have increased since the pre-industrial era (IPCC, 2014), which has led to the warming of the Earth's atmosphere (Karl and Trenberth, 2003). The impact of climate change is not uniform but varies regionally on Earth.

This study examines the changes in precipitation, temperature and climate extremes in India. This chapter discusses:

- Analysis of precipitation and temperature in India for observed climate (1951-2010)
- Bias-correction of GCM outputs for four different RCP scenarios
- Analysis of precipitation and temperature in India for projected climate (2006-2100)
- Analysis of climate extremes (25 indices) over observed and projected climate
  - 11 precipitation extremes
  - 14 temperature extremes

6.2 Study area and data used

6.2.1 Observed data

The study area for this study was India. The analysis was carried out at carried out over 0.5°×0.5° grids of IMD. High resolution (0.25°×0.25°) gridded precipitation

dataset was obtained from the IMD (Pai et al., 2014). The high-resolution precipitation data was regridded to 0.5-degree grid points using Inverse Distance Weighting (IDW) Interpolation technique. IMD provides temperature data at coarse resolution (1° × 1°), which was not suitable for this study. Therefore, temperature data (i.e., maximum and minimum daily temperature) from Sheffield et al. (2006) was used. The dataset was developed by Terrestrial Hydrology Research Group, Princeton University and is available at 0.25° × 0.25° resolution. Figure 6.1 shows these three data grids in India. Mishra et al. (2014) used this temperature dataset from Sheffield et al. (2006) and compared with the IMD temperature records for the overlapping period (1969-2005) in India. The comparison suggested that temperature data from Sheffield et al. (2006) follows the seasonal cycle and temporal and spatial variability in India.

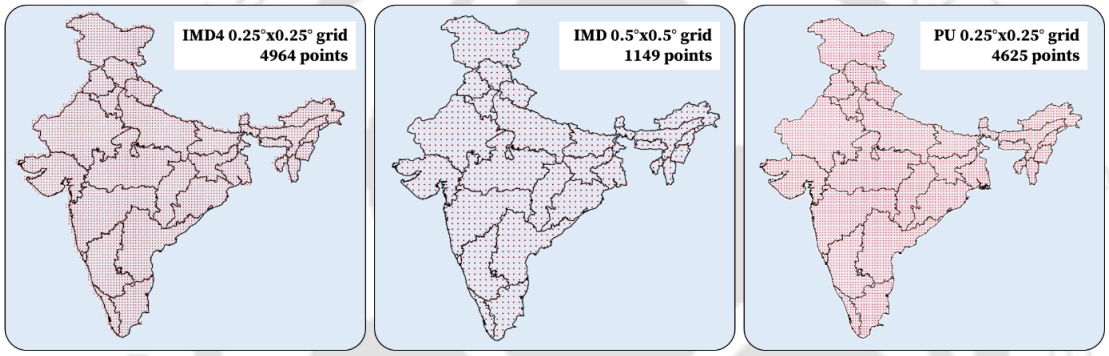

Figure 6.1: IMD4 (0.25°×0.25°), IMD (0.5°×0.5°) and PU (0.25°×0.25°) grids in India.

6.2.2 GCM data

For projected climate, daily outputs of precipitation and air temperature were obtained from the 20 GCMs that participated in CMIP5 (Table 6.1). CMIP5 based GCMs provide outputs for four RCPs. All four RCPs were considered in this study.

6.3 Methods used

6.3.1 Bias correction

Outputs from the GCMs are generally biased and are rarely used directly. The biases arise due to the systematic errors in the climate model simulations, which occur because of the limited spatial resolution and simplified physics and thermodynamics. Our lack of understanding of different atmospheric processes also leads to deviation of model outputs from the actual scenarios. Therefore, it becomes essential to bias-correct

Table 6.1: GCMs and RCPs used in this study.

S. N.	Institute Name	Model Name	Scenario Used				
			Historical	RCP 2.6	RCP 4.5	RCP 6.0	RCP 8.5
1	BCC	bcc_csm1-1	Yes	Yes	Yes	Yes	Yes
2	BNU	BNU-ESM	Yes	Yes	Yes	No	Yes
3	CCCma	Can-ESM2	Yes	Yes	Yes	No	Yes
4	CMCC	CMCC-CM	Yes	No	Yes	No	Yes
5		CMCC-CMS	Yes	No	Yes	No	Yes
6	CNRM	CM5	Yes	Yes	Yes	No	Yes
7	CSIRO-BOM	ACCESS1-0	Yes	No	Yes	No	Yes
8		ACCESS1-3	Yes	No	Yes	No	Yes
9	CSIRO-QCCCE	CSIRO-Mk3-6-0	Yes	Yes	Yes	Yes	Yes
10	ICHEC	EC-EARTH	Yes	Yes	Yes	No	Yes
11	INM	INMCM4	Yes	No	Yes	No	Yes
12	IPSL	IPSL-CM5A-LR	Yes	Yes	Yes	Yes	Yes
13		IPSL-CM5A-MR	Yes	Yes	Yes	Yes	Yes
14		IPSL-CM5B-LR	Yes	No	Yes	No	Yes
15	LASG-CESS	FGOALS-g2	Yes	Yes	Yes	No	Yes
16	MOHC	HadGEM2-CC	Yes	No	Yes	No	Yes
17		HadGEM2-ES	Yes	Yes	Yes	Yes	Yes
18	NOAA-GFDL	GFDL_CM3	Yes	Yes	Yes	No	Yes
19		GFDL_ESM2G	Yes	Yes	Yes	Yes	Yes
20		GFDL_ESM2M	Yes	Yes	Yes	Yes	Yes
Total number of models used			20	13	20	7	20

the GCM outputs so that it adequately represents the actual patterns. For this work, the method suggested by Mahmood and Babel (2013) was used for bias correction of GCM outputs. Observed precipitation and temperature datasets were used for the bias correction of model outputs. The bias-corrected data for the past period was compared with

observed data in terms of magnitude and frequencies. The bias correction methodology is described in detail in Section 5.4.1.

6.3.2 Climate extremes

For this analysis, all the indices discussed in Section 5.4.6 were used. In addition, two indices (R90p and R99p) were also used. The computation of R90p and R99p is similar to R95p, but instead of the 95th percentile of precipitation on wet days used in R95p, 90th and 99th percentile of precipitation are used for R90p and R99p, respectively.

6.4 Results and discussion

6.4.1 Analysis of precipitation and temperature

Figures 6.2, 6.3 and 6.4 show the changes in mean annual precipitation (MAP), daily maximum temperature (Tmax) and daily minimum temperature (Tmin), respectively, over the observed and projected periods, and Figures 6.5, 6.6 and 6.7 show the country-average annual values for the same variables. Figure 6.2(a-c) presents the comparison of observed and multi-model average (MMA) MAP over the period 1975-2005. The MMA captured the spatial pattern of the observed precipitation. The projected scenarios (Figures 6.2d-o) showed an increase in the precipitation for the 21st century. The increase in precipitation was higher for the higher RCPs. RCP8.5 scenario had the highest increase in precipitation all over the country, which was highest in the western parts of the country. Some parts of western India had an increase of about 80-100% for the period 2071-2100 under RCP8.5. Overall, the precipitation is projected to increase for the 21st century. The country-average precipitation also showed an increasing trend for all scenarios; however, there was a considerable variation between different model projections (Figure 6.5). RCP8.5 had larger projections compared to other RCPs. Mann-Kendall trend test also indicated the statistically significant increasing trend in precipitation for all the RCPs (Table 6.2). The increasing trend was highest for RCP8.5 with a magnitude of 3.31 mm/year. The magnitudes of the trend for RCP2.6, RCP4.5 and RCP6.0 were 0.89, 1.65 and 1.47 mm/year, respectively.

Figure 6.3(a-c) presents the comparison of observed and MMA Tmax. The MMA had similar spatial variation as the observed Tmax, and the difference between observed and MMA was very less. The bias-corrected Tmax from GCMs showed an increase in

temperature for all scenarios. The increase in Tmax was higher for high emission RCPs. RCP8.5 showed the highest rise in Tmax, which exceeds 6°C in some areas for the late 21st century. Though there was an increase in Tmax for the whole country, there was spatial variation in the magnitude of increase. In general, the increase was higher in the Himalayan regions. The country-average Tmax had an increasing trend for all four RCPs (Figure 6.6). RCP2.6 showed a trend of stabilizing after 2052, which is consistent with global studies. RCP4.5 had an increasing trend throughout, except for last ten year. RCP6.0 and RCP8.5 had an increasing trend up to 2100 and there was no stabilization. The magnitudes of linear trend for RCP2.6, RCP4.5, RCP6.0 and RCP8.5 were 0.01, 0.02, 0.03 and 0.05 °C/year, respectively (Table 6.2).

Like Tmax, the bias-corrected Tmin also had similar patterns as observed Tmin (Figure 6.4a-c). The difference between MMA and observed was very less. A consistent increase in Tmin was found for all the scenarios over different periods. The high emission scenarios showed a more significant increase in Tmin. For the worst scenario (RCP8.5), the increase in Tmin was greater than 5°C all over the country. The country-average Tmin increased for all RCPs (Figure 6.7). RCP2.6 projections were found to stabilize after 2050, whereas the projections showed continuous increasing trend thought-out the 21st century for other RCPs. Trends for all RCPs were found statistically significant in this case (Table 6.2). The magnitudes of the linear trend for RCP2.6, RCP4.5, RCP6.0 and RCP8.5 were 0.01, 0.03, 0.03 and 0.06 °C/year, respectively. From the magnitude of the linear trend, it was found that the trend in Tmin was greater than Tmax. Therefore, Tmin is anticipated to increase faster compared to Tmax.

6.4.2 Analysis of climate extremes

Figures 6.8 - 6.31 show the change in the different climate extremes during the observed period (1951-2010) and the projected period (2011-2100). Observed period was divided into two parts: Observed 1 (1951-1980) and Observed 2 (1981-2010). The projected period was divided into three parts of 30 years: F1 (2011-2040), F2 (2041-2070) and F3 (2071-2100).

6.4.2.1 Temperature Extremes

Figure 6.8 shows the results for Maximum Tmax (TXx). TXx represents the maximum value of Tmax in a year. The spatial pattern of TXx was same for Observed 1

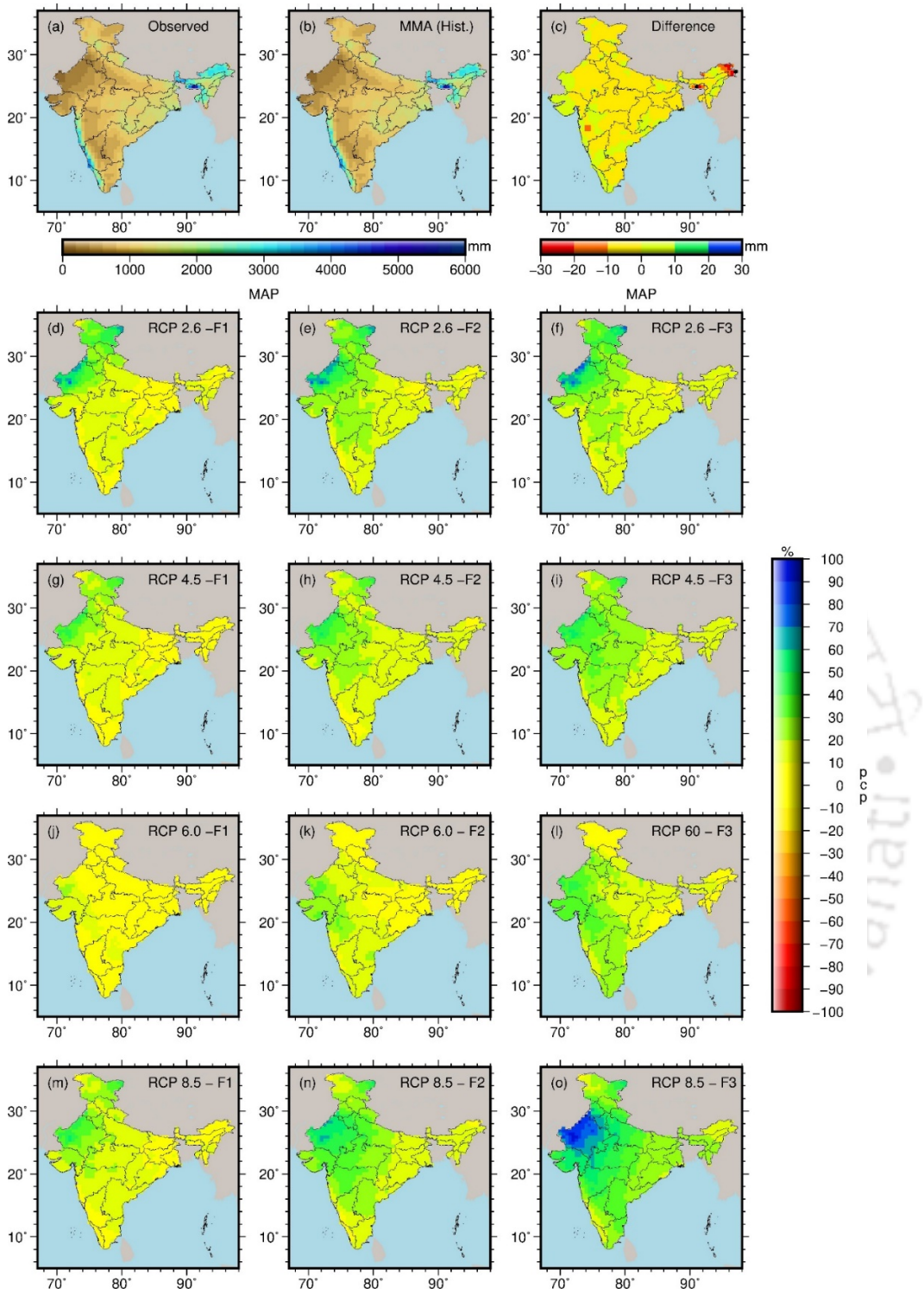

Figure 6.2: Change in mean annual precipitation (MAP) in India over observed and projected climate. (a) MAP over the observed period (1975-2005), (b) bias-corrected multi model average (MMA) MAP from historical run of the GCMs, (c) difference between observed and MMA, (d-o) percent change in MAP under RCPs with respect to observed MAP. F1, F2 and F3 denote the periods of 2011-2040, 2041-2070, and 2071-2100.

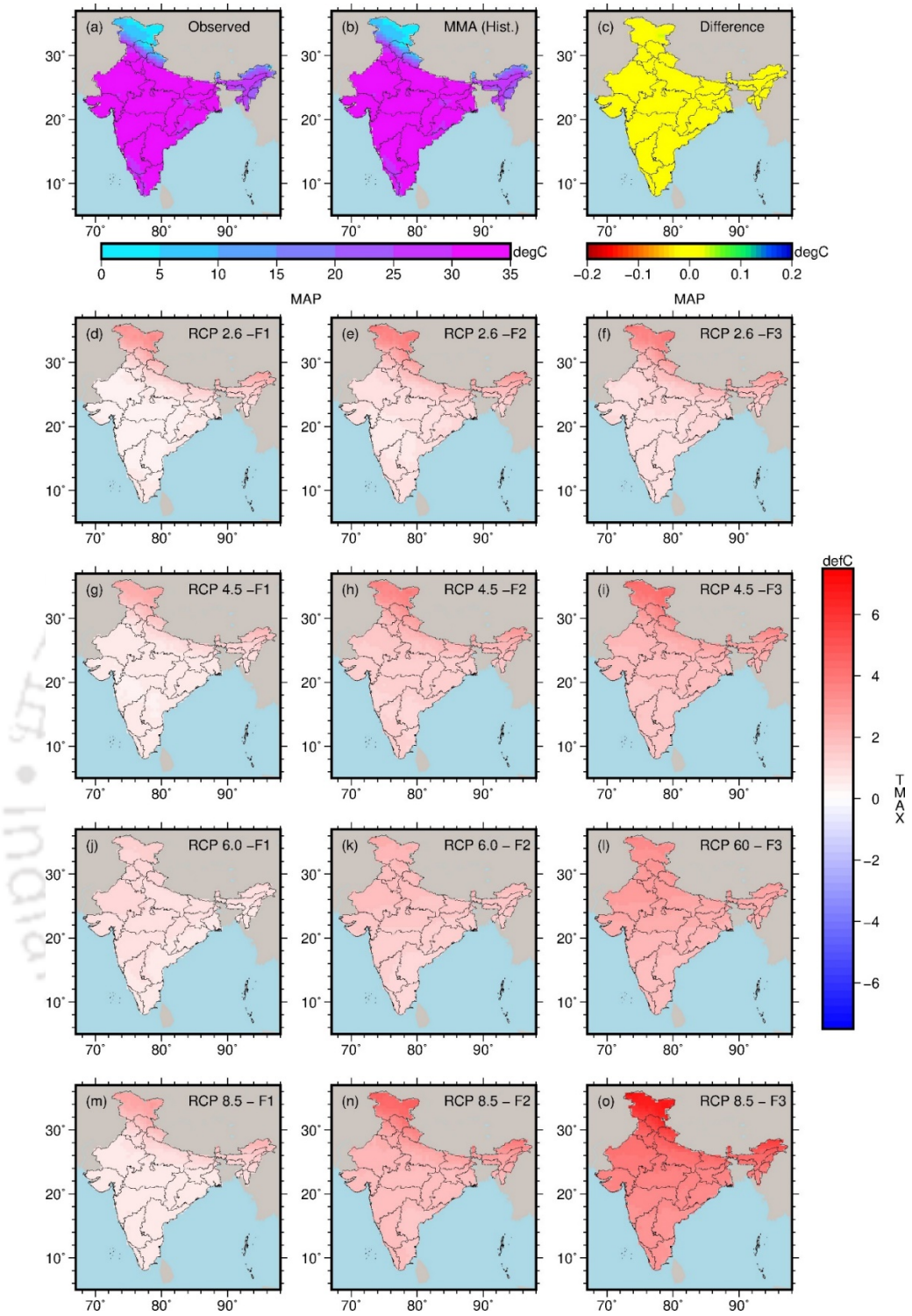

Figure 6.3: Change in mean annual daily maximum temperature (Tmax) in India over observed and projected climate. (a) Tmax over the observed period (1975-2005), (b) bias-corrected multi model average (MMA) Tmax from historical run of the GCMs, (c) difference between observed and MMA, (d-o) change in Tmax under RCPs with respect to observed Tmax. F1, F2 and F3 denote the periods of 2011-2040, 2041-2070, and 2071-2100.

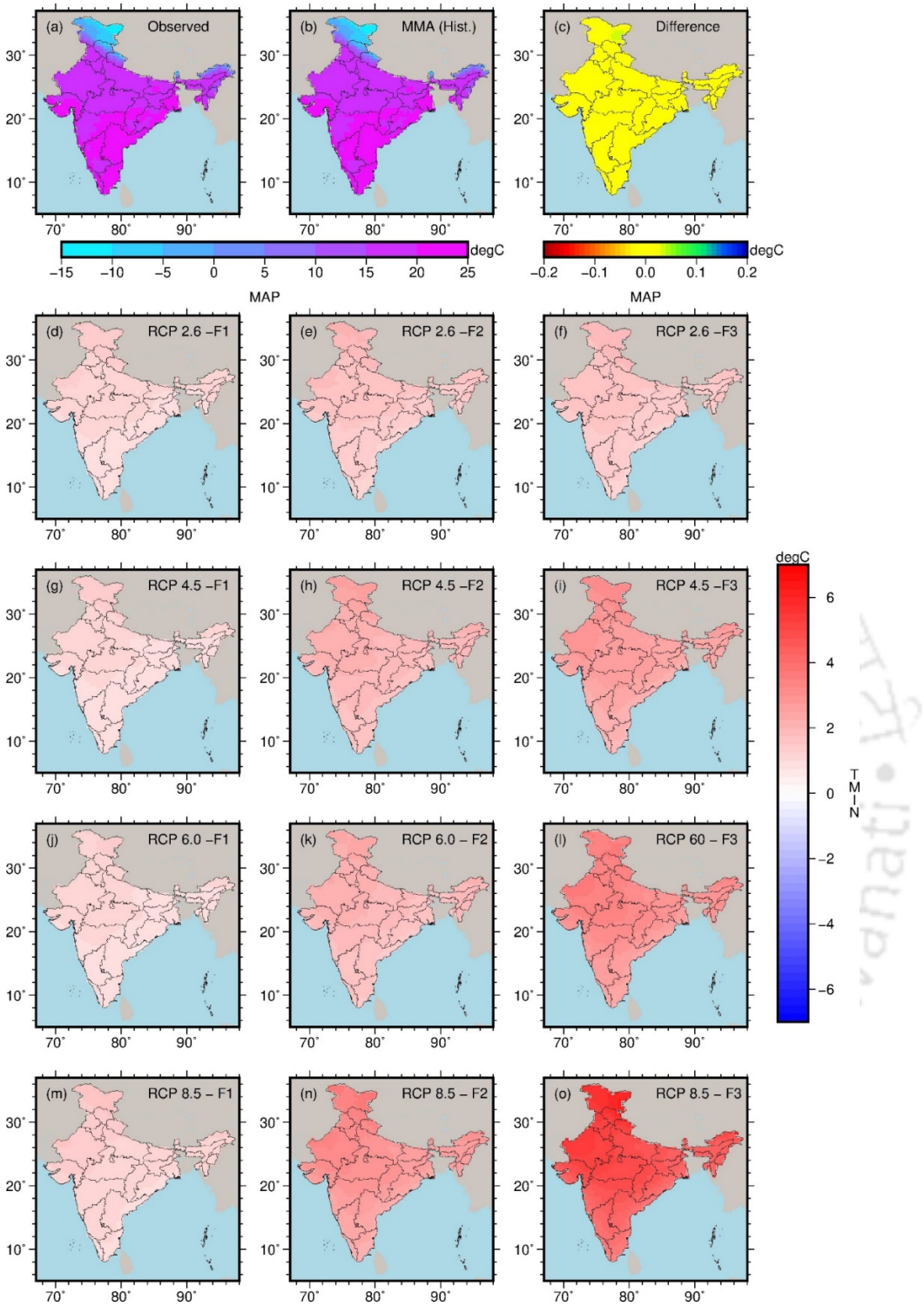

Figure 6.4: Change in mean annual daily minimum temperature (Tmin) in India over observed and projected climate. (a) Tmin over the observed period (1975-2005), (b) bias-corrected multi model average (MMA) Tmin from historical run of the GCMs, (c) difference between observed and MMA, (d-o) change in Tmin under RCPs with respect to observed Tmin. F1, F2 and F3 denote the periods of 2011-2040, 2041-2070, and 2071-2100.

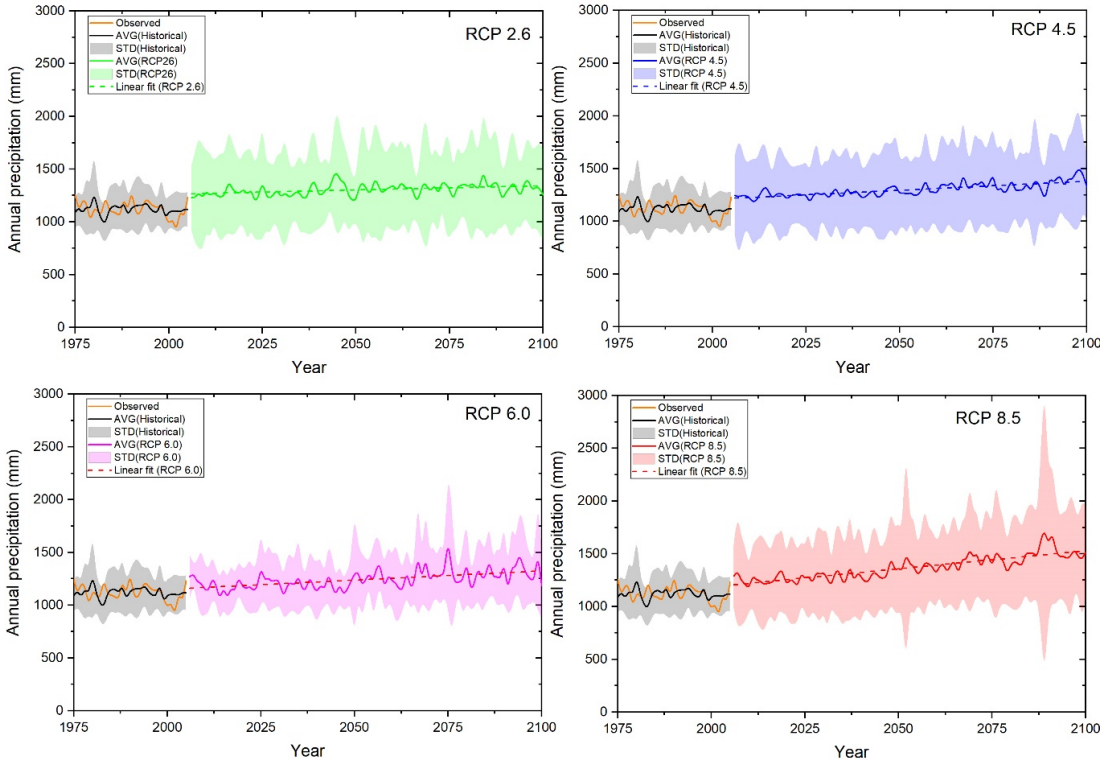

Figure 6.5: The country-average annual precipitation for the period 1975-2100 for different RCPs. The solid line shows the multi model average (MMA) values and the shaded area shows the standard deviation (SD) of multi model projections.

and Observed 2. The higher values of TXx were found for central and western parts of the country, whereas the Himalayan region had lower values of TXx. Figure 6.8(c) shows the changes in TXx between Observed 2 and Observed 1. There was an increase in TXx in some parts of the south and north India, whereas there was a decrease in TXx in central, eastern and northeastern parts of the country. The projected scenarios indicated an increase in TXx for all RCPs. Similar to temperature, the increase in TXx was higher for Himalayan regions. Some regions of north India had an increase in TXx of more than 6°C for period 2071-2100 for RCP8.5. Figure 6.9 shows the results for the change analysis of Minimum Tmax (TXn), which is computed as the minimum value of Tmax during the year. The spatial pattern of TXn was similar for Observed 1 and Observed 2 . TXn had an increasing gradient from north to south. The value of TXn in some parts of the Himalayas was as low as − 20°C. However, the TXn increased from Observed 1 to Observed 2 in northern, northwestern and southern parts of the country. In the northeastern and central parts of the country, there was a decrease in TXn between Observed 1 and Observed 2. All projected scenarios showed an increase in TXn; however, the increase was higher in Himalayan regions. Similar results were found the

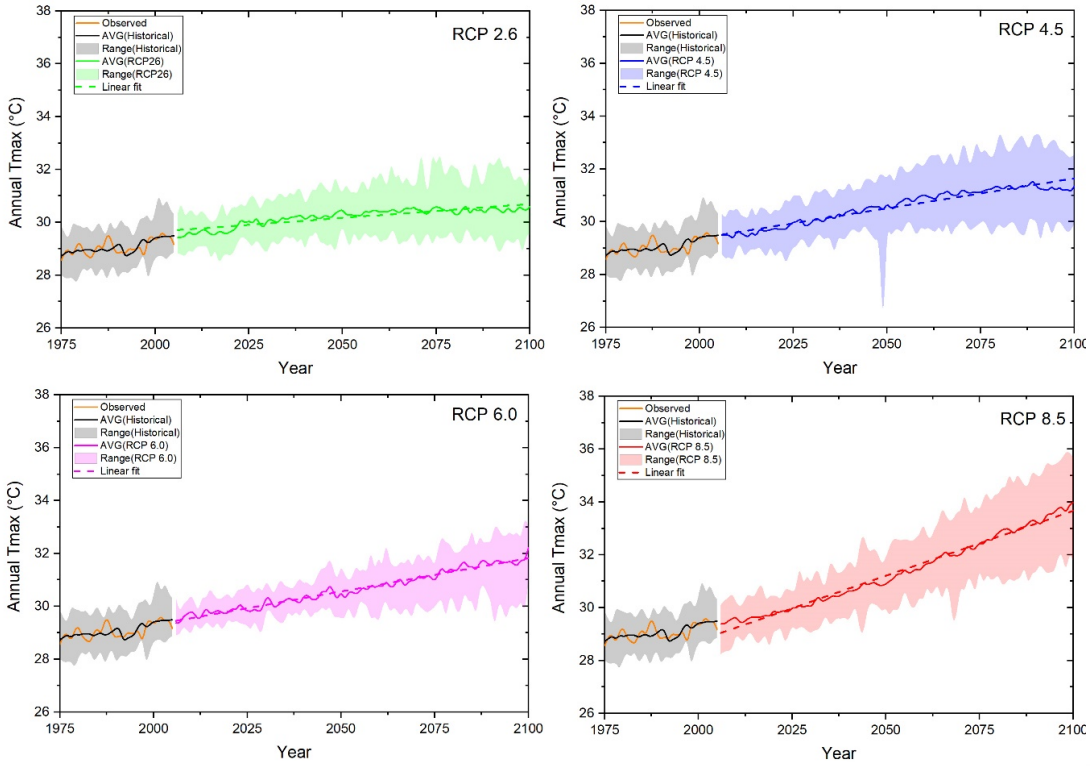

Figure 6.6: The country-average annual daily maximum temperature (Tmax) for the period 1975-2100 for different RCPs. The solid line shows the multi model average (MMA) values and the shaded area shows the range of multi model projections.

Maximum Tmin (TNx, Figure 6.10) and Minimum Tmin (TNn, Figure 6.11).

Figures 6.12-6.15 show the results for warm days (TX90p), cool days (TX10p), warm nights (TN90p) and cool nights (TN10p), respectively. These indices are expressed as the percent of the number of days in years having Tmax/Tmin below/above the threshold. The value of TX90p was found to increase over the observed period as well as the projected period (Figure 6.12). The country-average value of TX90p increased from 11.41% for Observed 1 to 11.66% for Observed 2 . There was large spatial variation in the TX90p. Between periods Observed 1 and Observed 2, TX90p increased in southern parts of the country by about 5-11%. A drastic increase in warm days was found for the projected climate. The country-average values of TX90p for RCP2.6 were 17.42%, 19.59% and 19.59% for F1, F2 and F3, respectively, for RCP4.5 were 17.29%, 22.45% and 25.67% for F1, F2 and F3, respectively, for RCP6.0 were 17.43%, 21.92% and 27.86% for F1, F2 and F3, respectively, and for RCP8.5 were 17.88%, 26.04% and 36.43% for F1, F2 and F3, respectively. Cool days (TX10p) decreased drastically under projected climate scenarios. Figure 6.13 compares the changes in TX10p with

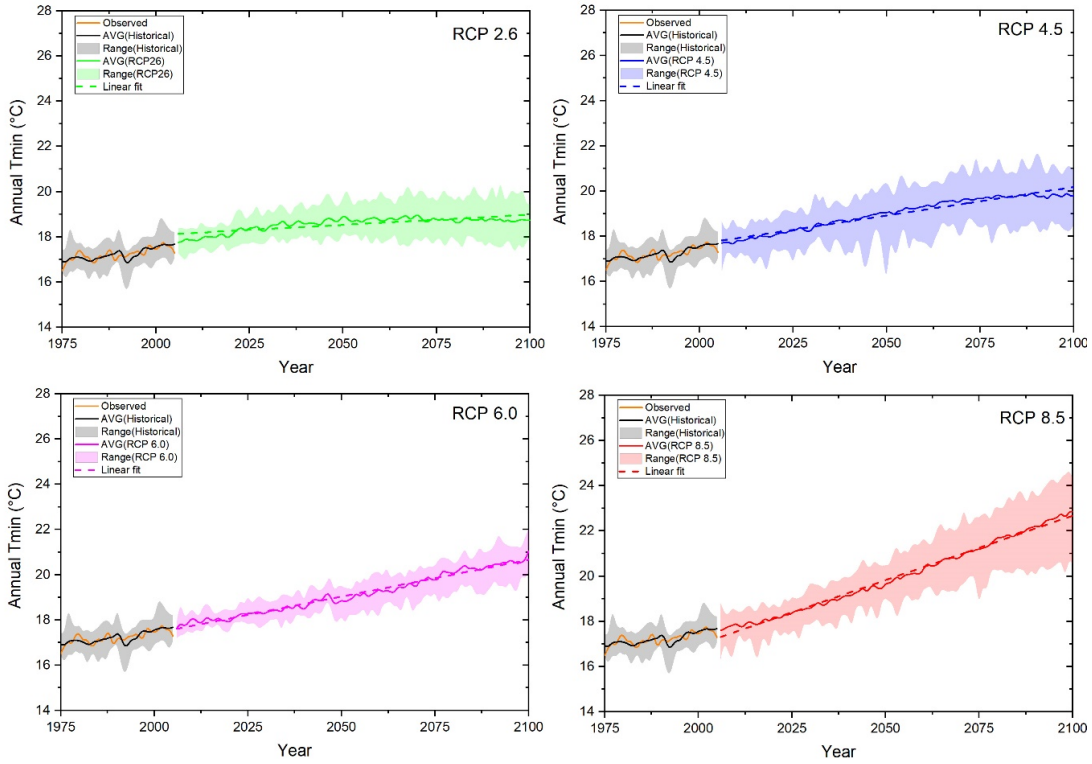

Figure 6.7: The country-average annual daily minimum temperature (Tmin) for the period 1975-2100 for different RCPs. The solid line shows the multi model average (MMA) values and the shaded area shows the range of multi model projections.

observed data. The value of TX10p varied between 7.83% and 21.64% for Observed 1 and between 6.26% and 14.66% for Observed 2 over India. The country-average values for Observed 1 was 11.41% and for Observed 2 was 9.58%. TX10p reduced significantly over the projected period. The country-average values of TX10p for RCP2.6 were 8.61%, 7.36% and 7.12% for F1, F2 and F3, respectively, for RCP4.5 were 8.53%, 5.59 and 4.35% for F1, F2 and F3, respectively, for RCP6.0 were 7.80%, 5.84% and 3.45% for F1, F2 and F3, respectively, and for RCP8.5 were 8.46%, 4.37% and 1.96% for F1, F2 and F3, respectively. Under the extreme condition (RCP8.5), the number of cool days reduced to less than ten days in some parts of the country. Every part of the country is anticipated to experience reduction in the cool days; however, the magnitude of reduction varied in different regions.

Similar indices that are based on Tmin are cool nights and warm nights. Like warm days and cool days, the warm nights were found to increase, whereas the cool nights were found to decrease (Figures 6.14 and 6.15). The number of warm nights increased by about 50% in some parts of the country for the period F3 under the extreme

Table 6.2: Trend analysis of the precipitation, Tmax and Tmin under projected scenarios.

Precipitation			
RCP	p-value	Z stat.	Slope (mm/yr)
RCP2.6	0	3.49	0.89
RCP4.5	0	7.1	1.65
RCP6.0	0	4.08	1.47
RCP8.5	0	8.66	3.31
Tmax			
RCP	p-value	Z-stat.	Slope (°C/yr.)
RCP2.6	0	10.13	0.01
RCP4.5	0	12.23	0.02
RCP6.0	0	12.39	0.03
RCP8.5	0	13.76	0.05
Tmin			
RCP	p-value	Z-stat.	Slope (°C/yr.)
RCP2.6	0	7.93	0.01
RCP4.5	0	13.04	0.03
RCP6.0	0	13.17	0.03
RCP8.5	0	13.93	0.06

scenario. The country-average value of TN90p was 11.07% for Observed 1 and 13.60% for Observed 2 . Under the projected climate, the country-average value increased to 23.34%, 27.35% and 27.04% for RCP2.6 for F1, F2 and F3, respectively, to 23.73%, 32.58% and 37.45% for RCP4.5 for F1, F2 and F3, respectively, to 23.10%, 31.54% and 41.14% for RCP6.0 for F1, F2 and F3, respectively, and to 25.02%, 39.76% and 53.14% for RCP8.5 for F1, F2 and F3, respectively. Cool nights had a similar trend as cool days. A decrease in cool nights was found for all parts of the country. During the observed period, the country-average cool nights decreased from 11.35% during Observed 1 to 8.91% during the Observed 2 , which shows there was a reduction of 2.44%. The cool nights reduced further for different RCPs. In some parts of the country, cool nights

decreased to less than 10 days per year by the end of the century.

Tropical nights (TR), which is the number of days with Tmin > 20°C, plays a vital role for humans as the human body requires to cool down after a hot day. During a tropical night, the temperature stays high (>20°C), which makes it hard for the human body to cool down. A drastic increase in TR may also lead to an increase in mortality. Figure 6.16 shows the analysis of TR over the observed and projected climate. There's a considerable spatial variation in TR over the country. The southern parts of the country had TR as high as the length of the year, whereas the Himalayan regions had TR as low as 0 day. The spatial pattern of TR remained the same between Observed 1 and Observed 2; however, there was a significant change in values, especially in Western Ghats regions and in northeast India. There was an increase of about 30-60 days in some parts of south India between Observed 1 and Observed 2. The country-average TR increased from 180 days during Observed 1 to 187 days during Observed 2 . Consistent with the increase in temperature, a rise in TR was found for all projected scenarios. Western Ghats in the south had the most significant increase under projected climate. For RCP2.6, the country-average TR was found 203, 210, and 210 days for period F1, F2 and F3, respectively. For RCP4.6, the country-average TR was found 203, 217 and 226 days for F1, F2 and F3, respectively. For RCP6.0, the country-average TR was found 203, 215 and 231 days for F1, F2 and F3, respectively. For the extreme scenario, i.e., RCP8.5, the country-average TR was found 206, 229 and 255 days for F1, F2 and F3, respectively. The analysis suggested that there was an increase in TR and are further anticipated to increase in projected climate.

Summer days (SU) is the number of days with Tmax greater than 25°C (Figure 6.17). The index is important because not only that it is difficult for humans to stay under warm condition, but it also plays an important role in electricity consumption for cooling. SU had large spatial variation in India ranging from 0 day in Himalayan regions to 365/366 days in southern parts. Between the observed periods, there were significant changes in SU in some parts of the country. The country-average SU increased from 297.45 days for Observed 1 to 298.261 days for Observed 2 . Persistent increase in SU was found for the projected climate. The increase was higher in the northern parts of the country. There was no significant change in the value of SU for southern parts of the country as the value of the index was already maximum for these regions during the observed period. The country-average values of SU for RCP2.6 were 303, 307 and

307 days for F1, F2 and F3, respectively, for RCP4.5 were 301.76, 309.78, and 314.12 days for F1, F2 and F3, respectively, for RCP6.0 were 300.95, 306.65, and 314.72 days for F1, F2 and F3, respectively, and for RCP8.5 were 302.24, 314.05 and 324.34 days for F1, F2 and F3, respectively.

Frost days (FD) is the count of days with Tmin less than 0°C. FD is not very important for most parts of India as only some parts of the Indian Himalayan Region has temperature lower than 0°C. However, FD is analysed in this study as it is one of the critical indicators to assess the impact of climate change on snow/ice processes. FD ranged between 0 day in most parts of the country to 365/366 in the Himalayan regions (Figure 6.18). There was a decrease in FD between the Observed 1 and Observed 2 s. The country-average FD decreased from 22.4 days for Observed 1 to 21.5 days for Observed 2 . A drastic decrease in FD under projected climate was observed as all projected scenarios indicated a decrease in FD in Himalayan regions. The country-average values of FD for RCP2.6 were 19.57, 18.81 and 18.96 days for F1, F2 and F3, respectively, for RCP4.5 were 19.71, 18.09 and 17.10 days for F1, F2 and F3, respectively, for RCP6.0 were 19.85, 18.25 and 16.48 days for F1, F2 and F3, respectively, and for RCP8.5 were 19.43, 16.57 and 13.53 days for F1, F2 and F3, respectively.

Another important index for ice/snow process is Ice days (ID). The ID is the count of days with Tmax less than 0°C. The ID is also important for Himalayan regions. Like FD, ID also had zero value for most parts of the country (Figure 6.19). While most parts of the country had no ID, some parts of Indian Himalayan Region had ID as high as 170 days. Like FD, the ID also decreased from Observed 1 to Observed 2 . The country-average value of ID decreased from 176.7 days for Observed 1 to 168.8 days for Observed 2. The ID is expected to further decrease under projected climate. The country-average values of ID for RCP2.6 were 149.08, 142.84 and 144.77 days for F1, F2 and F3, respectively, for RCP4.5 were 152.59, 139.96 and 133.43 days for F1, F2 and F3, respectively, for RCP6.0 were 161.07, 150.06 and 134.66 days for F1, F2 and F3, respectively, and for RCP8.5 were 150.85, 130.44 and 105.18 days for F1, F2 and F3, respectively.

Diurnal temperature range (DTR) is the variation between a high temperature and a low temperature that occurs during the same day. It plays an important role in some agricultural crops. DTR had large spatial variation in India (Figure 6.20). The coastal areas had lower values of DTR, whereas the central and western regions had higher

values of DTR. The changes in DTR during the observed period had a gradient from north to south. A decrease in DTR was found for most parts of the country, whereas an increase in DTR was found in the southern parts. The country-average value of DTR decreased from 12.07°C for Observed 1 to 11.83°C for Observed 2 . Under the projected climate, the changes in DTR were different for Himalayan regions compared to the remaining parts of the country. Increase in DTR was found for the Himalayan region, whereas a decrease was found for the rest of the country. The country-average DTR was found to decrease under the projected climate. The country-average values of DTR for RCP2.6 were 11.61, 11.55 and 11.61 °C for F1, F2 and F3, respectively, for RCP4.5 were 11.63, 11.60 and 11.56 °C for F1, F2 and F3, respectively, for RCP6.0 were 11.69, 11.55 and 11.40 °C for F1, F2 and F3, respectively, and for RCP8.5 were 11.58, 11.33 and 11.10 °C for F1, F2 and F3, respectively.

Growing season length (GSL) is the number of days in the year when the plant growth takes place. It plays a very important role in agriculture in cold areas. In India, the weather conditions are suitable for agriculture throughout the year in most of the parts. Figure 6.21 shows the analysis of GSL. The value of GSL is equal to the number of days in a year for most parts of the country. However, the value of GSL was lower for some snow-covered Himalayan regions.

6.4.2.2 Precipitation Extremes

Consecutive dry days (CDD) is the maximum number of consecutive days in a year with precipitation less than 1 mm. CDD is an important indicator for the analysis of drought, changing precipitation patterns and intensity. Figure 6.22 shows the results for the analysis of CDD over the observed and projected climates. CDD varies in India from as low as 20-50 days to as high as 150-180 days. The high precipitation regions of northeast India and the Western Ghats had lower values of CDD, whereas the arid regions in western India had higher values of CDD. Significant changes in CDD were found over the observed period. CDD decreased in the parts of western and southern India. Increase in CDD was observed in parts of western (mainly in the states of Gujarat and Maharashtra) and central India. The country-average CDD decreased from 77 days for Observed 1 to 75.98 days for Observed 2 . The projected climate showed an increase in CDD for most parts of the country except for the central India. The country-average values of CDD for RCP2.6 were 75.20, 74.58 and 74.08 days for F1, F2 and F3, respec-

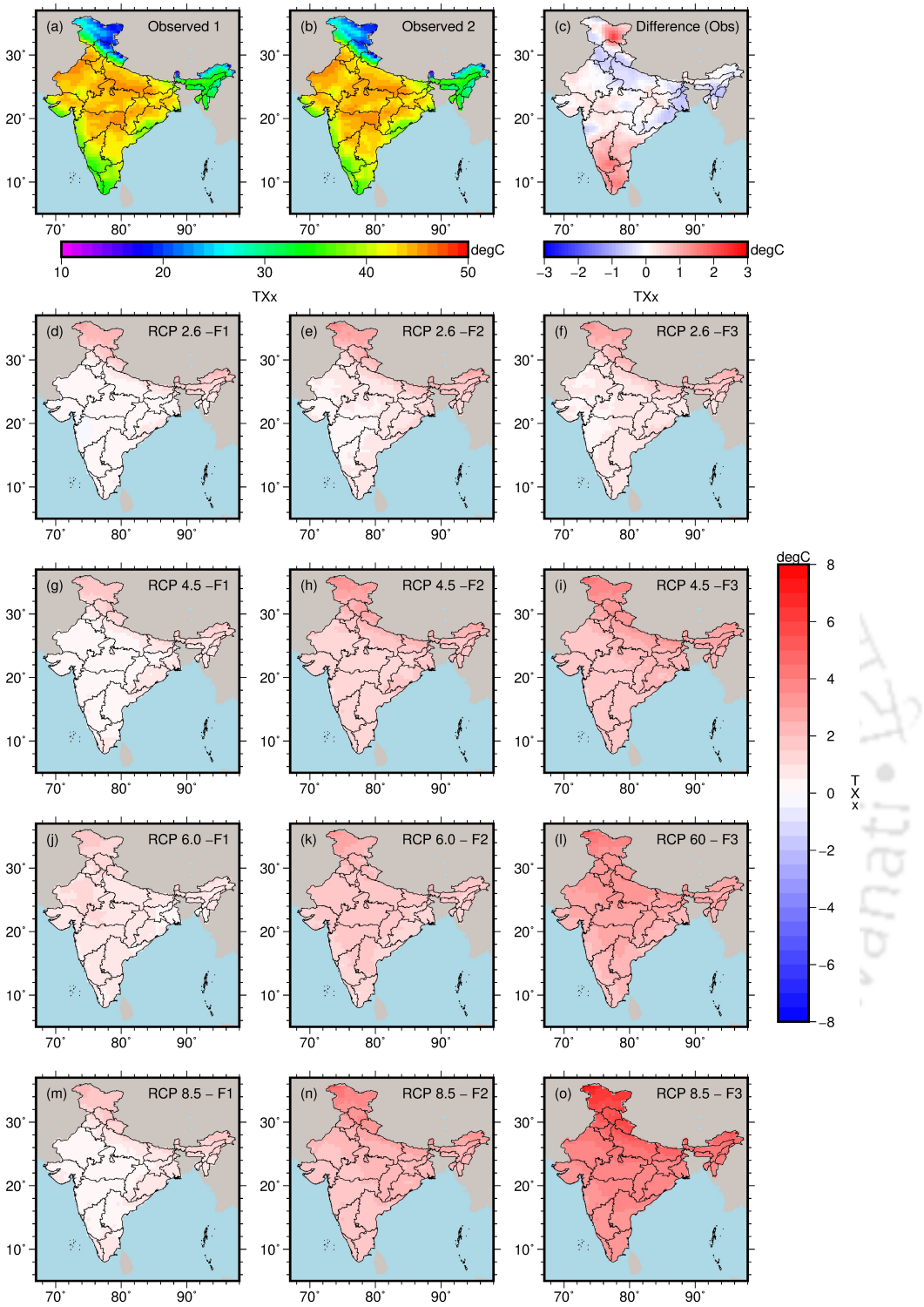

Figure 6.8: Change in mean annual TXx in India over observed and projected climate. TXx over the observed period: (a) Observed 1: 1951-1980 and (b) Observed 2: 1981-2010. (c) The change in Observed 2 with respect to Observed 1. (d-o) Changes in TXx under RCPs with respect to Observed 2. F1, F2 and F3 denote the periods of 2011-2040, 2041-2070, and 2071-2100.

tively, for RCP4.5 were 76.05, 76.23 and 75.75 days for F1, F2 and F3, respectively, for RCP6.0 were 79.27, 80.20 and 80.23 days for F1, F2 and F3, respectively, and for

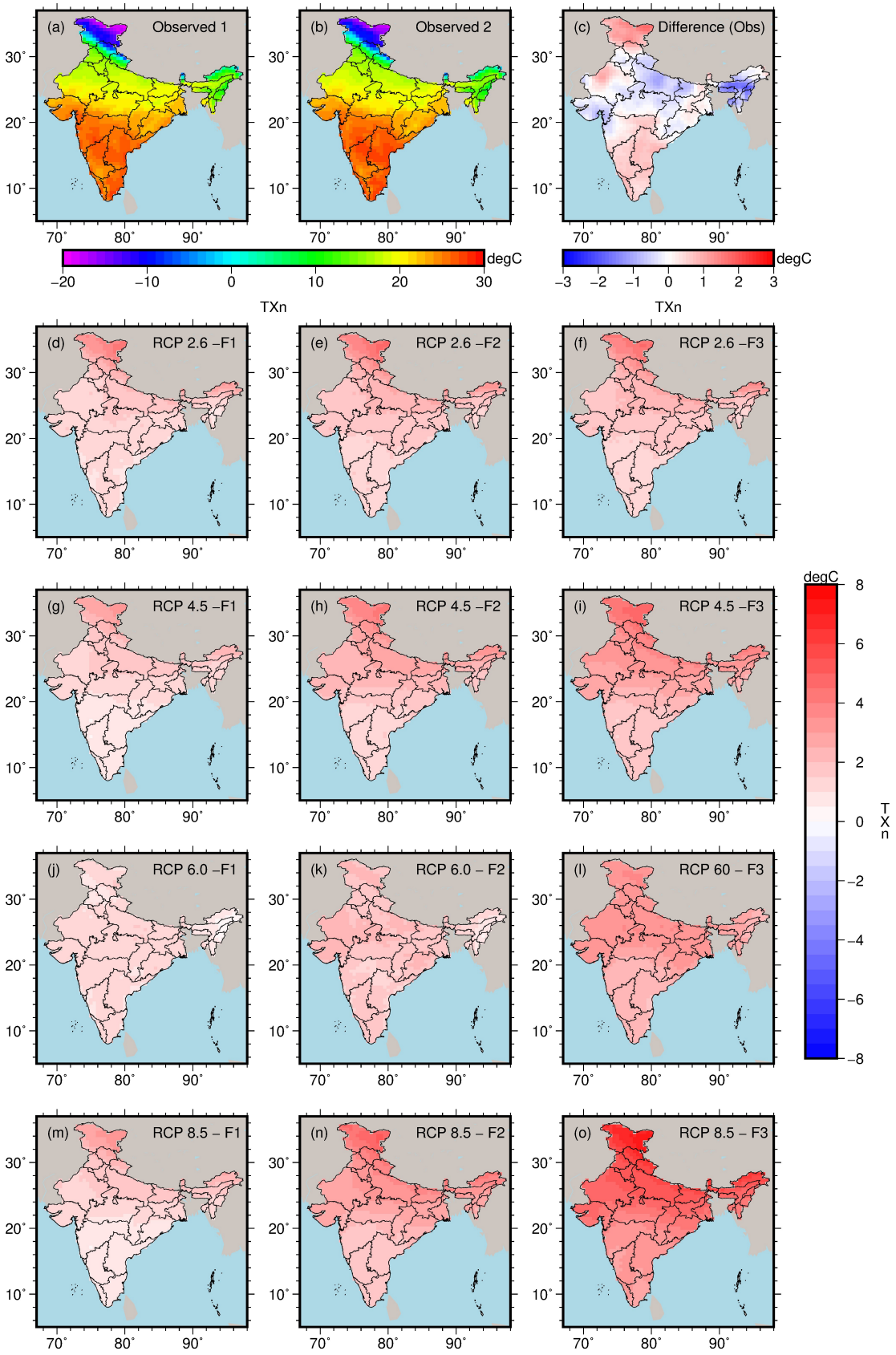

Figure 6.9: Same as Figure 6.8 but for TXn.

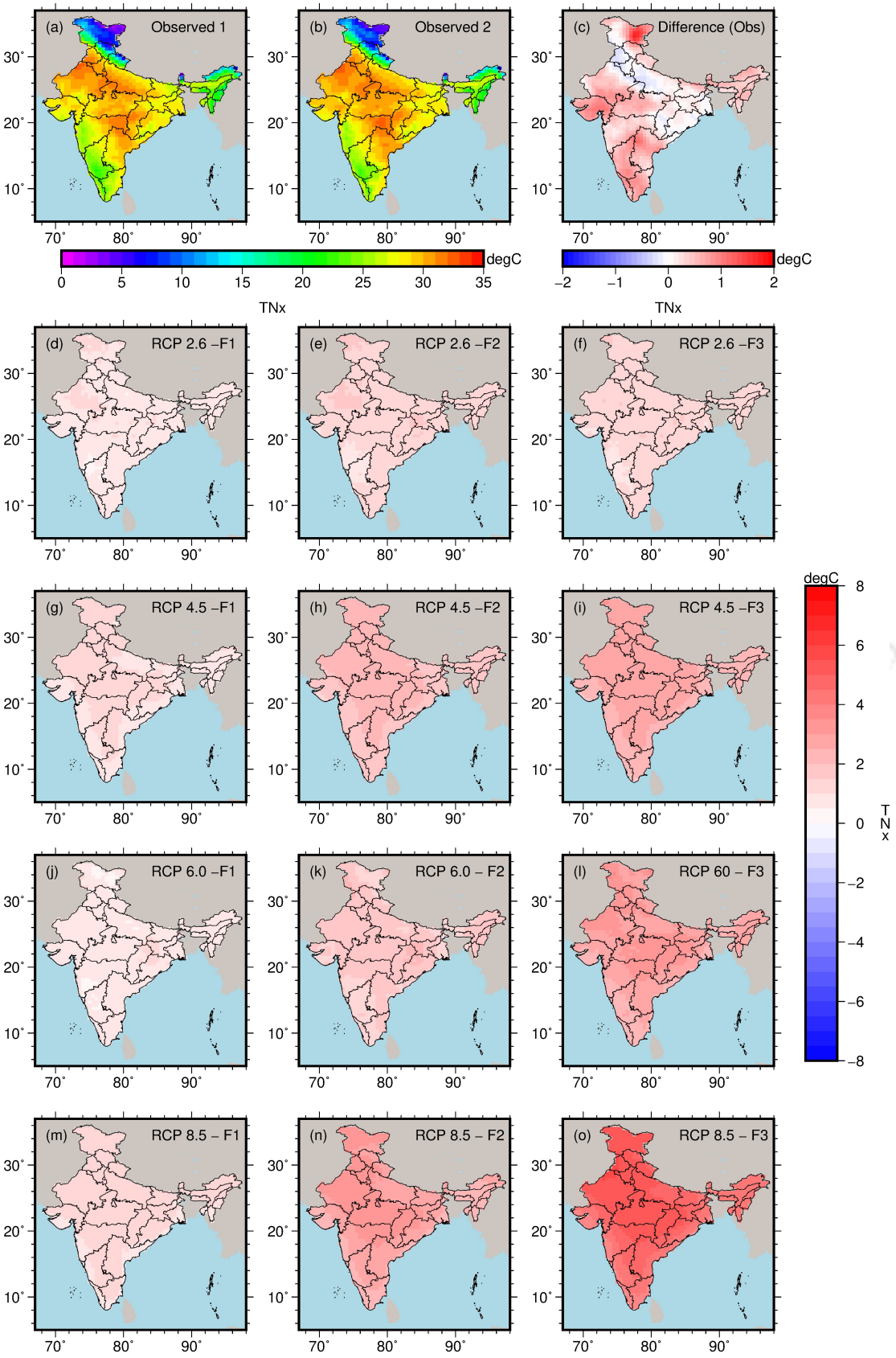

Figure 6.10: Same as Figure 6.8 but for TNx.

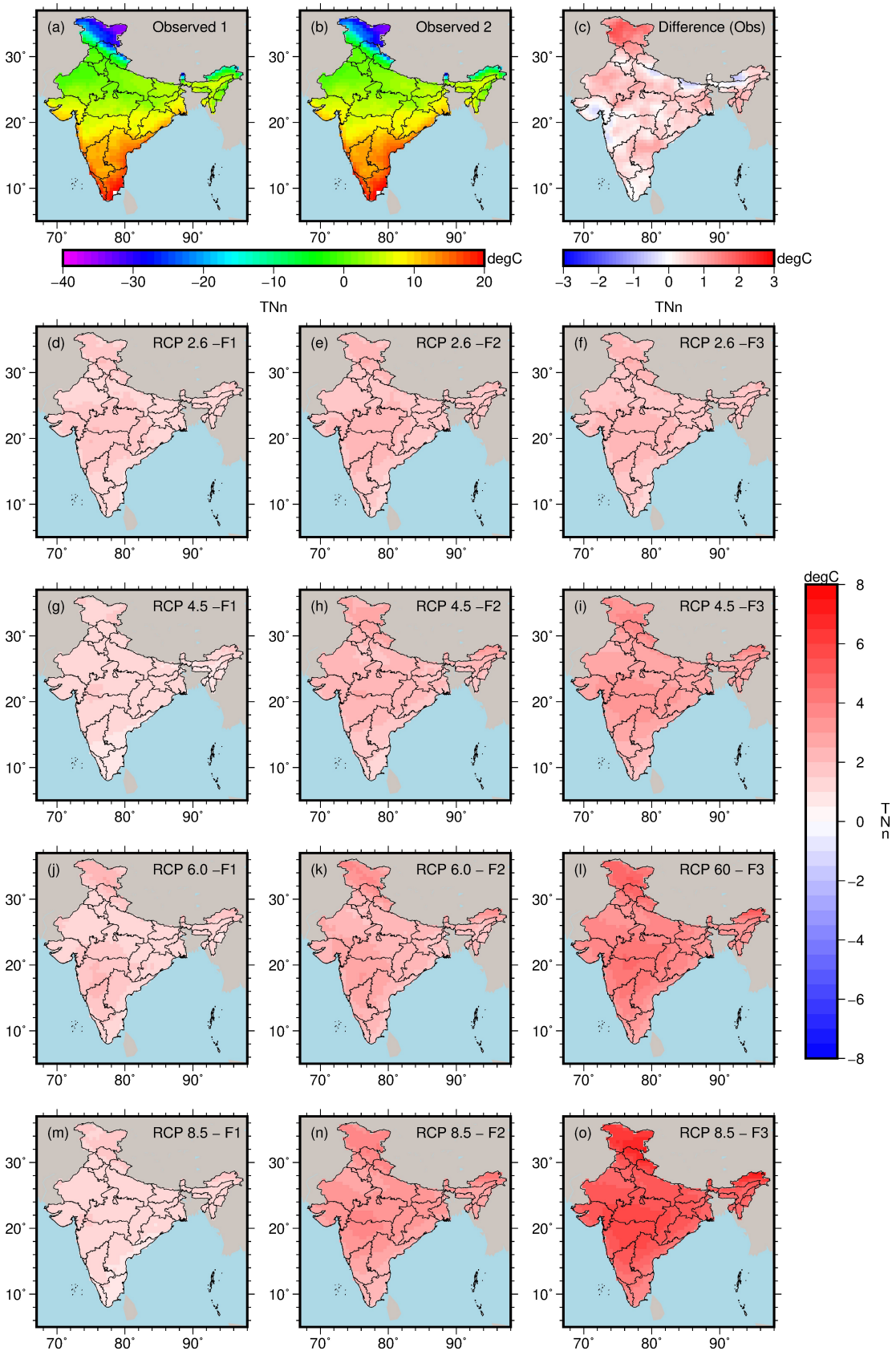

Figure 6.11: Same as Figure 6.8 but for TNn.

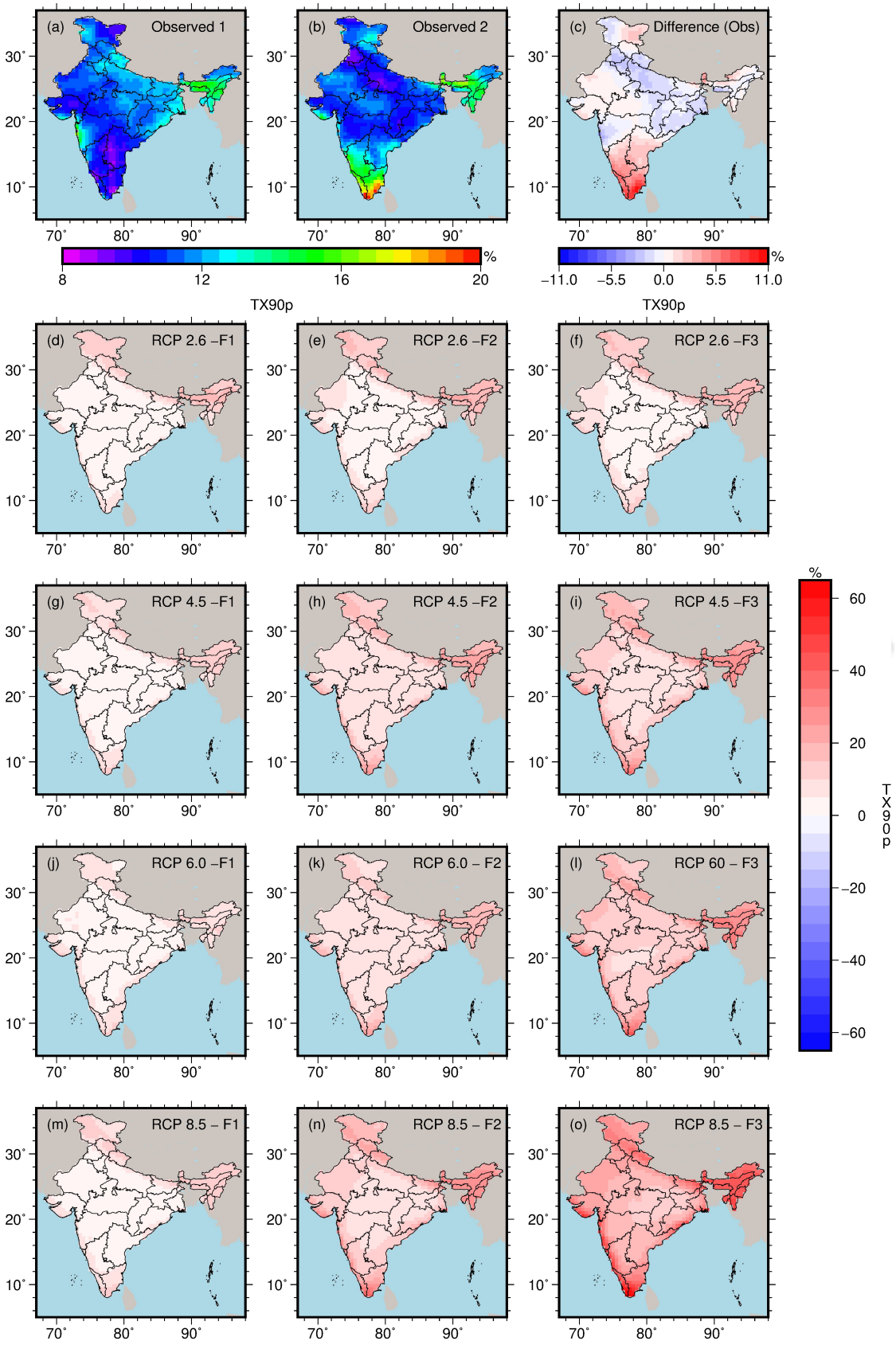

Figure 6.12: Same as Figure 6.8 but for TX90p.

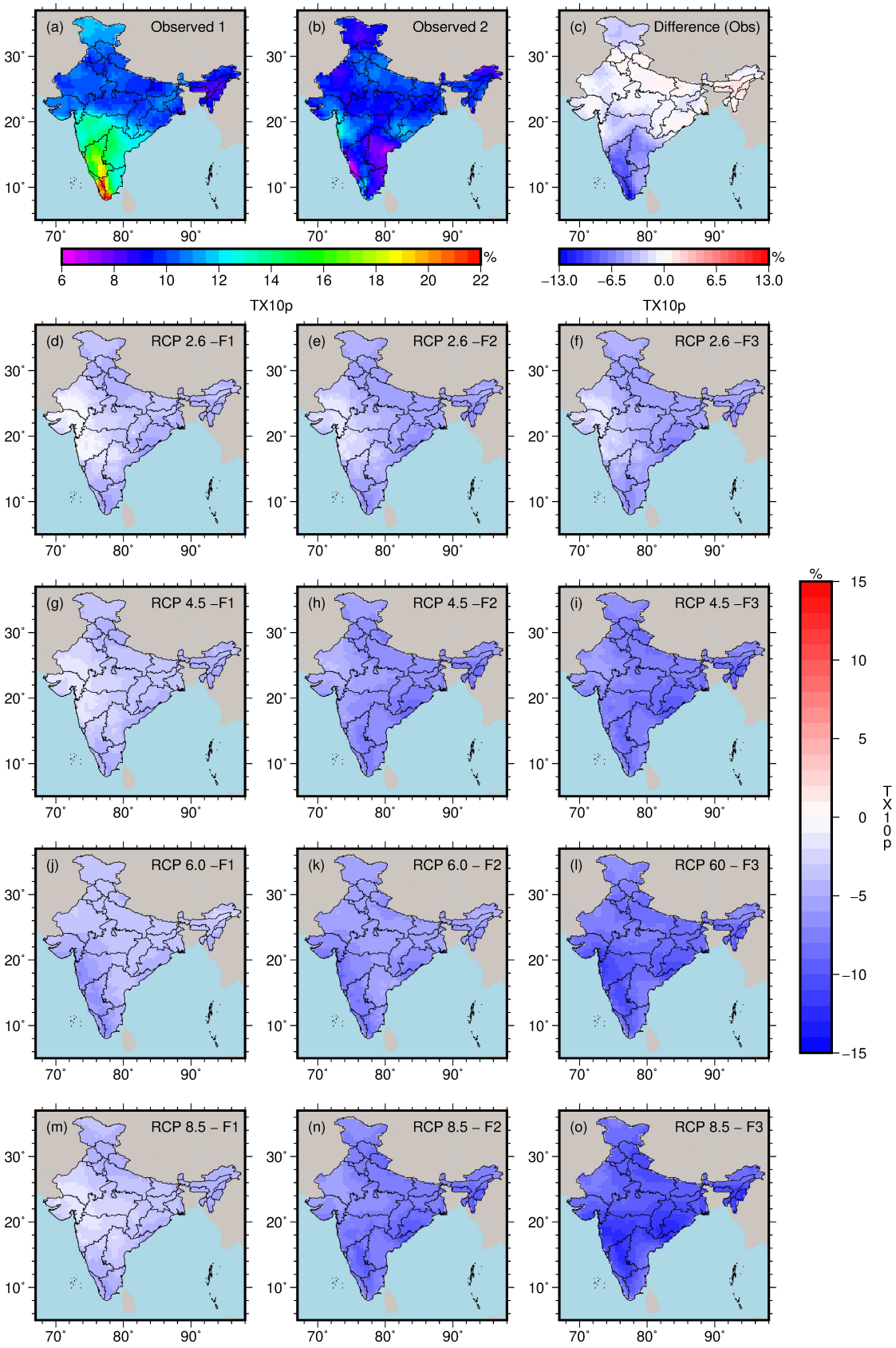

Figure 6.13: Same as Figure 6.8 but for TX10p.

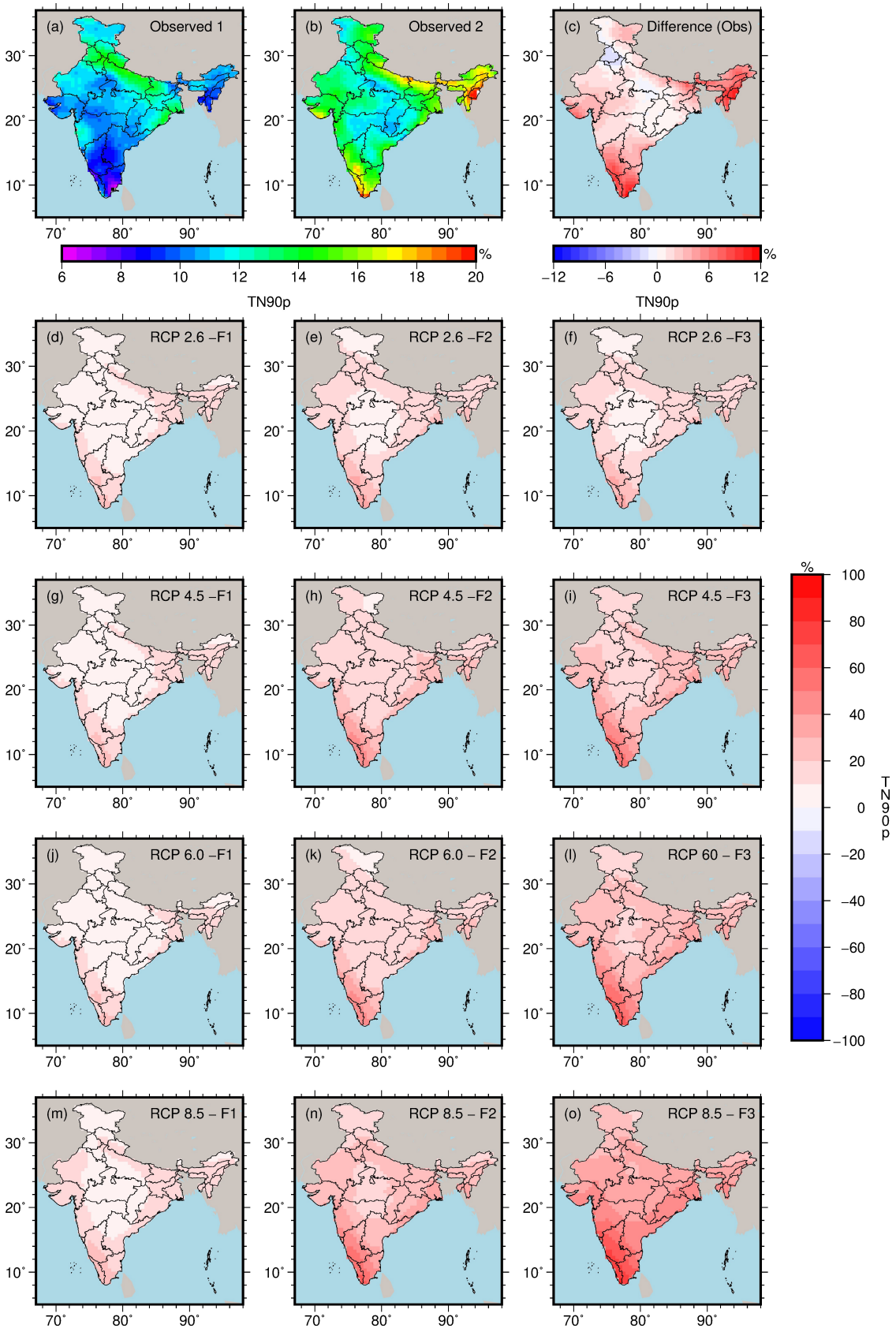

Figure 6.14: Same as Figure 6.8 but for TN90p.

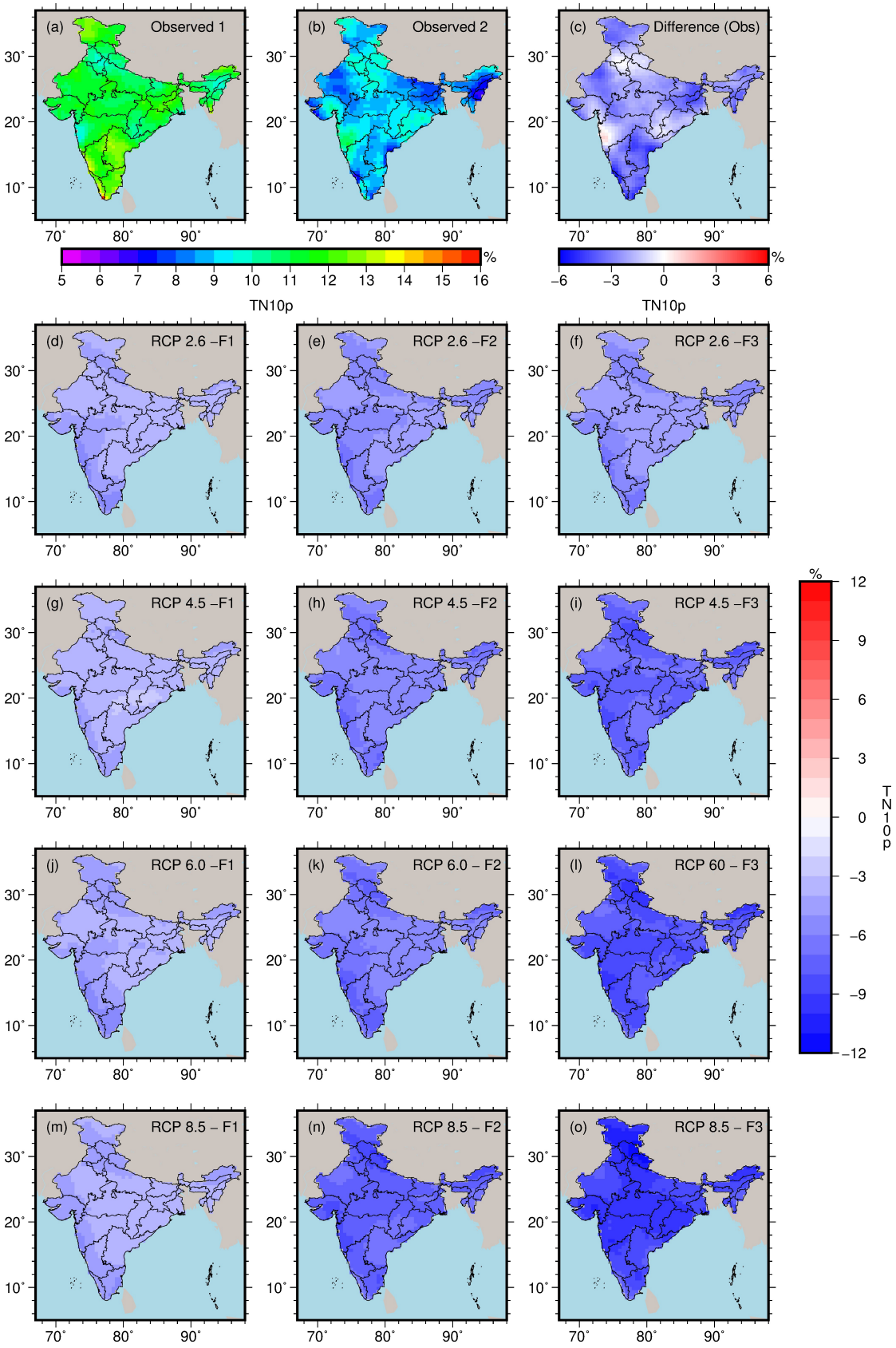

Figure 6.15: Same as Figure 6.8 but for TN10p.

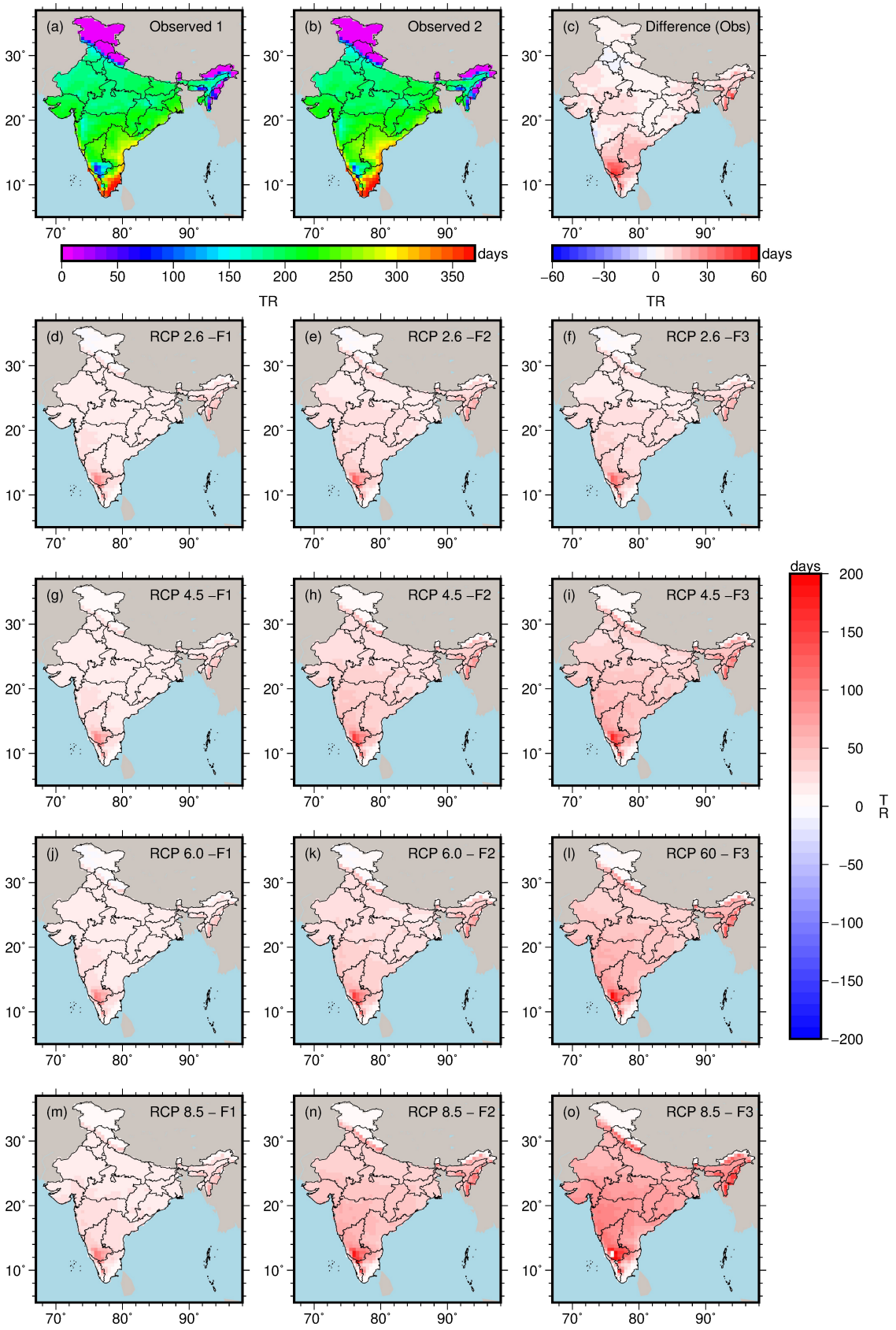

Figure 6.16: Same as Figure 6.8 but for TR.

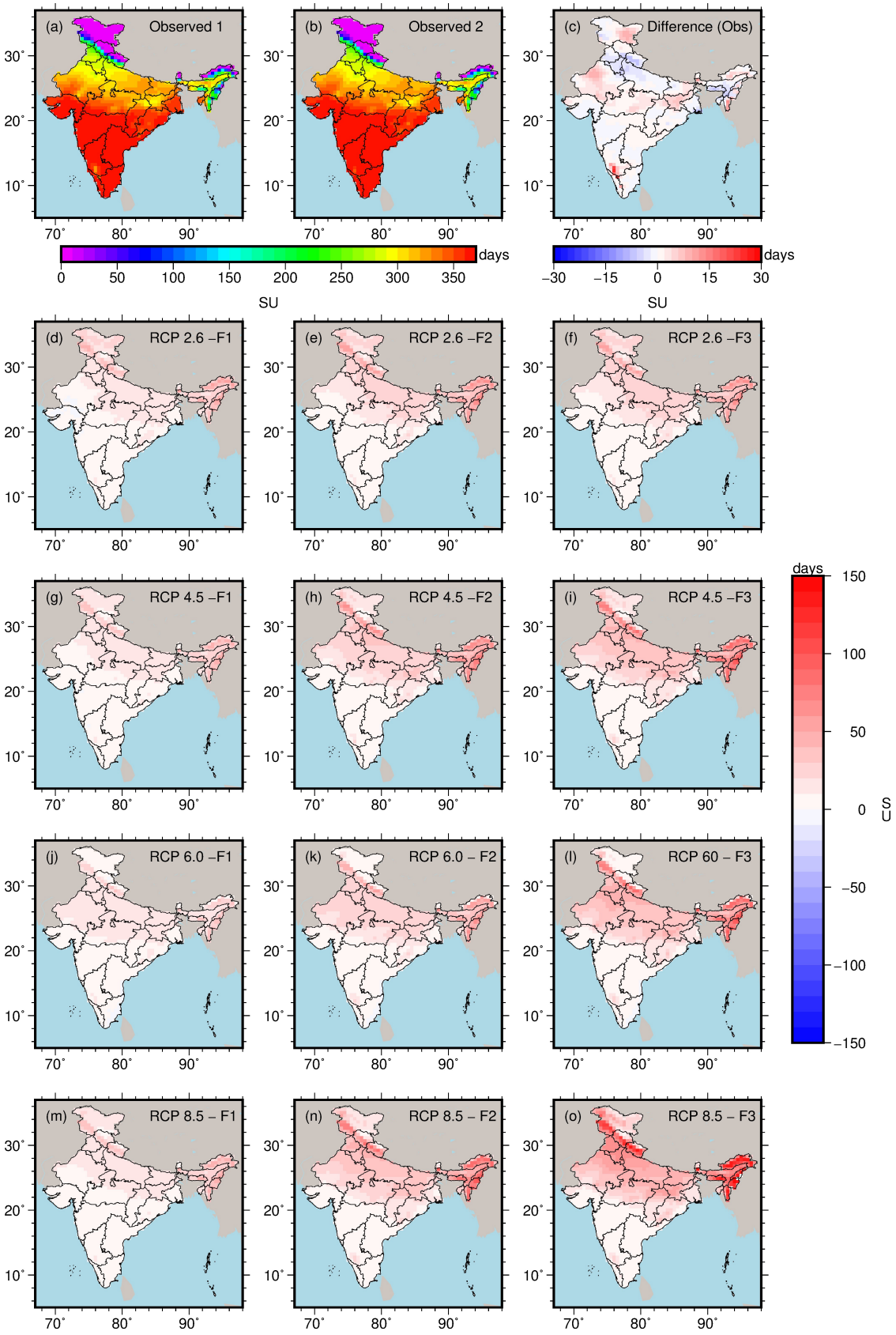

Figure 6.17: Same as Figure 6.8 but for SU.

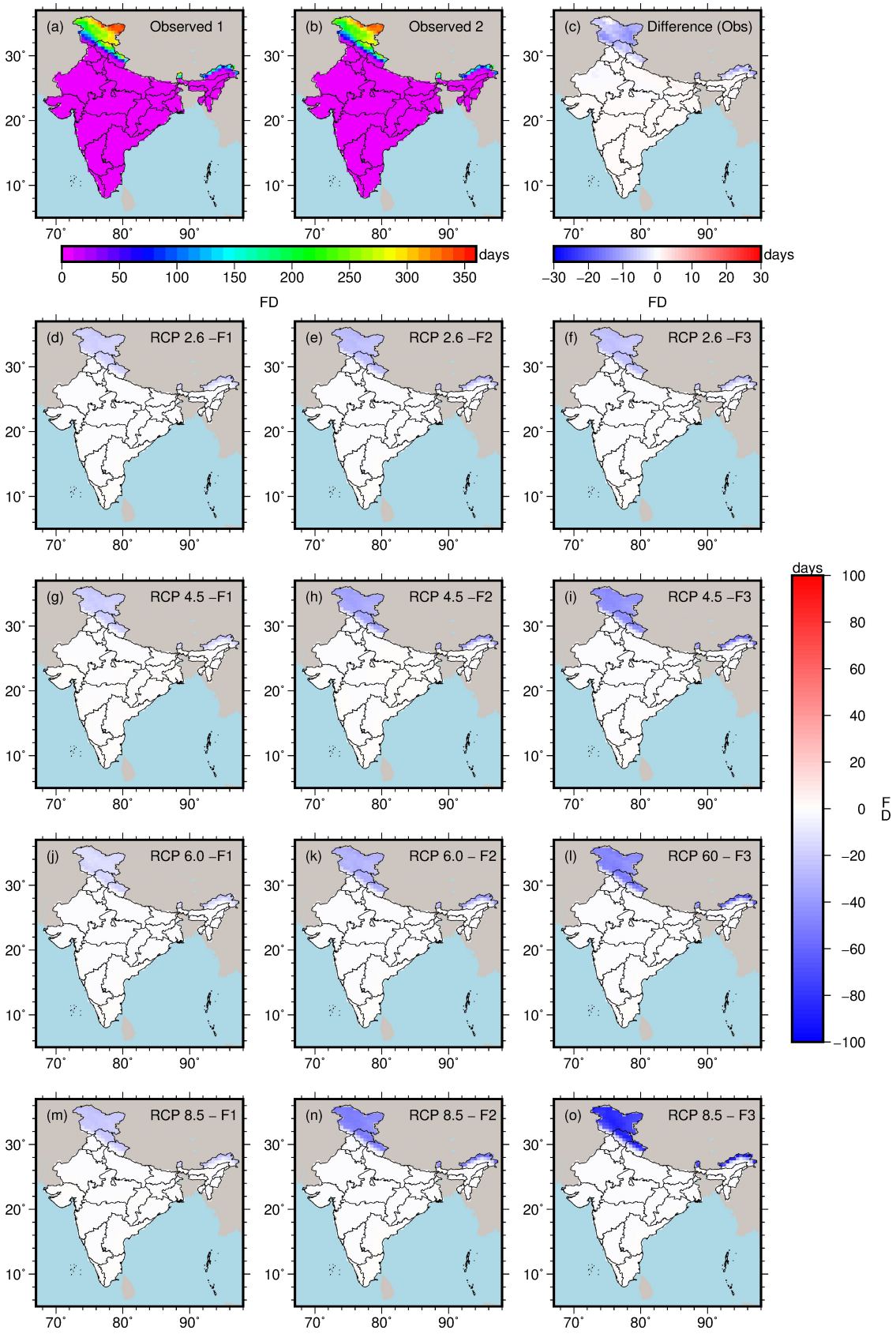

Figure 6.18: Same as Figure 6.8 but for FD.

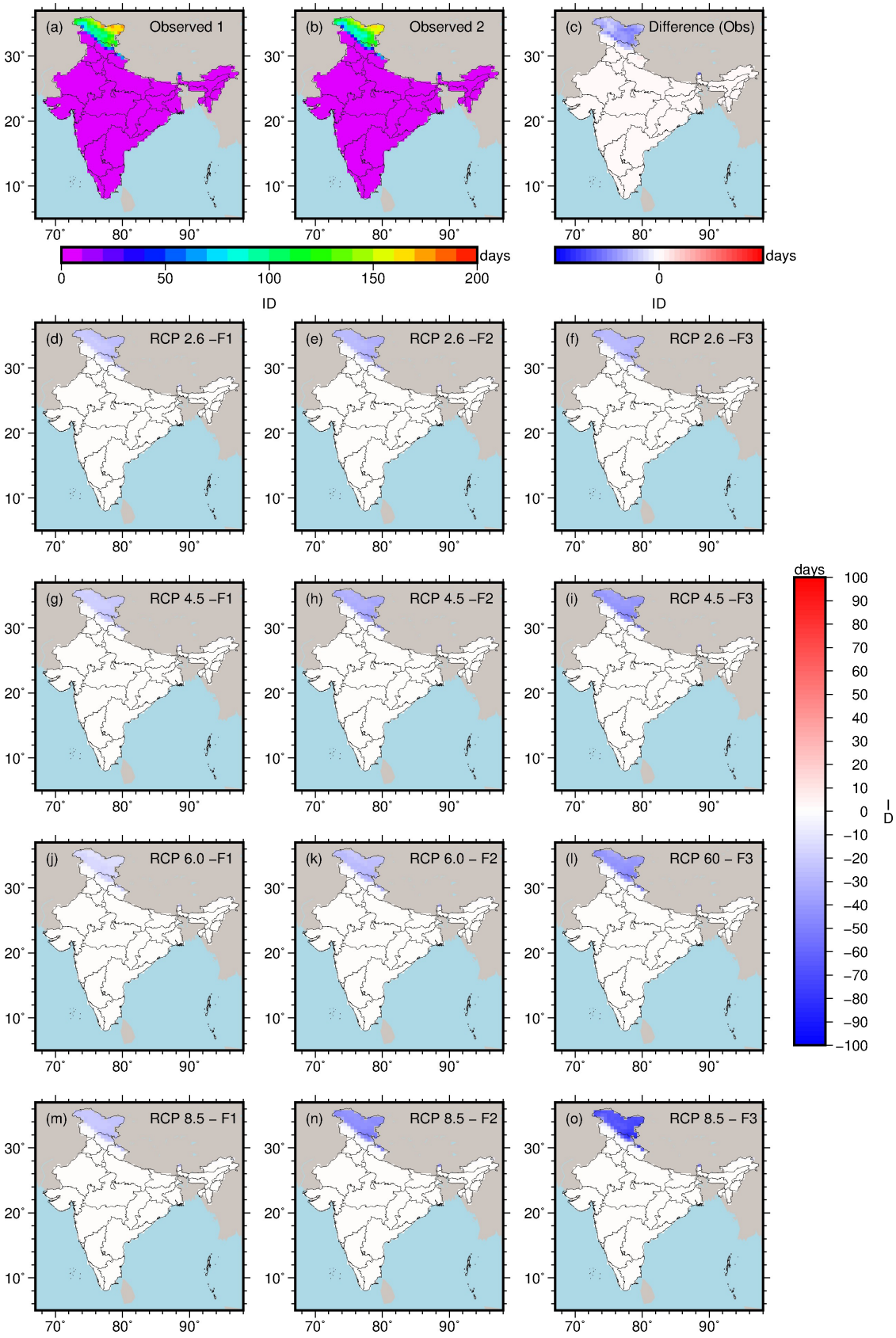

Figure 6.19: Same as Figure 6.8 but for ID.

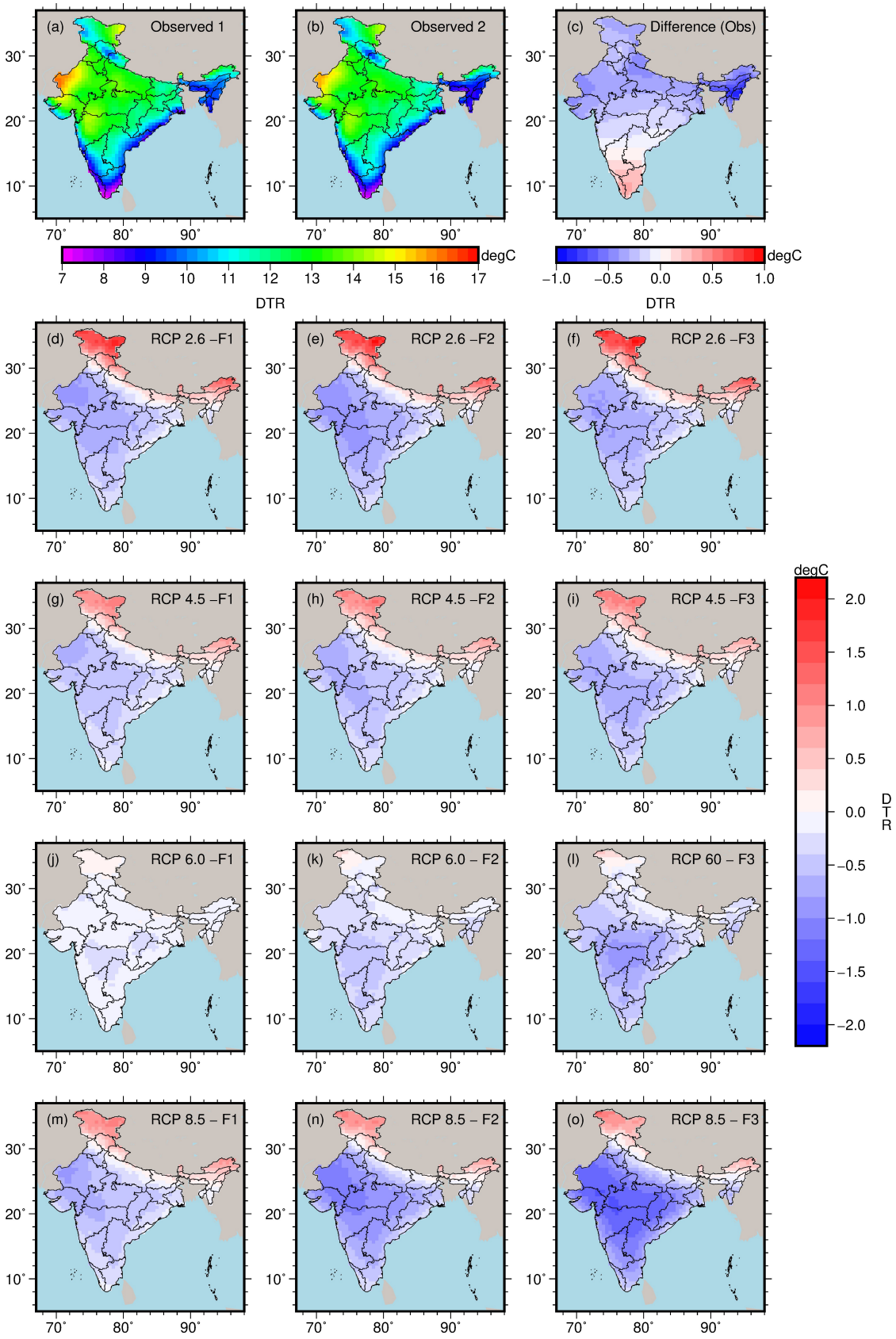

Figure 6.20: Same as Figure 6.8 but for DTR.

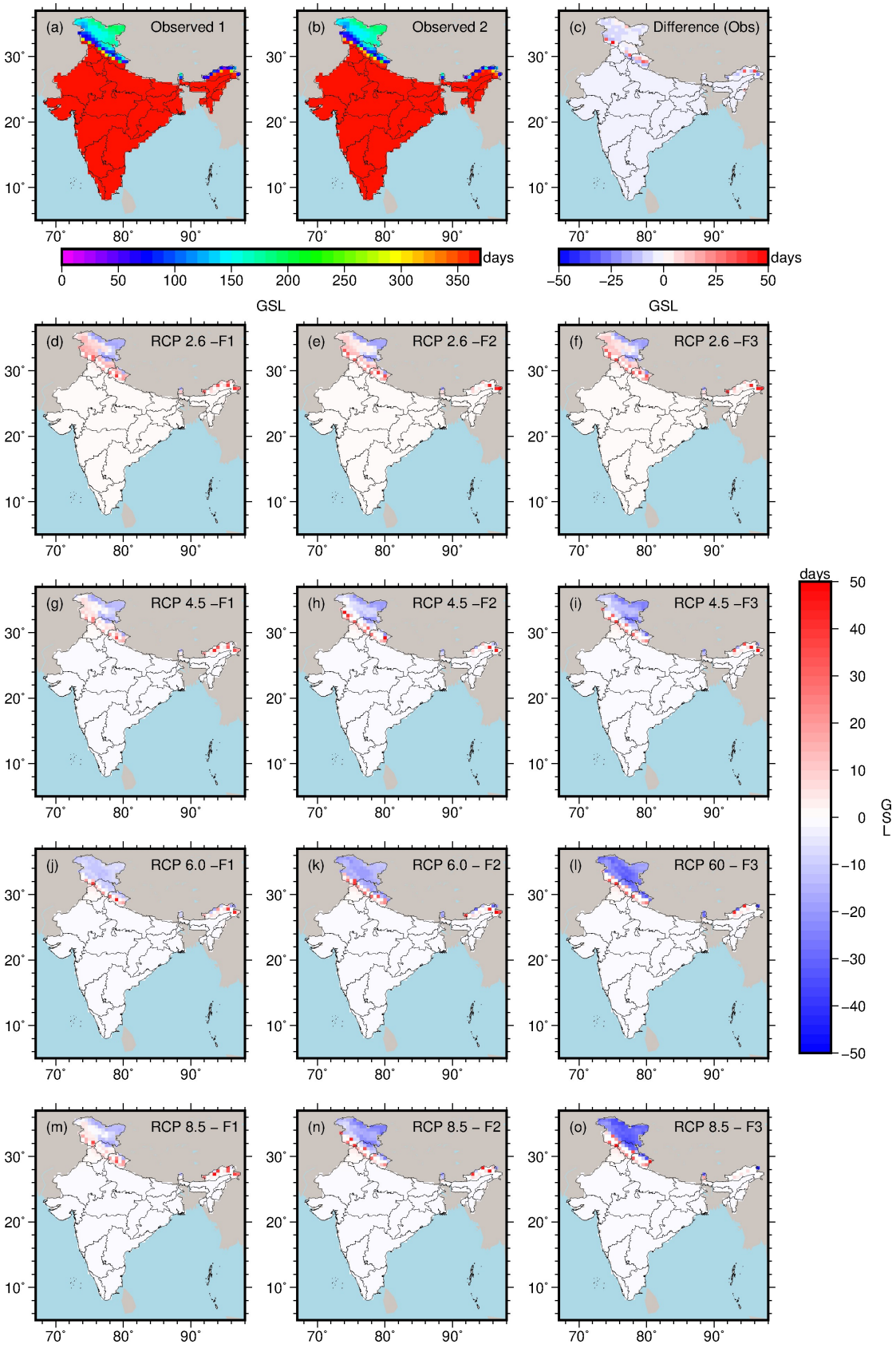

Figure 6.21: Same as Figure 6.8 but for GSL.

RCP8.5 were 75.65, 76.66 and 77.84 days for F1, F2 and F3, respectively.

Consecutive wet days (CWD) is the maximum number of consecutive days in a year with precipitation greater than 1 mm. The spatial variation in CWD follows the spatial variation in precipitation (Figure 6.23). CWD was higher for parts of northeast and Western Ghats. Arid regions had fewer CWD. The country-average value of CWD was 23.10 days for Observed 1 , which reduced to 20.40 days for Observed 2 . Some parts of northeast India showed an increase in CWD over the observed period. For projected climate, RCP2.6, RCP4.5 and RCP8.5 showed an increase in CWD, but RCP6.0 showed a decrease in CWD for most parts of the country.

R10 is the number of heavy precipitation days, which is computed as the number of days in a year having daily precipitation greater than 10 mm. The spatial variation in R10 was similar to spatial variation in precipitation (Figure 6.24). In some parts of Western Ghats and northeast, the value of R10 was greater than 80 days. There was no significant variation in R10 between Observed 1 and Observed 2 except in some parts of north and northeast India. The country-average value of R10 decreased slightly from 33.79 days for Observed 1 to 33.49 days for Observed 2 . Most of the projected scenarios showed an increase in R10 throughout the country. For RCP6.0, some parts of north and northeast India showed a decrease in R10 as well. The country-average values of R10 for RCP2.6 were 36.25, 37.52 and 37.95 days for F1, F2 and F3, respectively, for RCP4.5 were 34.69, 36 and 37.46 days for F1, F2 and F3, respectively, for RCP6.0 were 32.48, 33.80 and 35.77 days for F1, F2 and F3, respectively, and for RCP8.5 were 34.93, 37.07 and 39.49 days for F1, F2 and F3, respectively. Increase in R10 may lead to an increase in flood risk.

R20 is also a similar index, which represents the number of very heavy precipitation days. It is computed as the number of days in a year having daily precipitation greater than 20mm. R20 followed the similar pattern as R10 (Figure 6.25). R20 was as high as 50-75 days in some parts of northeast India and Western Ghats. The country-average value of R20 remained the same over the observed period with the values of 14.50 days for Observed 1 and 14.58 days for Observed 2 . Increase in R20 was found for some parts of northeast and north India, whereas some parts on northeast India, particularly in the state of Arunachal Pradesh, showed a decrease in R20. All the projected scenarios showed an increase in R20. The increase in R20 was higher for northern and northeastern parts of the country. The country-average values of R20 for RCP2.6 were

16.59, 17.2 and 17.34 days for F1, F2 and F3, respectively, for RCP4.5 were 16.57, 17.47 and 18.23 days for F1, F2 and F3, respectively, for RCP6.0 were 16.36, 17.30 and 18.84 days for F1, F2 and F3, respectively, and for RCP8.5 were 16.78, 18.40 and 20.25 days for F1, F2 and F3, respectively. Increase in R20 was consistent with the increase in R10 and precipitation. The analysis indicates increasing risk of flash floods in northern and northeast India.

Wet days (R90p), very wet days (R95p) and extremely wet days (R99p) are three indices that tell about the amount of precipitation during heavy precipitation events. The numbers, 90, 95 and 99, denote the thresholds considered for the calculation of these indices. For example, R95p is the sum of daily precipitation on the days when daily precipitation is greater than 95th percentile threshold of the wet-day precipitation distribution derived from the base period. Similarly, R90p and R99p are based on 90th and 99th percentile, respectively. Figures 6.26, 6.27 and 6.28 show the results for the R90p, R95p and R99p, respectively. The spatial patterns of R90p, R95p and R99p were found similar, but there were differences in magnitude of the indices. Higher values of these indices were found in high precipitation areas. The patterns of the changes during the observed period were also theimilar for these indices. Increase in these indices was found for parts of north, northeast and south, whereas a decrease in these indices was found for parts of northeast and central India. These indices are anticipated to further increase under the projected climate. A large increase in these indices was found for the Western Ghats.

Maximum 1-day precipitation (RX1day) and Maximum consecutive 5-day precipitation (RX5day) are used to assess flood risks due to heavy rain conditions. RX1day is maximum 1-day precipitation amount, and RX5day is the maximum 5-day precipitation computed over the 5-day interval. RX1day ranged between 18.35 mm and 162.11 mm for Observed 1 and between 25.50mm and 203.74 mm for Observed 2 (Figure 6.29). The country-average RX1day increased from 67.68 mm for Observed 1 to 74.31 mm for Observed 2 . Most of the projected scenarios indicated an increase in RX1day. The country-average values of RX1day for RCP2.6 were 74.24, 77.92 and 75.76 mm for F1, F2 and F3, respectively, for RCP4.5 were 81.89, 87.31 and 91.85 mm for F1, F2 and F3, respectively, for RCP6.0 were 86.15, 91.74 and 99.82 mm for F1, F2 and F3, respectively, and for RCP8.5 were 83.90, 94.18 and 108.41 mm for F1, F2 and F3, respectively. The value of RX5day increased from 160.37 mm for Observed 1 to 166.96 mm

for Observed 2 (Figure 6.30). The country-average values of RX5day for RCP2.6 were 172.14, 182.45 and 179.02mm for F1, F2 and F3, respectively, for RCP4.5 were 187.01, 202.98 and 214.65 mm for F1, F2 and F3, respectively, for RCP6.0 were 201.89, 216.22 and 240 mm for F1, F2 and F3, respectively, and for RCP8.5 were 191.54, 219.62 and 254.18 mm for F1, F2 and F3, respectively. The substantial increase in RX5day may result in floods in major cities in India. Figure 6.30 shows that the increase in RX5day was higher in western parts of the country. These parts of the country have faced huge floods in the past, for example, Mumbai floods of 2005.

Simple daily intensity index (SDII) is the average precipitation on the wet days (days with precipitation greater than 1mm). It is an indicator of the intensity of the precipitation throughout the year. SDII varied between 3.79 mm/day and 24.84 mm/day for the observed period (Figure 6.31). Increase in SDII was found in parts of north India, whereas a significant decrease in SDII was found for some parts of the northeast. The country-average SDII increased from 10.09 mm/day for Observed 1 to 10.38 mm/day for Observed 2 . SDII is projected to further increase for RCPs. The country-average values of SDII for RCP2.6 were 10.41, 10.77 and 10.66 mm/day for F1, F2 and F3, respectively, for RCP4.5 were 11, 11.50 and 11.80 mm/day for F1, F2 and F3, respectively, for RCP6.0 were 11.23, 11.66 and 12.36 mm/day for F1, F2 and F3, respectively, and for RCP8.5 were 11.09, 12 and 13 mm/day for F1, F2 and F3, respectively.

Figure 6.32 shows the results for change analysis of annual total wet-day precipitation (PRCPTOT). There were drastic changes in PRCPTOT in some parts of the country, for example, in the states of Jammu and Kashmir, and Arunachal Pradesh. There was a slight change in PRCPTOT from 1107 mm for Observed 1 to 1113 mm for Observed 2 . However, there was a large increase in spatial variability. The range of PRCPCP for Observed 2 was 156-4910 mm compared to 183-4289 mm for Observed 1 . The projected scenarios showed a consistent increase in PRCPTOT for the 21st century. The country-average values of PRCPTOT for RCP2.6 were 1278, 1326 and 1323 mm for F1, F2 and F3, respectively, for RCP4.5 were 1248, 1306 and 1357 mm for F1, F2 and F3, respectively, for RCP6.0 were 1188, 1246 and 1337 mm for F1, F2 and F3, respectively, and for RCP8.5 were 1265, 1368 and 1493 mm for F1, F2 and F3, respectively.

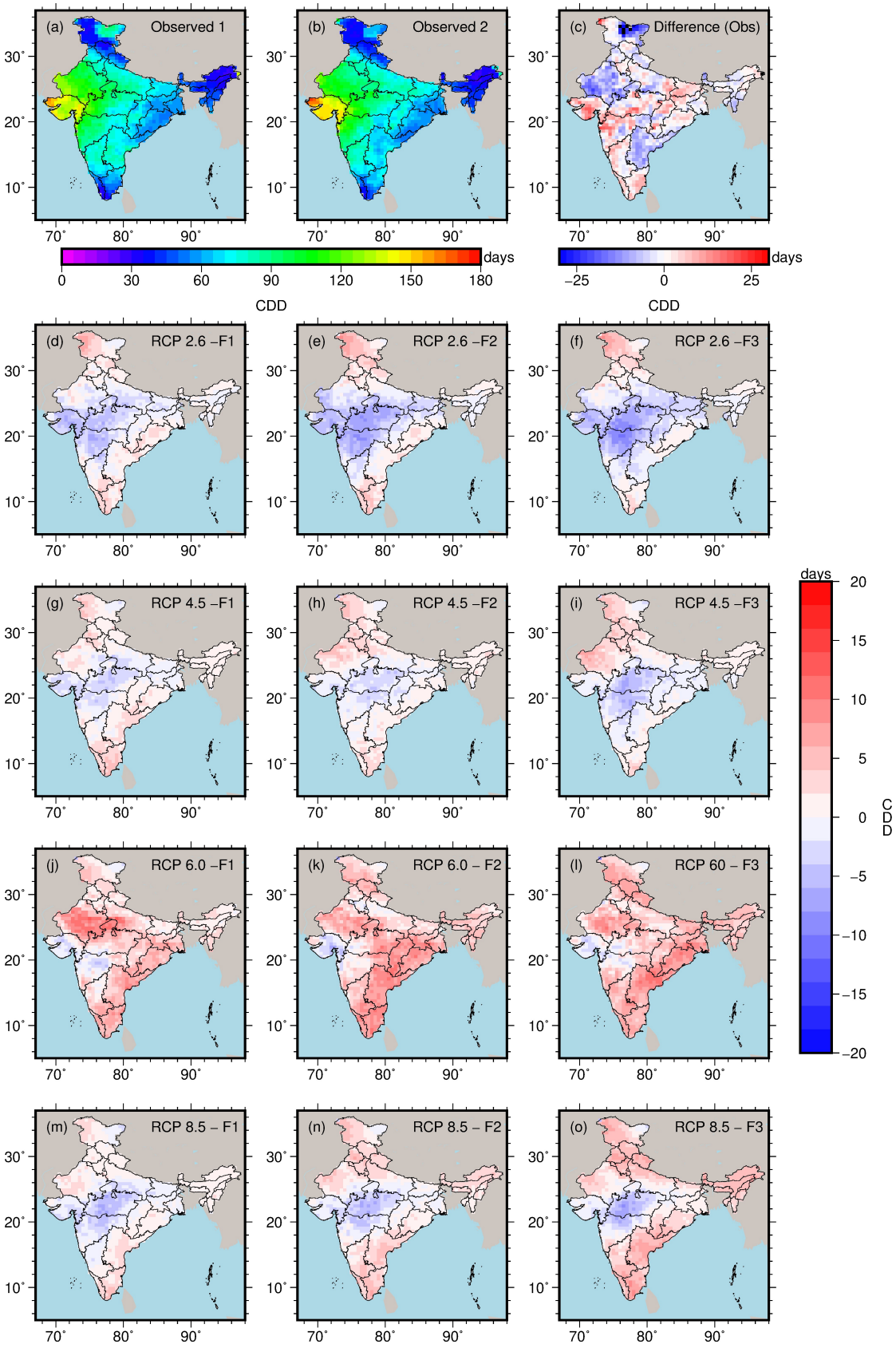

Figure 6.22: Same as Figure 6.8 but for CDD.

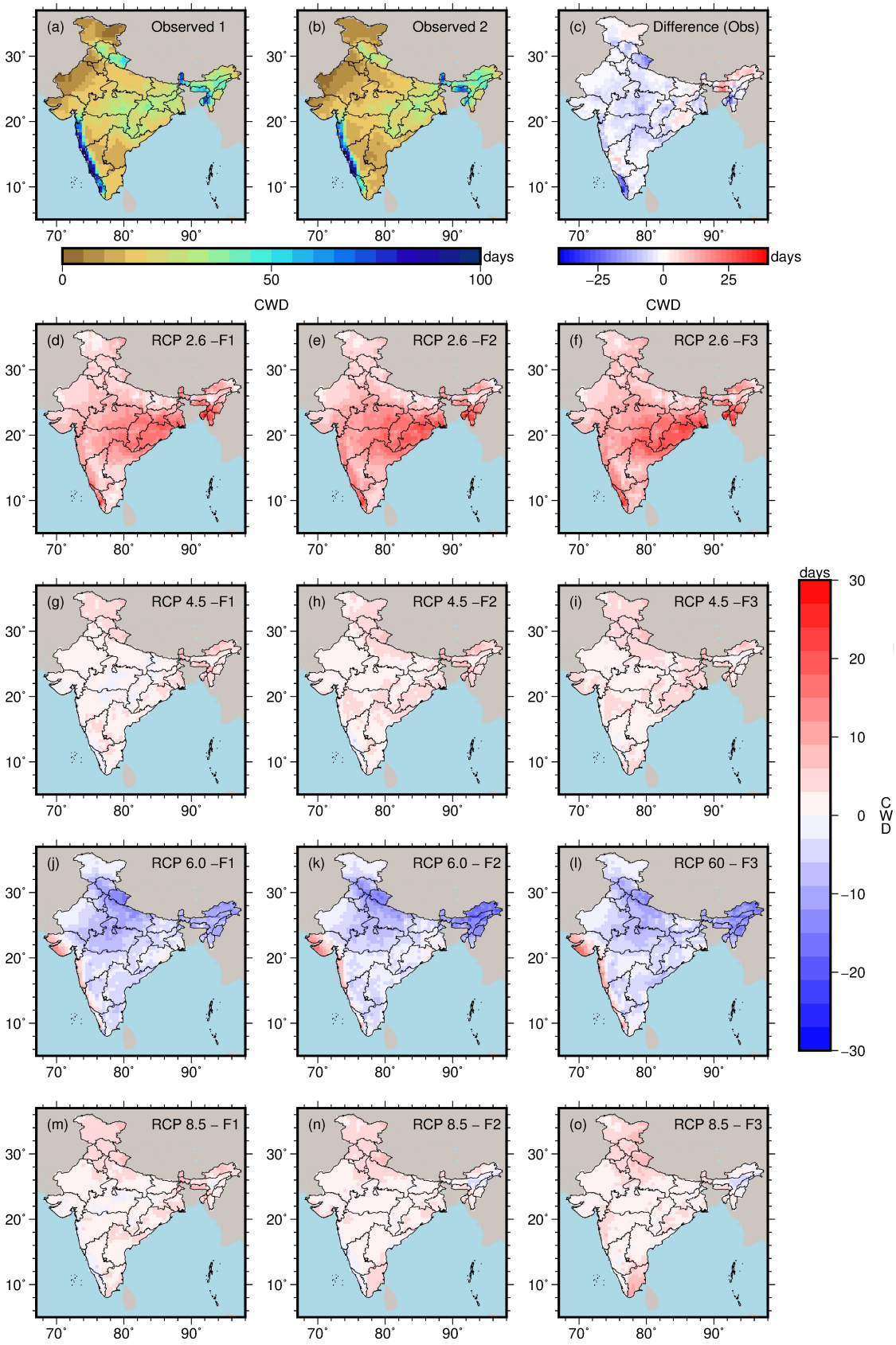

Figure 6.23: Same as Figure 6.8 but for CWD.

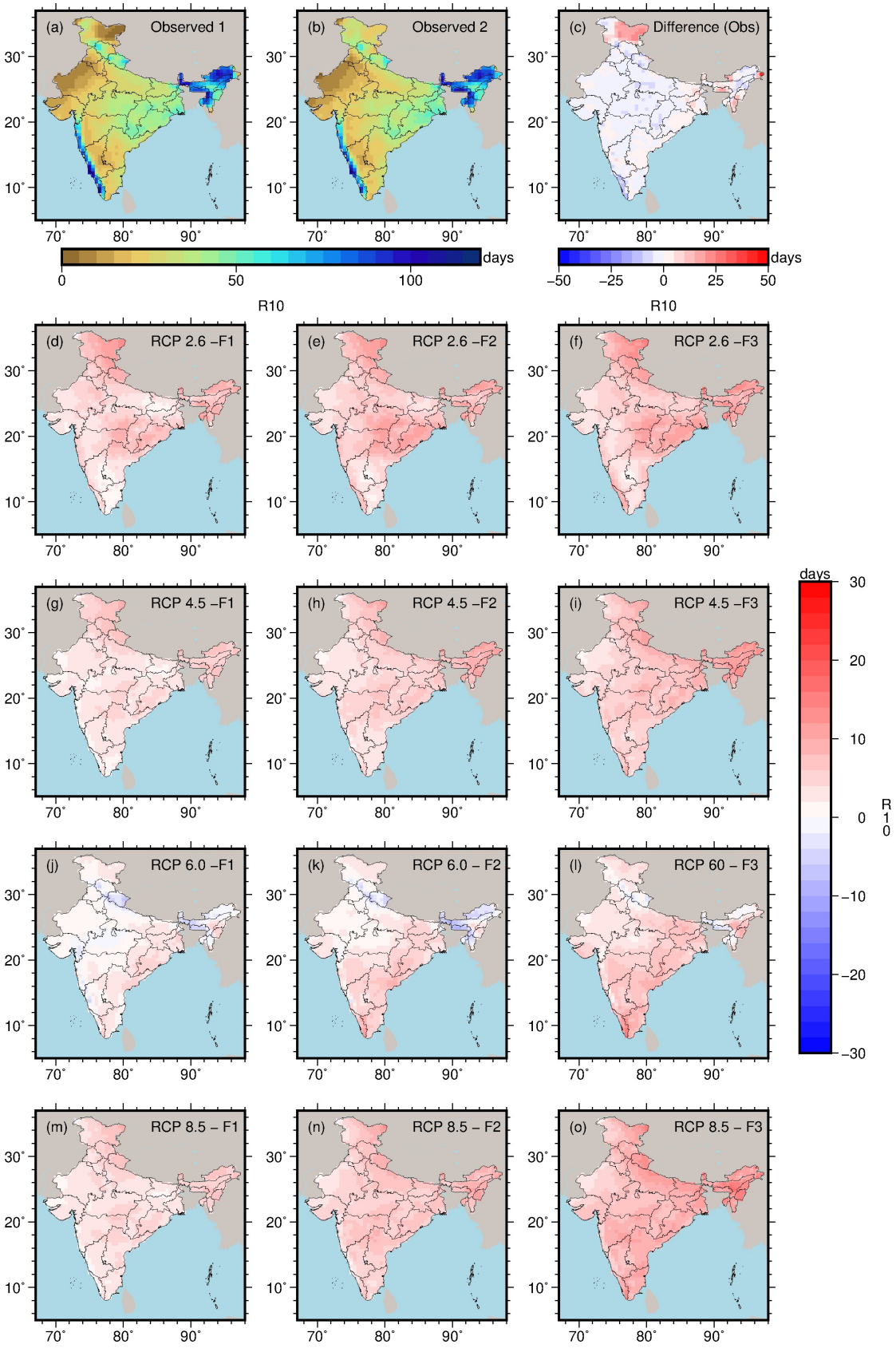

Figure 6.24: Same as Figure 6.8 but for R10.

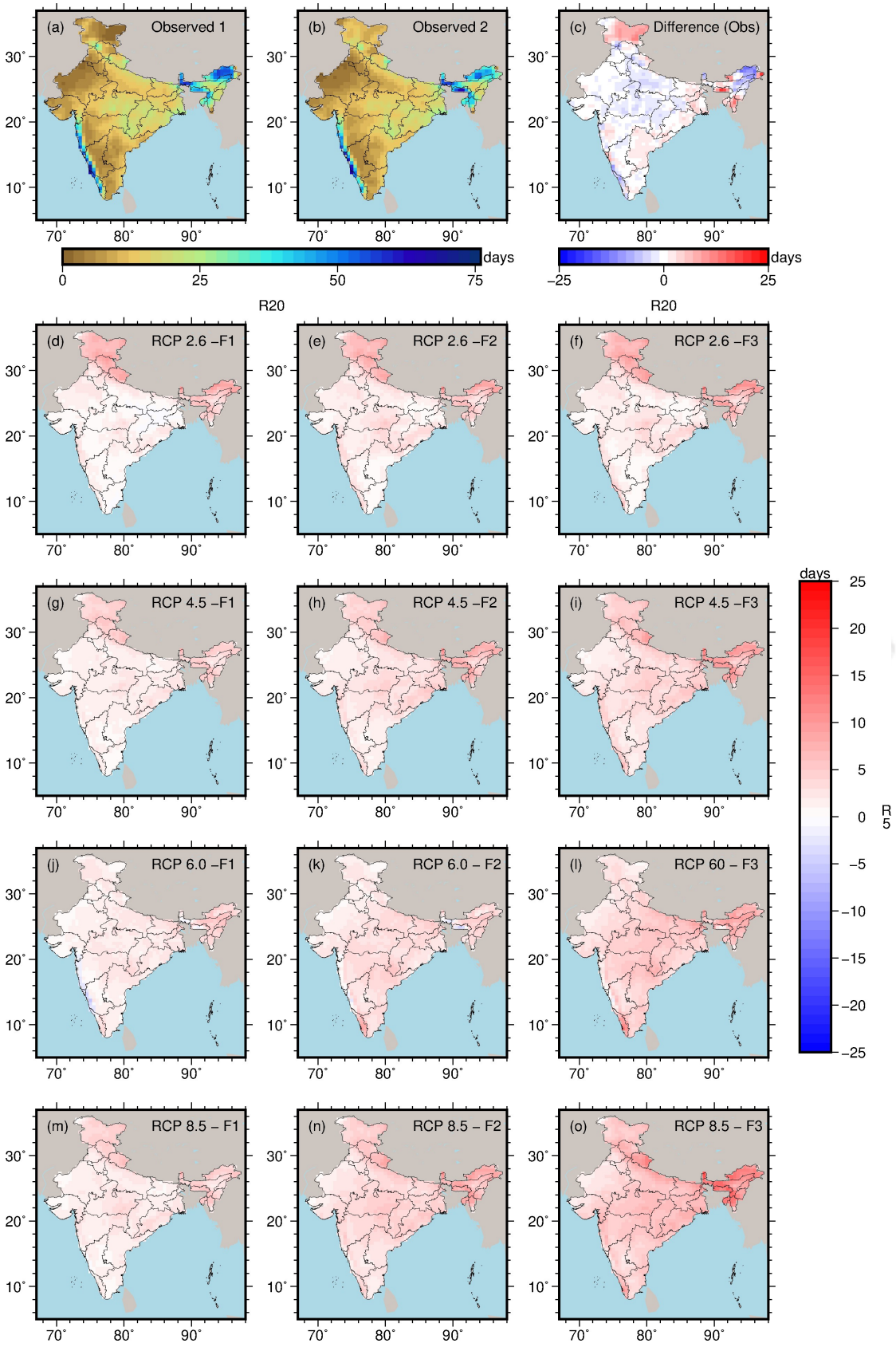

Figure 6.25: Same as Figure 6.8 but for R20.

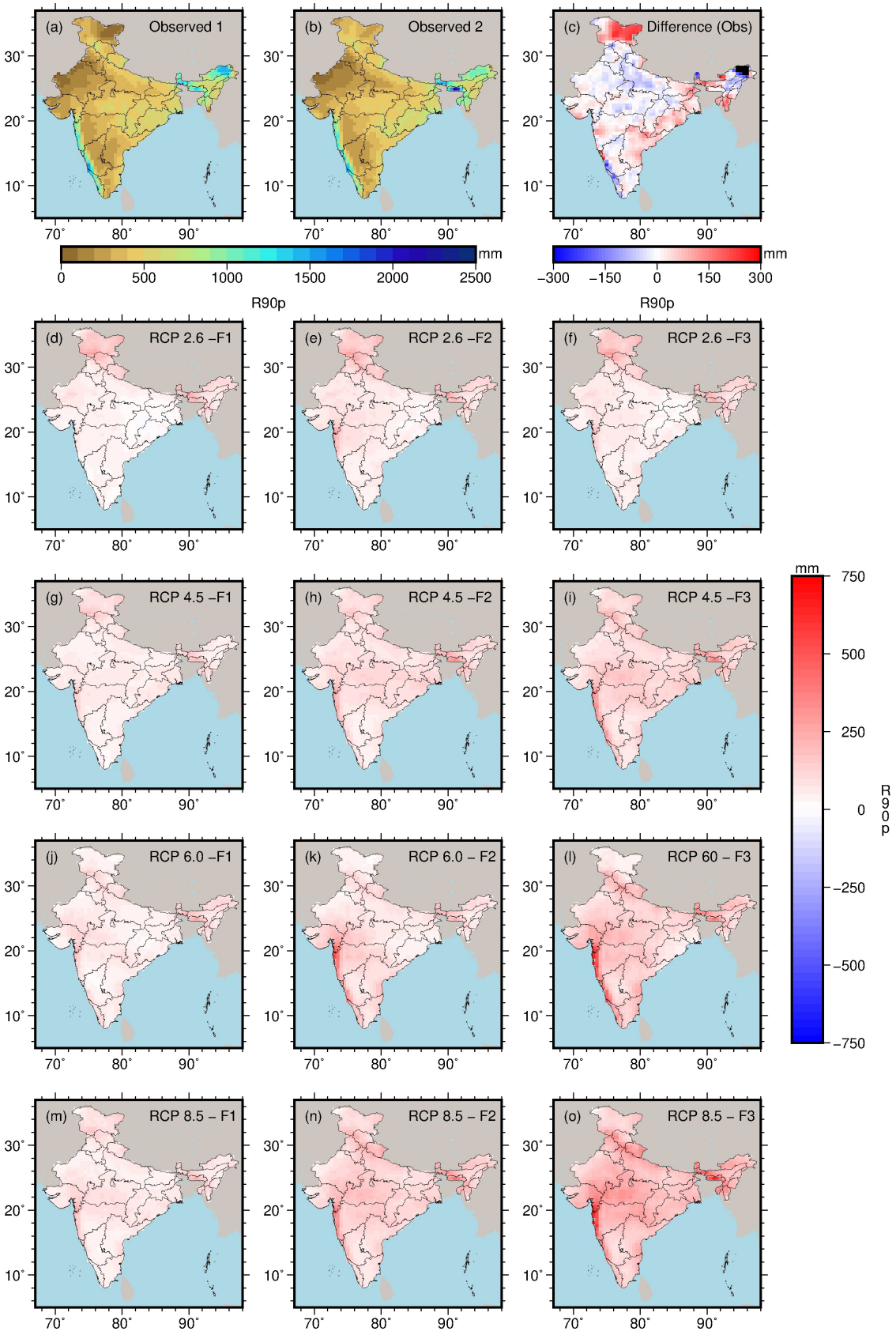

Figure 6.26: Same as Figure 6.8 but for R90p.

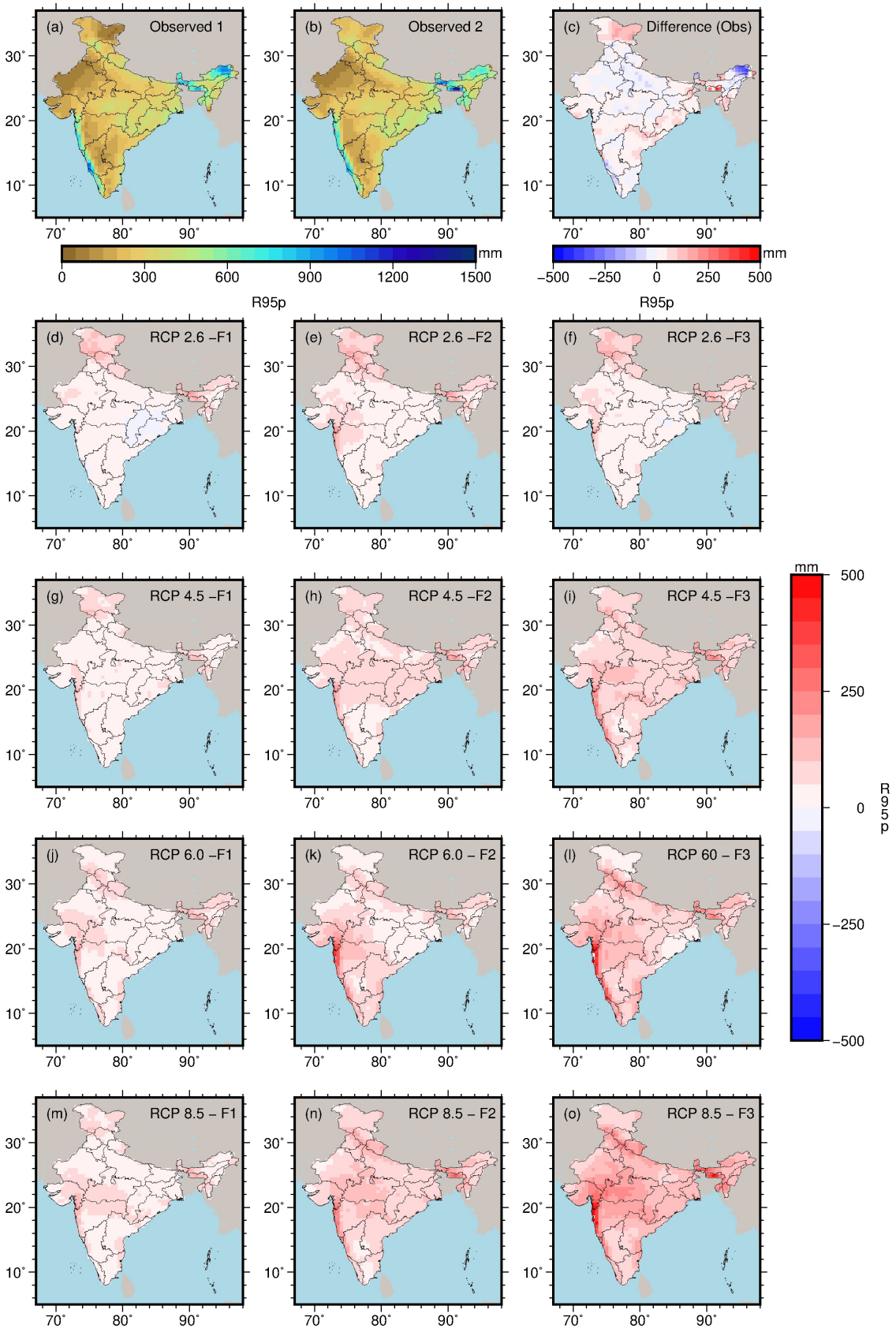

Figure 6.27: Same as Figure 6.8 but for R95p.

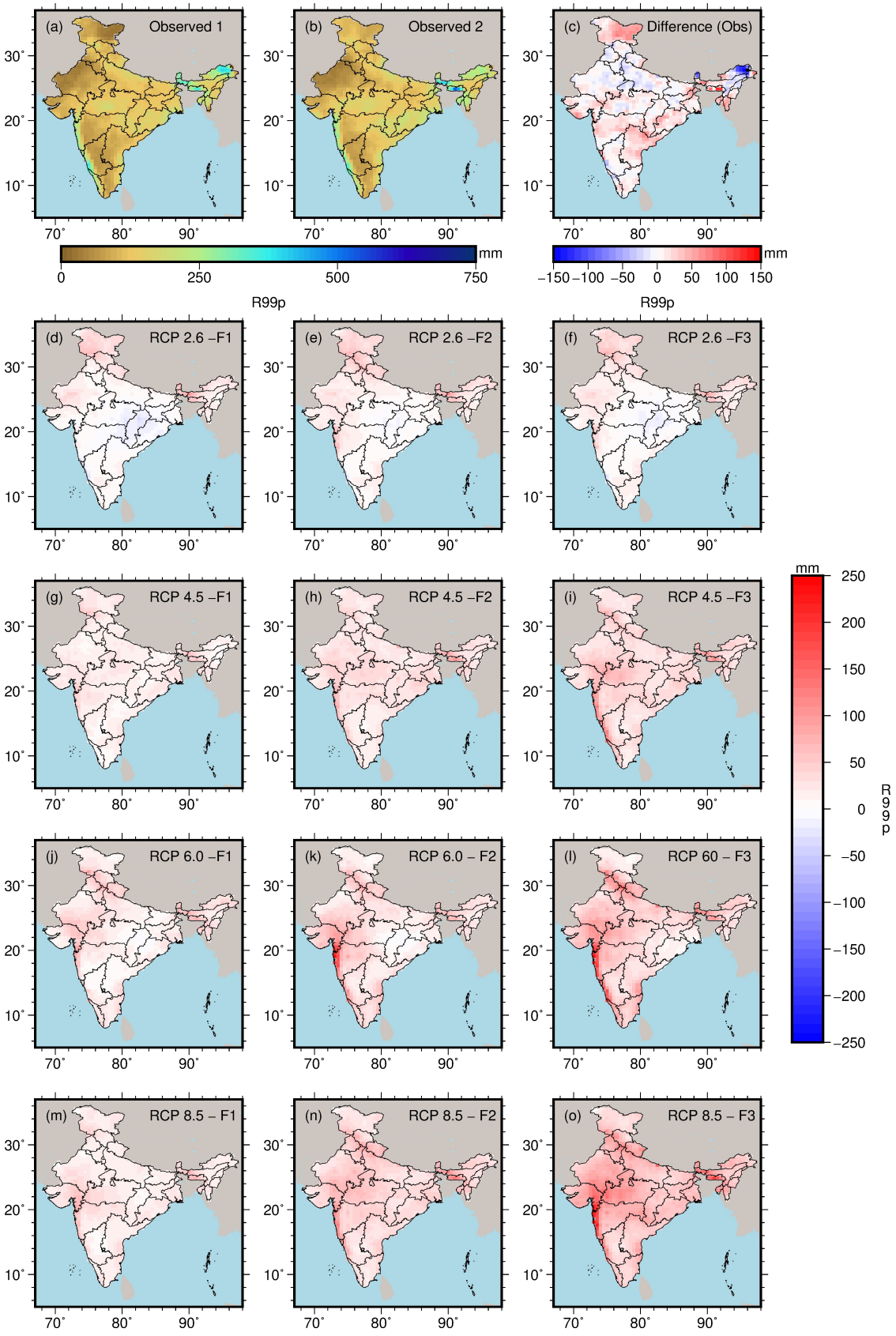

Figure 6.28: Same as Figure 6.8 but for R99p.

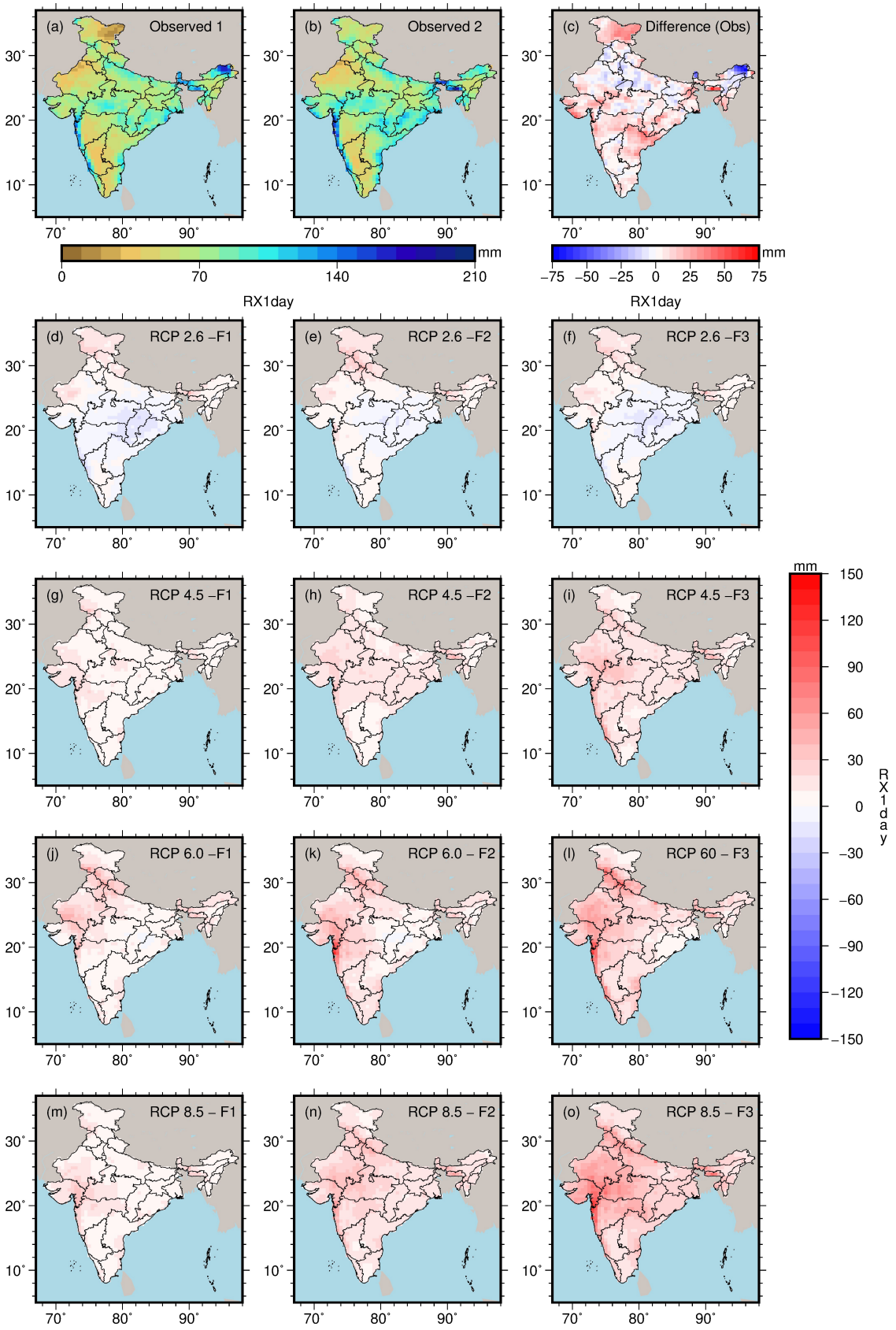

Figure 6.29: Same as Figure 6.8 but for RX1day.

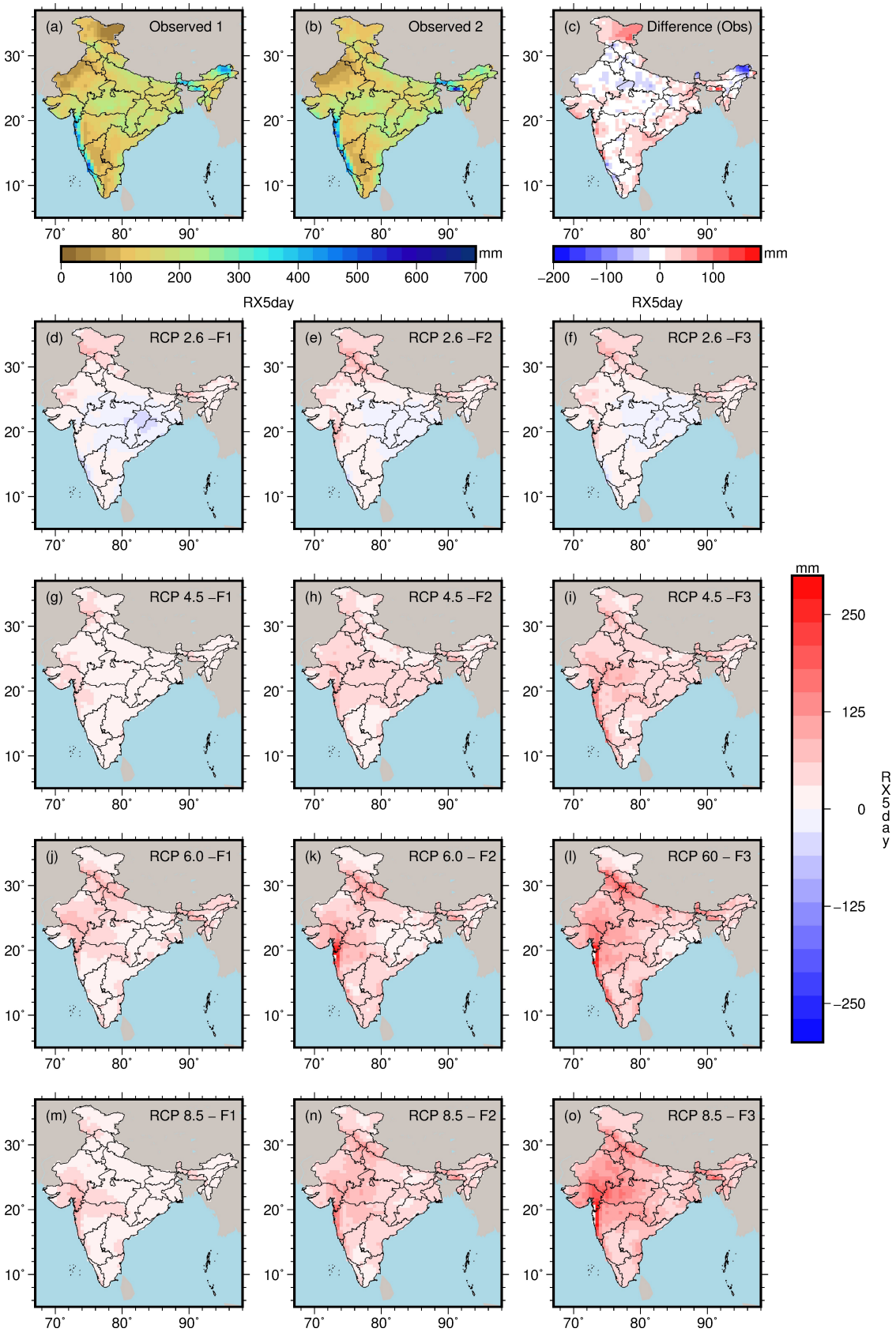

Figure 6.30: Same as Figure 6.8 but for RX5day.

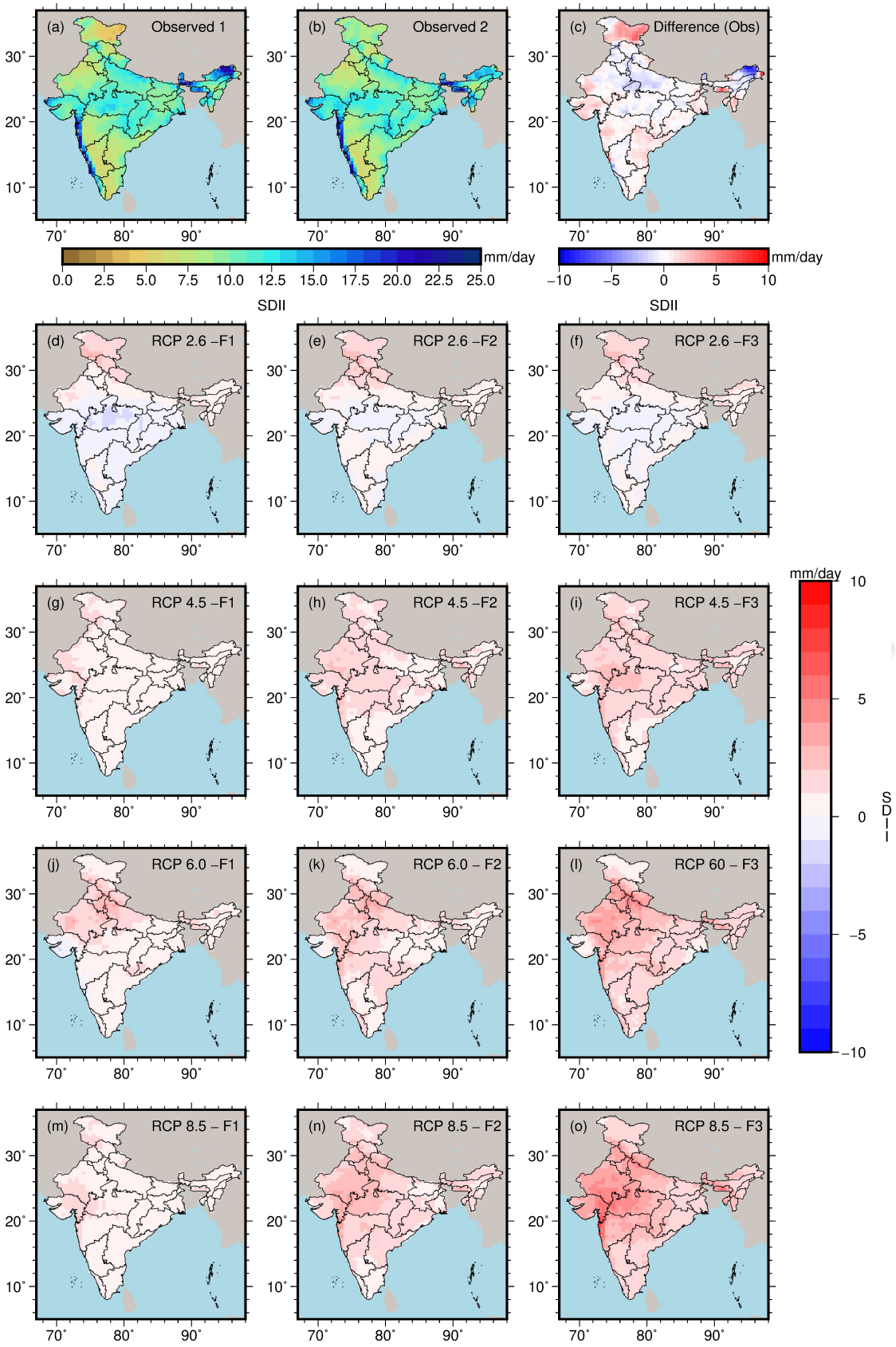

Figure 6.31: Same as Figure 6.8 but for SDII.

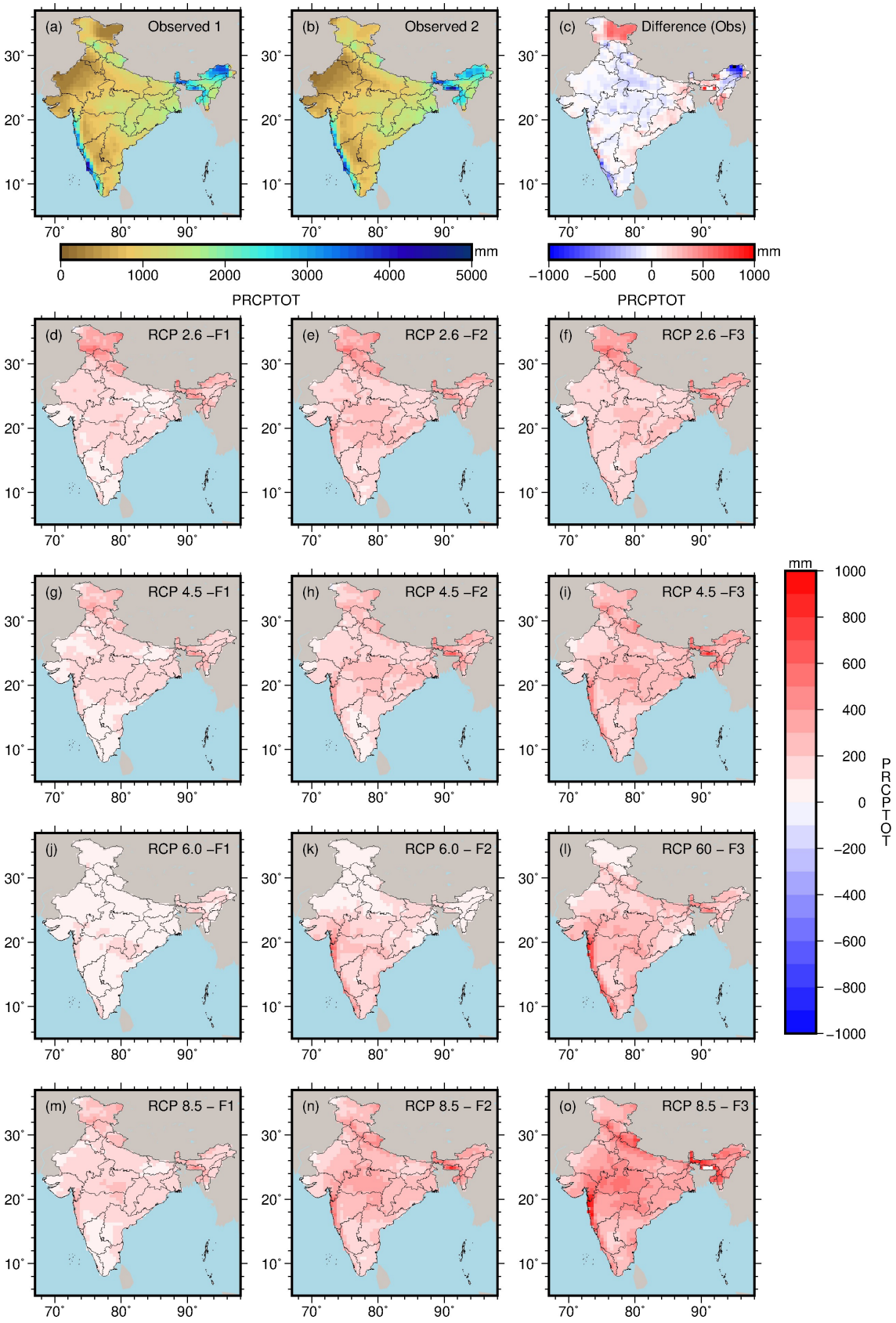

Figure 6.32: Same as Figure 6.8 but for PRCPTOT.

6.4.3 Basin scale analysis of precipitation and temperature

The analysis of changes in precipitation and temperature was also carried out at the basin scale. The river basin definition is adopted from Watershed Atlas of India (India-WRIS, 2014), as described in Section 3.3.1. Figures 6.33, 6.34 and 6.35 show the bar charts of basin-wise precipitation, Tmax and Tmin, respectively. The Basin Id's used are as per Watershed Atlas of India, as shown in Table 3.3. The results are shown for observed period (1975-2005), GCMs based historical scenarios (1975-2005) and GCM based RCP projections (F1: 2011-2040, F2: 2041-2070 and F3: 2071-2100).

Basin Id. 2c had the highest precipitation for the observed period of 2,627 mm/year, whereas the bias-corrected MMA precipitation for the basin was 2,623 mm/year for the same period. On the other hand, Basin Id. 1 had the least precipitation of 733 mm/year for the observed period, whereas the bias-corrected MMA precipitation for the basin was 732 mm/year. Similarly, the bias-corrected MMA historical run of GCMs was in good agreement with the observed precipitation at the basin scale. Increase in precipitation was found for all the river basins in India. Precipitation increased from lower to higher emission scenarios, i.e., higher values were projected for RCP8.5 compared to RCP2.6 or RCP4.5. Increase in precipitation was greater than 200-300 mm for basins with higher annual precipitation such as Basin Ids. 2b, 2c and 14. Changes in precipitation in five major basins (Basin Ids. 1, 2a, 2b, 3 and 4) are discussed in detail in this section; however, increase in precipitation was found for every river basin.

Basin Id. 1 (Indus basin) had the least precipitation among all basins during the period 1975-2005 as the basin covers a large arid region of Western India. Increase of about 20-30% in precipitation was observed for the basin under different RCPs. Under the extreme scenario, i.e., RCP8.5, the percent increase in precipitation was found to be 22.8%, 28.1% and 37.3% for F1, F2 and F3, respectively. Basin Id. 2a (Ganga basin) is the largest basin in the country. The mean annual precipitation in the basin for the observed period was 1,049 mm. Significant increase in the precipitation was found for the basin for different RCPs. The basin is expected to experience 18% to 38% increase in precipitation under different RCPs by the end of the 21st century. Basin Id. 2b (Brahmaputra basin) is one of the highest rainfall receiving basins in the country. The average precipitation in the basin during the observed period was 2,522 mm/year. Consistent with other basins, an increase in precipitation was found in this basin as well. The basin is expected to experience 4 - 10% higher precipitation during F1, 4 - 13.2%

higher precipitation during F2 and 9.7 - 19.3% higher precipitation for F3, compared to the observed period for different RCPs. In general, the increase in precipitation was higher for RCP8.5 compared to other RCPs. Basin Ids. 3 (Godavari) and 4 (Krishna) are located in peninsular India. The annual precipitation in the observed period for the Godavari and Krishna basin was 1,114 mm/year and 944 mm/year, respectively. The bias-corrected MMA historical precipitation was nearly equal for both the basins. Like basins in the north and northeast, both of these basins are also expected to receive higher precipitation under RCPs. Comparing the extreme scenario (RCP8.5) for the F3 period, the Godavari and Krishna basin are expected to receive 35.7% and 31.2% higher precipitation compared to the observed period. Likewise, all other basins were also found to experience higher under climate change scenarios. Mahi basin (Basin Id. 10), which is one of the least precipitation receiving basin, is expected to have the highest increase (in terms of percent change) in precipitation.

Indus basin (Basin Id. 1) has the lowest temperature among all basins with Tmax of 20.2 °C and Tmin of 7.44 °C for the observed period. A large part of the Indus basin is in the Himalayan region, which has very low temperature. Basin Id. 17 has the highest temperature with Tmax of 33.59 °C and Tmin of 23.25 °C. Increase in temperature was found for all the basins; however, the Indus basin is anticipated to experience a higher increase in temperature compared to other basins. Under RCP8.5, the basin average Tmax and Tmin in the Indus basin are projected to increase by 5.32 °C and 5.48 °C, respectively, for F3 period compared to the observed period. In general, the basins in north India (close to the Himalayan belt) are anticipated to have a higher increase in temperature.

6.5 Conclusions

Assessment of the changes in precipitation, temperature and climate extremes was carried out using over India using observed data and bias-corrected outputs of 20 climate models considering the four Representative Concentration Pathways (RCPs). Further, analysis of changes in climate extremes (11 precipitation indices and 14 temperature indices) was carried out over observed and projected climate. This study found that climate change has affected the precipitation and temperature patterns in different parts of the country. The multimodel assessment of the precipitation showed an increasing trend in both precipitation and temperature for most of the parts of the country for

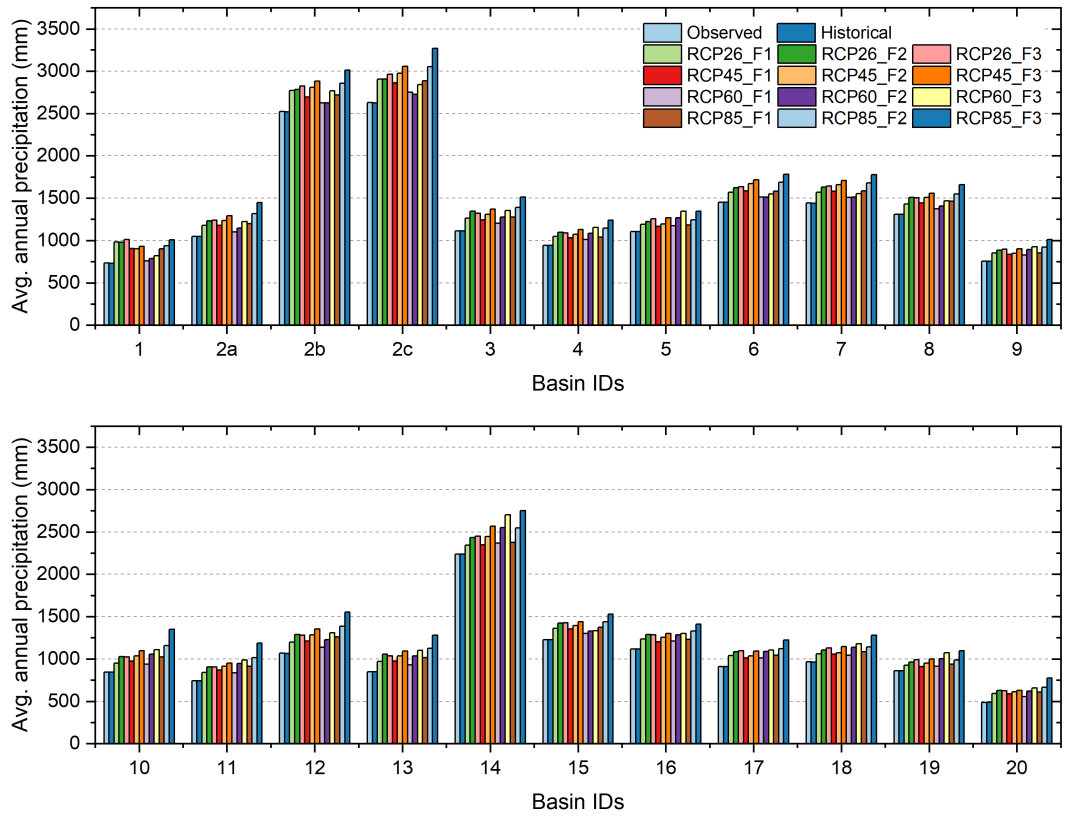

Figure 6.33: Changes in basin scale precipitation.

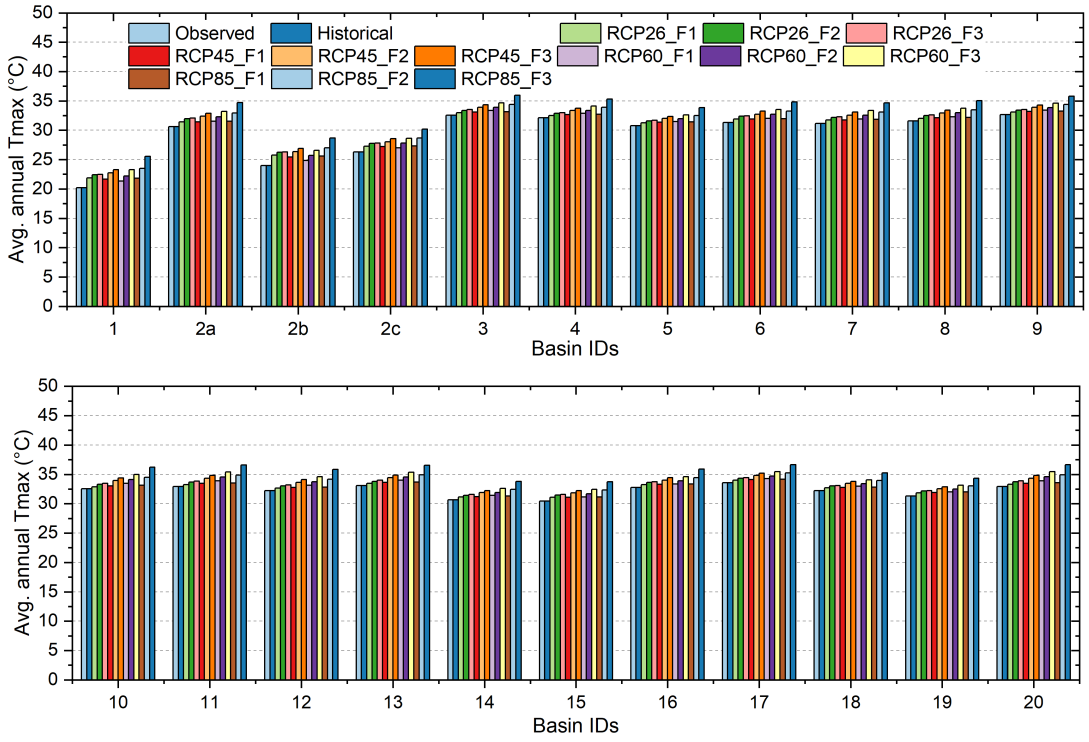

Figure 6.34: Changes in basin scale Tmax.

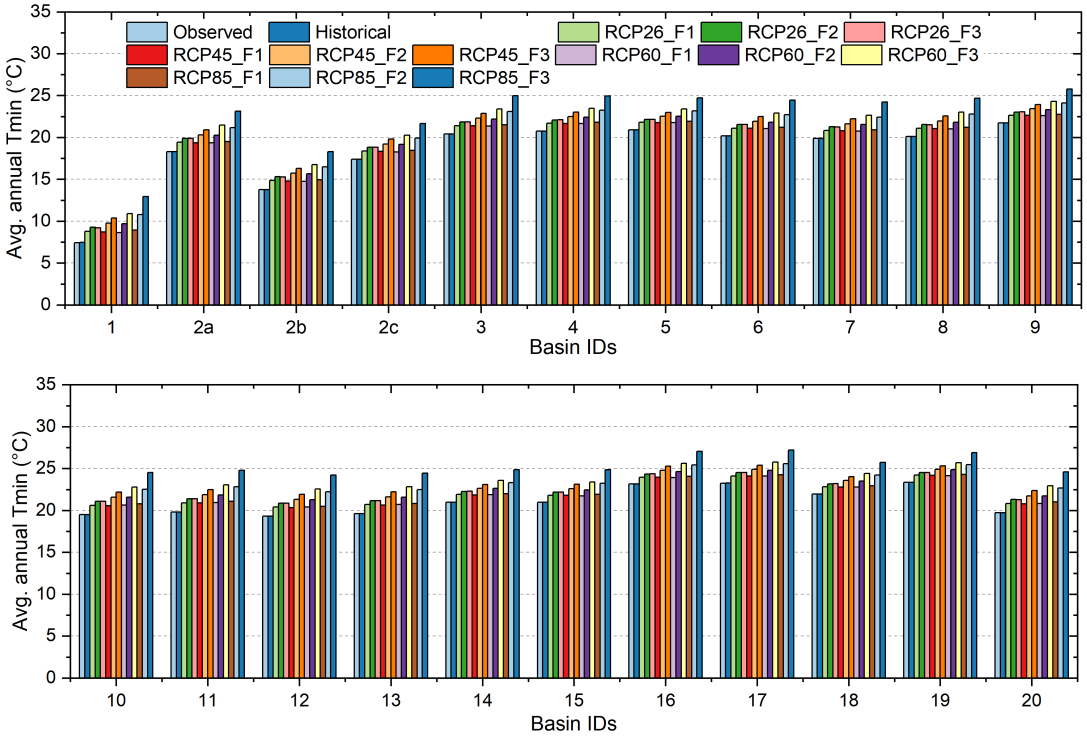

Figure 6.35: Changes in basin scale Tmin.

all RCPs. There was a large spatial heterogeneity in the changes in precipitation and temperature. The western regions of the country are anticipated to experience the higher increase in the precipitation for the projected climate. Increase in temperature was found higher for the Himalayan regions of the country. The country-average precipitation and temperature had a significant increasing trend for all RCPs; however, the trend in daily minimum temperature was higher than in daily maximum temperature. The changes in climate extremes were consistent with the increase in temperature and precipitation. A drastic increase in warm days and warm nights was found for all parts of the country whereas a drastic decrease in cool nights and cool days was found. A decrease in frost days and ice days was found in the Himalayan regions. Tropical nights and summer days were found to increase. The diurnal temperature range was found to increase in Himalayan regions, whereas it is anticipate to decrease in other parts of the country. Consecutive dry days were found to increase in most parts of the country except for central India. On the other hand, consecutive wet days were found to increase in most parts of the country. The heavy precipitation days were also found to increase along with the precipitation during the very wet days and the maximum 1 day and 5 days precipitation.

भारतीय प्रौद्योगिकी संस्थान गुवाहाटी
Indian Institute of Technology Guwahati

7

Conclusions and Recommendations

7.1 A brief review of the work done

This study presented a framework for the analysis of the ecosystem resilience of terrestrial ecosystems to droughts. The framework was developed using the basic concept of resilience and ecosystem water use efficiency. Ecosystem resilience analysis was performed at different scales in India. The ecosystem resilience at different scales was related to the controlling factors. Further, a detailed analysis of ecosystem water use efficiency was performed in India along with the role of climatic controls. Hydrological resilience analysis of a river basin in India was carried out based on two measures of resilience. The impact of climate change on the hydrology of the river basin was assessed using climate models and hydrological modelling. Four General Circulation Models (GCMs) and two Representative Concentration Pathways (RCPs) were used to evaluate the changes in the basin's hydrology under the projected climate. Finally, the impact of climate change on precipitation, temperature and climate extremes in India was assessed using 20 GCMs and four RCPs. Twenty-five climate indices were used for the analysis of climate extremes.

7.1.1 Ecosystem resilience analysis

Utilizing the concept of resilience, an ecosystem resilience framework was developed to study the impact of dry conditions on the productivity of terrestrial ecosystems. The framework was based on ecosystem water use efficiency (WUE_e), which is defined as the ratio of carbon uptake and water used by the ecosystem. Based on the ratio of WUE_e during dry period and normal WUE_e, a resilience index (R_d) was proposed. Four different classes of resilience were formed based on the values of R_d. The analysis

was carried out at different scales in India such as river basin, district, land cover and climate types. Significant variation in WUE_e was found at all scales in India. Among river basins, the Brahmaputra basin had the highest WUE_e due to the presence of forest. Land cover scale analysis revealed higher WUE_e for forest classes. Temperate climate type had higher WUE_e compared to other climate types. The resilience analysis at basin scale found that only six out of twenty-two basins were resilient to dry conditions, whereas other basins were found non-resilient. Seven basins were found slightly non-resilient, three were found moderately non-resilient and remaining six basins were found severely non-resilient. The resilience analysis at land cover scale revealed that only evergreen forests were resilient, and the climate type scale resilience analysis revealed that only temperate climate was resilient.

At district scale, the districts along the lower Himalayan regions had higher WUE_e due to moderate NPP and low ET. However, these regions had a decreasing trend in WUE_e. Central India had low WUE_e, but the region had an increasing trend. The resilience analysis at district scale revealed that, out of 634 districts, only 241 (≈38%) districts were resilient. On the other hand, number of districts with slightly, moderately and severely non-resilient classes was 180 (≈28.4%), 80 (≈12.6%) and 133 (≈21%), respectively. In general, the forest dominated districts were found higher resilient. Out of 30 states and UTs, only 10 had more than 50% resilient area, which were located mainly in the lower Himalayan region.

7.1.2 Spatiotemporal analysis of WUE_e

Pixel level analysis of WUE_e was carried out to understand the spatiotemporal variation of WUE_e in India. WUE_e plays an important role in understanding the impacts of climate change on terrestrial ecosystems. This study performed an analysis of the spatiotemporal pattern, trend and controlling factors of annual WUE_e in India over 2000-2014. The spatiotemporal pattern in WUE_e across India was consistent with the distribution of different biomes and climate types. Higher WUE_e for northeastern regions and lower Himalayan belt was found, whereas the arid areas of western India had the least WUE_e. The inter-annual variability in WUE_e was higher for the western arid regions due to highly fluctuating rainfall patterns. An increasing trend was found for country-average WUE_e with a magnitude of 0.0058 gC m^{-2} mm^{-1} yr^{-1}, whereas previous study had reported a decreasing trend in global average WUE_e. This shows

that there was a contrast in the response of terrestrial ecosystems to climate change in India and globally. Pixel-level trend analysis revealed an increasing trend in central India and decreasing trend along the lower Himalayan region. The trend in WUE_e in different parts of the country could be explained with the trend in controlling climatic factors (precipitation, temperature and solar radiation). Correlation analysis was performed between WUE_e and climatic factors to understand the climatic controls on WUE_e. Precipitation was the main climatic factor affecting WUE_e in the western, central and eastern India; Temperature in the mountainous Himalayan regions; and Solar radiation in some parts of northeast and northwest. Most of the land cover types had non-significant trends except for Deciduous Broadleaf Forest and Woody Savanas. In general, the land cover types with lower WUE_e had an increasing trend and the land cover types with higher WUE_e had a decreasing trend.

This study further explored the impact of anthropogenic activities on the terrestrial ecosystem productivity. Correlation analysis between Gross State Domestic Product (GSDP) and NPP was carried out at state scale in India. Some states had positive correlation between GSDP and NPP, indicating no or less impact of anthropogenic activities on NPP. However, the analysis found that the development activities had adversely affected (i.e., negative correction) the NPP in four forest-dominated states (3 in northeast and 1 in north). Forest Survey of India (FSI) has reported a reduction in forests in these states in recent decades, which was attributed to different human activities.

7.1.3 Hydrological Resilience in Teesta River Basin

A resilience-based analysis was performed in the Teesta River basin to understand the hydrologic changes in the basin under the changing climate. Analysis of changes in precipitation, temperature (both daily maximum and minimum) and climate extremes (both precipitation and temperature indices) was performed to four different CMIP5 based GCMs incorporating two RCPs (RCP4.5 and RCP8.5) . A total of 23 indices (14 temperature indices and 9 precipitation indices) were analysed for both past (1951-2010) and projected (2011-2100) climates. There were substantial changes in precipitation and temperature patterns as well as in the climate extremes in the basin for both observed as well as projected climate. In general, warming and increase in precipitation were found, which increased from RCP4.5 to RCP8.5. Significant increasing trends (p-value < 0.05) were found for all sub-basins for both temperature and precipitation

for the 21st century. The basin average annual precipitation is projected to increase by 225mm, 283mm and 385mm for period 2011 to 2040, 2041 to 2070, and 2071 to 2100, respectively, under RCP4.5 and by 160mm, 418mm and 751mm for period 2011 to 2040, 2041 to 2070, and 2071 to 2100, respectively, under RCP8.5 compared to 1951-2010 period. The basin average maximum daily temperature is projected to increase by 0.46°C, 0.90°C and 1.13°C for period 2011 to 2040, 2041 to 2070, and 2071 to 2100, respectively, for RCP4.5 and by 0.54°C, 1.18°C and 1.92°C for period 2011 to 2040, 2041 to 2070, and 2071 to 2100, respectively, for RCP8.5, compared to 1951-2010 period. The basin average minimum daily temperature is projected to increase by 0.4°C, 0.75°C, and 1°C for period 2011 to 2040, 2041 to 2070, and 2071 to 2100, respectively, for RCP4.5 and by 0.5°C, 1.2°C and 2°C for period 2011 to 2040, 2041 to 2070, and 2071 to 2100, respectively, for RCP8.5, compared to 1951-2010 period. Precipitation indices showed an increase in high precipitation events and decrease in dry days. Temperature indices showed a drastic increase in warm days and warm nights along with the decrease in cool days and cool nights. Trend analysis of seasonal precipitation indicated an increasing trend in both monsoon and non-monsoon precipitation in the region for projected climate, whereas some sub-basins had decreasing trend in monsoon precipitation for observed climate.

The hydrological processes in the basin were simulated using Soil and Water Assessment Tool (SWAT), which was calibrated using SWAT-Calibration and Uncertainty Programs (SWAT-CUP). SWAT-simulated streamflow also showed an increasing trend under both RCPs, whereas the increase in streamflow was noticeably higher for the winter months compared to other months. The contribution of snowfall to precipitation reduced, whereas the contribution of snowmelt to water yield remained the same for winter months and decreased for spring months. The standardized precipitation index (SPI) based drought analysis indicated a reduction in drought events under the projected climate. The intensity and duration of drought events were also found to reduce towards the end of the 21st century. “Deviation from normal” and “Time to recover” were used to assess the resilience in the basin. These measures suggested an increase in the basin’s resilience to dry period under projected climate. Both average deviation and recovery time reduced for projected climate for both RCPs, which clearly shows the higher resilience of the basin to dry conditions.

7.1.4 Changes in Precipitation, Temperature and Climate Extremes

This study examined the changes in precipitation, temperature and climate extremes over India at 0.5° × 0.5° resolution. The study was carried over the 1951-2100 period using observed data (1951-2010) and climate model outputs (2011-2100). The precipitation and temperature from 20 GCMs and four RCPs were corrected for bias before using for the analysis. Further, analysis of changes in climate extremes (11 precipitation indices and 14 temperature indices) was carried out over observed and projected climate. This study found that climate change has affected the precipitation and temperature patterns in different parts of the country. Increase in precipitation and temperature was found for different parts of the country. Comparing RCPs, it was found that the higher RCPs projected higher increase in these variables. The western parts of the country had largest percent increase in the precipitation. The projected increase in precipitation was as high as 80-100% for the period 2071-2100 under RCP8.5 in some parts of western India. Like precipitation, there was spatial heterogeneity in increase in temperature as well. The Himalayan regions were projected to experience higher increase in temperature than other parts of the country. The trend analysis of country-average precipitation and temperature revealed significant increasing trend for all RCPs. The slope of the trend in daily minimum temperature was found higher than that for daily maximum temperature.

Like temperature, substantial changes were found for temperature extremes. Consistent with the increase in temperature, the number of warm nights and warm days were projected to increase drastically in the 21st century. On the other hand, the number of cool nights and cool days were projected to decrease. The snow indices, which were used to study the snow patterns over Himalayan regions, revealed a drastic reduction in the frost days and ice days in the regions. The diurnal temperature range was found to increase in Himalayan regions, whereas it decreased in other parts of the country. The summer days and tropical nights were also projected to increase. The precipitation extremes indicated increase in heavy precipitation events. There was increase in consecutive dry days in most parts of the country except for central India. The heavy precipitation days were also found to increase along with the precipitation during the very wet days and the maximum 1 day and 5 days precipitation.

7.2 Key contributions of the Thesis

- A framework for ecosystem resilience analysis was proposed. This framework was used at different scales in India to understand the resilience of terrestrial ecosystems to droughts. Most of the terrestrial ecosystems in India were found non-resilient to droughts. Forest-dominated ecosystems had higher resilience.
- A spatiotemporal assessment of Ecosystem Water Use Efficiency (WUE_e) was carried out at pixel scale in India. Analysis of trend and controlling factors of WUE_e was also performed.
- A hydrological resilience framework was used in Teesta river basin to analyse the basin's response to dry conditions. An investigation of the changes in hydroclimatology of the basin was also performed.
- Outputs of twenty General Circulation Models (GCMs) were corrected for bias to perform a high-resolution analysis of changes in precipitation and temperature in India. Twenty five climate indices were studied to examine changes in extreme climatic events.

7.3 Recommendations for future work

This study provides a framework for the resilience analysis of natural systems to dry periods. The study also presented an analysis of climate change impacts on precipitation, temperature and climate extremes in India. To carry out further research in this direction, this study may be useful. The scope of future research discussed as follows:

1. The resilience analysis framework developed in this study was applied using satellite-based datasets. Ground observation may be utilized to reduce the uncertainties associated with the data.
2. The hydrological resilience study was carried out for only one river basin; however, a comparison of different river basins can be carried out using the proposed methodology.
3. Dynamic Vegetation Model (DVM) can be used to predict the primary productivity under future climate to assess the impact of climate change on terrestrial ecosystems.

Bibliography

Abbaspour, K. (2007). "User Manual for SWAT-CUP, SWAT Calibration and Uncertainty Analysis Programs." , Swiss Federal Institute of Aquatic Science and Technology, Eawag, Dübendorf, Switzerland.

Abbaspour, K. C., Faramarzi, M., Ghasemi, S. S., and Yang, H. (2009). "Assessing the impact of climate change on water resources in Iran." *Water Resources Research*, 45(10), 1–16.

Abbaspour, K. C., Johnson, C. A., and van Genuchten, M. T. (2004). "Estimating Uncertain Flow and Transport Parameters Using a Sequential Uncertainty Fitting Procedure." *Vadose Zone Journal*, 3(4), 1340–1352.

Adger, W. N., Hughes, T. P., Folke, C., Carpenter, S. R., and Rockström, J. (2005). "Social-Ecological Resilience to Coastal Disasters." *Science*, 309(5737), 1036–1039.

Amarasinghe, P., Liu, A., Egodawatta, P., Barnes, P., McGree, J., and Goonetilleke, A. (2016). "Quantitative assessment of resilience of a water supply system under rainfall reduction due to climate change." *Journal of Hydrology*, 540, 1043–1052.

Anav, A., Friedlingstein, P., Beer, C., Ciais, P., Harper, A., Jones, C., Murray-Tortarolo, G., Papale, D., Parazoo, N. C., Peylin, P., Piao, S., Sitch, S., Viovy, N., Wiltshire, A., and Zhao, M. (2015). "Spatiotemporal patterns of terrestrial gross primary production: A review." *Reviews of Geophysics*, 53, 785–818.

Anderies, J. M., Folke, C., Walker, B., and Ostrom, E. (2013). "Aligning key concepts for global change policy: Robustness, resilience, and sustainability." *Ecology and Society*, 18(2).

Andermann, C., Longuevergne, L., Bonnet, S., Crave, A., Davy, P., and Gloaguen, R. (2012). "Impact of transient groundwater storage on the discharge of Himalayan rivers." *Nature Geoscience*, 5, 127–132.

Anghileri, D., Pianosi, F., and Soncini-Sessa, R. (2014). "Trend detection in seasonal data: From hydrology to water resources." *Journal of Hydrology*, 511, 171–179.

Arnell, N. W. (1999). "Climate change and global water resources." *Global Environmental Change*, 9(June), S31–S49.

Arnell, N. W. and Gosling, S. N. (2016). "The impacts of climate change on river flood risk at the global scale." *Climate Change*, 134(3), 387–401.

Arnold, J. G., Allen, P. M., and Bernhardt, G. (1993). "A comprehensive surface-groundwater flow model." *Journal of Hydrology*, 142(1-4), 47–69.

Arnold, J. G., Moriasi, D. N., Gassman, P. W., Abbaspour, K. C., White, M. J., Srinivasan, R., Santhi, C., Harmel, R. D., van Griensven, A., Liew, M. W. V., Kannan, N., and Jha, M. K. (2012). "SWAT: Model use, calibration, and validation." *Transactions of the ASABE*, 55(4), 1491–1508.

Arnold, J. G., Srinivasan, R., Muttiah, R. S., and Williams, J. R. (1998). "Large area hydrologic modeling and assessment part I: Model development." *Journal of the American Water Resources Association*, 34(1), 73–89.

Babar, S. and Ramesh, H. (2015). "Streamflow Response to Land Use–Land Cover Change over the Nethravathi River Basin, India." *Journal of Hydrologic Engineering*, 20(10), 05015002.

Banger, K., Tian, H., Tao, B., and Ren, W. (2015). "Terrestrial net primary productivity in India during 1901 – 2010 : contributions from multiple environmental changes." *Climate Change*, 132, 575–588.

Beer, C., Reichstein, M., Tomelleri, E., Ciais, P., Jung, M., Carvalhais, N., Rödenbeck, C., Arain, M. A., Baldocchi, D., Bonan, G. B., Bondeau, A., Cescatti, A., Lasslop, G., Lindroth, A., Lomas, M., Luyssaert, S., Margolis, H., Oleson, K. W., Roupsard, O., Veenendaal, E., Viovy, N., Williams, C., and Woodward, F. I. (2010). "Terrestrial Gross Carbon Dioxide Uptake: Global Distribution and Covariation with Climate." *Science*.

Berghuijs, W. R., Woods, R. A., and Hrachowitz, M. (2014). "A precipitation shift from snow towards rain leads to a decrease in streamflow." *Nature Climate Change*, 4, 583–586.

Bergkamp, G. (1998). "Hydrologic influences on the resilience of Quercus spp. dominated geoecosystems in central Spain." *Geomorphology*, 23(2-4), 101–126.

Bhutiyani, M. R., Kale, V. S., and Pawar, N. J. (2010). "Climate change and the precipitation variations in the northwestern Himalaya: 1866-2006." *International Journal of Climatology*, 30(4), 535–548.

Bookhagen, B. and Burbank, D. W. (2010). "Toward a complete Himalayan hydrological budget: Spatiotemporal distribution of snowmelt and rainfall and their impact on river discharge." *Journal of Geophysical Research: Earth Surface*, 115(F03019), 1–25.

Botter, G., Basso, S., Rodriguez-iturbe, I., and Rinaldo, A. (2013). "Resilience of river flow regimes." *Proceedings of the National Academy of Sciences*, 110(32), 12925–12930.

Breshears, D. D., Cobb, N. S., Rich, P. M., Price, K. P., Allen, C. D., Balice, R. G., Romme, W. H., Kastens, J. H., Floyd, M. L., Belnap, J., Anderson, J. J., Myers, O. B., and Meyer, C. W. (2005). "Regional vegetation die-off in response to global-change-type drought." *Proceedings of the National Academy of Sciences of the United States of America*, 102(42), 15144–15148.

Broxton, P. D., Zeng, X., Sulla-Menashe, D., and Troch, P. A. (2014). "A global land cover climatology using MODIS data." *Journal of Applied Meteorology and Climatology*, 53(6), 1593–1605.

Cao, M. K. and Woodward, F. I. (1998). "Dynamic responses of terrestrial ecosystem carbon cycling to global climate change." *Nature*, 393(6682), 249–252.

Chaturvedi, R. K., Gopalakrishnan, R., Jayaraman, M., Bala, G., Joshi, N. V., Sukumar, R., and Ravindranath, N. H. (2011). "Impact of climate change on Indian forests: A dynamic vegetation modeling approach." *Mitigation and Adaptation Strategies for Global Change*, 16(2), 119–142.

Chen, H., Xu, C.-Y., and Guo, S. (2012). "Comparison and evaluation of multiple GCMs, statistical downscaling and hydrological models in the study of climate change impacts on runoff." *Journal of Hydrology*, 434, 36–45.

Chou, C., Chiang, J. C., Lan, C. W., Chung, C. H., Liao, Y. C., and Lee, C. J. (2013). "Increase in the range between wet and dry season precipitation." *Nature Geoscience*, 6, 263–267.

Chow, V. T., Maidment, D. R., and Mays., L. W. (1988). *Applied Hydrology*. McGraw-Hill, New York, 2010 edition.

Ciais, P., Reichstein, M., Viovy, N., Granier, A., Ogée, J., Allard, V., Aubinet, M., Buchmann, N., Bernhofer, C., Carrara, A., Chevallier, F., De Noblet, N., Friend, a. D., Friedlingstein, P., Grünwald, T., Heinesch, B., Keronen, P., Knohl, A., Krinner, G., Loustau, D., Manca, G., Matteucci, G., Miglietta, F., Ourcival, J. M., Papale, D., Pilegaard, K., Rambal, S., Seufert, G., Soussana, J. F., Sanz, M. J., Schulze, E. D., Vesala, T., and Valentini, R. (2005). "Europe-wide reduction in primary productivity caused by the heat and drought in 2003." *Nature*, 437, 529–533.

Ciais, P., Tans, P. P., Trolier, M., White, J. W. C., and Francey, R. J. (1995). "A large northern hemisphere terrestrial CO2 sink indicated by the 13C/12C ratio of atmospheric CO2." *Science*, 269, 1098–1102.

Cowie, J. (2012). *Climate change: biological and human aspects*. Cambridge University Press, New York.

Dai, A. and NCAR, N. C. f. A. R. S. (2017). "The Climate Data Guide: Palmer Drought Severity Index (PDSI), <https://climatedataguide.ucar.edu/climate-data/palmer-drought-severity-index-pdsi>.

Dale, V. H., Joyce, L. A., McNulty, S., and Neilson, R. P. (2000). "The interplay between climate change, forests, and disturbances." *Science of the Total Environment*, 262, 201–204.

Dalezios, N. R. (2017). "A Review of Drought Indices." *International Journal of Constructive Research in Civil Engineering*, 3(4).

Dams, J., Nossent, J., Senbeta, T., Willems, P., and Batelaan, O. (2015). "Multi-model approach to assess the impact of climate change on runoff." *Journal of Hydrology*, 529, 1601–1616.

Dash, S. K. and Hunt, J. C. R. (2007). "Variability of climate change in India.." *Current Science (00113891)*, 93(6).

Dash, S. K., Jenamani, R. K., Kalsi, S. R., and Panda, S. K. (2007). "Some evidence of climate change in twentieth-century India." *Climatic change*, 85(3-4), 299–321.

Déry, S. J., Hernández-Henríquez, M. A., Burford, J. E., and Wood, E. F. (2009). "Observational evidence of an intensifying hydrological cycle in northern Canada." *Geophysical Research Letters*, 36(13), 1–5.

Devi, G. K., Ganasri, B. P., and Dwarakish, G. S. (2015). "A Review on Hydrological Models." *International Conference on Water Resources, Coastal And Ocean Engineering (ICWRCOE 2015)*, Vol. 4, 1001–1007.

Dile, Y. T. and Srinivasan, R. (2014). "Evaluation of CFSR climate data for hydrologic prediction in data-scarce watersheds: An application in the blue nile river basin." *Journal of the American Water Resources Association*, 50(5), 1226–1241.

Easterling, D. R. (2000). "Climate Extremes: Observations, Modeling, and Impacts." *Science*, 289(5487), 2068–2074.

Ellison, D., Morris, C. E., Locatelli, B., Sheil, D., Cohen, J., Murdiyarso, D., Gutierrez, V., van Noordwijk, M., Creed, I. F., Pokorny, J., Gaveau, D., Spracklen, D. V., Tobella, A. B., Ilstedt, U., Teuling, A. J., Gebrehiwot, S. G., Sands, D. C., Muys, B., Verbist, B., Springgay, E., Sugandi, Y., and Sullivan, C. A. (2017). "Trees, forests and water: Cool insights for a hot world." *Global Environmental Change*, 43, 51–61.

Elmqvist, T., Folke, C., Nystrom, M., Peterson, G., Bengtsson, J., Walker, B., and Norberg, J. (2003). "Response diversity, ecosystem change, and resilience." *Frontiers in Ecology and the Environment*, 1(9), 488–494.

Faramarzi, M., Abbaspour, K. C., Ashraf Vaghefi, S., Farzaneh, M. R., Zehnder, A. J. B., Srinivasan, R., and Yang, H. (2013). "Modeling impacts of climate change on freshwater availability in Africa." *Journal of Hydrology*, 480, 85–101.

Fiering, M. B. (1982a). "A Screening Model to Quantify Resilience." *Water Resources Research*, 18(1), 27–32.

Fiering, M. B. (1982b). "Alternative Indices of Resilience." *Water Resources Research*, 18(1), 33–39.

Fiering, M. B. (1982c). "Estimates of resilience indices by simulation." *Water Resources Research*, 18(1), 41–50.

Fiering, M. B. (1982d). "Estimating resilience by canonical analysis." *Water Resources Research*, 18(1), 51–57.

Folke, C. (2006). "Resilience: The emergence of a perspective for social-ecological systems analyses." *Global Environmental Change*, 16(3), 253–267.

Folke, C. (2016). "Resilience (Republished)." *Ecology and Society*, 21(4), 44.

Fowler, H. J., Blenkinsop, S., and Tebaldi, C. (2007). "Linking climate change modelling to impacts studies: Recent advances in downscaling techniques for hydrological modelling." *International Journal of Climatology*, 27(12), 1547–1578.

Francis, R. and Bekera, B. (2014). "A metric and frameworks for resilience analysis of engineered and infrastructure systems." *Reliability Engineering and System Safety*, 121(2014), 90–103.

FSI (2009). "India State of Forest Report 2009." , Forest Survey of India.

FSI (2011). "India State of Forest Report 2011." , Forest Survey of India.

FSI (2015). "India State of Forest Report 2015." , Forest Survey of India.

Fuka, D. R., Walter, M. T., Macalister, C., Degaetano, A. T., Steenhuis, T. S., and Easton, Z. M. (2014). "Using the Climate Forecast System Reanalysis as weather input data for watershed models." *Hydrological Processes*, 28(22), 5613–5623.

Ganin, A. A., Massaro, E., Gutfraind, A., Steen, N., Keisler, J. M., Kott, A., Mangoubi, R., and Linkov, I. (2016). "Operational resilience: concepts, design and analysis." *Scientific Reports*, 6, 19540.

Gerten, D., Lucht, W., Schaphoff, S., Cramer, W., Hickler, T., and Wagner, W. (2005). "Hydrologic resilience of the terrestrial biosphere." *Geophysical Research Letters*, 32(21), L21408.

Ghosh, S., Das, D., Kao, S.-C., and Ganguly, A. R. (2012). "Lack of uniform trends but increasing spatial variability in observed Indian rainfall extremes." *Nature Climate Change*, 2(2), 86.

Ghosh, S., Luniya, V., and Gupta, A. (2009). "Trend analysis of Indian summer monsoon rainfall at different spatial scales." *Atmospheric science letters*, 10(4), 285–290.

Goroshi, S., Singh, R. P., Pradhan, R., and Parihar, J. S. (2014). "Assessment of net primary productivity over India using Indian geostationary satellite (INSAT-3A) data."

The International Archives of the Photogrammetry, Remote Sensing and Spatial Information Sciences, Vol. XL, Hyderabad, ISPRS Technical Commission VIII Symposium, 9–12.

Gosain, A. K., Rao, S., and Arora, A. (2011). "Climate change impact assessment of water resources of India." *Current Science*, 101, 356–371.

Gosain, A. K., Rao, S., and Basuray, D. (2006). "Climate change impact assessment on hydrology of Indian river basins." *Current Science*, 90(3), 346–353.

Goswami, B. N., Venugopal, V., Sengupta, D., Madhusoodanan, M. S., and Xavier, P. K. (2006). "Increasing trend of extreme rain events over India in a warming environment." *Science*, 314(5804), 1442–1445.

Goswami, U. P., Hazra, B., and Goyal, M. K. (2018). "Copula-based probabilistic characterization of precipitation extremes over North Sikkim Himalaya." *Atmospheric Research*, 212, 273–284.

Goyal, M. K., Panchariya, V. K., Sharma, A., and Singh, V. (2018). "Comparative Assessment of SWAT Model Performance in two Distinct Catchments under Various DEM Scenarios of Varying Resolution, Sources and Resampling Methods." *Water Resources Management*, 32(2), 805–825.

Green, W. and Ampt, G. (1911). "Studies on soil phyics, 1. The flow of air and water through soils." *The Journal of Agricultural Science*, 4(1), 1–24.

Hallegatte, S., Green, C., Nicholls, R. J., and Corfee-Morlot, J. (2013). "Future flood losses in major coastal cities." *Nature Climate Change*, 3, 802–806.

Hamed, K. H. and Rao, A. R. (1998). "A modified Mann-Kendall trend test for autocorrelated data." *Journal of Hydrology*.

Harder, P., Pomeroy, J. W., and Westbrook, C. J. (2015). "Hydrological resilience of a Canadian Rockies headwaters basin subject to changing climate , extreme weather , and forest management." *Hydrological Processes*, 29, 3905–3924.

Hashimoto, T., Stedinger, J. R., and Loucks, D. P. (1982). "Reliability, resiliency, and vulnerability criteria for water resource system performance evaluation." *Water Resources Research*, 18(1), 14–20.

Hayes, M. J., Svoboda, M. D., Wilhite, D. A., and Vanyarkho, O. V. (1999). "Monitoring the 1996 drought using the standardized precipitation index." *Bulletin of the American Meteorological Society*, 80(3), 429–438.

Held, I. M. and Soden, B. J. (2006). "Robust Responses of the Hydrological Cycle to Global Warming." *Journal of Climate*, 19, 5686–5699.

Holling, C. S. (1973). "Resilience and Stability of Ecological Systems." *Annual Review of Ecology and Systematics*, 4, 1–23.

Holling, C. S. (1986). "The resilience of terrestrial ecosystems: local surprise and global change." *Sustainable Development of the Biosphere*, W. C. Clark and R. E. Munn, eds., Cambridge University Press, Cambridge, 292–320.

Holling, C. S. (1996). "Engineering Resilience versus Ecological Resilience." *Engineering Within Ecological Constraints*, National Academies Press, Washington.

Howden, S. M., Soussana, J.-F., Tubiello, F. N., Chhetri, N., Dunlop, M., and Meinke, H. (2007). "Adapting agriculture to climate change." *Proceedings of the National Academy of Sciences of the United States of America*, 104(50), 19691–19696.

Huang, L., He, B., Han, L., Liu, J., Wang, H., and Chen, Z. (2017a). "A global examination of the response of ecosystem water-use efficiency to drought based on MODIS data." *Science of The Total Environment*, 601-602, 1097–1107.

Huang, M., Piao, S., Sun, Y., Ciais, P., Cheng, L., Mao, J., Poulter, B., Shi, X., Zeng, Z., and Wang, Y. (2015). "Change in terrestrial ecosystem water-use efficiency over the last three decades." *Global Change Biology*, 21(6), 2366–2378.

Huang, M., Piao, S., Zeng, Z., Peng, S., Ciais, P., Cheng, L., Mao, J., Poulter, B., Shi, X., Yao, Y., Yang, H., and Wang, Y. (2016). "Seasonal responses of terrestrial ecosystem water-use efficiency to climate change." *Global Change Biology*, 22(6), 2165–2177.

Huang, X., Deng, J., Wang, W., Feng, Q., and Liang, T. (2017b). "Impact of climate and elevation on snow cover using integrated remote sensing snow products in Tibetan Plateau." *Remote Sensing of Environment*, 190, 274–288.

Huntington, T. G. (2006). "Evidence for intensification of the global water cycle: Review and synthesis." *Journal of Hydrology*, 319(1-4), 83–95.

Huxman, T. E., Smith, M. D., Fay, P. a., Knapp, A. K., Shaw, M. R., Loik, M. E., Smith, S. D., Tissue, D. T., Zak, J. C., Weltzin, J. F., Pockman, W. T., Sala, O. E., Haddad, B. M., Harte, J., Koch, G. W., Schwinning, S., Small, E. E., and Williams, D. G. (2004). "Convergence across biomes to a common rain-use efficiency." *Nature*, 429(6992), 651–654.

India-WRIS (2014). "Watershed Atlas of India." , Central Water Commision and National Remote Sensing Center ISRO.

IPCC (2001). "Third Assessment Report of the Intergovernmental Panel on Climate Change IPCC (WG I & II)." , Cambridge Univ. Press, Cambridge.

IPCC (2007). "Climate Change 2007: Synthesis report. Contribution of working group I, II and III to the fourth assessment report of the Intergovernmental Panel on Climate Change.

IPCC (2013). "Climate Change 2013: The Physical Science Basis. Contribution of Working Group I to the Fifth Assessment Report of the Intergovernmental Panel on Climate Change." , Cambridge University Press, Cambridge, United Kingdom and New York, NY, USA.

IPCC (2014). "IPCC, 2014: Climate Change 2014: Synthesis Report. Contribution of Working Groups I, II and III to the Fifth Assessment Report of the Intergovernmental Panel on Climate Change." , Intergovernmental Panel on Climate Change.

Jain, S. K. and Kumar, V. (2012). "Trend analysis of rainfall and temperature data for India." *Current Science*, 102(1), 37–49.

Jones, H. (2004). "What is water use efficiency?." *Water Use Efficiency in Plant Biology*, M. Bacon, ed., Blackwell Publishing Ltd., 27–41.

Kalnay, E., Kanamitsu, M., Kistler, R., Collins, W., Deaven, D., Gandin, L., Iredell, M., Saha, S., White, G., Woollen, J., Zhu, Y., Leetmaa, A., Reynolds, R., Chelliah, M., Ebisuzaki, W., Higgins, W., Janowiak, J., Mo, K. C., Ropelewski, C., Wang, J., Jenne, R., and Joseph, D. (1996). "The NCEP/NCAR 40-Year Reanalysis Project." *Bulletin of the American Meteorological Society*, 77(3), 437–471.

Kang, Y., Khan, S., and Ma, X. (2009). "Climate change impacts on crop yield, crop water productivity and food security - A review." *Progress in Natural Science*, 19(12), 1665–1674.

Karl, T. R. and Trenberth, K. E. (2003). "Modern Global Climate Change." *Science*, 302(5651), 1719–1723.

Keenan, T. F., Hollinger, D. Y., Bohrer, G., Dragoni, D., Munger, J. W., Schmid, H. P., and Richardson, A. D. (2013). "Increase in forest water-use efficiency as atmospheric carbon dioxide concentrations rise.." *Nature*, 499(7458), 324–7.

Kendall, M. G. (1975). *Rank Correlation Methods*. Griffin.

Kottek, M., Grieser, J., Beck, C., Rudolf, B., and Rubel, F. (2006). "World map of the Köppen-Geiger climate classification updated." *Meteorologische Zeitschrift*, 15(3), 259–263.

Krishna, A. P. (2005). "Snow and glacier cover assessment in the high mountains of Sikkim Himalaya." *Hydrological Processes*, 19(12), 2375–2383.

Kumar, K. R., Sahai, A. K., Kumar, K. K., Patwardhan, S. K., Mishra, P. K., Revadekar, J. V., Kamala, K., and Pant, G. B. (2006). "High-resolution climate change scenarios for India for the 21st century." *Current science*, 90(3), 334–345.

Kumar, M. N., Murthy, C. S., Sai, M. V. R. S., and Roy, P. S. (2009). "On the use of Standardized Precipitation Index (SPI) for drought intensity assessment." *Meteorological Applications*, 16, 381–389.

Kundzewicz, Z. W., V. Krysanova, R. E. Benestad, Ø. Hov, M. Piniewski, and I. M. Otto (2018). "Uncertainty in climate change impacts on water resources." *Environmental Science & Policy*, 79, 1–8.

Leng, G., Tang, Q., and Rayburg, S. (2015). "Climate change impacts on meteorological, agricultural and hydrological droughts in China." *Global and Planetary Change*, 126, 23–34.

Li, H., Beldring, C.-y. X. S., Merete, L., and Sharad, T. (2016). "Water Resources Under Climate Change in Himalayan Basins." 843–859.

Li, Y. and Lence, B. J. (2007). "Estimating resilience for water resources systems." *Water Resources Research*, 43(7), 1–11.

Liu, Y., Xiao, J., Ju, W., Zhou, Y., and Wang, S. (2015). "Water use efficiency of China ' s terrestrial ecosystems and responses to drought." *Scientific Reports*, 5, 13799.

Loomis, R. and Connor, D. (1992). *Crop ecology: productivity and management in agricultural systems*. Cambridge University Press.

Madhusudhan, L. (2015). "Agriculture Role on Indian Economy." *Business and Economics Journal*, 06(04), 1000176.

Mahmood, R. and Babel, M. S. (2013). "Evaluation of SDSM developed by annual and monthly sub-models for downscaling temperature and precipitation in the Jhelum basin, Pakistan and India." *Theoretical and Applied Climatology*, 113(1-2), 27–44.

Maier, H. R., Lence, B. J., Tolson, B. A., and Fosch, R. O. (2001). "First-order reliability method for estimating reliability, vulnerability, and resilience." *Water Resource Research*, 37(3), 779–790.

Mallya, G., Mishra, V., Niyogi, D., Tripathi, S., and Govindaraju, R. S. (2015). "Trends and variability of droughts over the Indian monsoon region." *Weather and Climate Extremes*, 12, 43–68.

Mann, H. B. (1945). "Nonparametric tests against trend." *Econometrica*, 13, 245–259.

Marty, C. (2008). "Regime shift of snow days in Switzerland." *Geophysical Research Letters*, 35(12), 1–5.

Mckee, T. B., Doesken, N. J., and Kleist, J. (1993). "The relationship of drought frequency and duration to time scales." *AMS 8th Conference on Applied Climatology*, (January), 179–184.

McMichael, A. J., Campbell-Lendrum, D., Kovats, S., Edwards, S., Wilkinson, P., Wilson, T., and Nicholls, R. (2004). "Global Climate Change." *Comparative quantification of health risks : global and regional burden of disease attributable to selected major risk factors.*, E. Majid, A. D.Lopez, A. A. Rodgers, and Murray, eds., World Health Organisation, Geneva, 1543–1650.

Meehl, G. A. and Tebaldi, C. (2004). "More frequent, and longer lasting heat waves in the 21st century." *Science*, 305(5686), 994–997.

Milly, P. C. D., Wetherald, R. T., Dunne, K. a., and Delworth, T. L. (2002). "Increasing risk of great floods in a changing climate.." *Nature*, 415(6871), 514–517.

Mishra, A. K. and Desai, V. R. (2005). "Drought forecasting using stochastic models." *Stochastic Environmental Research and Risk Assessment*, 19, 326–339.

Mishra, V., Aadhar, S., Akarsh, A., Pai, S., and Kumar, R. (2016). "On the frequency of the 2015 monsoon season drought in the Indo-Gangetic Plain." *Geophysical Research Letters*, (November).

Mishra, V. and Lilhare, R. (2016). "Hydrologic sensitivity of Indian sub-continental river basins to climate change." *Global and Planetary Change*, 139, 78–96.

Mishra, V., Shah, R., and Thrasher, B. (2014). "Soil Moisture Droughts under the Retrospective and Projected Climate in India." *Journal of Hydrometeorology*, 15(6), 2267–2292.

Mondal, A., Narasimhan, B., Sekhar, M., and Mujumdar, P. P. (2016). "Hydrologic Modelling." *Proceedings of the Indian National Science Academy*, 82(3).

Monteith, J. L. (1972). "Solar Radiation and Productivity in Tropical Ecosystems." *The Journal of Applied Ecology*, 9(3), 747.

Moy, W.-S., Cohon, J. L., and ReVelle, C. S. (1986). "A Programming Model for Analysis of the Reliability, Resilience, and Vulnerability of a Water Supply Reservoir." *Water Resources Research*, 22(4), 489–498.

Mu, Q., Heinsch, F. A., Zhao, M., and Running, S. W. (2007). "Development of a global evapotranspiration algorithm based on MODIS and global meteorology data." *Remote Sensing of Environment*, 111, 519–536.

Mu, Q., Zhao, M., and Running, S. W. (2011a). "Evolution of hydrological and carbon cycles under a changing climate." *Hydrological Processes*, 25(26), 4093–4102.

Mu, Q., Zhao, M., and Running, S. W. (2011b). "Improvements to a MODIS global terrestrial evapotranspiration algorithm." *Remote Sensing of Environment*, 115, 1781–1800.

Mu, Q., Zhao, M., and Running, S. W. (2013). "MODIS Global Terrestrial Evapotranspiration (ET) Product (MOD16A2/A3) - ATBD Collection 5." , Missoula.

Mudryk, L. R., Kushner, P. J., Derksen, C., and Thackeray, C. (2017). "Snow cover response to temperature in observational and climate model ensembles." *Geophysical Research Letters*, 44(2), 919–926.

Narsimlu, B., Gosain, A. K., and Chahar, B. R. (2013). "Assessment of Future Climate Change Impacts on Water Resources of Upper Sind River Basin , India Using SWAT Model." 3647–3662.

Nayak, R. K., Dadhwal, V. K., Patel, N. R., and Dutt, C. B. S. (2011). "Inter-annual variability of net ecosystem productivity over India." *The International Archives of the Photogrammetry, Remote Sensing and Spatial Information Sciences*, 34(Part XXX), 125–128.

Nayak, R. K., Patel, N. R., and Dadhwal, V. K. (2010). "Estimation and analysis of terrestrial net primary productivity over India by remote-sensing-driven terrestrial biosphere model." *Environmental Monitoring and Assessment*, 170(1-4), 195–213.

Nayak, R. K., Patel, N. R., and Dadhwal, V. K. (2013). "Inter-annual variability and climate control of terrestrial net primary productivity over India." *International Journal of Climatology*, 33(1), 132–142.

Nayak, R. K., Patel, N. R., and Dadhwal, V. K. (2015). "Spatio-temporal variability of net ecosystem productivity over India and its relationship to climatic variables." *Environmental Earth Sciences*, 74(2), 1743–1753.

Neitsch, S. L., Arnold, J. G., Kiniry, J. R., and Williams, J. R. (2011). "Soil & Water Assessment Tool Theoretical Documentation Version 2009."

Nemani, R. R., Keeling, C. D., Hashimoto, H., Jolly, W. M., Piper, S. C., Tucker, C. J., Myneni, R. B., and Running, S. W. (2003). "Climate-driven increases in global terrestrial net primary production from 1982 to 1999.." *Science (New York, N.Y.)*, 300(5625), 1560–1563.

Niu, S., Xing, X., Zhang, Z., Xia, J., Zhou, X., Song, B., Li, L., and Wan, S. (2011). "Water-use efficiency in response to climate change: From leaf to ecosystem in a temperate steppe." *Global Change Biology*, 17(2), 1073–1082.

NRC (2012). *Disaster Resilience: A National Imperative*. Committee on Increasing National Resilience to Hazards and Disasters Committee on Science, Engineering, and Public Policy, National Academies Press, Washington (nov).

Oki, T. and Kanae, S. (2006). "Global hydrological cycles and world water resources." *Science*, 313(5790), 1068–1072.

Oreskes, N. (2004). "The Scientific Consensus on Climate Change." *Science*, 306(December), 1686.

Pai, D. S., Sridhar, L., Rajeevan, M., Sreejith, O. P., Satbhai, N. S., and Mukhopadhyay, B. (2014). "Development of a new high spatial resolution (0.25° × 0.25°) long period (1901-2010) daily gridded rainfall data set over India and its comparison with existing data sets over the region." *Mausam*, 65(1), 1–18.

Parmesan, C. and Yohe, G. (2003). "A globally coherent fingerprint of climate change impacts across natural systems." *Nature*, 421, 37–42.

Pearson, R. G. and Dawson, T. P. (2003). "Predicting the impacts of climate change on the distribution of species: Are bioclimate envelope models useful?." *Global Ecology and Biogeography*, 12(5), 361–371.

Peel, M. C., Finlayson, B. L., and McMahon, T. A. (2007). "Updated world map of the Koppen-Geiger climate classification." *Hydrology and Earth System Sciences*, 11, 1633–1644.

Peñuelas, J., Canadell, J. G., and Ogaya, R. (2011). "Increased water-use efficiency during the 20th century did not translate into enhanced tree growth." *Global Ecology and Biogeography*, 20(4), 597–608.

Peñuelas, J. and Filella, I. (2001). "Responses to a warming world.." *Science*, 294(5543), 793–795.

Peterson, G., Allen, C. R., and Holling, C. S. (1997). "Ecological Resilience, Biodiversity, and Scale." *Ecosystems*, 1(1), 6–18.

Peterson, T. C. (2005). "Climate Change Indices." *World Meteorological Organization Bulletin*, 54(2), 83–86.

Peterson, T. J., Western, A. W., and Argent, R. M. (2012). "Analytical methods for ecosystem resilience : A hydrological investigation." *Water Resources Research*, 48(W10531), 1–16.

Ponce Campos, G. E., Moran, M. S., Huete, A., Zhang, Y., Bresloff, C., Huxman, T. E., Eamus, D., Bosch, D. D., Buda, A. R., Gunter, S. a., Scalley, T. H., Kitchen, S. G., McClaran, M. P., McNab, W. H., Montoya, D. S., Morgan, J. a., Peters, D. P. C., Sadler,

E. J., Seyfried, M. S., and Starks, P. J. (2013). "Ecosystem resilience despite large-scale altered hydroclimatic conditions.." *Nature*, 494(7437), 349–352.

Qi, M., Feng, M., Sun, T., and Yang, W. (2016). "Resilience changes in watershed systems : A new perspective to quantify long-term hydrological shifts under perturbations." *Journal of Hydrology*, 539, 281–289.

Racoviteanu, A. E., Arnaud, Y., Williams, M. W., and Manley, W. F. (2015). "Spatial patterns in glacier characteristics and area changes from 1962 to 2006 in the Kanchenjunga-Sikkim area, eastern Himalaya." *Cryosphere*, 9(2), 505–523.

Randall, D. A. and Wood, R. A. (2007). "Climate Models and Their Evaluation." *Climate change 2007: The physical science basis.*, Cambridge University Press, 589–662.

Reichstein, M., Bahn, M., Ciais, P., Frank, D., Mahecha, M. D., Seneviratne, S. I., Zscheischler, J., Beer, C., Buchmann, N., Frank, D. C., Papale, D., Rammig, A., Smith, P., Thonicke, K., Van Der Velde, M., Vicca, S., Walz, A., and Wattenbach, M. (2013). "Climate extremes and the carbon cycle." *Nature*, 500(7462), 287–295.

Roxburgh, S. H., Berry, S. L., Buckley, T. N., Barnes, B., and Roderick, M. L. (2005). "What is NPP? Inconsistent accounting of respiratory fluxes in the definition of net primary production." *Functional Ecology*, 19, 378–382.

Roxy, M. K., Ghosh, S., Pathak, A., Athulya, R., Mujumdar, M., Murtugudde, R., Terray, P., and Rajeevan, M. (2017). "A threefold rise in widespread extreme rain events over central India." *Nature Communications*, 8(1), 1–11.

Rubel, F. and Kottek, M. (2010). "Observed and projected climate shifts 1901-2100 depicted by world maps of the Koppen-Geiger climate classification." *Meteorologische Zeitschrift*, 19(2), 135–141.

Running, S. W., Nemani, R. R., Heinsch, F. A., Zhao, M., Reeves, M., and Hashimoto, H. (2004). "A continuous satellite-derived measure of global terrestrial primary production." *BioScience*, 54(6), 547.

Sarkar, S. K., Bhattacharya, A., and Bhattacharya, B. (2003). "The river Ganga of northern India: An appraisal of its geomorphic and ecological changes." *Water Science and Technology*, 48(7), 121–128.

Sen, P. K. (1968). "Estimates of the regression coefficient based on Kendall's Tau." *Journal of the American Statistical Association*, 63(324), 1379–1389.

Shah, H. L. and Mishra, V. (2016). "Hydrologic Changes in Indian Subcontinental River Basins (1901–2012)." *Journal of Hydrometeorology*, 17(10), 2667–2687.

Sharma, K. D., Sorooshian, S., and Wheater, H. (2008). *Modelling Hydrological Processes in Arid and Semi Arid Areas*. New York.

Sharma, S. and Mujumdar, P. (2017). "Increasing frequency and spatial extent of concurrent meteorological droughts and heatwaves in India." *Scientific Reports*, 7(1), 15582.

Sharmila, S., Joseph, S., Sahai, A. K., Abhilash, S., and Chattopadhyay, R. (2015). "Future projection of Indian summer monsoon variability under climate change scenario: An assessment from CMIP5 climate models." *Global and Planetary Change*, 124, 62–78.

Sheffield, J., Goteti, G., and Wood, E. F. (2006). "Development of a 50-year high-resolution global dataset of meteorological forcings for land surface modeling." *Journal of Climate*, 19(13), 3088–3111.

Shekhar, M. S., Chand, H., Kumar, S., Srinivasan, K., and Ganju, A. (2010). "Climate-change studies in the western Himalaya." *Annals of Glaciology*, 51(54), 105–112.

Sillmann, J. and Roeckner, E. (2008). "Indices for extreme events in projections of anthropogenic climate change." *Climatic Change*, 86(1-2), 83–104.

Singh, D., Tsiang, M., Rajaratnam, B., and Diffenbaugh, N. S. (2014). "Observed changes in extreme wet and dry spells during the south Asian summer monsoon season." *Nature Climate Change*, 4, 456–461.

Singh, R. P., Rovshan, S., Goroshi, S. K., Panigrahy, S., and Parihar, J. S. (2011). "Spatial and temporal variability of net primary productivity (NPP) over terrestrial biosphere of India using NOAA-AVHRR based GLoPEM model." *Journal of the Indian Society of Remote Sensing*, 39(3), 345–353.

Singh, V. and Goyal, M. K. (2016). "Changes in climate extremes by the use of CMIP5 coupled climate models over eastern Himalayas." *Environmental Earth Sciences*, 75(9), 839.

Singh, V. and Goyal, M. K. (2017a). "Spatio-temporal heterogeneity and changes in extreme precipitation over eastern Himalayan catchments India." *Stochastic Environmental Research and Risk Assessment*, 31(10), 2527–2546.

Singh, V. and Goyal, M. K. (2017b). "Unsteady High Velocity Flood Flows and the Development of Rating Curves in a Himalayan Basin under Climate Change Scenarios." *Journal of Hydrologic Engineering*, 22(8), 04017023.

Singh, V., Sharma, A., and Goyal, M. K. (2017). "Projection of hydro-climatological changes over eastern Himalayan catchment by the evaluation of RegCM4 RCM and CMIP5 GCM models." *Hydrology Research*, 5, nh2017193.

Song, Q.-H., Fei, X.-H., Zhang, Y.-P., Sha, L.-Q., Liu, Y.-T., Zhou, W.-J., Wu, C.-S., Lu, Z.-Y., Luo, K., Gao, J.-B., and Liu, Y.-H. (2017). "Water use efficiency in a primary subtropical evergreen forest in Southwest China." *Scientific Reports*, 7, 43031.

Srinivasan, R., Ramanarayanan, T. S., Arnold, J. G., and Bednarz, S. T. (1998). "Large area hydrologic modeling and assessment part II: Model application." *Journal of the American Water Resources Association*, 34(1), 91–101.

Still, C. J., Berry, J. A., Collatz, G. J., and DeFries, R. S. (2003). "Global distribution of C 3 and C 4 vegetation: Carbon cycle implications." *Global Biogeochemical Cycles*, 17(1), 1–14.

Sun, Y., Piao, S., Huang, M., Ciais, P., Zeng, Z., Cheng, L., Li, X., Zhang, X., Mao, J., Peng, S., Poulter, B., Shi, X., Wang, X., Wang, Y.-P. P., and Zeng, H. (2016). "Global patterns and climate drivers of water-use efficiency in terrestrial ecosystems deduced from satellite-based datasets and carbon cycle models." *Global Ecology and Biogeography*, 25(3), 311–323.

Tang, X., Li, H., Desai, A. R., Nagy, Z., Luo, J., Kolb, T. E., Olioso, A., Xu, X., Yao, L., Kutsch, W., Pilegaard, K., Köstner, B., and Ammann, C. (2014). "How is water-use efficiency of terrestrial ecosystems distributed and changing on Earth?." *Scientific reports*, 4, 7483.

Tang, X., Ma, M., Ding, Z., Xu, X., Yao, L., Huang, X., Gu, Q., and Song, L. (2017). "Remotely Monitoring Ecosystem Water Use Efficiency of Grassland and Cropland in China's Arid and Semi-Arid Regions with MODIS Data." *Remote Sensing*, 9(6), 616.

Taylor, K. E., Stouffer, R. J., and Meehl, G. a. (2009). "A Summary of the CMIP5 Experiment Design." , <http://cmip-pcmdi.llnl.gov/cmip5/docs/Taylor_CMIP5_design.pdf>.

Taylor, K. E., Stouffer, R. J., and Meehl, G. A. (2012). "An overview of CMIP5 and the experiment design." *Bulletin of the American Meteorological Society*, 93(4), 485–498.

Thapliyal, V. and Kulshrestha, S. M. (1991). "Climate changes and trends over India." *Mausam*, 42(4), 333–338.

Thomey, M. L., Collins, S. L., Vargas, R., Johnson, J. E., Brown, R. F., Natvig, D. O., and Friggens, M. T. (2011). "Effect of precipitation variability on net primary production and soil respiration in a Chihuahuan Desert grassland." *Global Change Biology*, 17(4), 1505–1515.

Tian, H., Banger, K., Bo, T., and Dadhwal, V. K. (2014). "History of land use in India during 1880-2010: Large-scale land transformations reconstructed from satellite data and historical archives." *Global and Planetary Change*, 121, 78–88.

Tong, X. J., Li, J., Yu, Q., and Qin, Z. (2009). "Ecosystem water use efficiency in an irrigated cropland in the North China Plain." *Journal of Hydrology*, 374(3-4), 329–337.

Trenberth, K. E. (2011). "Changes in precipitation with climate change." *Climate Research*, 47(1-2), 123–138.

Trenberth, K. E., Dai, A., van der Schrier, G., Jones, P. D., Barichivich, J., Briffa, K. R., and Sheffield, J. (2014). "Global warming and changes in drought." *Nature Climate Change*, 4, 17–22.

Tripathi, P., Patel, N. R., and Kushwaha, S. (2017). "Estimating net primary productivity in tropical forest plantations in India using satellite-driven ecosystem model." *Geocarto International*, (May), 1–12.

Turner, D. P., Ritts, W. D., Cohen, W. B., Gower, S. T., Running, S. W., Zhao, M., Costa, M. H., Kirschbaum, A. A., Ham, J. M., Saleska, S. R., and Ahl, D. E. (2006). "Evaluation of MODIS NPP and GPP products across multiple biomes." *Remote Sensing of Environment*, 102(3-4), 282–292.

UNFCCC (1992). "United Nations Framework Convention on Climate Change (UNFCCC) - Article 1." , UNFCCC, Bonn, Germany.

USDA (1972). *US Department of Agriculture - Soil Conservation Service (USDA-SCS), National Engineering Handbook, Hydrology section*.

van Vuuren, D. P., Edmonds, J., Kainuma, M., Riahi, K., Thomson, A., Hibbard, K., Hurtt, G. C., Kram, T., Krey, V., Lamarque, J. F., Masui, T., Meinshausen, M., Nakicenovic, N., Smith, S. J., and Rose, S. K. (2011). "The representative concentration pathways: An overview." *Climatic Change*, 109(1), 5–31.

Vicente-Serrano, S. M., Beguería, S., and López-Moreno, J. I. (2010). "A multiscalar drought index sensitive to global warming: The standardized precipitation evapotranspiration index." *Journal of Climate*, 23(7), 1696–1718.

Vorosmarty, C. J., Green, P., Salisbury, J., and Lammers, R. B. (2014). "Global Water Resources : Vulnerability from Climate Change and Population Growth." *Science*, 289(2000), 284–288.

Walker, B., Holling, C. S., Carpenter, S. R., and Kinzig, A. (2004). "Resilience, adaptability and transformability in social – ecological systems." *Ecology and Society*, 9(2), 5.

Walker, B. and Salt, D. (2006). *Resilience thinking: Sustaining Ecosystems and People in a Changing World*. Washington.

Walker, B. and Salt, D. (2013). "A Crash Course in the Science of Resilience." *The Community Resilience Reader: Essential Resources for an Era of Upheaval*, D. Lerch, ed., number April, Island Press, Washington, Chapter 9, 163–178.

Walther, G.-r., Post, E., Convey, P., Menzel, A., Parmesan, C., Beebee, T. J. C., Fromentin, J.-m., I, O. H.-g., and Bairlein, F. (2002). "Ecological responses to recent climate change." *Nature*, 416, 389–395.

Wheeler, T. and Von Braun, J. (2013). "Climate change impacts on global food security." *Science*, 341(6145), 508–513.

White, A., Cannell, M. G., and Friend, A. D. (1999). "Climate change impacts on ecosystems and the terrestrial carbon sink: a new assessment." *Global Environmental Change*, 9, S21–S30.

Wilby, R. L., Wigley, T. M. L., Conway, D., Jones, P. D., Hewitson, B. C., Main, J., and Wilks, D. S. (1998). "Statistical downscaling of general circulation model output: A comparison of methods." *Water Resour. Res.*, 34(11), 2995–3008.

Xu, C., Liu, H., Anenkhonov, O. A., Korolyuk, A. Y., Sandanov, D. V., Balsanova, L. D., Naidanov, B. B., and Wu, X. (2017). "Long-term forest resilience to climate change indicated by mortality, regeneration, and growth in semiarid southern Siberia." *Global Change Biology*, 23(6), 2370–2382.

Xu, C. Y., Widén, E., and Halldin, S. (2005). "Modelling hydrological consequences of climate change - Progress and challenges." *Advances in Atmospheric Sciences*, 22(6), 789–797.

Xue, B.-L., Guo, Q., Otto, A., Xiao, J., and Tao, S. (2015). "Global patterns , trends , and drivers of water use efficiency from 2000 to 2013." *Ecosphere*, 6(October), 1–18.

Yang, Y., Guan, H., Batelaan, O., McVicar, T. R., Long, D., Piao, S., Liang, W., Liu, B., Jin, Z., and Simmons, C. T. (2016). "Contrasting responses of water use efficiency to drought across global terrestrial ecosystems." *Scientific Reports*, 6(November 2015), 23284.

Yu, G., Chen, Z., Piao, S., Peng, C., Ciais, P., Wang, Q., Li, X., and Zhu, X. (2014). "High carbon dioxide uptake by subtropical forest ecosystems in the East Asian monsoon region." *Proc Natl Acad Sci*, 111(13), 4910–4915.

Zhao, M., Heinsch, F. A., Nemani, R. R., and Running, S. W. (2005). "Improvements of the MODIS terrestrial gross and net primary production global data set." *Remote Sensing of Environment*, 95(2), 164–176.

Zhao, M. and Running, S. W. (2010). "Drought-induced reduction in global terrestrial net primary production from 2000 through 2009." *Science*, 329(5994), 940–943.

Zhao, M., Running, S. W., and Nemani, R. R. (2006). "Sensitivity of Moderate Resolution Imaging Spectroradiometer (MODIS) terrestrial primary production to the accuracy of meteorological reanalyses." *Journal of Geophysical Research: Biogeosciences*, 111(1), 1–13.

Publications

Journals

1. **Ashutosh Sharma** and Manish Kumar Goyal (2018) "District-level assessment of the ecohydrological resilience to hydroclimatic disturbances and its controlling factors in India" *Journal of Hydrology*, 564, 1048–1057. [IF: 4.405]

2. **Ashutosh Sharma** and Manish Kumar Goyal. (2018) "Assessment of ecosystem resilience to hydroclimatic disturbances in India" *Global Change Biology*, 24(2), e432–e441. [IF: 8.88]

3. **Ashutosh Sharma** and Manish Kumar Goyal, "Assessment of the Changes in Precipitation, Temperature and Climate Extremes in Teesta River Basin in Indian Himalayan Region under Climate Change", *Atmospheric Research*, 231, 104670. [IF: 4.114]

Not published

- "Analysis of hydrological resilience of Teesta river basin to dry conditions under past and projected climate" - *Under preparation*
- "The Spatiotemporal Pattern of Ecosystem Water Use Efficiency and its Controlling Factors in India" - *Under preparation*
- "Analysis of changes in precipitation, temperature and climate extremes in India using multiple General Circulation Models" - *Under preparation*

Conferences

1. **Ashutosh Sharma**, Manish Kumar Goyal and Arup Kumar Sarma (2018) "Comparative assessment of ecosystem resilience to droughts in two large scale river basins in India", AGU Fall Meeting 2018, Session: H51K: Drought: Dynamics, Impacts, Resilience, and Mitigation I Posters, Washington DC, US. 10-14 Dec 2018.

2. **Ashutosh Sharma**, Manish Kumar Goyal and Arup Kumar Sarma. "Remote sensing based assessment of terrestrial ecosystem resilience to droughts in India". Midwest Big Data Hub Digital Agriculture All Hands meeting, University of Nebraska-Lincoln, 21 September 2018.